Physiological and Pathological Characterization of Alpha-Synuclein Oligomers

Physiological and Pathological Characterization of Alpha-Synuclein Oligomers

A dissertation presented

by

Eric Sloan Luth

to

The Division of Medical Sciences

in partial fulfillment of the requirements

for the degree of

Doctor of Philosophy

in the subject of

Neurobiology

Harvard University

Cambridge, Massachusetts

April 2014

Dissertation Advisor: Dr. Dennis Selkoe Eric Sloan Luth

Physiological and Pathological Characterization of Alpha-Synuclein Oligomers

Abstract

α-Synuclein (αSyn) is highly abundant cytosolic protein whose conversion into insoluble fibrils is a pathological hallmark of Parkinson's disease (PD) and other synucleinopathies. Despite decades of research, fundamental questions regarding αSyn biology are unresolved. Soluble, prefibrillar oligomers, not their fibrillar end products, are believed to be neurotoxic in humans and in disease models, but their mechanism of action remains unknown. Evidence from our lab and others increasingly suggests that, in healthy cells, αSyn does not exist purely as an unfolded monomer, as the field has long believed, but also as aggregation-resistant, α-helical oligomers; however, their physiological role remains controversial. Thus, my aim was twofold: to characterize toxic αSyn species in the context of mitochondrial dysfunction, a central phenotypic feature of PD; and to purify helical αSyn oligomers from human brain to enable further characterization of physiological αSyn.

Because the neuronal populations vulnerable in PD are characterized by cytosolic Ca^{2+} oscillations that burden mitochondria, I investigated the direct relationship between αSyn aggregation and mitochondrial dysfunction in the context of mitochondrial Ca^{2+} stress. Using a reductionist system comprising isolated mitochondria and recombinant αSyn in various carefully characterized aggregation states, I observed that soluble, prefibrillar αSyn oligomers, but neither fibrillar nor monomeric αSyn, decreased the ability of mitochondria to retain Ca^{2+}, promoted

Ca^{2+}-induced swelling and depolarization, and accelerated cytochrome c release. These changes were seen only when mitochondria were energized with complex I substrates and were prevented by cyclosporin A, implicating the involvement of the mitochondrial permeability transition pore.

Then, I developed a protocol to successfully purify soluble αSyn from postmortem, non-diseased human cortex. CD spectroscopy revealed that brain-derived αSyn contained significantly more helical content than recombinant protein. Application of a crosslinking reagent to intact neurons and to partially purified αSyn samples showed for the first time that abundant αSyn oligomers exist natively in the brain, and that they survive several, but not all, purification steps. Together, my results suggests that factors which shift the equilibrium of native αSyn oligomers toward aggregation-prone monomers can drive the generation of prefibrillar oligomers that then contribute to the selective degeneration of Ca^{2+}-challenged neuronal populations in PD.

Table of Contents

Table of Figures

Chapter 2: Soluble, Prefibrillar α-Synuclein Oligomers Promote Complex I-Dependent, Ca^{2+}-Induced Mitochondrial Dysfunction

Chapter 3: Purification and Characterization of α-Synuclein from Human Brain

Appendix 3: Visualization of Cellular α-Synuclein Oligomers Using Intact Cell Crosslinking

Acknowledgements

This work would not have been possible without the support of many individuals. I would first like to thank my extraordinary mentor Dennis Selkoe. Dennis has been, and continues to be, incredibly supportive of my research and career goals, even when they fall outside of what is typical for his trainees. He has given me every opportunity to succeed, and I am grateful for that. I also want to thank Dennis for creating such a stimulating lab environment. Having such wonderful colleagues and friends in the CND made work fun and exciting even when the data were not (which, let's face it, was more often than I care to remember). In particular, I want to thank my fellow Tetramericans: Tim Bartels, Joanna Choi, Ulf Dettmer, Nora Kim, Andrew Newman, and Vidiya Sathananthan. I would like to acknowledge other Selkoe lab members with whom I have worked closely: Toby Cavanaugh, Allen Chen, Oliver Holmes, Soyon Hong, Beth Ostaszewski, Heather Rice, and Ting Yang. It has been a sincere pleasure working with you all. I would also like to thank Tracy Young-Pearse, my introduction to the Sekloe lab during my rotation, Matt LaVoie, and their labs for their comments, criticism, and camaraderie. In addition, I want to thank Irina Stavrovskaya and Bruce Kristal for their guidance and contributions. Thanks also to my DAC committee: Marcia Haigis, Tom Schwarz, and Bernardo Sabatini.

I am grateful to have an extremely supportive family. My parents, Linda and Jeff, and my brother Stuart are constant sources of encouragement and have guided me to where I am today. I want to thank my son Ben who is, literally and figuratively, the reason I get up in the morning. He always makes me laugh and motivates me to be the best person I can be. I would like to thank my boglen Luna for her unconditional friendship and love. Finally, I want to thank my incredible wife Emily, without whose love nothing in my life would be possible. Thank you for your unwavering support and patience, and for reminding me what is truly important in life.

Chapter 1

Introduction

Parkinson's Disease

In 1817 James Parkinson first described the "shaking palsy" that would come to bear his name. In the many years since this initial characterization of six cases, Parkinson's disease (PD) has come to be diagnosed as the 2nd most common neurodegenerative disorder. PD is diagnosed in 1% of individuals by the age of 65 and 5% by age 85 (Van Den Eeden et al., 2003). In total, as many as 0.3% of Americans suffer from the disease, with the total number of diagnosed individuals projected to more than double by 2050 (Kowal et al., 2013). PD costs our nation over $14 billon annually, and as our population ages, PD is poised to present even more of a clinical and financial burden (Kowal et al., 2013). While several genes have been implicated in familial forms of PD over the last 2 decades, the vast majority of cases, greater than 90%, are sporadic with no known inherited cause (Dauer and Przedborski, 2003).

The principal clinical features of PD are resting tremor, rigidity, bradykinesia or slowness of movement, and postural instability (Dauer and Przedborski, 2003). The cause of classical parkinsonian symptoms, the loss of dopamine stimulation of the striatum, was not discovered until over a century after they were initially described. In the central nervous system, initiation of movement takes place partly in the midbrain, specifically in a collection of neuronal clusters called the basal ganglia (Shulman et al., 2011). The basal ganglia consist of the striatum, globus pallidus, subthalamic nuclei, and substantia nigra (SN). Synapses that connect the basal ganglia nuclei with each other as well those that link the basal ganglia with the motor cortex via the thalamus form the so-called basal ganglia motor loop. The activity of the SN serves to modulate the activity of this loop through two different dopaminergic pathways originating in the striatum: the *direct* pathway, which increases the output of the motor cortex and therefore movement; and the *indirect* pathway, which ultimately has the opposite effect. Depletion of striatal dopamine

would be expected to 1) reduce activation of the direct pathway and 2) remove inhibition of the indirect pathway – both of which would result in the inhibition of movement (Shulman et al., 2011). Indeed, this is exactly what happens in the brains of individuals with PD.

Striatal dopamine is reduced in PD patients because the cells the produce and deliver this dopamine, the neurons of the substantia nigra pars compacta (SNc), are targeted by the disease (Ehringer and Hornykiewicz, 1960). It is believed that by the time parkinsonian symptoms appear, 80% of striatal dopamine and 50-60% of SNc dopaminergic neurons have been lost (Bernheimer et al., 1973; Riederer and Wuketich, 1976). This notable for two reasons: on one hand it suggests that one can lose an impressive number of these cells before there are noticeable behavioral implications; but on the other, it indicates the extent of disease progression before patients seek medical attention - both of which highlight the importance of efforts to develop sensitive biomarkers for early detection. At this point, the only effective molecular treatments for parkinsonian symptoms are L-3,4-dihydroxyphenylalanine (L-DOPA), a dopamine precursor that serves to ameliorate motor dysfunction by increasing the amount of dopamine produced by SNc neurons, and other drugs that act to increase the activity of dopamine in the nigrostriatal pathway. Unfortunately, enhancing dopaminergic tone does not affect the underlying cause of nigral degeneration, and, after many dopaminergic neurons are lost, such treatments can lose their efficacy (Olanow and Schapira, 2013).

Aside from selective neuronal loss, the other pathological hallmark of PD is the presence of insoluble aggregates in the soma and neurites of cells called Lewy bodies and Lewy neurites, respectively. These proteinaceous inclusion bodies appear as a dense core surrounded by a diffuse halo and are found areas affected by neuronal loss (Spillantini et al., 1997). Lewy pathology contains ubiquitin and other proteins such as synaptophysin (Nishimura et al., 1994)

and synphilin (Katsuse et al., 2003), but it is primarily composed of 10-14 nm in diameter fibrils of the protein α-synuclein (αSyn) (Spillantini et al., 1997). Though they are present in diseased regions, it is becoming increasingly clear that Lewy bodies themselves are not toxic, but rather they may represent an attempt by cells to sequester other toxic αSyn species (Reeve et al., 2012; Tanaka et al., 2004; Tompkins and Hill, 1997).

α-Synuclein in Familial and Sporadic Parkinson's Disease

αSyn is present in peripheral tissue such as cells of the erythroid lineage (Barbour et al., 2008; Dettmer et al., 2013), but it is most highly expressed in brain - with estimates that it represents 0.2%-1% of the total brain protein (Iwai et al., 1995; Tofaris et al., 2005). αSyn is a 140 amino acid protein that is localized primarily to presynaptic terminals. Its N terminus is marked by seven imperfect, 11-residue repeats that mediate the binding of αSyn to membranes – primarily small diameter vesicles and negatively charged phospholipids such as monosialoganglioside (GM1) (Martinez et al., 2007) and cardiolipin (Nakamura et al., 2008) – and the adoption of N-terminal helicity (Davidson et al., 1998). The vast majority (>90%) of the protein is soluble (Dettmer et al., 2013; George et al., 1995; Kahle et al., 2000), however, indicating that interactions with membranes may be transient. αSyn also contains an unfolded, acidic C-terminal tail and a highly hydrophobic central NAC domain (residues 61-95), so named because this peptide was identified as a non-amyloid-β component of plaques in Alzheimer's disease (Culvenor et al., 1999; Uéda et al., 1993).

Genetic evidence indicates that αSyn plays a causal role in the pathogenesis of PD. To date, 5 missense mutations (A53T, A30P, E46K, G51D, H50Q) have been discovered that lead to dominantly inherited PD (Kara et al., 2013). These patients display similar symptoms to those

suffering from idiopathic PD, though some mutations are more aggressive than others (Lesage et al., 2013; Zarranz et al., 2004). Duplication and triplication of the wild type αSyn locus are sufficient to cause PD with an onset and severity that varies with the gene dosage (Chartier-Harlin et al., 2004; Singleton et al., 2003). Aside from its involvement in familial PD, the presence of Lewy pathology in sporadic PD indicates that αSyn plays an important role in these cases as well.

Though the exact molecular stimuli remain unclear, under pathological conditions, this normally soluble protein undergoes a conversion into β-sheet-rich, insoluble fibrils found within Lewy pathology. This aberrant, amyloid-type aggregation of αSyn is dependent on the NAC domain (Giasson et al., 2001), which is absent in its aggregation-resistant family member β-synuclein (βSyn) (George, 2002). *In vitro* studies of recombinant protein have shown that aggregation from an unfolded monomer into fibrils occurs by way of a heterogeneous pool of soluble oligomeric intermediates (Breydo et al., 2012). Because of their correlation with neuronal loss in PD, Lewy bodies were long thought to be toxic to neurons; however, recent evidence suggests that these inclusions may serve to sequester soluble αSyn oligomers, now believed to represent the true neurotoxic species (Volles and Lansbury, 2003) - a hypothesis reminiscent of the changing attitudes regarding Aβ aggregates in the pathogenesis of AD (Haass and Selkoe, 2007).

Several lines of evidence from PD patients support the hypothesis that soluble αSyn oligomers, rather than insoluble fibrils, are the main neurotoxic species in PD and other such synucleinopathies. First, not all αSyn mutations that result in early onset PD lead to enhanced fibrilization (Conway et al., 2000). These familial PD mutations may have other effects on the structure and stability of physiological αSyn that will be addressed later. Second, insoluble Lewy

bodies are found in asymptomatic individuals (Knopman et al., 2003). And third, cells containing Lewy bodies are thought to be healthier than nearby neurons that lack Lewy bodies (Tompkins and Hill, 1997). *In vitro* data support this theory, as well. Oligomers produced from recombinant αSyn have been shown to permeabilize vesicles and create plasma membrane pores that result in Ca^{2+} influx and initiation of caspase-3-dependent cell death (Danzer et al., 2007; Volles et al., 2001).

The *in vivo* toxicity of oligomer-forming αSyn was elegantly addressed by recent publications. αSyn of different aggregation propensities were expressed in *C. elegans* and *Drosophila*. The authors observed an inverse correlation between β-sheet content/insolubility of the variants, as determined biophysically or by immunostaining, and neurotoxicity in these model organisms (Chen and Feany, 2005; Chen et al., 2009; Karpinar et al., 2009). Winner and colleagues (2011) similarly engineered αSyn mutants that either promote oligomerization or fibrilization as determined *in vitro*. Oligomer-forming, but not fibril-forming, variants resulted dopaminergic neuron loss when overexpressed in rat SN neurons by lentiviral infection. As analyses of PD brains have shown, however, there is no evidence indicating that αSyn oligomers exist only in brain regions that undergo neurodegeneration. This suggests that, on their own, soluble αSyn oligomers may not be inherently toxic but rather result in cytotoxicity when they are stabilized and present in an environment particularly vulnerable to their effects.

Phenotype of Vulnerable Neuronal Populations

The classical PD motor symptoms and their source, the stereotypical degeneration of SNc dopaminergic neurons, have been well characterized. Dopamine itself is often pointed to as the culprit for this selective loss since cytosolic DA is readily oxidized into toxic metabolites

(Greenamyre and Hastings, 2004); however additional evidence suggests that presence of dopamine on its own is not sufficient to explain the pattern of cell loss in PD. For one thing, if dopamine itself were leading to toxicity, it would be difficult to explain how chronic administration of the dopamine precursor L-DOPA can alleviate, rather than worsen, parkinsonian symptoms (Fahn, Parkinson Study Group, 2005). In addition, distinct dopaminergic populations are differentially susceptible in PD. For example, compared to the nigral dopaminergic neurons, those of the neighboring ventral tegmental area (VTA) are relatively spared (Dauer and Przedborski, 2003). Perhaps most importantly, non-DA areas are also targeted. PD-related degeneration in areas such as the cholinergic dorsal motor nucleus of the vagus (DMV), the noradrenergic locus ceruleus (LC), and serotonergic raphe nuclei (RN) are responsible for symptoms such as constipation, sleep disturbance, and depression, respectively (Surmeier and Schumacker, 2013).

The neuronal populations vulnerable in PD share a distinctive physiological phenotype in which they deal with high transmembrane Ca^{2+} current. Unlike their relatively spared VTA counterparts, SNc dopaminergic neurons possess an unusual, age-dependent reliance on Ca^{2+} influx through Cav1.3 L-type voltage-gated Ca^{2+} channels that contribute to their pacemaking activity (Chan et al., 2007) and lead to detectable oscillations in intracellular Ca^{2+} levels (Guzman et al., 2010). Moreover, their slow firing rate and extended spike duration allow for excessive Ca^{2+} influx through presynaptic voltage-gated Ca^{2+} channels. Elevated Ca^{2+} flux is also a feature of broad-spiking, spontaneously active neurons of the DMV, LC, and RN, among other vulnerable regions (Surmeier and Schumacker, 2013).

Careful regulation of intracellular Ca^{2+} is critical for proper neuronal function. Ca^{2+} regulates neurotransmitter release, stimulates ATP production, mediates synaptic plasticity, and

activates a host of transcription programs that result in, among other changes, cell growth, proliferation, and differentiation. The specific pathways activated in response to Ca^{2+} transients generated either by influx of extracellular Ca^{2+} or release from intracellular stores are dependent on the temporal and spatial dimensions, amplitude, and subcellular localization of the signal (Wojda et al., 2008). Excessive intracellular Ca^{2+} can lead to activation of Ca^{2+}-binding calpain proteases and caspases that can cleave enzymatic and structural proteins leading to cell death (Berliocchi et al., 2005; Wojda et al., 2008).

In addition to ATP-dependent plasma membrane pumps, neurons rely on fixed cytosolic Ca^{2+} buffering proteins (such as calbindin, calretinin, and parvalbumin) combined with uptake into intracellular Ca^{2+} stores to keep the cytosolic concentration low. Neurons at risk in PD display a reduced intrinsic buffering capacity. Nigral dopaminergic neurons have significantly lower levels of calbindin-D mRNA and protein in PD cases compared to controls (Iacopino and Christakos, 1990) and dopaminergic and non-dopaminergic regions lost in PD contain lower levels of Ca^{2+} binding proteins than those that are more resistant to the disease (B. G. Kim et al., 2000; McCarthy et al., 2012; Mouatt-Prigent et al., 1994; Yamada et al., 1990), suggesting that they rely more heavily on intracellular storage.

The cytosolic Ca^{2+} oscillations that occur in vulnerable populations place a substantial metabolic burden on mitochondria. Mitochondrial ATP is needed to operate transporters on the plasma and endoplasmic reticulum (ER) membranes that pump Ca^{2+} out of the cytosol in an effort to re-establish the steep concentration gradient that is reduced upon Ca^{2+} influx. Besides their critical role in ATP generation, mitochondria are also important Ca^{2+} buffering organelles in both physiological and pathological situations. Under physiological conditions, mitochondrial Ca^{2+} uptake through the ruthenium red-sensitive Ca^{2+} uniporter spatially and temporally

modulates intracellular Ca^{2+} transients and stimulates the production of ATP by activating multiple enzymes of the tricarboxylic acid cycle (Szabadkai and Duchen, 2008). L-type-mediated Ca^{2+} influx in particular can act to modulate ryanodine receptors and stimulate Ca^{2+}-induced-Ca^{2+}-release from the ER that, due its close proximity to mitochondria, results in an increase in mitochondrial Ca^{2+} concentration (Szabadkai and Duchen, 2008). Under pathological conditions, it is instrumental for execution of excitotoxic pathways (Stout et al., 1998), as mitochondrial Ca^{2+} overload leads to opening of the mitochondrial permeability transition pore (mPTP) (Baumgartner et al., 2009).

The mPTP is a multi-protein complex that is believed to consist of the mitochondrial outer membrane protein VDAC (voltage-dependent anion channel), the inner mitochondrial membrane protein ANT (adenine nucleotide translocator), and the matrix modulator cyclophilin-D. If the matrix Ca^{2+} concentration passes a critical threshold, cyclophilin D binds to ANT - a process prevented by the mPTP inhibitor cyclosporin A (CsA) – and allows ANT and VDAC to form a large conductance pore (Norenberg and Rao, 2007). Pore formation allows for the diffusion of solutes smaller than 1500 Da across both mitochondrial membranes, effectively abolishing mitochondrial membrane potential ($\Delta\Psi_m$). This permeability increase also results in the osmotic influx of H_2O due to the high concentration of matrix solutes, ultimately leading to mitochondrial swelling, outer membrane rupture, the release of cytochrome C, and downstream initiation of apoptosis (Petit et al., 1998). Oxidative stress favors the opening of the mPTP by inducing the crosslinking of matrix-facing cysteines residues of ANT that promotes binding of cyclophilin-D (Halestrap and Brenner, 2003).

Recent work has revealed that the mitochondria of vulnerable neurons do indeed exhibit signs of stress. The Surmeier lab used a mitochondria-targeted, redox-sensitive GFP and

observed brighter fluorescence (corresponding to a more oxidized matrix environment) in neurons within at-risk populations, including the SNc and DMV, compared to neurons from areas that are relatively spared, like the VTA (Goldberg et al., 2012; Guzman et al., 2010). The fluorescence/oxidation state of GFP could be reduced by antagonizing L-type Ca^{2+} channels or by blocking the mitochondrial Ca^{2+} uniporter with Ru360, suggesting that mitochondrial Ca^{2+} uptake contributes to this oxidative environment (Goldberg et al., 2012; Guzman et al., 2010). Mitochondrial Ca^{2+} uptake occurs due to the electrical and chemical gradient inside the matrix and its uptake partially dissipates the $\Delta\Psi_m$ needed for ATP synthesis. In order to re-establish the $\Delta\Psi_m$ to allow for optimal ATP synthesis and buffering of further cytosolic Ca^{2+} elevations, mitochondria must increase activity of the electron transport chain (ETC) and its associated proton pumping. In case of vulnerable neurons whose cytosolic Ca^{2+} concentrations are constantly oscillating, there are likely cycles of mitochondrial depolarization due to Ca^{2+} uptake, and repolarization due to stimulation of respiratory chain activity. Though the precise mechanisms linking ETC activity and the production of reactive oxygen species (ROS) are not fully understood, a greater flux of electrons into the respiratory chain raises the probability that some single electrons will be inappropriately transferred to O_2 prior to reaching complex IV (Lee et al., 2001; Rigoulet et al., 2011) especially under conditions of compromised ETC activity (see below). Regardless of how it is achieved, the basal level of oxidant stress in the mitochondria of vulnerable neurons may put them at risk of dysfunction caused by an additional stressor.

Mitochondrial Dysfunction in Parkinson's Disease

In the context of PD, mitochondrial stress could come in the form of the accumulation of damaged or dysfunctional mitochondrial components. For example, two proteins implicated in familial PD, Parkin and PINK-1, are believed to function in a mitochondrial quality control pathway. The mitochondrial network is constantly undergoing cycles of fission and fusion that serve to exchange membrane content (including proteins and lipids) and intra-mitochondrial components (such as mitochondrial DNA). Loss of function mutations in these PD-related genes may result in defective autophagic clearance of damaged or dysfunctional mitochondria (mitophagy) and their subsequent accumulation within the cell (Narendra et al., 2012).

Parkinsonism has repeatedly been linked to deficits in the activity of mitochondrial complex I, an inner mitochondrial membrane protein complex of at least 45 subunits and multiple assembly factors that serves as the entry point for NADH-linked substrates into the ETC (Koopman et al., 2010). Complex I catalyzes the transfer of electrons from NADH to ubiquinone via iron sulfur clusters and a flavin mononucleotide while also pumping protons from the matrix to the intermembrane space, thereby contributing to the proton gradient that is harnessed for ATP production (Mitchell, 1961). In 1983, Langston (1983) reported cases of illicit drug users who developed progressive parkinsonism with degeneration of the SN after inadvertently injecting 1-methyl-4-phenyl- 1,2,3,6-tetrahydropyridine (MPTP). MPTP is oxidized by monoamine oxidase in glia to MPP+, which is selectively taken up into dopaminergic neurons via dopamine transporter where it binds to and inhibits the activity of complex I (Langston et al., 1984). Epidemiological data indicate that exposure to pesticides such as rotenone, another specific complex I inhibitor (but one that is not selective for dopaminergic neurons), is also associated with PD (T. M. Dawson and V. L. Dawson, 2003). Use of MPTP and rotenone in primates,

rodents, and cell culture have become useful PD models since they reproduce features of the disease including oxidative stress, motor deficits (in animal models) and αSyn accumulation (Betarbet et al., 2002).

Multiple types of complex I dysfunction have been reported in the brains of sporadic PD patients. Spectrophotometric measurements of the enzymatic activity of mitochondrial ETC complexes harvested from post-mortem tissue revealed specific deficits in complex I activity compared to control tissue even in areas spared from frank cell loss (Keeney et al., 2006; Parker et al., 2008; Schapira et al., 1990). This supports the idea that certain brain regions are preferentially susceptible to the downstream effects of compromised mitochondrial function. In line with reports of reduced complex I activity, Keeney and colleagues (2006) detected elevated levels of protein carbonyls, a marker of oxidative damage, in the complex I subunits of PD patients that inversely correlated with proper complex I assembly and function. Furthermore, mitochondria from PD patients contain a higher proportion of mitochondrial DNA (mtDNA) mutations than do mitochondria from control tissue – an observation indicative of an oxidative matrix environment. These mtDNA mutations are likely both a consequence and cause of oxidative stress. ROS such as H_2O_2 are known to produce double-stranded DNA breaks. Mutations in mtDNA can lead to reduced expression of mitochondrial gene-encoded proteins or the expression of non-functional variants. Of the 13 proteins encoded by mtDNA, seven are complex I subunits and the others are subunits for complexes III and IV (Reeve et al., 2008). Improper ETC complex formation can impair the proper flow of electrons and lead to the generation of ROS, especially from complexes I and III (Rigoulet et al., 2011). ROS can act locally to oxidize ETC components and membrane lipids or target mtDNA, further contributing to oxidative challenges and bioenergetic failure.

α-Synuclein Accumulation Impairs Mitochondrial Function

It is becoming increasingly apparent that the accumulation of αSyn, as occurs in PD, is associated with a mislocalization of a pool of αSyn to the soma and processes (Roy, 2009) as well as a partial redistribution from the cytosol to the mitochondria. Cole and colleagues (2008) proposed that this redistribution might be heightened in times of oxidative or metabolic stress. Accordingly, another group used immunoelectron microscopy (immuno-EM) to demonstrate a preferential association of αSyn with mitochondria in rat SN neurons compared to cortical neurons (Zhang et al., 2008). Though it is still unclear how this transition occurs *in vivo*, PD patients and models show increased mitochondrial αSyn content that is associated with mitochondrial dysfunction, including complex I dysfunction, elevated ROS, reduced $\Delta\Psi_m$, altered Ca^{2+} homeostasis, and enhanced cytochrome c release (Chinta et al., 2010; Devi et al., 2008; Hsu et al., 2000; Martin et al., 2006; Parihar et al., 2008; Rhinn et al., 2012; Sarafian et al., 2013; Smith et al., 2005; Stichel et al., 2007). Devi et al. (2008) used ELISA and immuno-EM to show that the mitochondria from the SN of PD patients contained significantly more αSyn than did the SN from control tissue or the cerebellum from PD brain. These findings were supported by another group who recently reported an increase in mitochondrial αSyn in PD patients possessing an αSyn mRNA transcript isoform with an elongated 3' untranslated region associated with higher protein levels (Rhinn et al., 2012). Transfection of this isoform in rat cortical neurons confirmed a greater redistribution of αSyn to mitochondria from synaptic terminals compared to the short isoform, suggesting that αSyn concentration itself may somehow contribute to mitochondrial translocation (Rhinn et al., 2012).

The precise mitochondrial localization of redistributed αSyn is still controversial. As will be addressed further below, αSyn has a well-documented tendency to bind acidic phospholipids. The mitochondrial membranes, particularly the inner mitochondrial membrane, are enriched in cardiolipin (Daum, 1985), and fluorescence resonance energy transfer studies suggest that αSyn preferentially interacts with mitochondrial membranes *in vitro* (Nakamura et al., 2008). Several reports have described an outer mitochondrial membrane association for αSyn (Cole et al., 2008; Nakamura et al., 2008; 2011), but others indicate that, under conditions favorable for ATP production, it can be localize to the inner membrane as determined by immuno-EM and proteinase K digestion experiments (Devi et al., 2008; Liu et al., 2009; Zhang et al., 2008). Discrepancies in submitochondrial localization may be due to differences in the cell types examined or the degree or form of αSyn expressed within the cell. Though αSyn lacks a classical mitochondrial recognition sequence, truncation of the N-terminal 32 residues did abolish the mitochondrial import of αSyn in one system (Devi et al., 2008); however, since the N terminus is responsible for lipid-induced folding of αSyn, it is conceivable that this could be disruptive to the general structure and function of the protein (Bartels et al., 2010; Vamvaca et al., 2009).

Over the last 8 years there have been a multitude of reports that demonstrating that αSyn accumulation, and its subsequent association with mitochondria, is correlated with mitochondrial dysfunction. In the aforementioned study by Devi and colleagues (2008), the amount of mitochondrial αSyn in PD tissue was inversely correlated to the activity of complex I, but not other respiratory complexes. Overexpression of wild type and PD mutant αSyn in mice or cell lines also results in reduced complex I activity (Chinta et al., 2010; Devi et al., 2008; Stichel et al., 2007). These effects are not observed upon overexpression of an N-terminally truncated variant that fails to target to mitochondria (Devi et al., 2008). Further implying a direct role for

αSyn in complex I dysfunction, purified αSyn has been shown to dose-dependently reduce complex I activity in mitoplasts and freeze-fractured mitochondria (Devi et al., 2008; Liu et al., 2009). As may be expected by these reported effects on complex I function, overexpression of mutant and wild type αSyn is also associated with decreased $\Delta\Psi_m$ and elevated ROS levels and in a variety of cell types (Devi et al., 2008; Hsu et al., 2000; Li et al., 2013; Parihar et al., 2009; Smith et al., 2005). An increase in mitochondrially-generated ROS could be particularly problematic since, aside from its roles in oxidizing macromolecules and facilitating mitochondrial permeability transition, ROS have also been reported to promote the oligomerization of αSyn (Näsström et al., 2011), perhaps leading to a vicious cycle of oligomerization and mitochondrial dysfunction.

Recent studies suggest that apoptosis observed in αSyn transgenic organisms might be related to the activity of the mPTP. Genetic modulation of mPTP components rescued cytotoxicity in mice, *Drosophila*, and *C. elegans* models of αSyn overexpression (Büttner et al., 2013; Martin et al., 2013). Interestingly, the pro-apoptotic nuclease Endo-G, which is released from mitochondria upon mPTP opening, was observed within the nuclei of cells in PD, but not control brain sections (Büttner et al., 2013). These data in agreement with earlier reports that αSyn overexpression in cell lines promotes a redistribution of cytochrome c from the mitochondria into the cytosol (Parihar et al., 2008; Smith et al., 2005) that can be partially rescued by the mPTP inhibitor cyclosporin A (Smith et al., 2005), but not all αSyn transgenic mouse models with mitochondrial abnormalities show evidence of mPTP activation (Stichel et al., 2007).

There have been very few investigations into the effect of different forms of αSyn on intact mitochondrial function. Parihar and colleagues (2008) reported that aggregated, but not

monomeric αSyn, can increase markers of oxidative stress upon incubation with isolated mitochondria, but the aggregation state (fibrillar or oligomeric) was not characterized. Overall, the overexpression of αSyn is associated with a variety of mitochondrial phenotypes including complex I dysfunction, elevated ROS, reduced membrane potential, altered Ca^{2+} homeostasis, and enhanced cytochrome c release. That said, the direct effects of defined αSyn of aggregation states on mitochondria in the context of elevated Ca^{2+}, as experienced by the mitochondria of neurons vulnerable in PD, has not been investigated.

Physiological Function of α-Synuclein

Interest in alpha-synuclein intensified when it was identified as the main protein component in Lewy bodies associated with synucleinopathies (Spillantini et al., 1997), and appropriately, much research has been devoted to the role of its aggregation in disease pathogenesis. Studies linking αSyn to disease also spurred research into its physiological function. Independent of its recognition as a component of plaques in AD (Culvenor et al., 1999; Uéda et al., 1993), αSyn was first discovered in 1988 as a presynaptic protein by virtue of its identification in a cDNA library using an antisera to purified cholinergic synaptic vesicles from the electric ray *Torpedo californica* (Maroteaux et al., 1988). This report, and others (McLean et al., 2000) also detected αSyn in the nucleus in addition to its synaptic localization, leading to the name "synuclein". Its small size of ~14 kDa is below the molecular weight cutoff for the nuclear pore, so it is conceivable that its presence in the nucleus is a result of diffusion rather than a specific functional role (Bendor et al., 2013).

α-, β-, and γ-synuclein (γSyn) comprise the synuclein family of proteins, which is present only in vertebrates. There are no identified orthologs in other organisms. All synuclein family

members are mainly expressed in the nervous system, with α- and βSyn localized centrally, and γSyn present in peripheral nerves. Within species, the proteins share a highly conserved N terminus with considerable variability in the C-terminal ~40 amino acids (George, 2002). It is also noteworthy that βSyn lacks the residues corresponding to amino acids 53-63 in αSyn, a region that partially overlaps with the hydrophobic NAC domain that is required for the aggregation of αSyn into fibrils (Giasson et al., 2001). The N terminus of αSyn is also highly conserved across taxa; for example the human and mouse sequences are identical through the intial 42 amino acids and 95.3% identical overall (Lavedan, 1998). This suggests that N-terminal residues are ciritical for the proper structure and function of the protein.

The exact nature of αSyn's physiological function is not completely understood. There have been reports that αSyn functions as an inhibitor of phospholipase D-2, an enzyme responsible for generating the intracellular signaling molecule phosphatidic acid (Jenco et al., 1998); however, recent evidence argues against this (Rappley et al., 2009). Studies of synelfin, an avian homolog of αSyn, revealed abundant presynaptic expression that correlates spatially and temporally with zebra finch song learning, thus proposing a role for αSyn in synaptic plasticity (George et al., 1995). The imperfect repeats found in αSyn are similar to lipid binding domains of apolipoproteins (Weinreb et al., 1996) suggesting a role in the binding of lipids and vesicles. That being said, interaction with lipids may only be transient since over 90% of αSyn is found within the cytosol following fractionation (Dettmer et al., 2013; George et al., 1995; Kahle et al., 2000). Investigations in which the level of αSyn within cells or organisms has been modulated support predictions based on protein domain similarity and the presynaptic localization of αSyn. Low-level overexpression of aSyn in pheochromocytoma cells resulted in an increase in docked dense core vesicles and a corresponding reduction in vesicle fusion events (Larsen et al., 2006).

Inhibition of vesicle exocytosis was also observed upon mild overexpression in cultured neurons (Nemani et al., 2010), though effects on vesicle endocytosis may be dependent on the cell type examined (Ben Gedalya et al., 2009; Nemani et al., 2010). Along these lines, experiments using αSyn knockout mice revealed a mild increase in dopamine transmission upon repetitive stimulation, consistent with the idea that αSyn functions as a negative regulator of activity-dependent dopamine release. A more mild effect was seen in glutamatergic neurons (Abeliovich et al., 2000). Animals in which multiple synuclein family members have been genetically ablated have been reported to display elevated basal neurotransmitter release (Anwar et al., 2011), but this may be dependent on which synapses are analyzed (Burré et al., 2010). αSyn has also been proposed to act as a chaperone for the activity dependent assembly of neuronal SNARE (SNAP (soluble NSF attachment protein) receptor) complexes (Burré et al., 2010), though biochemical interaction with SNARE proteins remains controversial (Chandra et al., 2005; DeWitt and Rhoades, 2013).

In vitro examination of αSyn further supports a role for αSyn in lipid binding and membrane dynamics. Recombinant αSyn adopts stable, helical secondary structure upon lipid binding (Davidson et al., 1998), a process that is dependent on critical N-terminal amino acids (Bartels et al., 2010; Vamvaca et al., 2009). Fluorescence correlation spectroscopy indicates that αSyn has preference for a high degree of membrane curvature, as found in small diameter vesicles like synaptic vesicles (Middleton and Rhoades, 2010). Aside from this type of curvature-sensing, there are also reports of curvature-generation by high concentrations of recombinant αSyn (Varkey et al., 2010), and it has been proposed that these abilities may be related (Jensen et al., 2011). This preference for highly curved membranes and evidence that αSyn inhibits the *in vitro* fusion of small unilamellar vesicles, potentially by relieving stress

caused by curvature-induced lipid packing defects (Kamp et al., 2010), provide a degree of mechanistic insight into αSyn-induced alterations in exocytosis observed *in vivo*.

There is still much to be learned about how and with what molecular partners αSyn is acting within cells. Due to the strong connection between αSyn and neurodegenerative disease, research has focused on the role of αSyn in the brain; however, high expression of aSyn in erythrocytes (Barbour et al., 2008) suggests a broader role for the protein in vesicle/membrane dynamics rather than one specific to synaptic vesicles. Future examinations of possible erythrocyte phenotypes in knockout animals, for example, could provide insight into previously unobserved or underappreciated cellular roles for αSyn. Importantly, the vast majority of *in vitro* efforts to study physiological αSyn and its interaction with various lipid and protein molecules have relied on bacterially expressed recombinant protein. Recent work from our lab suggests that future investigations into the precise physiological function of αSyn would benefit from the availability of protein isolated under non-denaturing conditions from endogenously expressing sources (Bartels et al., 2011).

Rethinking the Native State of α-Synuclein

Original characterizations of bacterially expressed αSyn purified either under native or denaturing conditions indicated that the recombinant protein is unfolded and monomeric (Kim, 1997; Weinreb et al., 1996). Because of these experiments, the field has generally believed that αSyn is similarly unfolded and monomeric under endogenous expression conditions,and has therefore routinely used denaturing protocols to prepare αSyn for *in vitro* studies due to their simplicity.

A recent report from our laboratory challenged this assumption by using αSyn purified under non-denaturing conditions from human erythrocytes, an abundant endogenous source of αSyn (Barbour et al., 2008), and from human neuroblastoma cells (Bartels et al., 2011). This report demonstrated that native, human αSyn exists in large part as a helically folded oligomer that sized as a tetramer by scanning transmission electron microscopy and analytical ultracentrifugation. While it is well established that αSyn adopts a helical structure when associated with lipid vesicles, the inability of phosphate analysis to detect lipid content in the purified samples indicated that helicity of the oligomer observed by Bartels et al. is maintained in the absence of phospholipids. Importantly, incubation with the β-sheet-binding dye thioflavin T revealed that human cell-derived helical oligomers did not undergo amyloid-type aggregation, unlike bacterially expressed recombinant monomers (Bartels et al., 2011). This strongly suggests that these helical oligomers are physiological and not pathological species.

Understandably, these findings have inspired considerable debate in the field. Since this publication, the purification of helical oligomeric αSyn from human erythrocytes has been reproduced by one group (Westphal and Chandra, 2013), though not by another (Fauvet et al., 2012). A third group has recently published that mouse brain contains αSyn that is predominantly unfolded and monomeric, though the contribution of helical αSyn was downplayed (Burré et al., 2013). Still others have achieved helical oligomeric aSyn from bacterial expression protocols under certain conditions (Trexler and Rhoades, 2012; Wang et al., 2011), most notably those that allow for the N-terminal acetylation of the protein (Trexler and Rhoades, 2012). Mammalian αSyn appears to be exclusively N-acetylated (Anderson et al., 2006; Bartels et al., 2011; Ohrfelt et al., 2011), unlike the protein normally expressed in bacteria, and recent studies suggest that this post-translational modification is important for stabilizing

helical content (Maltsev et al., 2012; Trexler and Rhoades, 2012). The detection of oligomeric protein within intact, but not lysed cells (Dettmer et al., 2013; Klucken et al., 2006) and the difficulty in consistently purifying helical oligomers across labs speaks to their labile nature; however, it is presently unclear what conditions favor the destabilization of aggregation-resistant oligomers into aggregation-prone monomers.

It should be noted that studies of recombinant protein are appropriate and necessary for two reasons. First, unfolded monomeric αSyn clearly represents meaningful pool of total αSyn that no doubt plays a role within the cell. And second, investigations into the pathologic role of αSyn should focus on a form of the protein that undergoes spontaneous aggregation. As discussed above, helical oligomers are aggregation-resistant while unfolded monomers are aggregation-prone. Though it is unclear whether monomers on their own are toxic to cells, there is overwhelming evidence that toxicity is related to the aggregation of αSyn. That being said, a complete understanding of *physiological* αSyn and its function within neurons and other cells will require extensive examination of non-pathologic, helical oligomers.

Overview of Thesis

This goal of this thesis is to characterize oligomeric forms of αSyn in order to better understand their physiological and pathological relevance. αSyn has been heavily studied since it was discovered that this normally soluble protein undergoes a conversion into insoluble amyloid fibrils that accumulate as cytoplasmic aggregates termed Lewy bodies and Lewy neurites, the main cytopathological hallmarks of PD. A growing body of evidence from our lab and others suggests that αSyn does not exist purely as an unfolded monomer, as the field has long believed, but in an equilibrium between helical oligomers and unfolded monomers. Helical, oligomeric

αSyn is aggregation-resistant *in vitro* while the unfolded monomer readily aggregates into insoluble, β-sheet-rich amyloid-type fibrils through prefibrillar, oligomeric intermediates. Soluble, prefibrillar oligomers, not their fibrillar end products, have been reported to be neurotoxic *in vitro* and in disease models. My aim was twofold: to characterize toxic αSyn species in the context of mitochondrial dysfunction, a central phenotypic feature of PD; and to purify helical αSyn from human brain to enable further characterization of physiological αSyn.

Part 1: Soluble, Prefibrillar α-Synuclein Oligomers Promote Complex I-Dependent, Ca^{2+}-Induced Mitochondrial Dysfunction

The 1st part of this thesis is focused on exploring the direct relationship between two features of PD: αSyn aggregation and mitochondrial dysfunction. I modeled mitochondrial Ca^{2+} stress in a reductionist system composed of isolated mitochondria and recombinant human αSyn in various carefully characterized aggregation states. I observed that soluble, prefibrillar αSyn oligomers, but neither fibrillar nor monomeric αSyn, decreased the retention of exogenously added Ca^{2+}, promoted Ca^{2+}-induced mitochondrial swelling, and accelerated cytochrome c release, but only when mitochondria were energized with complex I substrates. αSyn-induced changes in mitochondrial parameters were prevented by cyclosporin A, implicating the involvement of the mitochondrial permeability transition pore. My results indicate that soluble, prefibrillar αSyn oligomers sensitize mitochondria to Ca^{2+}-induced permeability transition and reveal that the association of oligomeric αSyn with mitochondria can be particularly harmful to cells that experience elevated intracellular Ca^{2+} levels, such as those that are targeted in PD.

Part 2: Purification and Characterization of α-Synuclein from Human Brain

The 2nd part of this thesis is centered on understanding the physiological forms of αSyn present under normal conditions in the human brain and providing a means of enabling future studies of the function of this protein. In light of our recent studies suggesting that αSyn exists natively as a helical oligomer, I sought to purify and characterize native αSyn oligomers from the tissue most relevant to neurologic disease. Using a combination of ammonium sulfate precipitation, gel filtration, ion exchange, and affinity chromatography, I successfully purified soluble αSyn from postmortem, non-diseased human brain. Purified, brain-derived αSyn contained significantly more helical content than recombinant protein, as determined by CD spectroscopy. Application of the lysine-reactive crosslinker DSG to intact neurons and to partially purified αSyn samples revealed that abundant αSyn oligomers exist in the human brain under physiological conditions, and that they can survive several purification steps. This protocol has proved useful in identifying conditions that destabilize helical oligomers into monomers, and it will be important for future *in vitro* studies of the physiological function of native brain αSyn.

References

Abeliovich, A., Schmitz, Y., Fariñas, I., Choi-Lundberg, D., Ho, W.H., Castillo, P.E., Shinsky, N., Verdugo, J.M., Armanini, M., Ryan, A., Hynes, M., Phillips, H., Sulzer, D., Rosenthal, A., 2000. Mice lacking alpha-synuclein display functional deficits in the nigrostriatal dopamine system. Neuron 25, 239–252.

Anderson, J.P., Walker, D.E., Goldstein, J.M., de Laat, R., Banducci, K., Caccavello, R.J., Barbour, R., Huang, J., Kling, K., Lee, M., Diep, L., Keim, P.S., Shen, X., Chataway, T., Schlossmacher, M.G., Seubert, P., Schenk, D., Sinha, S., Gai, W.P., Chilcote, T.J., 2006. Phosphorylation of Ser-129 is the dominant pathological modification of alpha-synuclein in familial and sporadic Lewy body disease. J. Biol. Chem. 281, 29739–29752.

Anwar, S., Peters, O., Millership, S., Ninkina, N., Doig, N., Connor-Robson, N., Threlfell, S., Kooner, G., Deacon, R.M., Bannerman, D.M., Bolam, J.P., Chandra, S.S., Cragg, S.J., Wade-Martins, R., Buchman, V.L., 2011. Functional alterations to the nigrostriatal system in mice lacking all three members of the synuclein family. Journal of Neuroscience 31, 7264–7274.

Barbour, R., Kling, K., Anderson, J.P., Banducci, K., Cole, T., Diep, L., Fox, M., Goldstein, J.M., Soriano, F., Seubert, P., Chilcote, T.J., 2008. Red blood cells are the major source of alpha-synuclein in blood. Neurodegener Dis 5, 55–59.

Bartels, T., Ahlstrom, L.S., Leftin, A., Kamp, F., Haass, C., Brown, M.F., Beyer, K., 2010. The N-terminus of the intrinsically disordered protein α-synuclein triggers membrane binding and helix folding. Biophys. J. 99, 2116–2124.

Bartels, T., Choi, J.G., Selkoe, D.J., 2011. α-Synuclein occurs physiologically as a helically folded tetramer that resists aggregation. Nature 477, 107–110.

Baumgartner, H., Gerasimenko, J., Thorne, C., Ferdek, P., Pozzan, T., Tepikin, A., Petersen, O., Sutton, R., Watson, A., Gerasimenko, O., 2009. Calcium elevation in mitochondria is the main Ca2+ requirement for mitochondrial permeability transition pore (mPTP) opening. J. Biol. Chem. 284, 20796–20803.

Ben Gedalya, T., Loeb, V., Israeli, E., Altschuler, Y., Selkoe, D.J., Sharon, R., 2009. α-Synuclein and Polyunsaturated Fatty Acids Promote Clathrin-Mediated Endocytosis and Synaptic Vesicle Recycling 10, 218–234.

Bendor, J.T., Logan, T.P., Edwards, R.H., 2013. The function of α-synuclein. Neuron 79, 1044–1066.

Berliocchi, L., Bano, D., Nicotera, P., 2005. Ca2+ signals and death programmes in neurons. Philos. Trans. R. Soc. Lond., B, Biol. Sci. 360, 2255–2258.

Bernheimer, H., Birkmayer, W., Hornykiewicz, O., Jellinger, K., Seitelberger, F., 1973. Brain dopamine and the syndromes of Parkinson and Huntington. Clinical, morphological and neurochemical correlations. J. Neurol. Sci. 20, 415–455.

Betarbet, R., Sherer, T.B., Greenamyre, J.T., 2002. Animal models of Parkinson's disease. Bioessays 24, 308–318.

Breydo, L., Wu, J.W., Uversky, V.N., 2012. A-synuclein misfolding and Parkinson's disease. Biochim. Biophys. Acta 1822, 261–285.

Burré, J., Sharma, M., Tsetsenis, T., Buchman, V., Etherton, M.R., Südhof, T.C., 2010. Alpha-synuclein promotes SNARE-complex assembly in vivo and in vitro. Science 329, 1663–1667.

Burré, J., Vivona, S., Diao, J., Sharma, M., Brunger, A.T., Südhof, T.C., 2013. Properties of native brain α-synuclein. Nature 498, E4–6– discussion E6–7.

Büttner, S., Habernig, L., Broeskamp, F., Ruli, D., Vögtle, F.N., Vlachos, M., Macchi, F., Küttner, V., Carmona-Gutierrez, D., Eisenberg, T., Ring, J., Markaki, M., Taskin, A.A., Benke, S., Ruckenstuhl, C., Braun, R., Van den Haute, C., Bammens, T., van der Perren, A., Fröhlich, K.-U., Winderickx, J., Kroemer, G., Baekelandt, V., Tavernarakis, N., Kovacs, G.G., Dengjel, J., Meisinger, C., Sigrist, S.J., Madeo, F., 2013. Endonuclease G mediates α-synuclein cytotoxicity during Parkinson's disease. EMBO J 32, 3041–3054.

Chan, C.S., Guzman, J.N., Ilijic, E., Mercer, J.N., Rick, C., Tkatch, T., Meredith, G.E., Surmeier, D.J., 2007. 'Rejuvenation‘ protects neurons in mouse models of Parkinson’s disease. Nature 447, 1081–1086.

Chandra, S., Gallardo, G., Fernández-Chacón, R., Schlüter, O.M., Südhof, T.C., 2005. Alpha-synuclein cooperates with CSPalpha in preventing neurodegeneration. Cell 123, 383–396.

Chartier-Harlin, M.-C., Kachergus, J., Roumier, C., Mouroux, V., Douay, X., Lincoln, S., Levecque, C., Larvor, L., Andrieux, J., Hulihan, M., Waucquier, N., Defebvre, L., Amouyel, P., Farrer, M., Destée, A., 2004. Alpha-synuclein locus duplication as a cause of familial Parkinson's disease. Lancet 364, 1167–1169.

Chen, L., Feany, M.B., 2005. Alpha-synuclein phosphorylation controls neurotoxicity and inclusion formation in a Drosophila model of Parkinson disease. Nat. Neurosci. 8, 657–663.

Chen, L., Periquet, M., Wang, X., Negro, A., McLean, P.J., Hyman, B.T., Feany, M.B., 2009. Tyrosine and serine phosphorylation of alpha-synuclein have opposing effects on neurotoxicity and soluble oligomer formation. J. Clin. Invest. 119, 3257–3265.

Chinta, S.J., Mallajosyula, J.K., Rane, A., Andersen, J.K., 2010. Mitochondrial α-synuclein accumulation impairs complex I function in dopaminergic neurons and results in increased mitophagy in vivo. Neurosci. Lett. 486, 235–239.

Cole, N.B., DiEuliis, D., Leo, P., Mitchell, D.C., Nussbaum, R.L., 2008. Mitochondrial translocation of α-synuclein is promoted by intracellular acidification. Experimental Cell Research 314, 2076–2089.

Conway, K.A., Lee, S.J., Rochet, J.C., Ding, T.T., Williamson, R.E., Lansbury, P.T., 2000. Acceleration of oligomerization, not fibrillization, is a shared property of both alpha-synuclein mutations linked to early-onset Parkinson's disease: implications for pathogenesis and therapy. Proc. Natl. Acad. Sci. U.S.A. 97, 571–576.

Culvenor, J.G., McLean, C.A., Cutt, S., Campbell, B.C., Maher, F., Jäkälä, P., Hartmann, T., Beyreuther, K., Masters, C.L., Li, Q.X., 1999. Non-Abeta component of Alzheimer's disease amyloid (NAC) revisited. NAC and alpha-synuclein are not associated with Abeta amyloid. Am. J. Pathol. 155, 1173–1181.

Danzer, K.M., Haasen, D., Karow, A.R., Moussaud, S., Habeck, M., Giese, A., Kretzschmar, H., Hengerer, B., Kostka, M., 2007. Different Species of α-Synuclein Oligomers Induce Calcium Influx and Seeding. J Neuroscience. 27, 9220–9232.

Dauer, W., Przedborski, S., 2003. Parkinson's disease: mechanisms and models. Neuron 39, 889–909.

Daum, G., 1985. Lipids of mitochondria. Biochim. Biophys. Acta 822, 1–42.

Davidson, W.S., Jonas, A., Clayton, D.F., George, J.M., 1998. Stabilization of alpha-synuclein secondary structure upon binding to synthetic membranes. J. Biol. Chem. 273, 9443–9449.

Dawson, T.M., Dawson, V.L., 2003. Molecular pathways of neurodegeneration in Parkinson's disease. Science 302, 819–822.

Dettmer, U., Newman, A.J., Luth, E.S., Bartels, T., Selkoe, D., 2013. In vivo cross-linking reveals principally oligomeric forms of α-synuclein and β-synuclein in neurons and non-neural cells. J. Biol. Chem. 288, 6371–6385.

Devi, L., Raghavendran, V., Prabhu, B.M., Avadhani, N.G., Anandatheerthavarada, H.K., 2008. Mitochondrial import and accumulation of alpha-synuclein impair complex I in human dopaminergic neuronal cultures and Parkinson disease brain. Journal of Biological Chemistry 283, 9089–9100.

DeWitt, D.C., Rhoades, E., 2013. α-Synuclein Can Inhibit SNARE-Mediated Vesicle Fusion through Direct Interactions with Lipid Bilayers. Biochemistry 52, 2385–2387.

Ehringer, H., Hornykiewicz, O., 1960. [Distribution of noradrenaline and dopamine (3-hydroxytyramine) in the human brain and their behavior in diseases of the extrapyramidal system]. Klin. Wochenschr. 38, 1236–1239.

Fahn, S., Parkinson Study Group, 2005. Does levodopa slow or hasten the rate of progression of Parkinson's disease? J. Neurol. 252 Suppl 4, IV37–IV42.

Fauvet, B., Mbefo, M.K., Fares, M.-B., Desobry, C., Michael, S., Ardah, M.T., Tsika, E., Coune, P., Prudent, M., Lion, N., Eliezer, D., Moore, D.J., Schneider, B., Aebischer, P., El-Agnaf, O.M., Masliah, E., Lashuel, H.A., 2012. α-Synuclein in central nervous system and from erythrocytes, mammalian cells, and Escherichia coli exists predominantly as disordered monomer. J. Biol. Chem. 287, 15345–15364.

George, J.M., 2002. The synucleins. Genome Biol. 3, REVIEWS3002.

George, J.M., Jin, H., Woods, W.S., Clayton, D.F., 1995. Characterization of a novel protein regulated during the critical period for song learning in the zebra finch. Neuron 15, 361–372.

Giasson, B.I., Murray, I.V., Trojanowski, J.Q., Lee, V.M., 2001. A hydrophobic stretch of 12 amino acid residues in the middle of alpha-synuclein is essential for filament assembly. J. Biol. Chem. 276, 2380–2386.

Goldberg, J.A., Guzman, J.N., Estep, C.M., Ilijic, E., Kondapalli, J., Sanchez-Padilla, J., Surmeier, D.J., 2012. Calcium entry induces mitochondrial oxidant stress in vagal neurons at risk in Parkinson's disease. Nat. Neurosci. 15, 1414–1421.

Greenamyre, J.T., Hastings, T.G., 2004. Biomedicine. Parkinson's--divergent causes, convergent mechanisms. Science 304, 1120–1122.

Guzman, J.N., Sanchez-Padilla, J., Wokosin, D., Kondapalli, J., Ilijic, E., Schumacker, P.T., Surmeier, D.J., 2010. Oxidant stress evoked by pacemaking in dopaminergic neurons is attenuated by DJ-1 1–7.

Haass, C., Selkoe, D.J., 2007. Soluble protein oligomers in neurodegeneration: lessons from the Alzheimer's amyloid beta-peptide. Nat. Rev. Mol. Cell Biol. 8, 101–112.

Halestrap, A.P., Brenner, C., 2003. The adenine nucleotide translocase: a central component of the mitochondrial permeability transition pore and key player in cell death. Curr. Med. Chem. 10, 1507–1525.

Hsu, L.J., Sagara, Y., Arroyo, A., Rockenstein, E., Sisk, A., Mallory, M., Wong, J., Takenouchi, T., Hashimoto, M., Masliah, E., 2000. alpha-synuclein promotes mitochondrial deficit and oxidative stress. Am. J. Pathol. 157, 401–410.

Iacopino, A.M., Christakos, S., 1990. Specific reduction of calcium-binding protein (28-kilodalton calbindin-D) gene expression in aging and neurodegenerative diseases. Proc. Natl. Acad. Sci. U.S.A. 87, 4078–4082.

Iwai, A., Masliah, E., Yoshimoto, M., Ge, N., Flanagan, L., de Silva, H.A., Kittel, A., Saitoh, T., 1995. The precursor protein of non-A beta component of Alzheimer's disease amyloid is a presynaptic protein of the central nervous system. Neuron 14, 467–475.

Jenco, J.M., Rawlingson, A., Daniels, B., Morris, A.J., 1998. Regulation of phospholipase D2: selective inhibition of mammalian phospholipase D isoenzymes by alpha- and beta-synucleins. Biochemistry 37, 4901–4909.

Jensen, M.B., Bhatia, V.K., Jao, C.C., Rasmussen, J.E., Pedersen, S.L., Jensen, K.J., Langen, R., Stamou, D., 2011. Membrane curvature sensing by amphipathic helices: a single liposome study using α-synuclein and annexin B12. J. Biol. Chem. 286, 42603–42614.

Kahle, P.J., Neumann, M., Ozmen, L., Muller, V., Jacobsen, H., Schindzielorz, A., Okochi, M., Leimer, U., van Der Putten, H., Probst, A., Kremmer, E., Kretzschmar, H.A., Haass, C., 2000. Subcellular localization of wild-type and Parkinson's disease-associated mutant alpha -synuclein in human and transgenic mouse brain. J. Neurosci. 20, 6365–6373.

Kamp, F., Exner, N., Lutz, A.K., Wender, N., Hegermann, J., Brunner, B., Nuscher, B., Bartels, T., Giese, A., Beyer, K., Eimer, S., Winklhofer, K.F., Haass, C., 2010. Inhibition of mitochondrial fusion by α-synuclein is rescued by PINK1, Parkin and DJ-1. EMBO J 29, 3571–3589.

Kara, E., Lewis, P.A., Ling, H., Proukakis, C., Houlden, H., Hardy, J., 2013. α-Synuclein mutations cluster around a putative protein loop. Neurosci. Lett. 546, 67–70.

Karpinar, D.P., Balija, M.B.G., Kügler, S., Opazo, F., Rezaei-Ghaleh, N., Wender, N., Kim, H.-Y., Taschenberger, G., Falkenburger, B.H., Heise, H., Kumar, A., Riedel, D., Fichtner, L., Voigt, A., Braus, G.H., Giller, K., Becker, S., Herzig, A., Baldus, M., Jäckle, H., Eimer, S., Schulz, J.B., Griesinger, C., Zweckstetter, M., 2009. Pre-fibrillar alpha-synuclein variants with impaired beta-structure increase neurotoxicity in Parkinson's disease models. EMBO J 28, 3256–3268.

Katsuse, O., Iseki, E., Marui, W., Kosaka, K., 2003. Developmental stages of cortical Lewy bodies and their relation to axonal transport blockage in brains of patients with dementia with Lewy bodies. J. Neurol. Sci. 211, 29–35.

Keeney, P.M., Xie, J., Capaldi, R.A., Bennett, J.P., 2006. Parkinson's disease brain mitochondrial complex I has oxidatively damaged subunits and is functionally impaired and misassembled. Journal of Neuroscience 26, 5256–5264.

Kim, B.G., Shin, D.H., Jeon, G.S., Seo, J.H., Kim, Y.W., Jeon, B.S., Cho, S.S., 2000. Relative sparing of calretinin containing neurons in the substantia nigra of 6-OHDA treated rat parkinsonian model. Brain Research 855, 162–165.

Kim, J., 1997. Evidence that the precursor protein of non-A beta component of Alzheimer's disease amyloid (NACP) has an extended structure primarily composed of random-coil. Mol. Cells 7, 78–83.

Klucken, J., Outeiro, T.F., Nguyen, P., McLean, P.J., Hyman, B.T., 2006. Detection of novel intracellular alpha-synuclein oligomeric species by fluorescence lifetime imaging. The FASEB Journal 20, 2050–2057.

Knopman, D.S., Parisi, J.E., Salviati, A., Floriach-Robert, M., Boeve, B.F., Ivnik, R.J., Smith, G.E., Dickson, D.W., Johnson, K.A., Petersen, L.E., McDonald, W.C., Braak, H., Petersen, R.C., 2003. Neuropathology of cognitively normal elderly. J. Neuropathol. Exp. Neurol. 62, 1087–1095.

Koopman, W.J.H., Nijtmans, L.G.J., Dieteren, C.E.J., Roestenberg, P., Valsecchi, F., Smeitink, J.A.M., Willems, P.H.G.M., 2010. Mammalian mitochondrial complex I: biogenesis, regulation, and reactive oxygen species generation. Antioxid. Redox Signal. 12, 1431–1470.

Kowal, S.L., Dall, T.M., Chakrabarti, R., Storm, M.V., Jain, A., 2013. The current and projected economic burden of Parkinson's disease in the United States. Mov Disord. 28, 311–318.

Langston, J.W., Ballard, P., Tetrud, J.W., Irwin, I., 1983. Chronic Parkinsonism in humans due to a product of meperidine-analog synthesis. Science 219, 979–980.

Langston, J.W., Irwin, I., Langston, E.B., Forno, L.S., 1984. 1-Methyl-4-phenylpyridinium ion (MPP+): identification of a metabolite of MPTP, a toxin selective to the substantia nigra. Neuroscience Letters 48, 87–92.

Larsen, K.E., Schmitz, Y., Troyer, M.D., Mosharov, E., Dietrich, P., Quazi, A.Z., Savalle, M., Nemani, V., Chaudhry, F.A., Edwards, R.H., Stefanis, L., Sulzer, D., 2006. Alpha-synuclein overexpression in PC12 and chromaffin cells impairs catecholamine release by interfering with a late step in exocytosis. Journal of Neuroscience 26, 11915–11922.

Lavedan, C., 1998. The synuclein family. Genome Res. 8, 871–880.

Lee, I., Bender, E., Arnold, S., Kadenbach, B., 2001. New control of mitochondrial membrane potential and ROS formation--a hypothesis. Biol. Chem. 382, 1629–1636.

Lesage, S., Anheim, M., Letournel, F., Bousset, L., Honoré, A., Rozas, N., Pieri, L., Madiona, K., Dürr, A., Melki, R., Verny, C., Brice, A., for the French Parkinson's Disease Genetics (PDG) Study Group, 2013. G51D α-synuclein mutation causes a novel parkinsonian-pyramidal syndrome. Ann. Neurol. 73, 459–471.

Li, L., Nadanaciva, S., Berger, Z., Shen, W., Paumier, K., Schwartz, J., Mou, K., Loos, P., Milici, A.J., Dunlop, J., Hirst, W.D., 2013. Human A53T α-synuclein causes reversible deficits in mitochondrial function and dynamics in primary mouse cortical neurons. PLoS ONE 8, e85815.

Liu, G., Zhang, C., Yin, J., Li, X., Cheng, F., Li, Y., Yang, H., Uéda, K., Chan, P., Yu, S., 2009. α-Synuclein is differentially expressed in mitochondria from different rat brain regions and dose-dependently down-regulates complex I activity. Neurosci. Lett. 454, 187–192.

Maltsev, A.S., Ying, J., Bax, A., 2012. Impact of N-Terminal Acetylation of α-Synuclein on Its Random Coil and Lipid Binding Properties. Biochemistry 51, 5004–5013.

Maroteaux, L., Campanelli, J.T., Scheller, R.H., 1988. Synuclein: a neuron-specific protein localized to the nucleus and presynaptic nerve terminal. J. Neurosci. 8, 2804–2815.

Martin, L.J., Pan, Y., Price, A.C., Sterling, W., Copeland, N.G., Jenkins, N.A., Price, D.L., Lee, M.K., 2006. Parkinson's disease alpha-synuclein transgenic mice develop neuronal mitochondrial degeneration and cell death. Journal of Neuroscience 26, 41–50.

Martin, L.J., Semenkow, S., Hanaford, A., Wong, M., 2013. The mitochondrial permeability transition pore regulates Parkinson's disease development in mutant α-synuclein transgenic mice. Neurobiol. Aging 10.1016–j.neurobiolaging.2013.11.008.

Martinez, Z., Zhu, M., Han, S., Fink, A.L., 2007. GM1 specifically interacts with alpha-synuclein and inhibits fibrillation. Biochemistry 46, 1868–1877.

McCarthy, A., McKinley, J., Lynch, T., 2012. The inherent susceptibility of dorsal motor

nucleus cholinergic neurons to the neurodegenerative process in Parkinson's Disease. Front Neurol 3, 189.

McLean, P.J., Ribich, S., Hyman, B.T., 2000. Subcellular localization of alpha-synuclein in primary neuronal cultures: effect of missense mutations. J. Neural Transm. Suppl. 53–63.

Middleton, E.R., Rhoades, E., 2010. Effects of curvature and composition on α-synuclein binding to lipid vesicles. Biophys. J. 99, 2279–2288.

Mitchell, P., 1961. Coupling of phosphorylation to electron and hydrogen transfer by a chemi-osmotic type of mechanism. Nature 191, 144–148.

Mouatt-Prigent, A., Agid, Y., Hirsch, E.C., 1994. Does the calcium binding protein calretinin protect dopaminergic neurons against degeneration in Parkinson's disease? Brain Research 668, 62–70.

Nakamura, K., Nemani, V.M., Azarbal, F., Skibinski, G., Levy, J.M., Egami, K., Munishkina, L., Zhang, J., Gardner, B., Wakabayashi, J., Sesaki, H., Cheng, Y., Finkbeiner, S., Nussbaum, R.L., Masliah, E., Edwards, R.H., 2011. Direct membrane association drives mitochondrial fission by the Parkinson disease-associated protein alpha-synuclein. J. Biol. Chem. 286, 20710–20726.

Nakamura, K., Nemani, V.M., Wallender, E.K., Kaehlcke, K., Ott, M., Edwards, R.H., 2008. Optical reporters for the conformation of alpha-synuclein reveal a specific interaction with mitochondria. Journal of Neuroscience 28, 12305–12317.

Narendra, D., Walker, J.E., Youle, R., 2012. Mitochondrial quality control mediated by PINK1 and Parkin: links to parkinsonism. Cold Spring Harb Perspect Biol 4, a011338–a011338.

Näsström, T., Fagerqvist, T., Barbu, M., Karlsson, M., Nikolajeff, F., Kasrayan, A., Ekberg, M., Lannfelt, L., Ingelsson, M., Bergström, J., 2011. The lipid peroxidation products 4-oxo-2-nonenal and 4-hydroxy-2-nonenal promote the formation of α-synuclein oligomers with distinct biochemical, morphological, and functional properties. Free Radical Biology and Medicine 50, 428–437.

Nemani, V.M., Lu, W., Berge, V., Nakamura, K., Onoa, B., Lee, M.K., Chaudhry, F.A., Nicoll, R.A., Edwards, R.H., 2010. Increased expression of alpha-synuclein reduces

neurotransmitter release by inhibiting synaptic vesicle reclustering after endocytosis. Neuron 65, 66–79.

Nishimura, M., Tomimoto, H., Suenaga, T., Nakamura, S., Namba, Y., Ikeda, K., Akiguchi, I., Kimura, J., 1994. Synaptophysin and chromogranin A immunoreactivities of Lewy bodies in Parkinson's disease brains. Brain Research 634, 339–344.

Norenberg, M.D., Rao, K.V.R., 2007. The mitochondrial permeability transition in neurologic disease. Neurochem. Int. 50, 983–997.

Ohrfelt, A., Zetterberg, H., Andersson, K., Persson, R., Secic, D., Brinkmalm, G., Wallin, A., Mulugeta, E., Francis, P.T., Vanmechelen, E., Aarsland, D., Ballard, C., Blennow, K., Westman-Brinkmalm, A., 2011. Identification of novel α-synuclein isoforms in human brain tissue by using an online nanoLC-ESI-FTICR-MS method. Neurochem. Res. 36, 2029–2042.

Olanow, C.W., Schapira, A.H.V., 2013. Therapeutic prospects for Parkinson disease. Ann. Neurol. 74, 337–347.

Parihar, M.S., Parihar, A., Fujita, M., Hashimoto, M., Ghafourifar, P., 2008. Mitochondrial association of alpha-synuclein causes oxidative stress. Cell. Mol. Life Sci. 65, 1272–1284.

Parihar, M.S., Parihar, A., Fujita, M., Hashimoto, M., Ghafourifar, P., 2009. Alpha-synuclein overexpression and aggregation exacerbates impairment of mitochondrial functions by augmenting oxidative stress in human neuroblastoma cells. International Journal of Biochemistry and Cell Biology 41, 2015–2024.

Parker, W.D., Parks, J.K., Swerdlow, R.H., 2008. Complex I deficiency in Parkinson's disease frontal cortex. Brain Research 1189, 215–218.

Petit, P.X., Goubern, M., Diolez, P., Susin, S.A., Zamzami, N., Kroemer, G., 1998. Disruption of the outer mitochondrial membrane as a result of large amplitude swelling: the impact of irreversible permeability transition. FEBS Letters 426, 111–116.

Rappley, I., Gitler, A.D., Selvy, P.E., LaVoie, M.J., Levy, B.D., Brown, H.A., Lindquist, S., Selkoe, D.J., 2009. Evidence that alpha-synuclein does not inhibit phospholipase D. Biochemistry 48, 1077–1083.

Reeve, A.K., Krishnan, K.J., Turnbull, D., 2008. Mitochondrial DNA mutations in disease, aging, and neurodegeneration. Ann. N. Y. Acad. Sci. 1147, 21–29.

Reeve, A.K., Park, T.-K., Jaros, E., Campbell, G.R., Lax, N.Z., Hepplewhite, P.D., Krishnan, K.J., Elson, J.L., Morris, C.M., McKeith, I.G., Turnbull, D.M., 2012. Relationship between mitochondria and α-synuclein: a study of single substantia nigra neurons. Arch. Neurol. 69, 385–393.

Rhinn, H., Qiang, L., Yamashita, T., Rhee, D., Zolin, A., Vanti, W., Abeliovich, A., 2012. Alternative α-synuclein transcript usage as a convergent mechanism in Parkinson's disease pathology. Nature Communications 3, 1084.

Riederer, P., Wuketich, S., 1976. Time course of nigrostriatal degeneration in parkinson's disease. A detailed study of influential factors in human brain amine analysis. J. Neural Transm. 38, 277–301.

Rigoulet, M., Yoboue, E.D., Devin, A., 2011. Mitochondrial ROS generation and its regulation: mechanisms involved in H(2)O(2) signaling. Antioxid. Redox Signal. 14, 459–468.

Roy, S., 2009. The paradoxical cell biology of alpha-Synuclein. Results Probl Cell Differ 48, 159–172.

Sarafian, T.A., Ryan, C.M., Souda, P., Masliah, E., Kar, U.K., Vinters, H.V., Mathern, G.W., Faull, K.F., Whitelegge, J.P., Watson, J.B., 2013. Impairment of mitochondria in adult mouse brain overexpressing predominantly full-length, N-terminally acetylated human α-synuclein. PLoS ONE 8, e63557.

Schapira, A.H., Mann, V.M., Cooper, J.M., Dexter, D., Daniel, S.E., Jenner, P., Clark, J.B., Marsden, C.D., 1990. Anatomic and disease specificity of NADH CoQ1 reductase (complex I) deficiency in Parkinson's disease. Journal of Neurochemistry 55, 2142–2145.

Shulman, J.M., De Jager, P.L., Feany, M.B., 2011. Parkinson's disease: genetics and pathogenesis. Annu Rev Pathol 6, 193–222.

Singleton, A.B., Farrer, M., Johnson, J., Singleton, A., Hague, S., Kachergus, J., Hulihan, M., Peuralinna, T., Dutra, A., Nussbaum, R., Lincoln, S., Crawley, A., Hanson, M., Maraganore, D., Adler, C., Cookson, M.R., Muenter, M., Baptista, M., Miller, D., Blancato, J., Hardy, J.,

Gwinn-Hardy, K., 2003. alpha-Synuclein locus triplication causes Parkinson's disease. Science 302, 841.

Smith, W.W., Jiang, H., Pei, Z., Tanaka, Y., Morita, H., Sawa, A., Dawson, V.L., Dawson, T.M., Ross, C.A., 2005. Endoplasmic reticulum stress and mitochondrial cell death pathways mediate A53T mutant alpha-synuclein-induced toxicity. Human Molecular Genetics 14, 3801–3811.

Spillantini, M.G., Schmidt, M.L., Lee, V.M., Trojanowski, J.Q., Jakes, R., Goedert, M., 1997. Alpha-synuclein in Lewy bodies. Nature 388, 839–840.

Stichel, C.C., Zhu, X.-R., Bader, V., Linnartz, B., Schmidt, S., Lübbert, H., 2007. Mono- and double-mutant mouse models of Parkinson's disease display severe mitochondrial damage. Human Molecular Genetics 16, 2377–2393.

Stout, A.K., Raphael, H.M., Kanterewicz, B.I., Klann, E., Reynolds, I.J., 1998. Glutamate-induced neuron death requires mitochondrial calcium uptake. Nat. Neurosci. 1, 366–373.

Surmeier, D.J., Schumacker, P.T., 2013. Calcium, Bioenergetics, and Neuronal Vulnerability in Parkinson's Disease 288, 10736–10741.

Szabadkai, G., Duchen, M.R., 2008. Mitochondria: the hub of cellular Ca2+ signaling. Physiology (Bethesda) 23, 84–94.

Tanaka, M., Kim, Y.M., Lee, G., Junn, E., Iwatsubo, T., Mouradian, M.M., 2004. Aggresomes formed by alpha-synuclein and synphilin-1 are cytoprotective. J. Biol. Chem. 279, 4625–4631.

Tofaris, G.K., Tofaris, G.K., Spillantini, M.G., Spillantini, M.G., 2005. Alpha-synuclein dysfunction in Lewy body diseases. Mov. Disord. 20 Suppl 12, S37–44.

Tompkins, M.M., Hill, W.D., 1997. Contribution of somal Lewy bodies to neuronal death. Brain Research 775, 24–29.

Trexler, A.J., Rhoades, E., 2012. N-Terminal acetylation is critical for forming α-helical oligomer of α-synuclein. Protein Sci. 21, 601–605.

Uéda, K., Fukushima, H., Masliah, E., Xia, Y., Iwai, A., Yoshimoto, M., Otero, D.A., Kondo, J., Ihara, Y., Saitoh, T., 1993. Molecular cloning of cDNA encoding an unrecognized component of amyloid in Alzheimer disease. Proc. Natl. Acad. Sci. U.S.A. 90, 11282–11286.

Vamvaca, K., Volles, M.J., Lansbury, P.T., Jr., 2009. The First N-terminal Amino Acids of α-Synuclein Are Essential for α-Helical Structure Formation In Vitro and Membrane Binding in Yeast. J. Mol. Biol. 389, 413–424.

Van Den Eeden, S.K., Tanner, C.M., Bernstein, A.L., Fross, R.D., Leimpeter, A., Bloch, D.A., Nelson, L.M., 2003. Incidence of Parkinson's disease: variation by age, gender, and race/ethnicity. Am. J. Epidemiol. 157, 1015–1022.

Varkey, J., Isas, J.M., Mizuno, N., Jensen, M.B., Bhatia, V.K., Jao, C.C., Petrlova, J., Voss, J.C., Stamou, D.G., Steven, A.C., Langen, R., 2010. Membrane curvature induction and tubulation are common features of synucleins and apolipoproteins. J. Biol. Chem. 285, 32486–32493.

Volles, M.J., Lansbury, P.T., 2003. Zeroing in on the pathogenic form of alpha-synuclein and its mechanism of neurotoxicity in Parkinson's disease. Biochemistry 42, 7871–7878.

Volles, M.J., Lee, S.J., Rochet, J.C., Shtilerman, M.D., Ding, T.T., Kessler, J.C., Lansbury, P.T., 2001. Vesicle permeabilization by protofibrillar alpha-synuclein: implications for the pathogenesis and treatment of Parkinson's disease. Biochemistry 40, 7812–7819.

Wang, W., Perovic, I., Chittuluru, J., Kaganovich, A., Nguyen, L.T.T., Liao, J., Auclair, J.R., Johnson, D., Landeru, A., Simorellis, A.K., Ju, S., Cookson, M.R., Asturias, F.J., Agar, J.N., Webb, B.N., Kang, C., Ringe, D., Petsko, G.A., Pochapsky, T.C., Hoang, Q.Q., 2011. A soluble α-synuclein construct forms a dynamic tetramer. Proceedings of the National Academy of Sciences 108, 17797–17802.

Weinreb, P.H., Zhen, W., Poon, A.W., Conway, K.A., Lansbury, P.T., 1996. NACP, a protein implicated in Alzheimer's disease and learning, is natively unfolded. Biochemistry 35, 13709–13715.

Westphal, C.H., Chandra, S.S., 2013. Monomeric synucleins generate membrane curvature. J.

Biol. Chem. 288, 1829–1840.

Winner, B., Jappelli, R., Maji, S.K., Desplats, P.A., Boyer, L., Aigner, S., Hetzer, C., Loher, T., Vilar, M., Campioni, S., Tzitzilonis, C., Soragni, A., Jessberger, S., Mira, H., Consiglio, A., Pham, E., Masliah, E., Gage, F.H., Riek, R., 2011. In vivo demonstration that alpha-synuclein oligomers are toxic. Proceedings of the National Academy of Sciences 108, 4194–4199.

Wojda, U., Salinska, E., Kuznicki, J., 2008. Calcium ions in neuronal degeneration. IUBMB Life 60, 575–590.

Yamada, T., McGeer, P.L., Baimbridge, K.G., McGeer, E.G., 1990. Relative sparing in Parkinson's disease of substantia nigra dopamine neurons containing calbindin-D28K. Brain Research 526, 303–307.

Zarranz, J.J., Alegre, J., Gómez-Esteban, J.C., Lezcano, E., Ros, R., Ampuero, I., Vidal, L., Hoenicka, J., Rodriguez, O., Atarés, B., Llorens, V., Gomez Tortosa, E., del Ser, T., Muñoz, D.G., de Yebenes, J.G., 2004. The new mutation, E46K, of alpha-synuclein causes Parkinson and Lewy body dementia. Ann Neurol. 55, 164–173.

Zhang, L., Zhang, C., Zhu, Y., Cai, Q., Chan, P., Uéda, K., Yu, S., Yang, H., 2008. Semi-quantitative analysis of. Brain Research 1244, 40–52.

Chapter 2

Soluble, Prefibrillar α-Synuclein Oligomers Promote Complex I-Dependent, Ca^{2+}-Induced Mitochondrial Dysfunction

Contributions:

Experiments were designed by Eric Luth, Irina Stavrovskaya, and Dennis Selkoe. Measurements of mitochondrial parameters were performed by Eric Luth and Irina Stavrovskaya. Tim Bartels assisted Eric Luth with biophysical analysis of αSyn. All other experiments were performed by Eric Luth.

Abstract

α-Synuclein (αSyn) aggregation and mitochondrial dysfunction both contribute to the pathogenesis of Parkinson's disease (PD). While recent studies have suggested that mitochondrial association of αSyn may disrupt mitochondrial function, it is unclear what aggregation state of αSyn is most damaging to mitochondria and what conditions promote or inhibit the effect of toxic αSyn species. Since the neuronal populations most vulnerable in PD are characterized by large cytosolic Ca^{2+} oscillations that burden mitochondria, we examined mitochondrial Ca^{2+} stress in an *in vitro* system comprising isolated mitochondria and purified recombinant human αSyn in various aggregation states. Using fluorimetry to simultaneously measure 4 mitochondrial parameters, we observed that soluble, prefibrillar αSyn oligomers, but not monomeric or fibrillar αSyn, decreased the retention time of exogenously added Ca^{2+}, promoted Ca^{2+}-induced mitochondrial swelling and depolarization, and accelerated cytochrome c release. Inhibition of the permeability transition pore rescued these αSyn-induced changes in mitochondrial parameters. Interestingly, the mitotoxic effects of αSyn were specifically dependent upon both electron flow through complex I and mitochondrial uptake of exogenous Ca^{2+}. Our results suggest that soluble prefibrillar αSyn oligomers recapitulate several mitochondrial phenotypes previously observed in animal and cell models of PD: complex I-mediated dysfunction, altered membrane potential, disrupted Ca^{2+} homeostasis, and enhanced cytochrome c release. These data reveal how the association of oligomeric αSyn with mitochondria can be detrimental to the function of cells with high Ca^{2+}-handling requirements.

Introduction

Parkinson's disease (PD), the second most common neurodegenerative disease, is characterized by the conversion of the normally soluble cytoplasmic protein α-Synuclein (αSyn) into insoluble amyloid fibrils that accumulate as cytoplasmic aggregates termed Lewy bodies and Lewy neurites (Spillantini et al., 1997). Duplication or triplication of the wild-type αSyn locus causes gene dose-dependent early onset PD (Chartier-Harlin et al., 2004; Singleton et al., 2003), and 5 pathogenic missense mutations have been reported to cause autosomal dominant PD (Kara et al., 2013). Moreover, 3'UTR variants and other single nucleotide polymorphisms in the *SNCA* gene that lead to increased αSyn expression are found in a subset of cases of sporadic PD (Kim, 2013). In addition, mutations in glucocerebrosidase (*GBA1*), the most common genetic risk factor for PD, can elevate αSyn protein levels, perhaps via reduced lysosomal degradation (Cullen et al., 2011). Thus, impaired proteostasis of αSyn is likely a key step in the pathogenesis of PD and related human synucleinopathies.

A growing body of evidence suggests that αSyn normally exits in an equilibrium between partially helical tetramers and unfolded monomers (Bartels et al., 2011; Dettmer et al., 2013; Wang et al., 2011; Westphal and Chandra, 2013). Helical, oligomeric αSyn is aggregation-resistant *in vitro* (Bartels et al., 2011) while the unfolded monomer readily aggregates into insoluble, β-sheet-rich amyloid-type fibrils through soluble oligomeric intermediates (Conway et al., 2000). Recent studies indicate that these abnormal soluble oligomers, in contrast to the fibrillar end products, are neurotoxic *in vitro* and in disease models (Danzer et al., 2007; Karpinar et al., 2009; Volles and Lansbury, 2003; Winner et al., 2011). The pathological mechanisms of these toxic oligomeric intermediates and the basis for the selective vulnerability of certain brain regions to their effects have not been determined.

Many observations suggest that mitochondrial dysfunction is associated with PD. Toxins targeting complex I of the electron transport chain (ETC) can cause parkinsonism in humans and animal models (Betarbet et al., 2000; Burns et al., 1983; Langston and Ballard, 1983), and postmortem brain tissue of PD patients shows deficits in mitochondrial complex I activity (Janetzky et al., 1994; Parker et al., 1989; Schapira et al., 1989). Markers of mitochondrial oxidative stress, including oxidized complex I subunits (Keeney et al., 2006) and mtDNA mutations (Bender et al., 2006), are also elevated in PD patients, though it is unclear whether these are a cause or consequence of ETC dysfunction. The neuronal populations most impaired in PD, including the substantia nigra pars compacta, locus ceruleus, and dorsal motor nucleus of the vagus, share an unusual physiological phenotype: they consist primarily of broad-spike pacemaking neurons with high transmembrane Ca^{2+} currents and low Ca^{2+} buffering capacities (Surmeier and Schumacker, 2013). This combination places a great metabolic burden on mitochondria to continually re-establish the resting cytosolic Ca^{2+} concentration. Mitochondria-targeted, redox-sensitive GFP reveals a more oxidative mitochondrial environment in these neurons relative to those of regions less affected in PD (Goldberg et al., 2012; Guzman et al., 2010). The basal level of oxidant stress in the mitochondria of vulnerable neurons may put them at risk of dysfunction caused by an additional stressor.

Recent evidence suggests increased association of αSyn with mitochondria in PD patients and animal models (Büttner et al., 2013; Devi et al., 2008; Hsu et al., 2000; Martin et al., 2006; 2013; Rhinn et al., 2012; Stichel et al., 2007). An apparent partial subcellular redistribution of αSyn from the cytoplasm to the inner and outer mitochondrial membranes (Devi et al., 2008; G. Liu et al., 2009; Nakamura et al., 2011) is correlated with mitochondrial dysfunction, including increased oxidative stress, reduced mitochondrial membrane potential ($\Delta\Psi_m$), altered Ca^{2+}

homeostasis, and cytochrome c release (Büttner et al., 2013; Devi et al., 2008; Hsu et al., 2000; Martin et al., 2006; Parihar et al., 2008; Shavali et al., 2008; Stichel et al., 2007). Few studies have directly investigated the effect of different forms of αSyn on mitochondrial function. One reported that incubation of isolated mitochondria with aggregated αSyn can increase markers of oxidative stress, but the aggregation state (fibrillar or oligomeric) was not thoroughly characterized (Parihar et al., 2008). No previous studies have tested the role of mitochondrial Ca^{2+} stress or specific respiratory substrates on the ability of diverse αSyn species to induce mitochondrial dysfunction. It therefore remains unclear what form of αSyn is most damaging to mitochondrial function and which conditions promote or inhibit the effect of toxic αSyn species.

We sought to investigate the functional consequences of αSyn on Ca^{2+}-challenged mitochondria, with a particular focus on the αSyn aggregation state. We modeled mitochondrial Ca^{2+} stress in an *in vitro* system comprising isolated mitochondria and pure, recombinant, human αSyn at various aggregation states. Soluble, oligomeric αSyn aggregates generated by two independent methods, but not monomeric αSyn or mature fibrils, sensitized mitochondria to Ca^{2+}-induced dysfunction. The effects of oligomeric αSyn were observed only when mitochondria were respiring under complex I-dependent conditions and were challenged with exogenous Ca^{2+} addition. Our results demonstrate a specific effect of oligomeric αSyn on complex I-dependent function and reveal a mechanism by which the physical association of αSyn with mitochondria impairs their function.

Experimental Procedures

Purification and preparation of αSyn species

Purification:

Recombinant human αSyn was purified essentially as described (Weinreb et al., 1996). Briefly, *E. coli* transformed with human wildtype αSyn were grown to OD_{600} = 0.5-1, at which time isopropyl β-D-1-thiogalactopyranoside was added to 1 mM to induce αSyn expression. At OD_{600} = 1.5-1.8, bacteria were pelleted by centrifugation and boiled in anion exchange buffer (20 mM Tris, 25 mM NaCl, pH 8.0). Boiled bacterial lysate was purified sequentially by anion exchange chromatography (using 2 x 5 ml HiTrap Q HP columns, GE Healthcare) and size exclusion chromatography (using a Superdex 200 XK26/00 column, GE Healthcare). Protein not used immediately was lyophilized and stored at 4ºC. Lyophilized protein was reconstituted either in PBS or 10 mM ammonium acetate depending on the method used to prepare oligomers (see below).

Lag Phase preparation:

0.6 mg/ml recombinant αSyn in 10 mM ammonium acetate was incubated at 37°C with nutation. The aggregation state was monitored using Thioflavin T (ThT) fluorescence (see below). "Unaged" αSyn was sampled at time 0 (prior to 37°C incubation or nutation). αSyn aged 3 to 9 d without ThT fluorescence above background was considered "ThT^{neg}". αSyn that had plateaued in ThT fluorescence was considered "ThT^{pos}".

Sonicated preparation:

2 mg/ml recombinant αSyn in PBS was aggregated for 5 d at 37°C with nutation to form ThT^{pos} fibrils. To generate oligomers, αSyn fibrils were diluted to 1 mg/ml and sonicated at power level 50 for 5 x 10 strokes using a Sonic Dismembrator Model 300 (Fisher Scientific). Aliquots of the resultant material were frozen in liquid nitrogen and stored at -80°C. Fractions of

this material were prepared by serial differential centrifugation, first at 16,000 *g* for 5 min. The supernatant was transferred to a new tube and the pellet was resuspended in an equal volume of PBS. The 16,000 *g* supernatant was then spun at 100,000 *g* for 30 min at 4ºC. The supernatant was transferred to a new tube and the pellet was resuspended in an equal volume of PBS. The use of a programmable Ultrasonic Liquid Processor (Misonix) equipped with a microtip (settings: amplitude of 20, sonication for 1 s on and 1 s off for a total of 60 s) also produced αSyn oligomers with comparable bioactivity on mitochondria as those produced via our standard manual sonication technique. For both sonicated and lag phase preparations, concentrations of fibrillar and oligomeric αSyn listed are estimated based on the monomer concentration before aggregation as determined by A280 using a NanoDrop spectrophotometer (Thermo Scientific).

Electron microscopy:

αSyn fibrils, total sonicated αSyn, and 100,000 *g* soluble sonicated αSyn were each diluted 1:10 in PBS. 5 µl of these αSyn samples were adsorbed for 1 minute to a carbon coated grid that had been made hydrophilic by a 30 second exposure to a glow discharge. Excess liquid was removed with filter paper (Whatman) and the samples were stained with 0.75% uranyl formate for 30 seconds. After removing the excess uranyl formate with filter paper, the grids were examined using a TecnaiG² Spirit BioTWIN transmission electron microscope. Images were acquired with an AMT 2k CCD camera.

Dynamic light scattering:

Experiments were performed using a DynaPro (Wyatt Technology) instrument equipped with a 20°C temperature-controlled microsampler. αSyn samples in PBS were placed in a 1.5

mm path length quartz cuvette and light scattering was measured in 10 s intervals for 20 cycles. Data were analyzed using the Dynamic v.5 software.

Thioflavin T assays:

2.5 μM αSyn at various aggregation states (i.e. unaged/monomer, fibrils, sonicated oligomers and fractions thereof, and lag phase samples) was added in triplicate to 10 μM ThT in 10 mM glycine buffer, pH 9 to a total of 200 μl. Fluorescence at ex/em of 447/485 nm was measured in a black 96-well plate using the Synergy H1 Hybrid Reader (BioTek). Background fluorescence of buffer (PBS or 10 mM ammonium acetate) was subtracted from αSyn-containing samples. For aggregation seeding assays, 100 μl of 7-20 μM monomeric αSyn in PBS plus 1 mol% of αSyn "seeds" at various aggregation states and 10 μM ThT were added in triplicate to a black 96-well plate. Plates were incubated at 37°C under constant agitation at 300 RPM using a titer plate shaker (Lab Line Instruments). ThT fluorescence at ex/em of 447/485 nm was measured periodically as above.

Mitochondrial isolation:

All chemicals were purchased from Sigma-Aldrich unless stated otherwise. All procedures for animal use and euthanasia were approved by the institutional animal care and use committee. Liver mitochondria were isolated from ~11-13 weeks old mice by the standard differential centrifugation method in sucrose-based buffers as described previously (Baranov et al., 2008; Stavrovskaya et al., 2010) with some modifications. Briefly, the liver was homogenized in a buffer containing 240 mM sucrose, 10 mM K^+-HEPES, pH 7.4, 1 mM K^+-EGTA, and 0.5% fatty acid free bovine serum albumin (BSA), and centrifuged at 1,000 *g* for 10

min. The supernatant was then centrifuged for 8 min at 8,000 *g*. The resulting pellet was resuspended in the same buffer and centrifuged for 8 min at 8,000 *g*. The pellet from this spin was resuspended in 240 mM sucrose, 10mM K^+-HEPES, pH 7.4 and centrifuged again for 8 min at 8,000 *g*. The final mitochondrial pellet was resuspended in 0.2 ml of 240 mM sucrose, 10 mM K^+-HEPES, pH 7.4. All centrifugation steps were performed at 4ºC. Mitochondrial protein concentration was determined by the DC protein assay (BioRad) using BSA as a standard. The quality of isolated mitochondria was assessed by the respiratory control ratio (RCR), calculated as the ratio between the rates of respiration in state 3 (ADP-stimulated) and 4 (ADP-exhausted) (Chance and Williams, 1955). The RCR for mitochondria used in this study measured to be 4.9 ± 0.18 under the following conditions: 10 mM succinate, 1 μM rotenone, and 200 μM ADP.

Measurement of mitochondrial Ca^{2+} uptake capacity, membrane potential, NAD(P)H oxidation and swelling:

All chemicals were purchased from Sigma-Aldrich unless stated otherwise. The measurement of these parameters was performed simultaneously on a multichannel dye fluorimeter (C&L Instruments, Inc.) as described previously (Baranov et al., 2008; Stavrovskaya et al., 2010). Liver mitochondria were incubated in buffer containing 240 mM sucrose, 10 mM HEPES, pH 7.2, 1 mM KH_2PO_4, 3 μM EDTA, and either 5mM glutamate/malate or 5 mM succinate plus 1 μM rotenone and were used at a concentration of 0.25 mg of mitochondrial protein/ml. Changes to mitochondrial membrane potential ($\Delta\Psi_m$) were estimated by measuring changes in the fluorescence intensity of tetramethylrhodamine methyl ester (TMRM) (60 nM) (Life Technologies) at excitation and emission wavelengths of 543 and 590 nm, respectively. Mitochondrial Ca^{2+} flux was measured as the change in extramitochondrial Ca^{2+} concentration,

measured by fluorescence of CaGreen-5N (125 nM) (Life Technologies) at excitation and emission wavelengths of 482 and 535 nm, respectively. The redox state of pyridine nucleotides in the mitochondrial suspension was followed by monitoring NAD(P)H autofluorescence at excitation and emission wavelengths of 350 and 450 nm, respectively. Mitochondrial swelling was measured by light scattering at a wavelength of 587 nm. Mitochondria were challenged by single Ca^{2+} additions of 20-40 nmol Ca^{2+}/mg mitochondrial protein. Mitochondrial Ca^{2+} retention time (CRT) was defined as the time between Ca^{2+} addition and the plateau in CaGreen-5N fluorescence. To induce maximal swelling, the non-specific pore-forming agent alamethicin (Ala) was added to a final concentration of 2.5 μM at the conclusion of each run. Fluorimeter data were analyzed using Origin v.8.0 (OriginLab) software. The specific conditions of each experiment (i.e. substrates, inhibitors, concentration of Ca^{2+} or other mitochondrial permeability transition pore (mPTP) inducers, and αSyn species) are noted in the text. CRT was normalized to vehicle control.

Assessment of mitochondrial cytochrome c release:

30 μl aliquots were removed from vehicle- and αSyn-treated mitochondrial suspensions used for fluorescence analysis of mitochondrial parameters (see above) at timepoints corresponding approximately to 25, 50, 75, and 100% swelling of vehicle-treated mitochondria. Another aliquot was removed following the addition of 2.5 μM Ala, which was used to induce maximal swelling and cytochrome c release. Aliquots were centrifuged for 5 min at 14,000 *g* to pellet intact mitochondria. 12 μl of the supernatant were added to LDS sample buffer containing 5% β -mercaptoethanol and analyzed by SDS-PAGE/Western blot for released, soluble cytochrome c.

Assessment of mitochondria-associated αSyn:

Mitochondria were incubated as described for fluorescence measurements of mitochondrial parameters. In all cases, glutamate/malate and αSyn were added to the mitochondrial suspension. 20 μM Ca^{2+} or an equivalent volume of water was added 2 min after αSyn, and after 5 additional minutes, 200 μl aliquots of the suspension were removed. Aliquots were spun at 8,000 *g* for 10 min to pellet mitochondria, and the supernatant was removed. Mitochondrial pellets were washed 4 times in 50 μl assay buffer without substrates after which they were lysed with 50 μl of 1% NP40 lysis buffer (50 mM Tris, pH 7.5, 150 mM NaCl, 10 mM EDTA, 1% v/v nonidet P-40, complete mini EDTA-free protease inhibitor tablet) for 25 min on ice. Lysed mitochondria were spun for 5 min at 6,000 *g*, and the supernatant was collected. The supernatants of the mitochondrial suspension, washes, and lysed mitochondrial pellets were analyzed by SDS-PAGE/Western blot for αSyn. To quantify the total αSyn immunoreactivity of lysed mitochondrial pellets, densitometric analysis was performed using ImageJ (NIH).

SDS-PAGE/Western blotting:

Samples for western blotting were electrophoresed on Nu-PAGE 4-12% Bis-Tris gels (Life Technologies) with MES-SDS running buffer. Gels were then transferred onto 0.45 μm Immobilon-P PVDF membranes (Millipore) for 60 min at 400 mA constant current at 4°C in transfer buffer consisting of 25 mM Tris, 192 mM glycine, and 20% methanol. After transfer, membranes were blocked in 5% non-fat milk in PBS with 0.1% v/v Tween-20 (PBS-T) for 30 min at room temperature and then incubated in primary antibody either overnight at 4 °C or for 60 min at room temperature. Membranes were then washed 3 times for 5 min in PBS-T,

incubated with secondary antibody, washed 3 more times for 5 min in PBS-T, and then developed with ECL Plus or ECL Prime (GE-Amersham) according to the manufacturer's directions.

Antibodies:

2F12, an in-house generated mouse monoclonal antibody against αSyn (Dettmer et al., 2013) was used at 0.18 μg/ml in PBS-T plus 5% milk. The mouse monoclonal anti-cytochrome c antibody 7H8 (Santa Cruz) was used at 200 ng/ml in PBS-T plus 1% milk. Horseradish peroxidase-conjugated mouse secondary antibody (GE Healthcare) was diluted 1:10,000 in PBS-T plus 1% milk.

Statistical analysis:

Data are presented as the mean ± standard deviation (SD) unless otherwise specified. Comparisons across 2 groups were made using an unpaired *t*-test. When 3 or more groups were compared, a one-way ANOVA followed by a Tukey's multiple comparison's test were used. Data are considered significant at a p-value ≤ 0.05.

Results

Prefibrillar thioflavin T-negative αSyn promotes complex I-dependent, Ca^{2+}-mediated mitochondrial dysfunction:

To assess whether αSyn can directly compromise mitochondrial function, we prepared recombinant human αSyn for application to isolated mitochondria. To this end, we monitored the aggregation state of αSyn solutions incubated at 37°C under nutation. Assaying αSyn at different

time-points in this in *vitro* "aging" process using the amyloid binding dye thioflavin-T (ThT) produced a sigmoidal curve of ThT fluorescence (Figure 2.1A). We compared unaged monomer, aged ThT-negative ($ThT^{neg)}$ αSyn sampled during the aggregation lag phase, and ThT-positive (ThT^{pos}) aggregates (Figure 2.1A, blue, red, and green, respectively) for their ability to alter the function of mitochondria. We hypothesized that ThT^{neg} αSyn from the aggregation lag phase would be bioactive when applied to the isolated mitochondria, because this phase is characterized by the presence of soluble oligomers (Cremades et al., 2012; Fink, 2006; Volles et al., 2001) that are believed to be more toxic than ThT^{pos} fibrils that are abundant at the end stage of aggregation.

Mitochondrial stress was modeled by exposing isolated mitochondria to a single bolus of Ca^{2+} to induce eventual membrane permeabilization associated with a collapse of $\Delta\Psi_m$, release of endogenous and exogenously-administered Ca^{2+}, oxidation of pyridine nucleotides, and mitochondrial swelling. We used a fluorimeter-based assay to simultaneously measure these 4 parameters ($\Delta\Psi_m$, Ca^{2+} uptake/release, redox state of NAD(P)H, and swelling) in isolated mouse liver mitochondria. Figure 2.1B shows a representative record of these 4 mitochondrial parameters for mitochondria respiring with the complex I substrates glutamate and malate (complex I conditions) and exposed to a single Ca^{2+} addition in the absence (black traces) or the presence of 1 μM monomeric (blue traces) or aged, ThT^{neg} αSyn (red traces). Addition of mitochondria into the incubation buffer, as indicated by the labeled arrow, induced the sharp decline of the TMRM signal (i.e., TMRM concentration in the buffer) due to the accumulation and quenching of the dye by polarized mitochondria. The addition of Ca^{2+} at 180 s induced a transient depolarization (and therefore increase of TMRM signal) as well as a spike in extramitochondrial Ca^{2+} concentration before rapid uptake into mitochondria. Alamethicin

Figure 2.1: **Prefibrillar, ThT^{neg} αSyn sensitizes mitochondria to Ca^{2+}-induced dysfunction in a substrate-dependent manner.**

A. Sample aggregation timecourse of recombinant αSyn as measured by thioflavin T (ThT) fluorescence. 0.6 mg/ml αSyn was aged at 37°C under nutation and ThT fluorescence was monitored periodically. Unaged monomeric protein was obtained prior 37°C incubation, ThT-negative (ThT^{neg}) aged protein was sampled from the aggregation lag phase, and ThT-positive (ThT^{pos}) aged protein was collected once ThT fluorescence had plateaued. B. Representative traces of basic parameters of isolated liver mitochondria simultaneously measured by a multichannel fluorimeter in the presence of 5mM glutamate and 5 mM malate as substrates, either PBS vehicle (black traces), 1 μM monomeric αSyn (blue traces), or 1 μM ThT^{neg} αSyn (red traces), and a single 20 μM Ca^{2+} addition. Mitochondrial membrane potential ($\Delta\Psi_m$) was measured via TMRM fluorescence. Higher intensity corresponds to depolarized mitochondria. Ca^{2+} concentration in the suspension was measured as Ca-Green 5N fluorescence signal. The redox status of pyridine nucleotides was measured by NAD(P)H autofluorescence. Lower intensity corresponds to a more oxidized state of NAD(P)H. Mitochondrial swelling was measured the change in light scattering of the suspension. A decrease in scattering indicates a dilution of mitochondrial solutes due to swelling. Spikes result from additions of Ca^{2+}, αSyn or vehicle, and alamethicin (Ala), which was used at the conclusion of the measurement to induce maximal swelling. C. Quantification of the ability of aged, ThT^{neg} but not monomeric αSyn to reduce the mitochondrial retention time of 20 μM Ca^{2+} under complex I (glutamate and malate as substrates) but not complex II conditions (succinate as a substrate plus rotenone to inhibit complex I). Ca^{2+} retention time (CRT) was defined as time from Ca^{2+} addition to ultimate plateau of Ca-Green 5N fluorescence. Error bars represent the SD from at least 5 independent

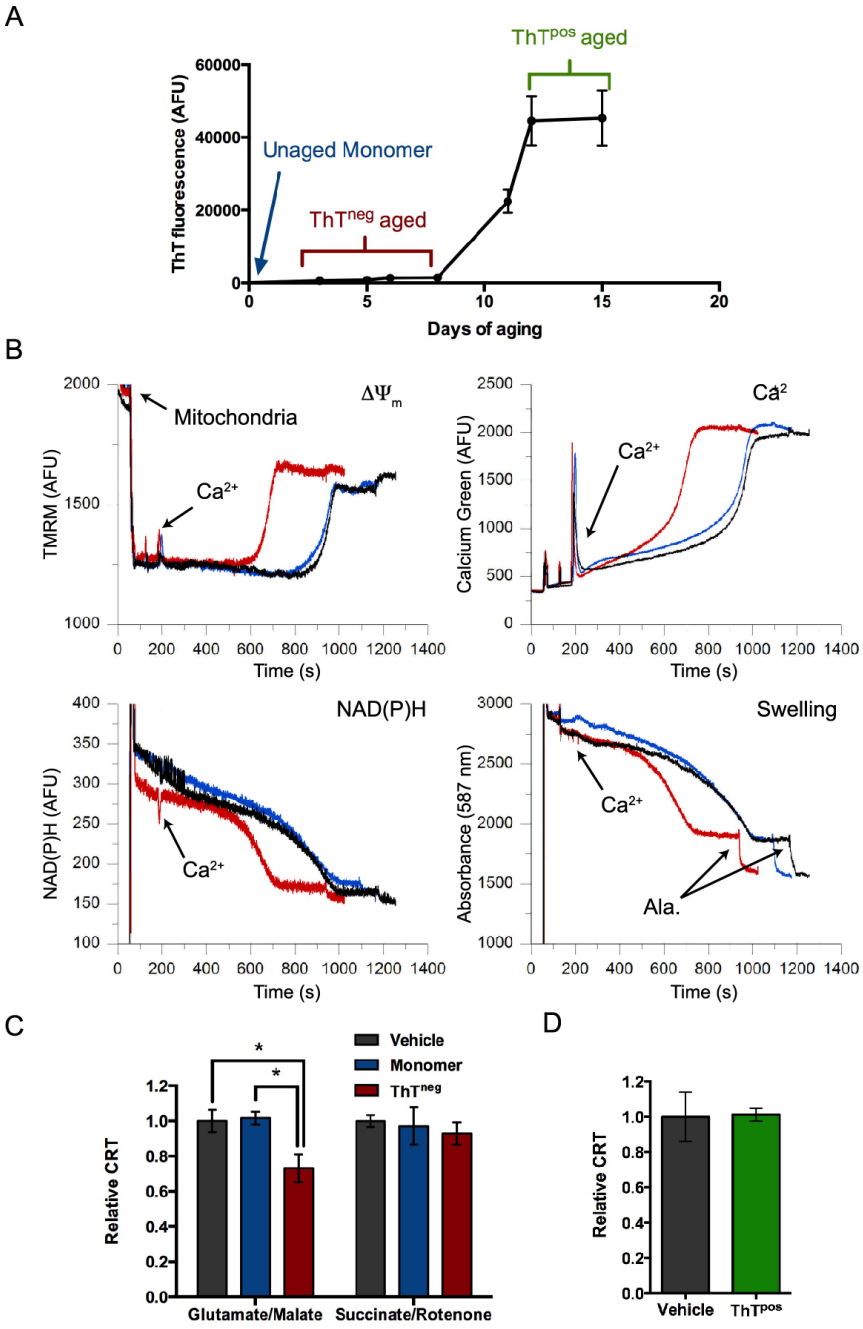

Figure 2.1 (Continued): **Prefibrillar, ThT^{neg} αSyn sensitizes mitochondria to Ca^{2+}-induced dysfunction in a substrate-dependent manner.**

experiments * = $p < 0.05$ ANOVA followed by Tukey's multiple comparisons test. D. The relative CRT of ThT^{pos} αSyn taken from end-stage plateau of fluorescence was compared to vehicle control. Error bars represent the SD of 4 independent experiments.

(Ala), a non-specific pore-forming agent, was added as a positive control to observe maximal mitochondrial swelling at the end of these measurements (note the rapid reduction in absorbance at 587 nm). Unaged, monomeric αSyn had no effect on mitochondrial Ca^{2+} retention time (CRT) while 1 μM ThT^{neg} αSyn significantly reduced mitochondrial CRT by 27% vs. control (Figure 2.1C). We found that αSyn sampled from the end-stage plateau of aggregation (ThT^{pos}) failed to reduce mitochondrial CRT (Figure 2.1D). Taken together, these data suggest that partially aged, ThT^{neg} αSyn, but not monomeric or highly aggregated, ThT^{pos} αSyn, sensitizes mitochondria to Ca^{2+}-mediated mitochondrial dysfunction.

Since the level of mitochondria-localized αSyn has been inversely correlated with complex I activity in the substantia nigra of PD patients (Devi et al., 2008), we investigated whether the effect of prefibrillar αSyn was restricted to complex I conditions. Therefore, instead of the complex I substrates glutamate and malate, we added the complex II substrate succinate and complex I inhibitor rotenone (complex II conditions). Interestingly, under complex II conditions, neither ThT^{neg} nor monomeric αSyn significantly affected CRT (Figure 2.1C) or the other mitochondrial parameters tested (data not shown). This result suggests that the ability of aged ThT^{neg} αSyn to sensitize mitochondria to Ca^{2+} is specifically dependent on electron flow through complex I and also serves as an important specificity control for our analytical method.

Duration of the aggregation lag phase is variable:

The data presented in Figure 1 highlight the fact that obtaining bioactive αSyn is critically dependent on predicting the timing of the aggregation lag phase and "catching" αSyn at the optimal oligomerization state. While the effects of aged, ThT^{neg} αSyn occurred consistently, the duration of the aggregation lag phase leading to activity varied considerably and was thus

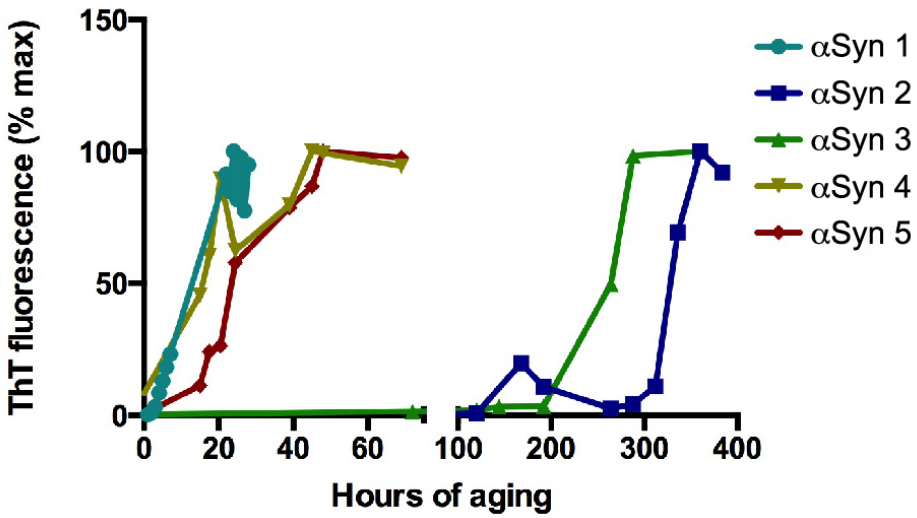

Figure 2.2: **Variation in αSyn aggregation kinetics.**

Aggregation state of 5 different 0.6 mg/ml αSyn samples incubated on different days under nutation at 37°C were monitored over time by ThT fluorescence. Note the broken abscissa and variation in duration of the aggregation lag phase prior to ThT positivity. Raw fluorescence values were normalized to the maximal fluorescence signal for each sample. Error bars were omitted to highlight differences among, rather than within samples.

difficult to predict *a priori*. Five examples of αSyn incubated under identical conditions on different days are displayed in Figure 2.2. In some cases the lag phase extended over several days, while in others the samples already contained ThT-binding species at early timepoints after the start of incubation (Fig. 2.2, note the broken abscissa). The kinetics of αSyn aggregation are known to be altered by many factors, including pH, temperature, sample volume, degree of agitation, protein concentration, and the presence of even a small amount of oligomeric "seeds". We therefore sought a more reproducible way of generating bioactive oligomers.

Characterization of α*Syn fibrils before and after sonication:*

Sonicated αSyn fibrils have recently been used to seed the aggregation of endogenous αSyn in cells and mice (Luk et al., 2012; 2009). Since mature αSyn fibrils can be prepared easily and reproducibly, we asked whether the mechanical disruption of fibrils into small species can produce oligomers that are functionally similar to the prefibrillar oligomers present during the aggregation lag phase (above). We first generated recombinant human αSyn fibrils (see Experimental Procedures) and characterized them by several techniques before and after sonication. Electron microscopy of non-sonicated fibrils revealed long, relatively uniform fibers hundreds of nm in length with diameters between 10 and 15 nm (Figure 2.3A). In contrast, sonicated fibril samples were more heterogeneous and included short fibril fragments as well as spherical αSyn aggregates (Figure 2.3B) Dynamic light scattering analysis revealed the average hydrodynamic radius of non-sonicated fibrils and sonicated fibrils to differ markedly at ~950.5 nm and ~40.0 nm, respectively (Figure 2.3C, note log scale). We examined the ensemble aggregation state of sonicated αSyn by incubating samples with the β-sheet-binding dye ThT. Sonicated αSyn was only 10% as fluorescent as non-sonicated fibrils (Figure 2.3D) illustrating a

Figure 2.3: Characterization of sonicated and non-sonicated αSyn fibrils.

A,B. Representative electron micrographs of αSyn aggregated at 2 mg/ml for 5 d under nutation before (A) and after (B) sonication. Sonicated fibrils contained a heterogeneous mixture of species including spherical oligomers and short fibril fragments. Scale bars = 100 nm. C. Hydrodynamic radii (Rh) of fibrils and sonicated fibrils as measured by dynamic light scattering. Error bars represent SEM of 3 and 7 replicates for fibrils and sonicated fibrils, respectively. D. Background-subtracted fluorescence values of 2.5 μM (based on starting monomer concentration) fibrillar, and sonicated αSyn fibrils in the presence of 10 μM ThT expressed as a percentage of signal obtained for fibrillar αSyn. Sonicated fibrils fluoresced with approximately 10% of the intensity of fibrils. Error bars represent SD of 3 independent experiments. E. An example aggregation timecourse of 7 μM monomeric αSyn seeded with 1 mol % of fibrillar, sonicated, or additional monomeric αSyn is shown. Sonicated and non-sonicated fibrils accelerated the aggregation of monomeric αSyn compared to additional monomeric αSyn. In this experiment, monomer-seeded αSyn was observed to acquire ThT positivity after 40 h of aging. 100,000 AFU represents the upper limit of detection of our instrument. Error bars represent the SD of 3-4 replicates. Similar data were obtained in 3 other independent experiments.

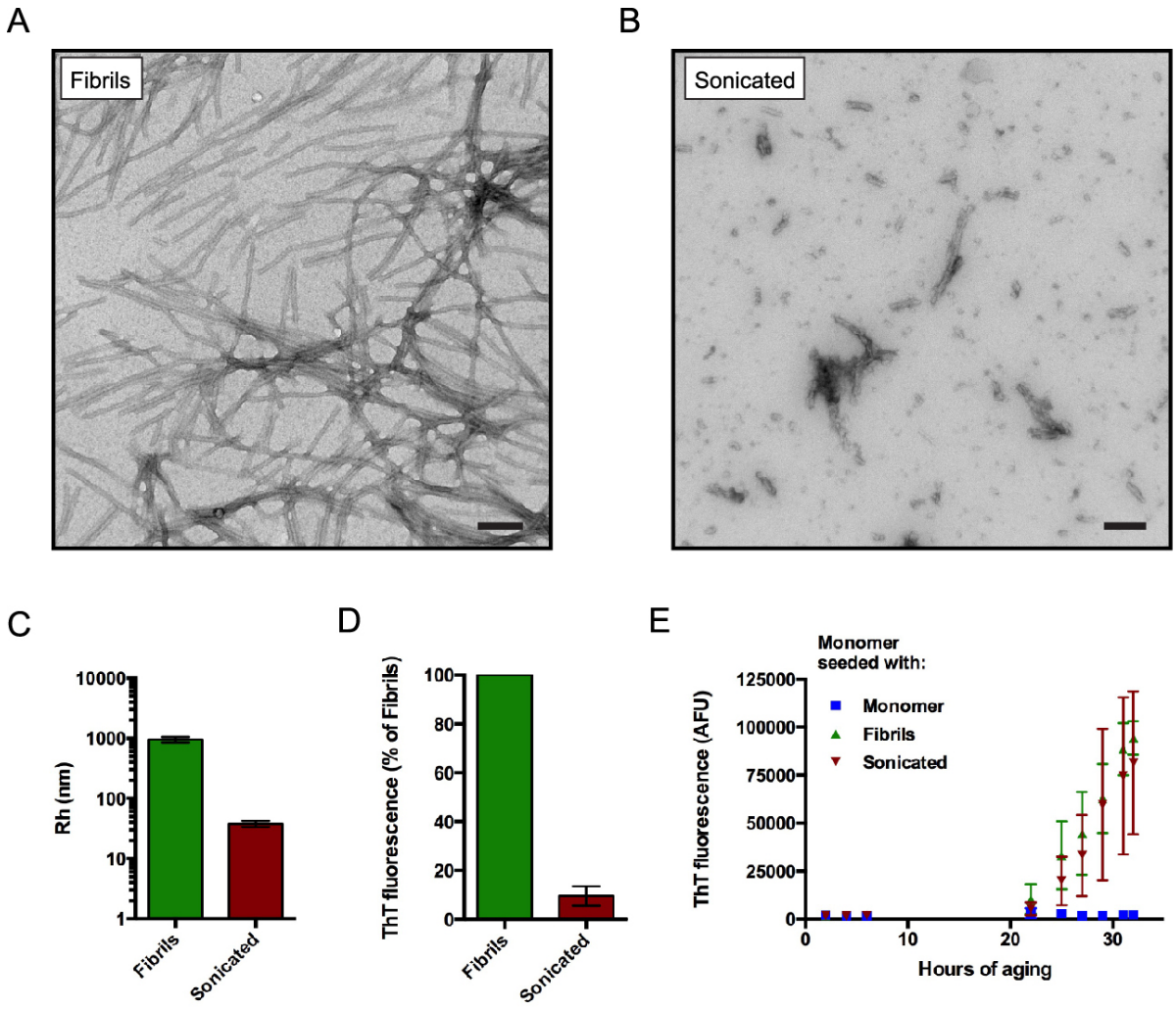

Figure 2.3 (Continued): **Characterization of sonicated and non-sonicated αSyn fibrils.**

substantial loss of β-sheet content. Despite this loss of β-sheet content, we observed that sonicated αSyn fibrils were able to seed the aggregation of monomeric αSyn (Figure 2.3E), confirming that they still contained species that they can serve as a template for further aggregation.

Sonicated αSyn fibrils recapitulate the mitochondrial effects of prefibrillar ThT^{neg} αSyn:

We compared sonicated and non-sonicated fibrils for their ability to alter the biochemical function of mitochondria. Under complex I conditions, sonicated αSyn reduced mitochondrial CRT in a dose-dependent manner, with the 1 μM and 2 μM doses causing significant 14% and 21% reductions, respectively (Figure 2.4A, B). This CRT reduction was again associated with commensurate acceleration in membrane depolarization, oxidation of endogenous pyridine nucleotides, and swelling of the mitochondria (Figure 2.4A). In contrast to the sonicated material, and in agreement with the ThT^{pos} samples described above (Fig. 1D), non-sonicated αSyn fibrils did not significantly alter CRT (Figure 2.4C) or the 3 other mitochondrial parameters we measured. Under complex II conditions, neither 1 μM nor 2 μM sonicated αSyn led to a reduction in CRT when incubated with mitochondria (Figure 2.4D, E). Together, these data confirm that oligomeric, but not ThT^{pos} fibrillar αSyn, promotes Ca^{2+}-induced mitochondrial dysfunction specifically under complex I conditions.

In general, the reduction of CRT by sonicated αSyn (1 μM) under complex I conditions was highly reproducible, but in 4 of 23 samples tested, no effect of the αSyn preparation could be detected. In the detailed characterization of the effects of αSyn on mitochondria that follows, we analyzed data from all those sonicated preparations that were found to be bioactive (i.e., 19 out of 23).

Figure 2.4: Sonicated αSyn fibrils promote Ca^{2+}-mediated mitochondrial dysfunction in a substrate-dependent manner.

A. Representative traces of basic parameters of isolated liver mitochondria ($\Delta\Psi_m$, extramitochondrial Ca^{2+}fluorescence, NAD(P)H autofluorescence, and mitochondrial swelling) simultaneously measured by a multichannel fluorimeter and recorded in the presence of a single 20 μM Ca^{2+} addition, 5 mM glutamate and 5 mM malate as substrates, and either PBS vehicle (black traces), 1 μM (red traces) or 2 μM (pink traces) sonicated αSyn fibrils. Spikes result from addition of mitochondria; arrows are used to indicate the time of Ca^{2+} addition. B. The CRT of mitochondria treated with 1 and 2 μM sonicated αSyn fibrils under complex I conditions (glutamate/malate-dependent respiration) were normalized to vehicle-treated mitochondria. Sonicated αSyn dose-dependently reduced CRT under these conditions. Error bars represent SD from at least 9 independent experiments * = $p < 0.05$ ANOVA followed by Tukey's multiple comparison's test. C. The relative CRT of isolated mitochondria respiring under complex I conditions and treated with non-sonicated αSyn fibrils was determined. Error bars represent SD from 5 independent experiments. D: Representative traces of parameters measured in isolated mitochondria under complex I conditions with either vehicle (black) or 1 μM sonicated αSyn fibrils (red). E: The CRT of mitochondria respiring under complex II conditions (succinate/rotenone-dependent respiration) and treated with 1 and 2 μM sonicated αSyn was compared to vehicle-treated mitochondria under identical conditions. Error bars represent SD from at least 4 independent experiments.

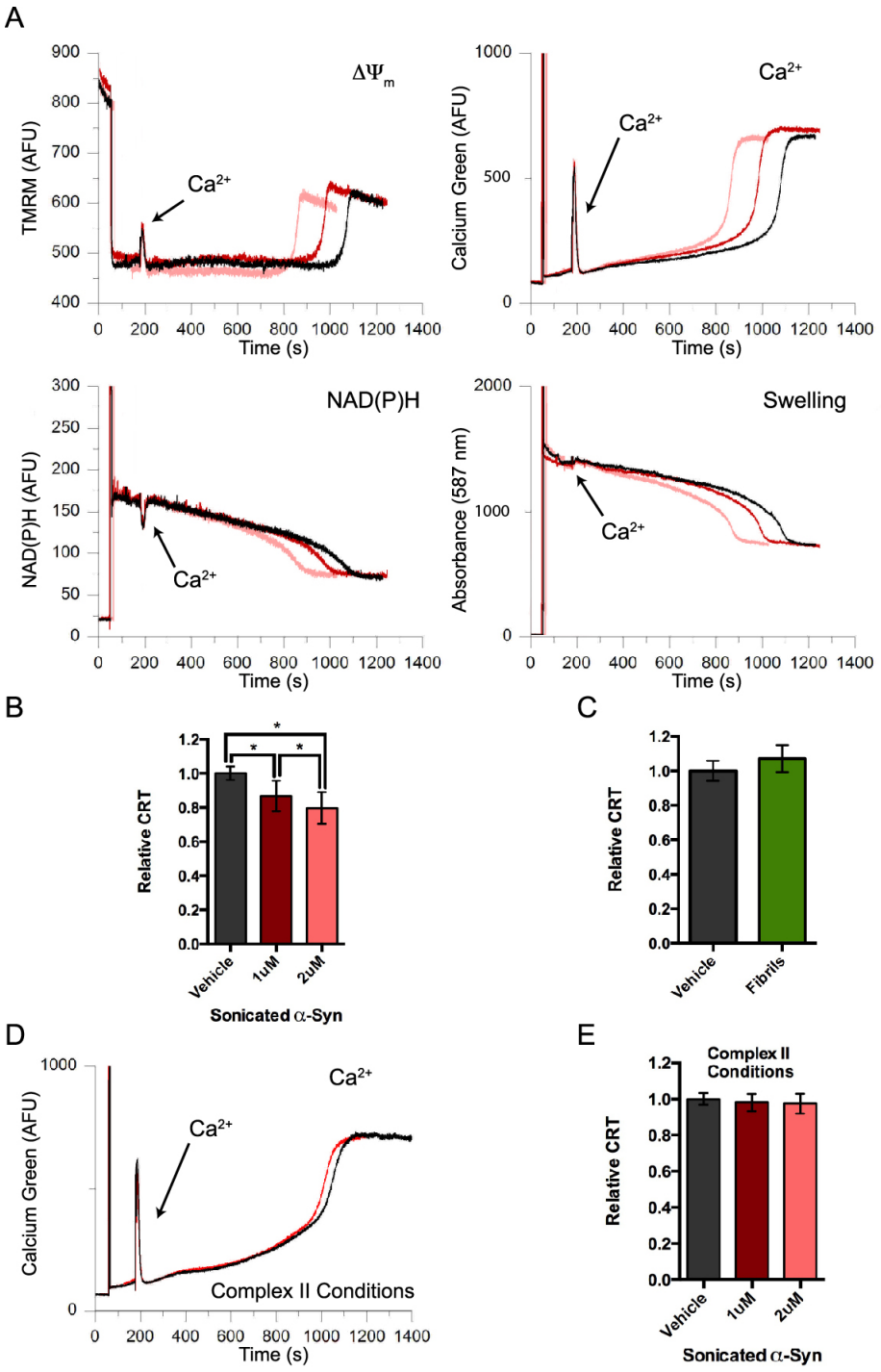

Figure 2.4 (Continued): Sonicated αSyn fibrils promote Ca^{2+}-mediated mitochondrial dysfunction in a substrate-dependent manner.

Bioactivity of sonicated αSyn *is contained within a 100,000* g *supernatant:*

We sought to further define the bioactive component of the sonicated αSyn fibril preparation. Analysis of the CRT-reduction capability of the 16,000 *g* supernatant revealed that it contained equivalent bioactivity compared to the total sonicated material (Figure 2.5). To determine whether the active component was retained in a high speed supernatant, we fractionated the total sonicated material via ultracentrifugation at 100,000 *g*. Electron microscopy of the 100,000 *g*-soluble and -insoluble fractions showed a near complete separation of small, rounded oligomers and large amyloid fibril fragments into the supernatant and pellet, respectively (Figure 2.6A, B). Further analysis using dynamic light scattering revealed that the 100,000 *g* supernatant contained oligomers with a mean hydrodynamic radius of 20.3 nm compared to monomeric αSyn and the 100,000 *g* pellet which had mean hydrodynamic radii of 3.8 nm and 42.8 nm, respectively (Figure 2.6C). Moreover, the 100,000 *g* supernatant was able to seed the aggregation of monomeric αSyn much faster than did additional monomer (Figure 2.6D), suggesting that it contains misfolded species that can promote the conversion of unfolded protein into β-sheet-rich aggregates. When applied to mitochondria, the 100,000 *g* supernatant significantly reduced CRT to a degree equivalent to the total sonicated sample, while the volume-normalized pellet failed to reduce CRT (Figure 2.6E). Though the pellet contained considerably less material than the supernatant as determined by total protein assays, subsequent experiments showed that the protein in the pellet had no capability to decrease CRT when protein normalized (data not shown). Together, these data demonstrate that sonication of αSyn fibrils produces entirely soluble oligomers that can disrupt mitochondrial Ca^{2+} homeostasis,

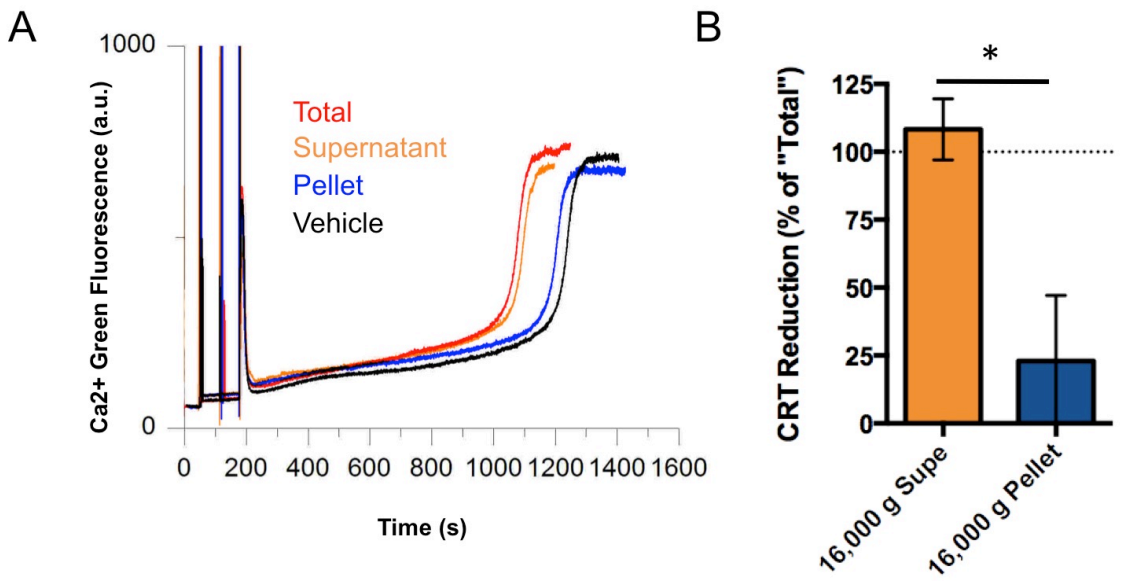

Figure 2.5: **16,000 *g* soluble fraction of sonicated αSyn fibrils contains bioactive protein**. A. Ca^{2+} flux measurements of mitochondria treated with total sonicated material (red), the soluble (orange) and insoluble (blue) fractions from a 16,000 *g* centrifugation step, or vehicle (black) were compared. B. CRT reduction upon treatment with the 16,000 *g* supernatant and pellet of the total sonicated material were compared. Data are represented as percent CRT reduction compared to total sonicated material from the same αSyn preparation. Error bars represent the SD from 3 independent experiments. * = $p < 0.05$ using student's T-test.

Figure 2.6: **100,000 *g* soluble fraction of sonicated αSyn fibrils contains bioactive oligomers**. A,B. Representative electron micrographs of sonicated αSyn fibrils fractionated into a 100,000 *g* supernatant (A) and pellet (B). Large fibril fragments pellet at this speed while smaller, rounded oligomers remain soluble. Scale bars = 100 nm. C. Comparison of the hydrodynamic radii (Rh) of αSyn monomer and the 100,000 *g* supernatant and pellet of sonicated αSyn fibrils as measured by dynamic light scattering. Error bars represent SEM of 3, 5, and 3 replicates for fibrils, 100,000 *g* supernatant, and 100,000 *g* pellet, respectively. D. Soluble oligomers present in the 100,000 *g* supernatant can seed the aggregation of monomeric αSyn. Monomeric αSyn at 20 μM was seeded with 1 mol % of additional monomeric αSyn or the 100,000 *g* supernatant of sonicated fibrils. An aggregation timecourse representative of 3 independent experiments is shown. Error bars represent the SD of 3-4 replicates. E. CRT reduction upon treatment with the 100,000 *g* supernatant and pellet of the total sonicated material were compared. Data are represented as percent CRT reduction compared to total sonicated material from the same αSyn preparation. Error bars represent the SD from 3 independent experiments. * = $p < 0.05$ using student's T-test.

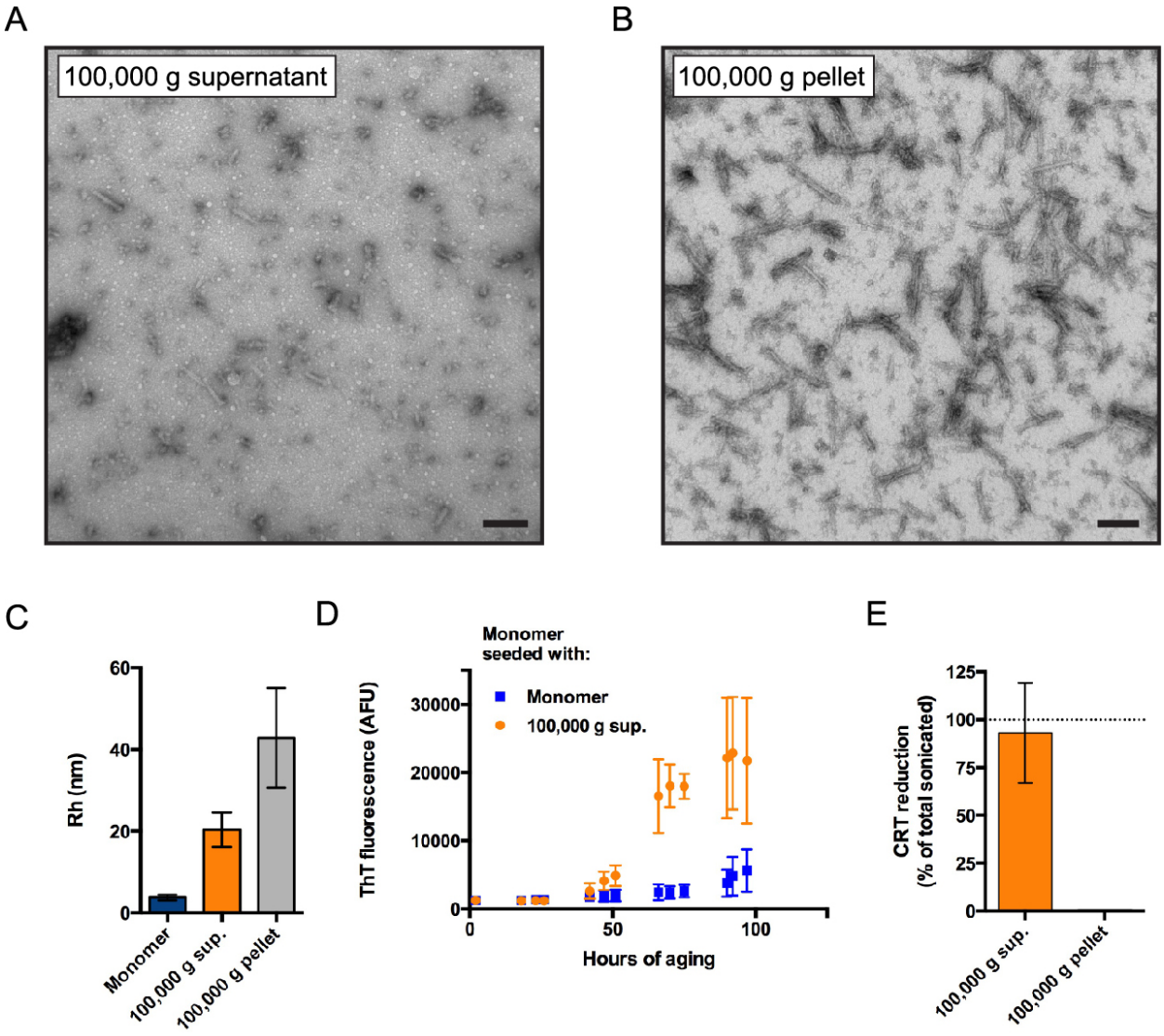

Figure 2.6 (Continued): **100,000 *g* soluble fraction of sonicated αSyn fibrils contains bioactive oligomers**.

while larger αSyn species that pellet under these conditions (intact fibrils and larger fragments thereof) have no significant effect on mitochondrial function.

Sonicated fibrils promote Ca^{2+}-mediated mitochondrial dysfunction and associated cytochrome c release via permeability transition pore induction:

There is mounting evidence that under pathophysiological conditions within a cell, the exposure of mitochondria to elevated cytosolic Ca^{2+} can result in mitochondrial damage via a permeability transition mechanism (Di Lisa et al., 2001; Lemasters et al., 1998; Scorrano et al., 1999). The induction of opening of the mitochondrial permeability transition pore (mPTP) is associated with membrane depolarization and release of intra-mitochondrial Ca^{2+}. These changes are followed closely by the rupture of the outer mitochondrial membrane and subsequent release of cytochrome c, which in an intact cell could lead to the downstream initiation of apoptosis (Petit et al., 1998).

To ascertain whether the opening of the mPTP was responsible for the αSyn-induced and Ca^{2+}-mediated changes in mitochondrial parameters documented above, we examined the effect of the specific mPTP inhibitor cyclosporin A (CsA). As expected, preincubation of the mitochondria with 1 μM CsA prevented the CRT reduction by sonicated αSyn fibrils (Figure 2.7A, left panel, purple trace) and the associated decrease in the time to complete mitochondrial swelling (Figure 2.7A, right panel, purple trace). We next determined whether the earlier onsets of mitochondrial Ca^{2+} release and swelling caused by incubation with sonicated αSyn oligomers were accompanied by premature cytochrome c release. We removed aliquots of the vehicle- and αSyn-treated mitochondrial suspensions at timepoints corresponding to approximately 25, 50, 75, and 100% swelling of vehicle-treated mitochondria. Another aliquot was removed following the

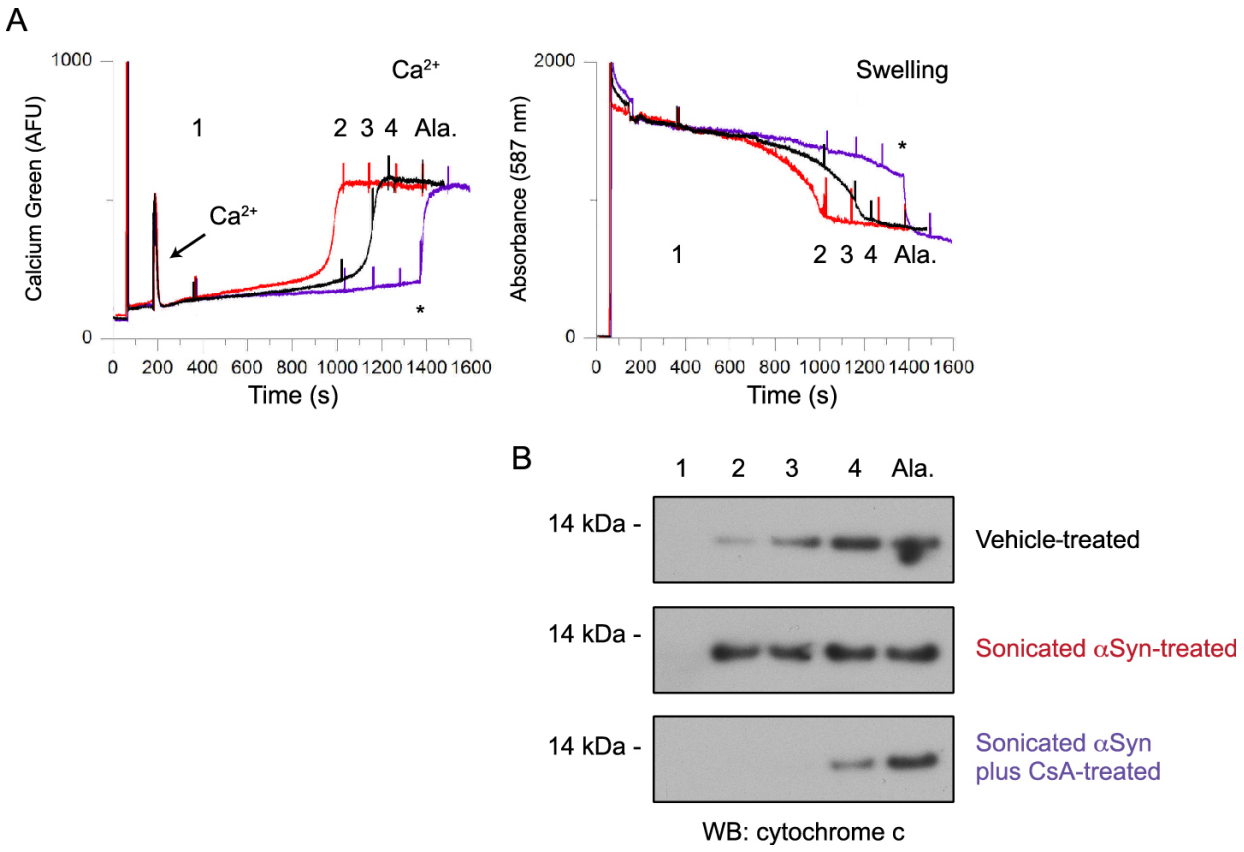

Figure 2.7: αSyn-induced changes in Ca^{2+} flux and swelling are due to activity of mPTP and are accompanied by cytochrome c release.

A. Comparison of extramitochondrial Ca^{2+} fluorescence (left) and swelling (right) of mitochondria incubated with vehicle (black), 1 μM sonicated αSyn (red) and 1 μM sonicated fibrils plus 1 μM cyclosporin A (CsA; purple). Experiments were conducted with the addition of 20 μM Ca^{2+} under complex I conditions. 30 μl aliquots were removed at the indicated times (1-4, Ala) and further processed for analysis in B. * = addition of Ala. Traces are representative of 4 independent experiments. B. Aliquots removed from the suspensions shown in A were centrifuged at 14,000 *g* for 5 min. The supernatants were run on SDS-PAGE, Western blotted, and probed with an antibody against cytochrome c to detect cytochrome c released from damaged mitochondria. Western blots are representative of 4 independent experiments.

addition of Ala, which was used to induce maximal swelling and cytochrome c release. Western blots of the supernatants from all these aliquots indicated that the detection of released cytochrome c correlated with the degree of swelling (change in light scattering) in the mitochondrial suspension as a whole (Figure 2.7B). Importantly, CsA preincubation also prevented αSyn-induced cytochrome c release (Figure 2.7B) suggesting that, in our system, this swelling occurs as a consequence of mPTP opening rather than via direct membrane permeabilization by αSyn oligomers.

Activity of sonicated αSyn is dependent on exogenous Ca^{2+} uptake:

Thus far, we had only investigated whether αSyn can alter mitochondrial function in the presence of exogenously added Ca^{2+}. We therefore asked whether the ability of sonicated αSyn to alter mitochondrial function under complex I conditions was dependent on added Ca^{2+}. For this purpose, we incubated the isolated mitochondria with sonicated αSyn but without addition of exogenous Ca^{2+}. No changes in all 4 measured mitochondrial parameters ($\Delta\Psi_m$, Ca^{2+} flux, NAD(P)H oxidation state and swelling) were detected for incubation times up to one hour (Figure 2.8A). To confirm that effects of sonicated αSyn are mediated by exogenous Ca^{2+}, we asked whether sonicated αSyn fibrils sensitized mitochondria to a non-Ca^{2+} inducer of mPTP opening, the bifunctional hydrophobic thiol-cross linking agent phenylarsine oxide (PhAsO) (Bernardi et al., 1992). As in the absence of exogenous Ca^{2+}, we observed no sensitizing effect of αSyn in the presence of 10 μM PhAsO (Figure 2.8B). We then specifically tested whether Ca^{2+} uptake into mitochondria, rather than simply its presence in the mitochondrial suspension, was required to observe αSyn–induced changes to mitochondrial parameters. Preincubation with the specific inhibitor of the mitochondrial Ca^{2+} uniporter Ru360 (10 μM) was sufficient to

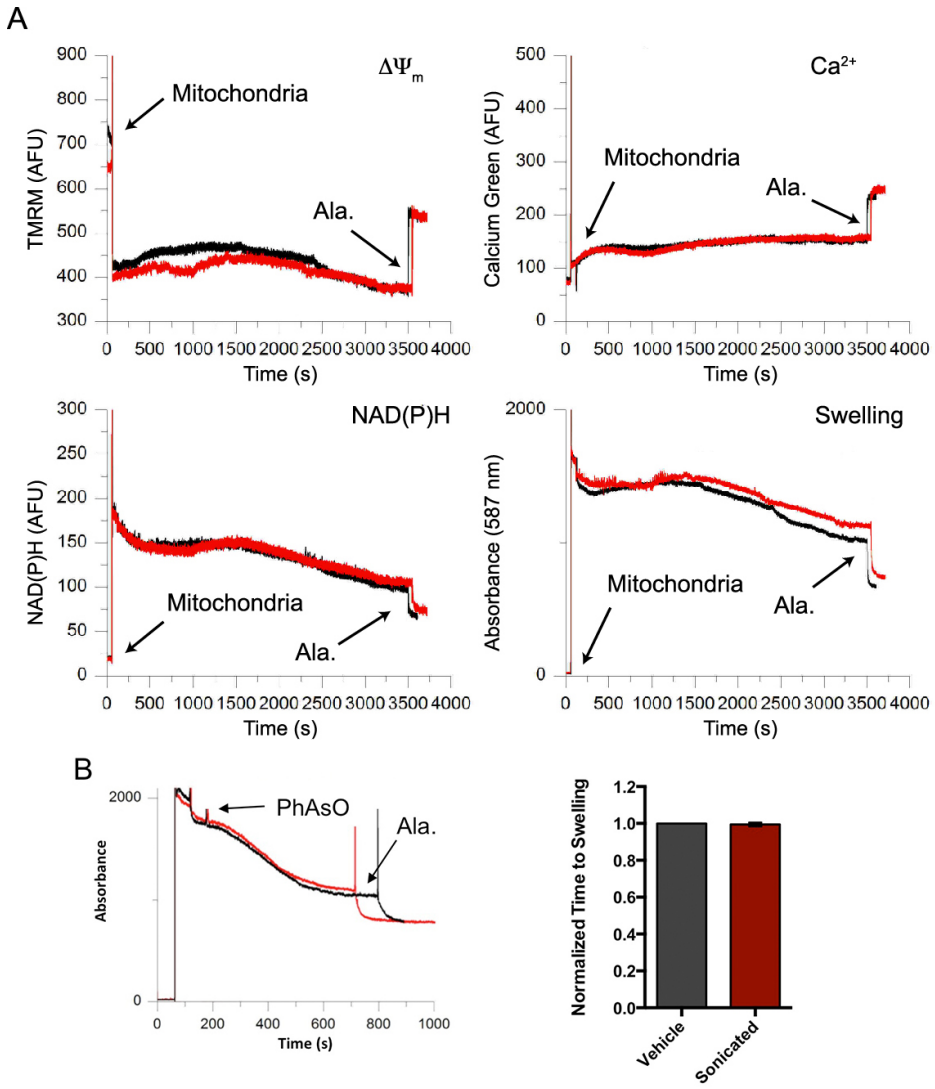

Figure 2.8: **αSyn does not affect mitochondrial parameters in the absence of added Ca^{2+}.** Comparison of mitochondrial suspensions incubated with vehicle control (black) or 1 μM sonicated αSyn fibrils (red) under complex I conditions in the absence of exogenous Ca^{2+}. Addition of sonicated αSyn resulted in no change in steady state $\Delta\Psi_m$, Ca^{2+} flux, oxidation state of pyridine nucleotides, or membrane swelling. Ala was added to induce swelling after 1 hour. Arrows = addition of mitochondria. Traces are representative of 4 independent experiments. B: Mitochondria treated with 10 uM PhAsO in the presence of vehicle control (black) or 1 μM sonicated αSyn fibrils (red) and in the absence of added Ca^{2+}. The normalized time to swelling was quantified. Error bars represent the SD from 4 independent experiments.

Figure 2.9: Mitochondrial Ca^{2+} cycling is necessary for αSyn-induced mPTP induction, but not binding.

A. Extramitochondrial Ca^{2+} (as determined by Ca-Green 5N fluorescence) of mitochondrial suspensions incubated with vehicle (black) or sonicated αSyn (red) and challenged with 20 μM Ca^{2+} in the absence (top) or presence of 10 μM Ru360, an inhibitor of the mitochondrial Ca^{2+} uniporter (bottom). Note that Ru360 prevents uptake of exogenous Ca^{2+}. Traces are representative of 4 independent experiments. B. Measurements of mitochondrial swelling (decrease in absorbance at 587 nm) obtained from incubations of the same αSyn and mitochondrial preparations shown in A. 20 μM Ca^{2+} was added to mitochondrial suspensions in the absence (top) or presence of 10 μM Ru360 (bottom). There is no Ca^{2+}-induced swelling in the presence of Ru360 whether αSyn is present or not. Traces are representative of 4 independent experiments. C. SDS-PAGE/western blot of the supernatant (S), washed pellets (W_1-W_4), and lysed pellets (L) of mitochondrial suspensions after brief incubation with sonicated αSyn in the presence or absence of 20 μM Ca^{2+}. Membranes were probed for αSyn (top panel) and cytochrome c (bottom panel). The majority of the incubated αSyn remains in the supernatant, but a fraction resists 4 washes in assay buffer and is specifically associated with the mitochondrial pellet. As expected, cytochrome c is only detectable in the lysed mitochondrial pellets suggesting mitochondria remain intact after these washes. Blots are representative of 4 independent experiments. D. Quantification of total αSyn immunoreactivity of lysed mitochondrial pellets (L) after incubation with sonicated αSyn in the presence or absence of $Ca^{2+}$and extensive washing. Total lane immunoreactivity was normalized to samples in which 20 μM Ca^{2+} was added to the αSyn/mitochondria suspension. Error bars represent the SD of 4 independent experiments.

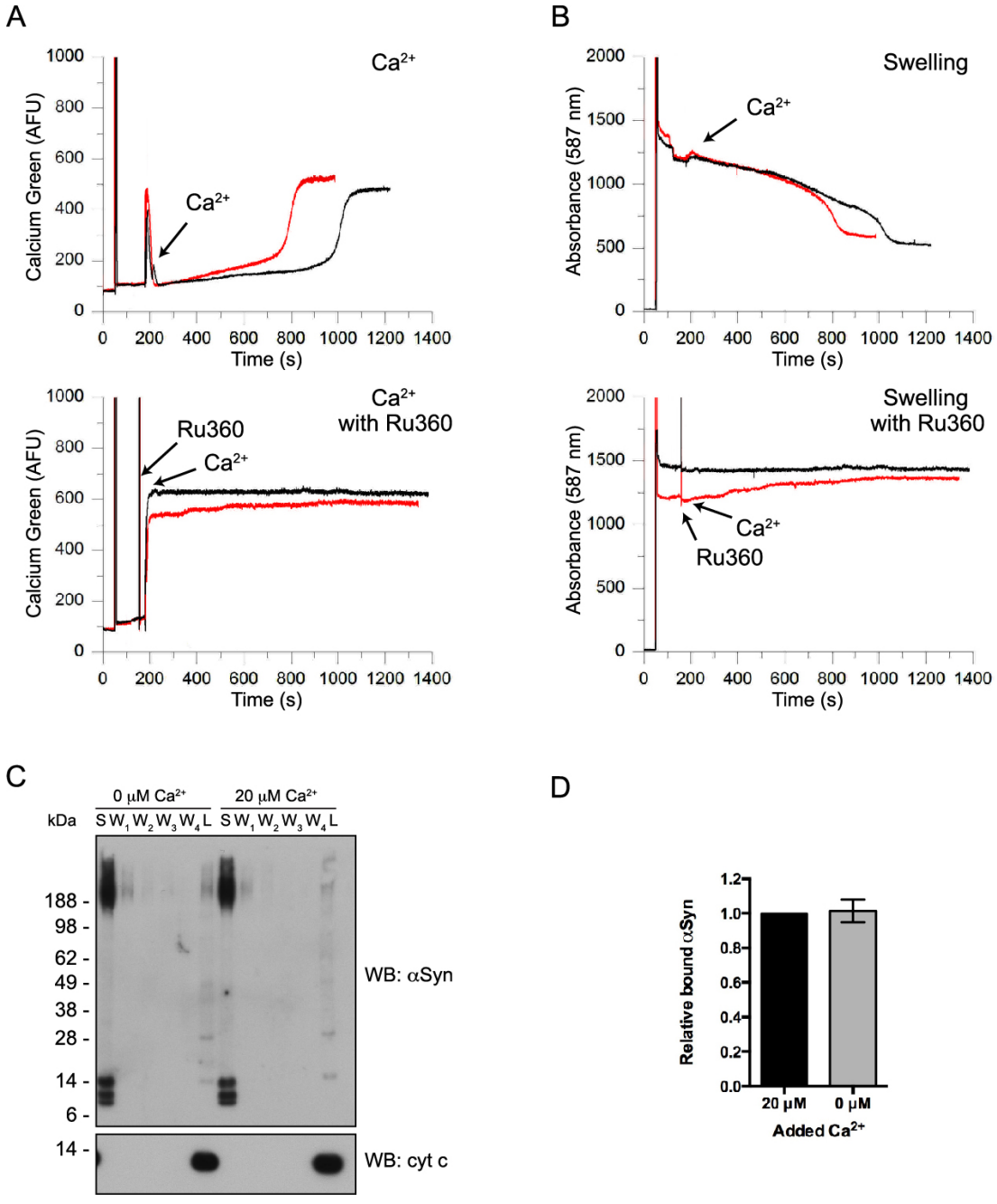

Figure 2.9 (Continued): Mitochondrial Ca^{2+} cycling is necessary for αSyn-induced mPTP induction, but not binding.

completely block uptake of exogenous Ca^{2+} (Figure 2.9A, compare bottom and top panels) and prevent the mPTP-inducing effects of sonicated αSyn, as exemplified by the swelling traces shown in Figure 2.9B. We observed no reduction in absorbance over time, indicating that αSyn did not promote mitochondrial swelling in the presence of Ru360 (compare top and bottom panels of Figure 2.9B). To determine whether exogenous Ca^{2+} enhanced the physical association of αSyn with mitochondria, we incubated mitochondria with sonicated αSyn in the presence or absence of 20 μM Ca^{2+}, ran the lysate of extensively washed mitochondrial pellets on SDS-PAGE, and blotted for αSyn. We observed no differences in the intensity or pattern of αSyn immunoreactivity in the lysed mitochondrial pellet (Figure 2.9C lanes "L", and Fig. 8D). This indicates that, while Ca^{2+} uptake is necessary for the downstream functional consequences of the αSyn/mitochondria association (i.e., CRT reduction and sensitization to mPTP opening), the association itself is not regulated by Ca^{2+} under our conditions. These data suggest that the addition of Ca^{2+} and the concomitant metabolic changes that accompany its uptake into mitochondria make the mitochondria vulnerable to the effects of bound αSyn.

Discussion

Evidence from many labs makes it increasingly clear that mitochondria are a principal target for aberrant accumulation of αSyn within the cell (Chinta et al., 2010; Choubey et al., 2011; Devi et al., 2008; Hsu et al., 2000; Martin et al., 2013; 2006; Parihar et al., 2008; Shavali et al., 2008; Stichel et al., 2007); however few studies have investigated the effects of different assembly forms of αSyn directly on the function of mitochondria. Here, we used a reductionist model system comprising isolated mitochondria and different, well-characterized forms of pure human αSyn to discover that highly soluble, prefibrillar αSyn oligomers, but not monomers or

ThT^{pos} fibrils, impair mitochondrial function. Further, we show that the toxicity of oligomeric αSyn is specifically dependent on both mitochondrial uptake of exogenous Ca^{2+} and electron flow through complex I.

The literature is replete with protocols for preparing αSyn oligomers (e.g., by incubation with supraphysiological levels of metal ions, lipids, detergents or oxidizing agents) that are either not further characterized or vary in their morphological, biochemical, and/or functional characteristics (Danzer et al., 2007; De Franceschi et al., 2011; Drescher et al., 2010; Giehm et al., 2011; Natalello et al., 2011; Näsström et al., 2011; Volles and Lansbury, 2002). In this study, we report highly complementary results using two independent methods for generating soluble prefibrillar αSyn oligomers in the absence of any additives: sonication of fully formed amyloid fibrils (sonicated prep) and collection of oligomers during the lag phase of initial aggregation (lag phase prep). Though oligomers obtained with the sonicated prep are formed by the sonication of fibrils and could therefore be considered "postfibrillar", they are capable of seeding the aggregation of monomeric protein into ThT^{pos} fibrils. Thus, for simplicity and to distinguish them from physiological, aggregation-resistant helical oligomers (Bartels et al., 2011; Dettmer et al., 2013), we refer herein to oligomers from the sonicated and lag phase preps as "prefibrillar oligomers". Both of these preparations produce closely similar effects on mitochondrial function, which argues against the likelihood of artifactual effects caused by a specific preparation of oligomers. Under the specific conditions discussed further below, αSyn generated using either of our protocols recapitulated several mitochondrial phenotypes previously reported in animal and cell models of PD, namely, complex I-mediated dysfunction, altered $\Delta\Psi_m$, disrupted Ca^{2+} homeostasis, and enhanced cytochrome c release.

Collectively, our data indicate that highly soluble prefibrillar oligomers, rather than larger, 100,000 *g*-pelletable oligomers or fibril fragments, can disrupt proper mitochondrial function. ThT assays suggest that our bioactive material is not β-sheet-rich; however, we cannot exclude the possibility that a small percentage of β-sheet-containing oligomers that do not avidly bind ThT contribute to our observed effects, especially in light of a propensity of the active material to act as a template for the formation of β-sheet-containing amyloid fibrils. Our sonicated prep was modeled in part after the sonicated preformed fibrils used by Lee and colleagues (Luk et al., 2012; 2009) who demonstrated the neuronal internalization of extracellularly applied sonicated fibrils and their ability to promote the aggregation of endogenous αSyn. To date, the colocalization, if any, of the seeded protein with mitochondria and the possible functional consequences for these organelles have not been assessed, but in light of our findings, they should be.

The mitochondria of neurons of the substantia nigra pars compacta and other brain regions vulnerable to PD are subjected to high Ca^{2+} concentrations due to regular influx through pacemaking L-type channels and low expression of cytosolic Ca^{2+} buffering proteins (Foehring et al., 2009; Goldberg et al., 2012; Guzman et al., 2010). We therefore studied the effects of αSyn on mitochondrial function in the context of elevated Ca^{2+} levels. We observed that bioactive prefibrillar αSyn disrupted basic mitochondrial parameters ($\Delta\Psi_m$, Ca^{2+} uptake/release, redox state of pyridine nucleotides, and swelling) only in the presence of exogenously added Ca^{2+}. Since Ru360 abolished this effect, we can conclude that the downstream effects of mitochondria-associated αSyn were dependent on the uptake of Ca^{2+} into the mitochondrial matrix.

The protective effects of CsA on our αSyn-induced changes in mitochondrial parameters demonstrated that addition of prefibrillar αSyn sensitized mitochondria to mPTP activation in our experiments. The acceleration of cytochrome c release in αSyn-treated mitochondria was likewise rescued by preincubation with CsA. This result suggests that cytochrome c release was also regulated by the mPTP in our system rather than by channels formed via direct permeabilization of the outer membrane by oligomeric αSyn, as had been suggested (Camilleri et al., 2013).

Ca^{2+}-induced mPTP opening can be broadly split into three main phases that could be accelerated by αSyn based on our new work: the "initiation phase", during which Ca^{2+} is taken up into the matrix through the mitochondrial Ca^{2+} uniporter; the "lag phase", during which mPTP components are recruited and assembled; and the and the "propagation phase", during which mPTP induction spreads through the population (Baranov et al., 2008). Our data showing the lack of direct effect of αSyn on $\Delta\Psi_m$ and the unimpaired initial uptake of Ca^{2+} both suggest that the first phase is not significantly affected by αSyn. There is also no apparent shift in the slope of the final propagation phase, suggesting no significant effect on that aspect of mPTP induction. This suggests that αSyn primarily acts during the lag phase, and accordingly, the lag phase is significantly shortened in our αSyn-treated mitochondria.

Alteration of the lag phase by prefibrillar oligomers is also consistent with our observing a clear-cut respiratory substrate-dependent effect. Our results show that prefibrillar αSyn oligomers sensitize mitochondria to Ca^{2+}-induced permeability transition under complex I, but not complex II conditions. Even mild inhibition of complex I function could be detrimental to mitochondria depolarized by Ca^{2+} uptake. Restoration and maintenance of the $\Delta\Psi_m$, a primary

defense against mPTP opening, would require increased electron flow into a compromised complex I.

Flux into and/or through, an impaired complex I would be expected to lead to initiation of a feed-forward cycle of increasing reactive oxygen species (ROS) generation (which occurs only minimally at complex II) and worsening complex I function. Our working hypothesis is that increased ROS may result, at least locally, from interactions between αSyn and complex I, one of the primary sites of mitochondrial ROS generation (Y. Liu et al., 2002). ROS are a principal sensitizer to Ca^{2+}-induced permeability transition active during the second/lag phase. ROS can act by oxidizing thiol groups of protein components of the mPTP and by promoting oxidation of membrane lipids (Kowaltowski et al., 2001), a process that itself creates secondary mPTP inducers (Kristal et al., 1996; Stavrovskaya et al., 2010).

In summary, we demonstrate for the first time a direct link between a particular form of αSyn assembly and mitochondrial dysfunction in a system that models the Ca^{2+} phenotype of cells affected in PD. Our data suggest that, in the context of PD, alterations in αSyn proteostasis that destabilize physiological α-helical oligomers or otherwise shift the equilibrium toward aggregation-prone monomeric αSyn may drive the generation of mitotoxic prefibrillar oligomers that then contribute to complex I-dependent dysfunction and the resultant degeneration of Ca^{2+}-challenged neuronal populations.

REFERENCES

Baranov, S.V., Stavrovskaya, I.G., Brown, A.M., Tyryshkin, A.M., Kristal, B.S., 2008. Kinetic model for Ca2+-induced permeability transition in energized liver mitochondria discriminates between inhibitor mechanisms. J. Biol. Chem. 283, 665–676.

Bartels, T., Choi, J.G., Selkoe, D.J., 2011. α-Synuclein occurs physiologically as a helically folded tetramer that resists aggregation. Nature 477, 107–110.

Bender, A., Krishnan, K.J., Morris, C.M., Taylor, G.A., Reeve, A.K., Perry, R.H., Jaros, E., Hersheson, J.S., Betts, J., Klopstock, T., Taylor, R.W., Turnbull, D.M., 2006. High levels of mitochondrial DNA deletions in substantia nigra neurons in aging and Parkinson disease 38, 515–517.

Bernardi, P., Vassanelli, S., Veronese, P., Colonna, R., Szabó, I., Zoratti, M., 1992. Modulation of the mitochondrial permeability transition pore. Effect of protons and divalent cations. J. Biol. Chem. 267, 2934–2939.

Betarbet, R., Sherer, T.B., MacKenzie, G., Garcia-Osuna, M., Panov, A.V., Greenamyre, J.T., 2000. Chronic systemic pesticide exposure reproduces features of Parkinson's disease. Nat. Neurosci. 3, 1301–1306.

Burns, R.S., Chiueh, C.C., Markey, S.P., Ebert, M.H., Jacobowitz, D.M., Kopin, I.J., 1983. A primate model of parkinsonism: selective destruction of dopaminergic neurons in the pars compacta of the substantia nigra by N-methyl-4-phenyl-1,2,3,6-tetrahydropyridine. Proc. Natl. Acad. Sci. U.S.A. 80, 4546–4550.

Büttner, S., Habernig, L., Broeskamp, F., Ruli, D., Vögtle, F.N., Vlachos, M., Macchi, F., Küttner, V., Carmona-Gutierrez, D., Eisenberg, T., Ring, J., Markaki, M., Taskin, A.A., Benke, S., Ruckenstuhl, C., Braun, R., Van den Haute, C., Bammens, T., van der Perren, A., Fröhlich, K.-U., Winderickx, J., Kroemer, G., Baekelandt, V., Tavernarakis, N., Kovacs, G.G., Dengjel, J., Meisinger, C., Sigrist, S.J., Madeo, F., 2013. Endonuclease G mediates α-synuclein cytotoxicity during Parkinson's disease. EMBO J 32, 3041–3054.

Camilleri, A., Zarb, C., Caruana, M., Ostermeier, U., Ghio, S., Högen, T., Schmidt, F., Giese, A., Vassallo, N., 2013. Mitochondrial membrane permeabilisation by amyloid aggregates and protection by polyphenols. Biochim. Biophys. Acta 1828, 2532–2543.

Chance, B., Williams, G.R., 1955. Respiratory enzymes in oxidative phosphorylation. IV. The respiratory chain. J. Biol. Chem. 217, 429–438.

Chartier-Harlin, M.-C., Kachergus, J., Roumier, C., Mouroux, V., Douay, X., Lincoln, S., Levecque, C., Larvor, L., Andrieux, J., Hulihan, M., Waucquier, N., Defebvre, L., Amouyel, P., Farrer, M., Destée, A., 2004. Alpha-synuclein locus duplication as a cause of familial Parkinson's disease. Lancet 364, 1167–1169.

Chinta, S.J., Mallajosyula, J.K., Rane, A., Andersen, J.K., 2010. Mitochondrial α-synuclein accumulation impairs complex I function in dopaminergic neurons and results in increased mitophagy in vivo. Neurosci. Lett. 486, 235–239.

Choubey, V., Safiulina, D., Vaarmann, A., Cagalinec, M., Wareski, P., Kuum, M., Zharkovsky, A., Kaasik, A., 2011. Mutant A53T alpha-synuclein induces neuronal death by increasing mitochondrial autophagy. J. Biol. Chem. 286, 10814–10824.

Conway, K.A., Lee, S.J., Rochet, J.C., Ding, T.T., Williamson, R.E., Lansbury, P.T., 2000. Acceleration of oligomerization, not fibrillization, is a shared property of both alpha-synuclein mutations linked to early-onset Parkinson's disease: implications for pathogenesis and therapy. Proc. Natl. Acad. Sci. U.S.A. 97, 571–576.

Cremades, N., Cohen, S.I.A., Deas, E., Abramov, A.Y., Chen, A.Y., Orte, A., Sandal, M., Clarke, R.W., Dunne, P., Aprile, F.A., Bertoncini, C.W., Wood, N.W., Knowles, T.P.J., Dobson, C.M., Klenerman, D., 2012. Direct observation of the interconversion of normal and toxic forms of α-synuclein. Cell 149, 1048–1059.

Cullen, V., Sardi, S.P., Ng, J., Xu, Y.-H., Sun, Y., Tomlinson, J.J., Kolodziej, P., Kahn, I., Saftig, P., Woulfe, J., Rochet, J.-C., Glicksman, M.A., Cheng, S.H., Grabowski, G.A., Shihabuddin, L.S., Schlossmacher, M.G., 2011. Acid β-glucosidase mutants linked to Gaucher disease, Parkinson disease, and Lewy body dementia alter α-synuclein processing. Ann. Neurol. 69, 940–953.

Danzer, K.M., Haasen, D., Karow, A.R., Moussaud, S., Habeck, M., Giese, A., Kretzschmar, H., Hengerer, B., Kostka, M., 2007. Different species of alpha-synuclein oligomers induce calcium influx and seeding. Journal of Neuroscience 27, 9220–9232.

De Franceschi, G., Frare, E., Pivato, M., Relini, A., Penco, A., Greggio, E., Bubacco, L., Fontana, A., de Laureto, P.P., 2011. Structural and morphological characterization of

aggregated species of α-synuclein induced by docosahexaenoic acid. J. Biol. Chem. 286, 22262–22274.

Dettmer, U., Newman, A.J., Luth, E.S., Bartels, T., Selkoe, D., 2013. In vivo cross-linking reveals principally oligomeric forms of α-synuclein and β-synuclein in neurons and non-neural cells. J. Biol. Chem. 288, 6371–6385.

Devi, L., Raghavendran, V., Prabhu, B.M., Avadhani, N.G., Anandatheerthavarada, H.K., 2008. Mitochondrial import and accumulation of alpha-synuclein impair complex I in human dopaminergic neuronal cultures and Parkinson disease brain. Journal of Biological Chemistry 283, 9089–9100.

Di Lisa, F., Menabò, R., Canton, M., Barile, M., Bernardi, P., 2001. Opening of the mitochondrial permeability transition pore causes depletion of mitochondrial and cytosolic NAD+ and is a causative event in the death of myocytes in postischemic reperfusion of the heart. J. Biol. Chem. 276, 2571–2575.

Drescher, M., van Rooijen, B.D., Veldhuis, G., Subramaniam, V., Huber, M., 2010. A stable lipid-induced aggregate of alpha-synuclein. J. Am. Chem. Soc. 132, 4080–4082.

Fink, A.L., 2006. The aggregation and fibrillation of alpha-synuclein. Acc. Chem. Res. 39, 628–634.

Foehring, R.C., Zhang, X.F., Lee, J.C.F., Callaway, J.C., 2009. Endogenous calcium buffering capacity of substantia nigral dopamine neurons. Journal of Neurophysiology 102, 2326–2333.

Giehm, L., Svergun, D.I., Otzen, D.E., Vestergaard, B., 2011. Low-resolution structure of a vesicle disrupting α-synuclein oligomer that accumulates during fibrillation. Proceedings of the National Academy of Sciences 108, 3246–3251.

Goldberg, J.A., Guzman, J.N., Estep, C.M., Ilijic, E., Kondapalli, J., Sanchez-Padilla, J., Surmeier, D.J., 2012. Calcium entry induces mitochondrial oxidant stress in vagal neurons at risk in Parkinson's disease. Nat. Neurosci. 15, 1414–1421.

Guzman, J.N., Sanchez-Padilla, J., Wokosin, D., Kondapalli, J., Ilijic, E., Schumacker, P.T., Surmeier, D.J., 2010. Oxidant stress evoked by pacemaking in dopaminergic neurons is

attenuated by DJ-1. Nature. 468,1–7.

Hsu, L.J., Sagara, Y., Arroyo, A., Rockenstein, E., Sisk, A., Mallory, M., Wong, J., Takenouchi, T., Hashimoto, M., Masliah, E., 2000. alpha-synuclein promotes mitochondrial deficit and oxidative stress. Am. J. Pathol. 157, 401–410.

Janetzky, B., Hauck, S., Youdim, M.B., Riederer, P., Jellinger, K., Pantucek, F., Zöchling, R., Boissl, K.W., Reichmann, H., 1994. Unaltered aconitase activity, but decreased complex I activity in substantia nigra pars compacta of patients with Parkinson's disease. Neuroscience Letters 169, 126–128.

Kara, E., Lewis, P.A., Ling, H., Proukakis, C., Houlden, H., Hardy, J., 2013. α-Synuclein mutations cluster around a putative protein loop. Neurosci. Lett. 546, 67–70.

Karpinar, D.P., Balija, M.B.G., Kügler, S., Opazo, F., Rezaei-Ghaleh, N., Wender, N., Kim, H.-Y., Taschenberger, G., Falkenburger, B.H., Heise, H., Kumar, A., Riedel, D., Fichtner, L., Voigt, A., Braus, G.H., Giller, K., Becker, S., Herzig, A., Baldus, M., Jäckle, H., Eimer, S., Schulz, J.B., Griesinger, C., Zweckstetter, M., 2009. Pre-fibrillar alpha-synuclein variants with impaired beta-structure increase neurotoxicity in Parkinson's disease models. EMBO J 28, 3256–3268.

Keeney, P.M., Xie, J., Capaldi, R.A., Bennett, J.P., 2006. Parkinson's disease brain mitochondrial complex I has oxidatively damaged subunits and is functionally impaired and misassembled. Journal of Neuroscience 26, 5256–5264.

Kim, H.-J., 2013. Alpha-Synuclein Expression in Patients with Parkinson“s Disease: A Clinician”s Perspective. Exp Neurobiol 22, 77–83.

Kowaltowski, A.J., Castilho, R.F., Vercesi, A.E., 2001. Mitochondrial permeability transition and oxidative stress. FEBS Letters 495, 12–15.

Kristal, B.S., Park, B.K., Yu, B.P., 1996. 4-Hydroxyhexenal is a potent inducer of the mitochondrial permeability transition. J. Biol. Chem. 271, 6033–6038.

Langston, J.W., Ballard, P.A., 1983. Parkinson's disease in a chemist working with 1-methyl-4-phenyl-1,2,5,6-tetrahydropyridine. N. Engl. J. Med. 309, 310.

Lemasters, J.J., Qian, T., Elmore, S.P., Trost, L.C., Nishimura, Y., Herman, B., Bradham, C.A., Brenner, D.A., Nieminen, A.L., 1998. Confocal microscopy of the mitochondrial permeability transition in necrotic cell killing, apoptosis and autophagy. Biofactors 8, 283–285.

Liu, G., Zhang, C., Yin, J., Li, X., Cheng, F., Li, Y., Yang, H., Uéda, K., Chan, P., Yu, S., 2009. α-Synuclein is differentially expressed in mitochondria from different rat brain regions and dose-dependently down-regulates complex I activity. Neurosci. Lett. 454, 187–192.

Liu, Y., Fiskum, G., Schubert, D., 2002. Generation of reactive oxygen species by the mitochondrial electron transport chain. Journal of Neurochemistry 80, 780–787.

Luk, K.C., Kehm, V., Carroll, J., Zhang, B., O'Brien, P., Trojanowski, J.Q., Lee, V.M.-Y., 2012. Pathological α-synuclein transmission initiates Parkinson-like neurodegeneration in nontransgenic mice. Science 338, 949–953.

Luk, K.C., Song, C., O'Brien, P., Stieber, A., Branch, J.R., Brunden, K.R., Trojanowski, J.Q., Lee, V.M.-Y., 2009. Exogenous alpha-synuclein fibrils seed the formation of Lewy body-like intracellular inclusions in cultured cells. Proceedings of the National Academy of Sciences 106, 20051–20056.

Martin, L.J., Pan, Y., Price, A.C., Sterling, W., Copeland, N.G., Jenkins, N.A., Price, D.L., Lee, M.K., 2006. Parkinson's disease alpha-synuclein transgenic mice develop neuronal mitochondrial degeneration and cell death. Journal of Neuroscience 26, 41–50.

Martin, L.J., Semenkow, S., Hanaford, A., Wong, M., 2013. The mitochondrial permeability transition pore regulates Parkinson's disease development in mutant α-synuclein transgenic mice. Neurobiol. Aging 10.1016–j.neurobiolaging.2013.11.008.

Nakamura, K., Nemani, V.M., Azarbal, F., Skibinski, G., Levy, J.M., Egami, K., Munishkina, L., Zhang, J., Gardner, B., Wakabayashi, J., Sesaki, H., Cheng, Y., Finkbeiner, S., Nussbaum, R.L., Masliah, E., Edwards, R.H., 2011. Direct membrane association drives mitochondrial fission by the Parkinson disease-associated protein alpha-synuclein. J. Biol. Chem. 286, 20710–20726.

Natalello, A., Benetti, F., Doglia, S.M., Legname, G., Grandori, R., 2011. Compact conformations of α-synuclein induced by alcohols and copper. Proteins 79, 611–621.

Näsström, T., Fagerqvist, T., Barbu, M., Karlsson, M., Nikolajeff, F., Kasrayan, A., Ekberg, M., Lannfelt, L., Ingelsson, M., Bergström, J., 2011. The lipid peroxidation products 4-oxo-2-nonenal and 4-hydroxy-2-nonenal promote the formation of α-synuclein oligomers with distinct biochemical, morphological, and functional properties. Free Radical Biology and Medicine 50, 428–437.

Parihar, M.S., Parihar, A., Fujita, M., Hashimoto, M., Ghafourifar, P., 2008. Mitochondrial association of alpha-synuclein causes oxidative stress. Cell. Mol. Life Sci. 65, 1272–1284.

Parker, W.D., Boyson, S.J., Parks, J.K., 1989. Abnormalities of the electron transport chain in idiopathic Parkinson's disease. Ann Neurol. 26, 719–723.

Petit, P.X., Goubern, M., Diolez, P., Susin, S.A., Zamzami, N., Kroemer, G., 1998. Disruption of the outer mitochondrial membrane as a result of large amplitude swelling: the impact of irreversible permeability transition. FEBS Letters 426, 111–116.

Rhinn, H., Qiang, L., Yamashita, T., Rhee, D., Zolin, A., Vanti, W., Abeliovich, A., 2012. Alternative α-synuclein transcript usage as a convergent mechanism in Parkinson's disease pathology. Nature Communications 3, 1084.

Schapira, A.H., Cooper, J.M., Dexter, D., Jenner, P., Clark, J.B., Marsden, C.D., 1989. Mitochondrial complex I deficiency in Parkinson's disease. Lancet 1, 1269.

Scorrano, L., Petronilli, V., Di Lisa, F., Bernardi, P., 1999. Commitment to apoptosis by GD3 ganglioside depends on opening of the mitochondrial permeability transition pore. J. Biol. Chem. 274, 22581–22585.

Shavali, S., Brown-Borg, H.M., Ebadi, M., Porter, J., 2008. Mitochondrial localization of alpha-synuclein protein in alpha-synuclein overexpressing cells. Neuroscience Letters 439, 125–128.

Singleton, A.B., Farrer, M., Johnson, J., Singleton, A., Hague, S., Kachergus, J., Hulihan, M., Peuralinna, T., Dutra, A., Nussbaum, R., Lincoln, S., Crawley, A., Hanson, M., Maraganore, D., Adler, C., Cookson, M.R., Muenter, M., Baptista, M., Miller, D., Blancato, J., Hardy, J., Gwinn-Hardy, K., 2003. alpha-Synuclein locus triplication causes Parkinson's disease. Science 302, 841.

Spillantini, M.G., Schmidt, M.L., Lee, V.M., Trojanowski, J.Q., Jakes, R., Goedert, M., 1997. Alpha-synuclein in Lewy bodies. Nature 388, 839–840.

Stavrovskaya, I.G., Baranov, S.V., Guo, X., Davies, S.S., Roberts, L.J., Kristal, B.S., 2010. Reactive gamma-ketoaldehydes formed via the isoprostane pathway disrupt mitochondrial respiration and calcium homeostasis. Free Radical Biology and Medicine 49, 567–579.

Stichel, C.C., Zhu, X.-R., Bader, V., Linnartz, B., Schmidt, S., Lübbert, H., 2007. Mono- and double-mutant mouse models of Parkinson's disease display severe mitochondrial damage. Human Molecular Genetics 16, 2377–2393.

Surmeier, D.J., Schumacker, P.T., 2013. Calcium, Bioenergetics, and Neuronal Vulnerability in Parkinson's Disease 288, 10736–10741.

Volles, M.J., Lansbury, P.T., 2002. Vesicle permeabilization by protofibrillar alpha-synuclein is sensitive to Parkinson's disease-linked mutations and occurs by a pore-like mechanism. Biochemistry 41, 4595–4602.

Volles, M.J., Lansbury, P.T., 2003. Zeroing in on the pathogenic form of alpha-synuclein and its mechanism of neurotoxicity in Parkinson's disease. Biochemistry 42, 7871–7878.

Volles, M.J., Lee, S.J., Rochet, J.C., Shtilerman, M.D., Ding, T.T., Kessler, J.C., Lansbury, P.T., 2001. Vesicle permeabilization by protofibrillar alpha-synuclein: implications for the pathogenesis and treatment of Parkinson's disease. Biochemistry 40, 7812–7819.

Wang, W., Perovic, I., Chittuluru, J., Kaganovich, A., Nguyen, L.T.T., Liao, J., Auclair, J.R., Johnson, D., Landeru, A., Simorellis, A.K., Ju, S., Cookson, M.R., Asturias, F.J., Agar, J.N., Webb, B.N., Kang, C., Ringe, D., Petsko, G.A., Pochapsky, T.C., Hoang, Q.Q., 2011. A soluble α-synuclein construct forms a dynamic tetramer. Proceedings of the National Academy of Sciences 108, 17797–17802.

Weinreb, P.H., Zhen, W., Poon, A.W., Conway, K.A., Lansbury, P.T., 1996. NACP, a protein implicated in Alzheimer's disease and learning, is natively unfolded. Biochemistry 35, 13709–13715.

Westphal, C.H., Chandra, S.S., 2013. Monomeric synucleins generate membrane curvature. J. Biol. Chem. 288, 1829–1840.

Winner, B., Jappelli, R., Maji, S.K., Desplats, P.A., Boyer, L., Aigner, S., Hetzer, C., Loher, T., Vilar, M., Campioni, S., Tzitzilonis, C., Soragni, A., Jessberger, S., Mira, H., Consiglio, A., Pham, E., Masliah, E., Gage, F.H., Riek, R., 2011. In vivo demonstration that alpha-synuclein oligomers are toxic. Proceedings of the National Academy of Sciences 108, 4194–4199.

Chapter 3

Purification and Characterization of α-Synuclein from Human Brain

Contributions:

Experiments were designed by Eric Luth, Tim Bartels, and Dennis Selkoe.

Crosslinking of intact brain cells was performed by Ulf Dettmer and Andrew Newman.

ELISAs were performed by Nora Kim.

All other experiments were performed by Eric Luth.

Abstract

Despite decades of research, the physiological function of the Parkinson's disease-related protein α-synuclein (αSyn) is not well understood. Almost all of the *in vitro* studies aimed at addressing this question have utilized bacterially-expressed recombinant protein with the assumption that αSyn exists in the human brain under non-pathological conditions in a similarly unfolded and monomeric state. Over the past few years, we have published multiple reports demonstrating that αSyn exits in neurons and other cell types a metastable oligomer that principally sizes as a tetramer. In contrast to recombinant αSyn, physiological oligomers purified from human erythrocytes and neuroblastoma cells are α-helical and aggregation resistant. In light of these studies, we sought to purify and characterize native αSyn from the tissue most relevant to neurologic disease, human brain. We successfully purified soluble αSyn from postmortem non-diseased human cortex using a combination of ammonium sulfate precipitation, gel filtration, ion exchange, and affinity chromatography. Crosslinking of the starting material and partially purified samples indicated that there are abundant αSyn oligomers in the human brain but that they can be destabilized under certain conditions. CD spectroscopy showed that purified, brain-derived αSyn contained significantly more helical content than recombinant protein. We envision that a slightly modified version of this protocol will be useful for obtaining helical αSyn for testing in functional assays and for identifying conditions that lead to the stabilization of these oligomers.

Introduction

α-Synuclein (αSyn) was first discovered in the *Torpedo* electric organ (Maroteaux, 1991), and subsequent studies have shown that it is highly expressed throughout the nervous system of

vertebrates, particularly in the brain (Iwai et al., 1995). Interest in the protein intensified after it was discovered that missense mutations in and genomic multiplications of *SNCA*, the gene that encodes αSyn, are sufficient to cause autosomal dominant forms of Parkinson's disease (PD) (Chartier-Harlin et al., 2004; Kara et al., 2013; Singleton et al., 2003). Moreover, αSyn was identified as the main component of Lewy bodies and Lewy neurites, insoluble protein aggregates that form the main cytopathological hallmark of PD and other synucleinopathies (Spillantini et al., 1997). Due to its prominent role in neurodegenerative diseases, there have been extensive investigations into possible pathological activities of αSyn with particular emphasis on the ability of this normally soluble protein to aggregate (Breydo et al., 2012; Cookson and van der Brug, 2008; Volles and Lansbury, 2003).

The precise physiological function of αSyn is still unclear. Though αSyn is primarily localized to the presynaptic terminal (George et al., 1995; Iwai et al., 1995), the vast majority of the protein appears cytosolic after cellular fractionation (Dettmer et al., 2013; George et al., 1995; Kahle et al., 2000). This indicates that associations with synaptic membranes are likely weak and/or transient. Animals lacking αSyn display relatively subtle deficits in synaptic function. Studies of knockout mice point to αSyn as a negative regulator of synaptic vesicle release under conditions of elevated neuronal activity (Abeliovich et al., 2000; Yavich et al., 2006; 2004). Consistent with this idea, mild overexpression of WT αSyn has been shown to interfere with synaptic vesicle exocytosis (Larsen et al., 2006; Nemani et al., 2010), though some other reported synaptic vesicle phenotypes may be related to the formation of toxic species (Boassa et al., 2013; Scott et al., 2010). It has also been proposed that αSyn acts to modulate membrane remodeling (Kamp et al., 2010; Varkey et al., 2010; Westphal and Chandra, 2013), perhaps as a chaperone for the SNARE complex (Burré et al., 2010), though biochemical

interaction with SNARE proteins remains controversial (Chandra et al., 2005; Dettmer et al., 2013; DeWitt and Rhoades, 2013). Well-controlled in vitro studies of pure αSyn with various membrane lipid and protein compositions could help elucidate a more defined role for the protein and aid in differentiating between physiological and pathological activities.

Due to initial studies characterizing the bacterially expressed recombinant protein as a natively unfolded monomer (Kim, 1997; Weinreb et al., 1996), the field has operated under the assumption that αSyn exists exclusively in this form under physiological conditions. As such, *in vitro* investigations into the function of αSyn have continued to employ unfolded recombinant protein. We recently demonstrated that αSyn also exists physiologically as an aggregation-resistant, helically folded tetramer based on a characterization of αSyn purified under non-denaturing conditions from human erythrocytes and neuroblastoma cells (Bartels et al., 2011). In follow-up studies using an intact cell crosslinking protocol that I helped develop (see Appendix 3), we showed that abundant non-pathological oligomers of αSyn, as well as the aggregation-resistant β-synuclein (βSyn), could be trapped in a variety of cells including primary neurons (Dettmer et al., 2013; Newman et al., 2013). A thorough understanding of how neuronal αSyn functions under non-pathological conditions will require *in vitro* examination of this emerging form of the protein.

While the biophysical and functional properties of monomeric αSyn have been extensively studied *in vitro*, and we have previously characterized α-helical tetramers isolated from human red blood cells, nothing is known about the properties of the helical αSyn oligomers found in the brain. A recent study described a purification of αSyn from mouse brain, albeit with limited details on the purification procedure (Burré et al., 2013). The amino acid sequence of mouse αSyn differs from that of human αSyn, most notably at residue 53 where rodents possess

a threonine (Hsu et al., 1998), reminiscent of the PD-causing A53T missense mutation in humans (Polymeropoulos et al., 1997). We therefore sought to develop a protocol to purify soluble αSyn from human brain, with the hope that characterizing isolated helical αSyn will aid in the study of the function of physiological oligomers and serve as a comparison to pathological conformations present in synucleinopathies. Here we describe a method for the purification of αSyn from postmortem human cortex. We show that this protocol yields pure αSyn with greater helical content than recombinant protein but that the degree of helicity is variable. Crosslinking of the starting material and partially purified samples followed by SDS-PAGE/WB revealed that αSyn oligomers are abundant in intact human neurons and are readily detectible at intermediate stages of purification; however, chromatography steps designed to purify αSyn to homogeneity may lead to the destabilization of native oligomers.

Experimental Procedures

Purification of Synucleins from Human Brain

Homogenization and ultracentrifugation:

Frozen cortices with no evidence of αSyn pathology were provided by Dr. M. Frosch (Massachusetts General Hospital/Harvard NeuroDiscovery Center) under an institutional review board (IRB)-approved protocol. Approximately 20 g of white and gray matter from frozen cortical slices was cut into ~1 cm^3 pieces and placed in a glass homogenizer 3.5 volumes phosphate buffered saline (PBS) with protease inhibitor cocktail (0.5 mg/ml leupeptin, aprotinin, and 0.2 mg/ml pepstatin-A). Homogenization was performed with 24 strokes of a Teflon-coated pestle in an Overhead Stirrer (Wheaton) at power level 2.4. Total homogenates were centrifuged at 230,000 *g* for 50 min at 4°C to collect the truly soluble protein.

Ammonium sulfate precipitation (ASP):

Ammonium sulfate was added to the supernatant of the ultracentrifugation step to a final concentration of 55%, after which samples were incubated at 4°C for 60 min under nutation, and then centrifuged for 20 min at 20,000 *g* at 4°C to pellet precipitated αSyn. At this stage, αSyn-containing pellets were either dried and stored at -80°C or immediately processed for size exclusion chromatography.

Size exclusion chromatography (SEC):

Pellets were resuspended in 5-8 ml of anion exchange buffer A (20 mM HEPES pH 8, 25 mM NaCl, 1 mM EDTA) and injected onto a Superdex 200 XK26/100 gel filtration column (GE Healthcare) that had been equilibrated in anion exchange buffer A. The column was washed with anion exchange buffer A at 1 ml/min, and 1.5 ml fractions were collected. SDS-PAGE/Western blotting (WB) was performed (see below) to identify αSyn-containing fractions.

Anion exchange chromatography (AEC):

SEC fractions that contained αSyn but minimal amounts of key contaminating proteins were pooled and loaded onto an equilibrated MonoQ anion exchange column (GE Healthcare) at a rate of 0.5 ml/min. αSyn was eluted using a gradient from 100% anion exchange buffer A to 50% anion exchange buffer A and 50% anion exchange buffer B (20 mM HEPES pH 8, 1,000 mM NaCl, 1 mM EDTA). αSyn eluted at approximately 300 mM NaCl. As before, fractions were probed for the presence of αSyn by SDS-PAGE/WB and for purity by SDS-

PAGE/Coomassie staining. AEC fractions that contained αSyn, but not βSyn were used for thiopropyl Sepharose 6b incubation.

Thiopropyl Sepharose 6b (TS6b) incubation:

TS6b resin (GE Healthcare) was prepared by washing dried beads with 200 ml MilliQ water/0.25 g of dried beads over filter paper. Hydrated beads were then made into slurry by adding MilliQ water to adjust the volume to 1 ml slurry/0.25 g dried beads. αSyn-containing AEC fractions were incubated with TS6b resin at a ratio of 1.5:1 overnight at 4°C with circular rotation. The αSyn-containing supernatant was collected by centrifugation for 5 min at 1,500 *g* at 4°C.

β-synuclein:

Purification of βSyn was performed identically to αSyn purification except that TS6b was incubated with AEC fractions that contained βSyn, but not αSyn.

Circular Dichroism (CD) Spectroscopy:

Following purification, αSyn was exchanged into 10 mM ammonium acetate using Zeba spin desalting columns (Thermo Fisher), lyophilized, and resuspended in 10 mM ammonium acetate at a concentration of approximately 10 uM. αSyn samples were added to a 1 mm path length quartz cuvette and analyzed using a J-815 CD spectrometer (Jasco). Spectra from at least 7 recordings were averaged. A background spectrum of 10 mM ammonium acetate was subtracted from all αSyn spectra. Calculations of helicity were performed using the following formula, as in (Scholtz et al., 1991): $f_{helix} = ([\Theta]_{222} - [\Theta]_{coil})/([\Theta]_{helix} - [\Theta]_{coil})$ where % helicity =

(100)(f_{helix}). The mean-residue ellipticities at 222 nm for completely helical and unfolded/random coil peptides were obtained from $[\Theta]_{helix} = -40{,}000(1-2.5/n) + 100T/°C$ and $[\Theta]_{coil} = 640 - 45T/°C$. $n = 140$, the number of amino acids in the αSyn polypeptide, and $T = 20°C$

Mass Spectrometry (MS):

Gel samples submitted for digestion by trypsin were digested using method described previously (Shevchenko et al., 1996). Samples were analyzed on an ABI model 4800 TOF/TOF Matrix Assisted Laser Desorption (MALDI) mass spectrometer Applied Biosystems, Foster City, CA). It is a research grade time of flight instrument equipped with delayed extraction technology and a reflectron for resolution of up to 20,000 (FWHH) with MSMS capability by way of tandem TOF/TOF technology. Samples previously digested were prepared by mixing 0.5 µl of sample with 0.5 µl of alpha cyano-4-hydroxy-trans-cinnamic acid (10mg/ml in 70% acetonitrile 0.1%TFA). The sample is rinsed after drying with 0.1%TFA. Intact mass analysis is also performed on the 4800 but run in linear mode, and spotted using 3,5-Dimethoxy-4-hydroxycinnamic acid (10mg/ml in 70% acetonitrile 0.1%TFA) and calibrated using an external calibration. Data was analyzed using the Mascot algorithm by searching against the updated non-redundant database from NCBI.

Determination of protein concentrations:

Total protein concentrations were determined by BCA assay (Thermo Scientific) according to the manufacturer's instructions. αSyn concentrations were determined using an in-house developed sandwich ELISA for total αSyn. 96-well Multi-Array High Bind plates (MSD, Meso Scale Discovery) were coated with the capture antibody 2F12 diluted (6.7 ng/µl) in Tris-

buffered saline with 0.1% Tween-20 (TBS-T) in 30 µl volumes/well and incubated at 4°C overnight. Following emptying of the wells, plates were blocked for 1 h at RT in blocking buffer (5% MSD Blocker A; TBS-T). After 3 washes with TBS-T, samples diluted in TBS-T with 1% MSD Blocker A and 0.5% nonidet P-40 were loaded and incubated at 4°C overnight. Sulfo-tagged SOY1 mAb (detection Ab) was generated using Sulfo-Tag-NHS-Ester (MSD), diluted in blocking buffer (6.7 ng/µl), added to the plate (30 µl volumes/well) and shaken for 1 h at RT. Following 3 washes, MSD Reader buffer was added and the plates were immediately measured using a MSD Sector 2400 imager.

Crosslinking:

For crosslinking of purified or partially purified samples, 1 µl Dithiobis[succinimidyl propionate] (DSP) or disuccinimidyl glutarate (DSG) dissolved in dimethyl sulfoxide was added to 50 µl of sample to a variety of concentrations noted in the text and figure legends. Typically, and to adjust for changes in total protein concentration, a starting concentration of 0.5 mM DSG/DSP was used for total homogenates, total soluble protein fractions (supernatants from the ultracentrifugation step), and ammonium sulfate precipitated samples; and 0.25 mM was used for SEC and AEC fractions. Upon addition of DSP or DSG, samples were incubated quiescently at 37°C for 30 min, after which 2.5 µl of 1 M Tris pH 7.6 was added and samples were incubated at room temperature for 15 min under nutation to quench crosslinking reactions.

For intact-cell crosslinking of human brain tissue, samples (human cortical biopsy) were finely minced by two rounds on a McIlwain Tissue Chopper (model MTC/2E, Mickle Laboratory Engineering Co., blade distance set to 100 µm); the sample was turned by 90° for the second round of mincing. Human cerebral cortex biopsies were obtained fresh from middle-aged

subjects undergoing focal ablative surgery for epilepsy who were otherwise healthy and had no evidence of synucleinopathy or other neurodegenerative disease; the sample was obtained from unaffected, discarded tissue and analyzed fresh (storage on ice <1hr). The minced brain samples were transferred to 15 ml tubes containing ~5 ml PBS/PI, and the solution containing the intact brain pieces was resuspended by gentle shaking without homogenization. From this suspension, aliquots were transferred to 1.5 mL tubes, which were spun at 1,500 g for 5 min at RT. Supernatants were discarded, and pellets (bits of intact tissue) underwent crosslinking, routinely at a ratio of 1000 µl of 1 mM DSG in PBS/PI per 100 mg tissue or else 1000 µl of 2 mM DSP/100 mg tissue. The suspensions were incubated at 37°C for 30 min while shaking, followed by spinning at 1,500 g for 5 min at RT. After crosslinking, the supernatant was discarded, and the pellet was resuspended in PBS/PI (in 25-50% of the volume of the crosslinking solution), followed by sonication (Sonic Dismembrator model 300, Fisher Scientific; microtip setting = 40; 2 x 15 sec). Spinning at 800 g for 5 min at 4°C yielded the postnuclear supernatant. A second spin at 100,000 g for 60 min at 4°C yielded the cytosolic material in the supernatant. Crosslinked samples were stored on ice (for immediate use) or at -20°C.

SDS-PAGE for Western blotting (WB) or Coomassie staining:

Samples were prepared using MilliQ water and 4x sample buffer containing LDS plus 20% β-mercaptoethanol (βME) (for crosslinked samples), or without βME (for non-crosslinked samples). Samples were electrophoresed on Nu-PAGE 4-12% Bis-Tris gels (Life Technologies) with MES-SDS running buffer.

Western blotting (WB) and Coomassie Staining:

Gels were then transferred onto 0.45 μm Immobilon-P PVDF membranes (Millipore) for 60 min at 400 mA constant current at 4°C in transfer buffer consisting of 25 mM Tris, 192 mM glycine, and 20% methanol. After transfer, membranes were blocked in 5% non-fat milk in PBS with 0.1% v/v Tween-20 (PBS-T) for 30 min at room temperature and then incubated in primary antibody either overnight at 4 °C or for 60 min at room temperature. Membranes were then washed 3 times for 5 min in PBS-T, incubated with secondary antibody, washed 3 more times for 5 min in PBS-T, and then developed with ECL Plus or ECL Prime (GE-Amersham) according to the manufacturer's directions. For Coomassie staining, gels were incubated in MilliQ water for 10 min and then stained using Gel Code Blue for 45 min at room temperature. Gels were destained by washing with MilliQ water.

Storage Condition Testing:

SEC fractions containing αSyn were aliquoted into either standard or low-binding centrifuge tubes and stored at room temperature (RT), 4°C, -20°C, or -80°C. Aliquots were periodically probed for αSyn using SDS-PAGE/WB with the 2F12 antibody. Aliquots stored at RT and 4°C were sampled at day 0, and then once a day for 5 additional days. Aliquots stored at -20°C and -80°C were sampled prior to freezing and then following each of 5 freeze/thaw cycles.

Antibodies:

2F12 and SOY1, monoclonal mouse antibodies (mAb) against αSyn were generated by immunizing αSyn -/- (KO) mice with αSyn purified from human erythrocytes. Hybridoma cell lines were generated by fusion of mouse splenocytic B lymphocytes with X63-Ag8.653 myeloma cells. Antibodies were generated and purified from hybridoma supernatant by Cell

Essentials (Boston, MA). For WB, 2F12 was used at 0.18 μg/ml in 5% milk. Another mouse monoclonal AB, 15G7, was generously provided by the Haass lab (Kahle et al., 2000), and the rabbit polyclonal αSyn antibody C20 was purchased from Santa Cruz. The following commercially available antibodies were also used**:** mAb EP1537Y to β-synuclein (Novus Biologicals) and mAb NSE-P1 to γ-enolase (Santa Cruz).

Results

Purification of αSyn from human brain:

We designed and carried out a 5-step protocol for the purification of soluble αSyn from the cerebral cortex of humans with no evidence of αSyn pathology (Figure 3.1A). We detected abundant αSyn in cortical white matter in addition to gray matter (Figure 3.2A) and therefore included both in our preparations. To minimize the possibility disrupting intermolecular interactions within αSyn oligomers we avoided the use of detergents during our purification. As such, total cortical matter was homogenized in PBS plus protease inhibitors. Though this method does not extract membrane-associated αSyn, we and others have previously shown that the protein is predominantly (≥90%) localized to the cytosol (Dettmer et al., 2013; George et al., 1995; Kahle et al., 2000). Using an αSyn-specific, in-house developed ELISA coupled with total protein assays, we estimated that αSyn comprised ~0.3% of total cytosolic protein (Figure 3.2B), in line with published findings (Iwai et al., 1995). PBS homogenates were spun at 240,000g to pellet all membrane components and insoluble protein. Since we were interested only in physiological forms of αSyn, we wanted to avoid all possible contribution from αSyn found in insoluble Lewy bodies should they exist in this non-diseased tissue. Ammonium

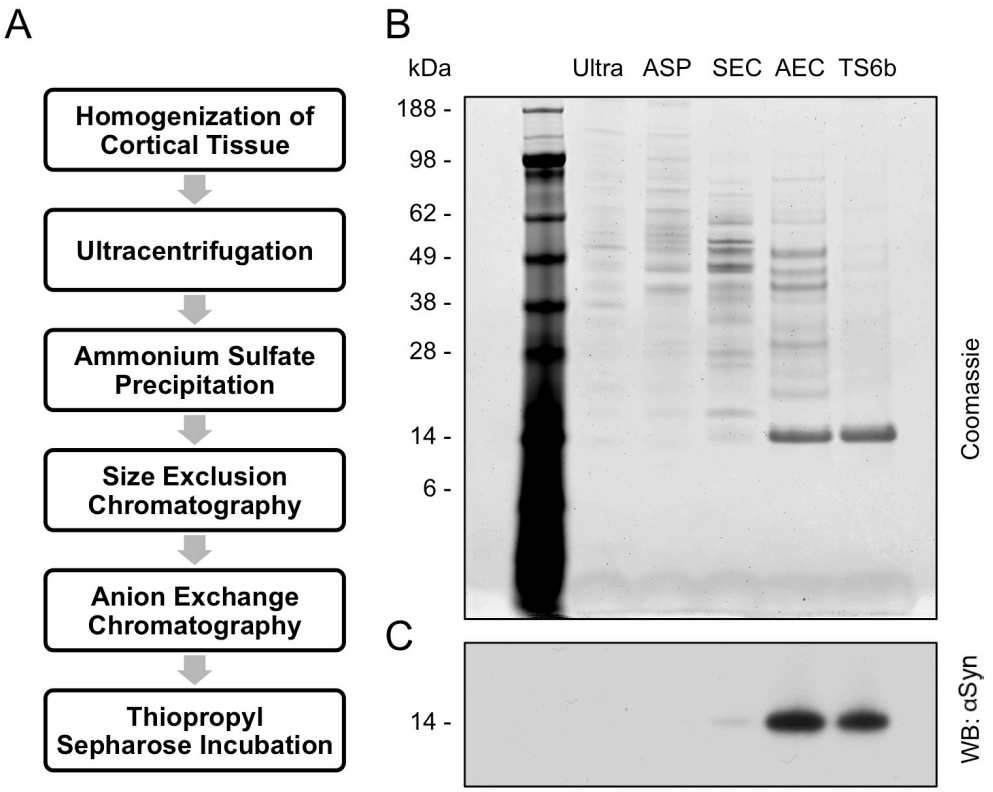

Figure 3.1: Purification of αSyn from human cortex.

A. Schematic of the strategy used to purify αSyn from human cortex. B. 400 ng of samples from after each stage of the purification were run on SDS-PAGE and stained with Coomassie blue. C. 30 ng of samples from after each purification step were run on SDS-PAGE and probed for αSyn using the antibody 2F12. All samples were taken after the chromatography step listed at the top of their respective lanes. Ultra = ultracentrifugation, ASP = ammonium sulfate precipitation, SEC = size exclusion chromatography, AEC = anion exchange chromatography, TS6b = thiopropyl Sepharose 6b incubation.

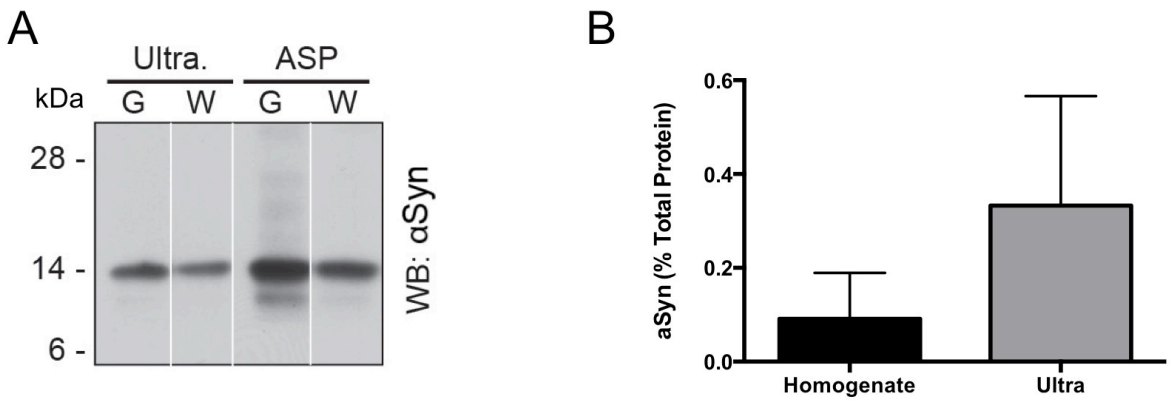

Figure 3.2: Abundant αSyn is present in cortical gray and white matter.

A. Cortical gray and white matter both contain αSyn. Gray matter (G) and white matter (W) were separated prior to homogenization and processed through the ammonium sulfate purification (ASP) step. Protein normalized samples of gray and white matter from after the ultracentrifugation (ultra.) and ASP steps were run on SDS-PAGE and probed for αSyn. B. The total protein concentration as determined by BCA assay and αSyn content as measured by ELISA were used to calculate the percentage of αSyn in crude cortical homogenates and the supernatant following ultracentrifugation. Error bars represent the standard deviation from 4 independent experiments**.**

sulfate was added to the supernatant to a final concentration of 55% in order to precipitate aSyn quantitatively. The resuspended pellet was applied to a Superdex 200 column for size exclusion chromatography (SEC), and fractions containing aSyn were pooled and further purified using anion exchange chromatography (AEC). αSyn-containing fractions were collected, and purification was completed using thiopropyl Sepharose 6b (TS6b) resin in batch mode. Since aSyn lacks cysteines, it remained in the supernatant, while the few remaining contaminants bound to this resin and were pelleted by centrifugation.

Samples from each stage of the purification were protein normalized and run on SDS-PAGE (Figure 3.1B,C). Coomassie blue staining of ~400 ng of total protein first revealed a 14 kDa band (the molecular weight of the αSyn monomer) corresponding to αSyn after SEC. This band was greatly enriched following AEC, and was the only band remaining following the final TS6b pull-down of contaminating proteins (Figure 3.1B). Western blotting of 30 ng of protein with the mouse monoclonal aSyn antibody 2F12 matched what was observed with Coomassie blue staining: the 14 kDa αSyn band was strongly enhanced after AEC and was retained by incubation with thiopropyl Sepharose 6b (Figure 3.1C). Importantly, we tested a panel of three aSyn antibodies and detected the purified protein with each of them (Figure 3.3A), but not with an antibody directed against its homologue, β-synuclein (βSyn) (Figure 3.3B). Next we confirmed the purity of αSyn using mass spectrometry. Enzymatic digestion and LC-MS/MS of the final supernatant following thiopropyl Sepharose incubation identified aSyn as the only human protein present in the sample. Analysis of the digested fragments revealed 65% coverage of the amino acid sequence and the presence of an N-terminal acetylation (Figure 3.3C), as we had previously observed for aSyn purified from human erythrocytes (Bartels et al., 2011). No additional post-translational modifications were detected. Intact mass spectrometry (which is

Figure 3.3: Enrichment of αSyn during purification.

A. Increasing concentrations of purified αSyn were run on SDS-PAGE and probed with 3 different monoclonal αSyn antibodies, 2F12, 15G7, and C20 which all detect the final purified sample. B. βSyn could not be detected in the AEC fraction and subsequent supernatant from TS6b incubation but was observed in the AEC start and all previous steps. C. Mass spectrometry was performed on the final purified sample. Following TS6b incubation, the sample was loaded for SDS-PAGE and the gel was stopped as soon as the sample entered the gel. The entire sample was excised, digested, and analyzed by mass spectrometry. The αSyn sequence covered by observed peptide fragments is shown in red. D. The fold enrichment of αSyn after each purification step was calculated by dividing the percentage of total protein that is αSyn at each step by the percentage of αSyn in the starting homogenate. E. The percent of soluble αSyn remaining after each chromatography step was plotted. On average, approximately 7.5% of the total soluble αSyn was ultimately collected. Error bars represent the standard deviation from 4 independent experiments.

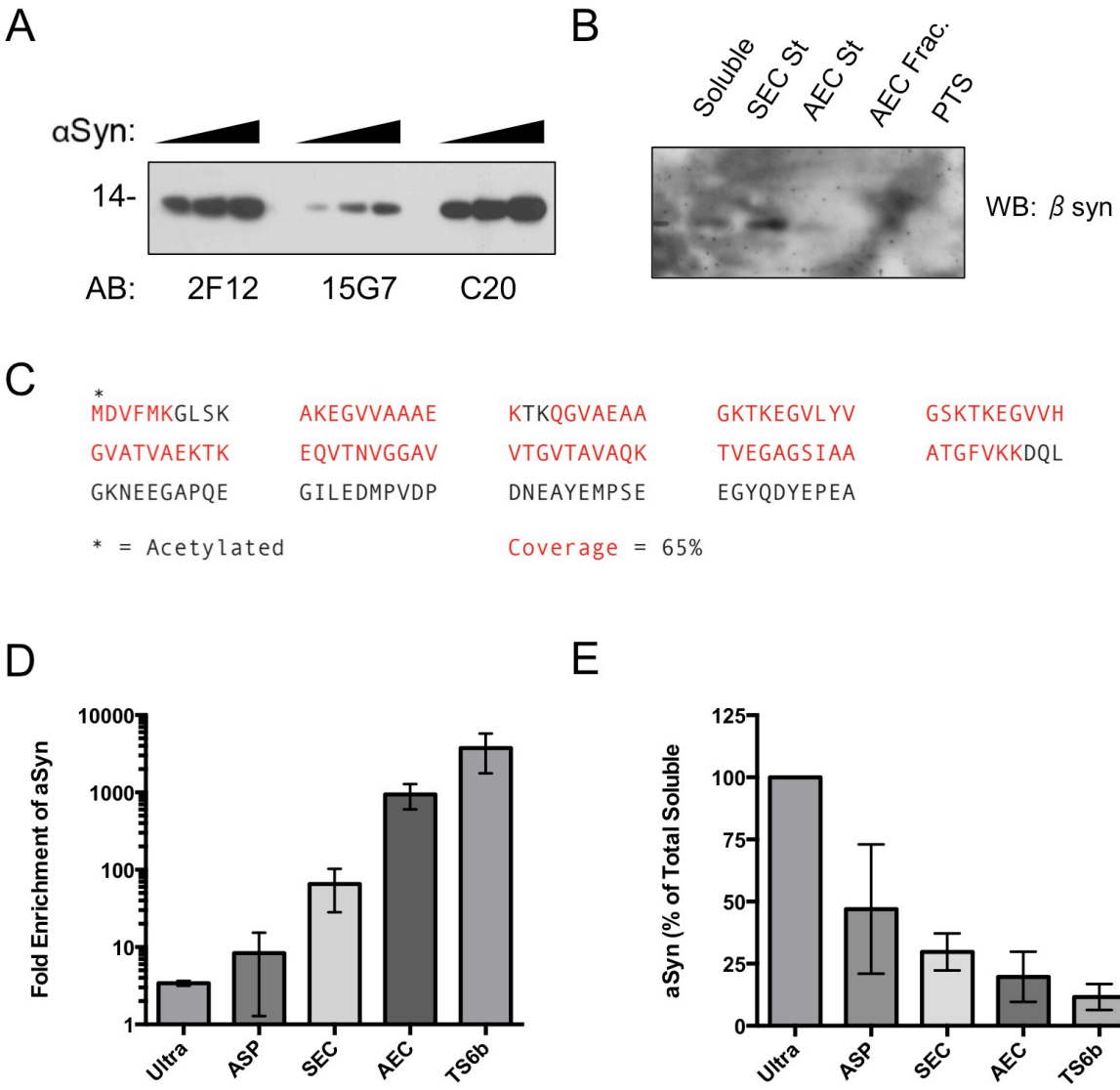

Figure 3.3 (Continued): Enrichment of αSyn during purification.

performed under conditions that do not maintain intermolecular interactions) revealed a molecular mass of 14,527 Da**,** consistent with an N acetylated protein without additional post-translational modifications.

Total protein and aSyn content were measured after each stage of purification by a BCA assay and an in-house developed, αSyn-specific sandwich ELISA, respectively. From these results, we calculated the progressive degrees of enrichment of αSyn during the purification (Figure 3.3D). SEC and AEC were particularly effective, with each enriching for αSyn by approximately one order of magnitude. Ultimately, this protocol provided a > 3,500 fold enrichment of αSyn from the starting total homogenate of cortical tissue and yielded 5-10% of the total cytosolic αSyn (Figure 3.3E). We typically obtained approximately 100-200 μg of pure αSyn starting from 20-25 g of cortex.

As a matter of best practice, we tried to avoid storing the protein solutions until the purification was completed; however, we occasionally did need to store the partially purified samples. We therefore investigated whether different storage conditions affected the stability of partially purified (following SEC), brain-derived αSyn (Figure 3.4). For samples stored in either standard or low-binding tubes at room temperature or 4°C, the αSyn levels appeared consistent over the course of 5 days. For samples frozen at -20°C, the amount of detectable αSyn appeared to decrease with each successive freeze/thaw cycle regardless of whether standard or low-binding tubes were used for storage, though this effect was greater in standard tubes. Flash freezing in liquid nitrogen and storing at -80°C did not lead to αSyn loss even after 5 freeze/thaw cycles. Based on these findings, we used low-binding tubes for all possible αSyn-containing fractions and stored these samples at 4°C (for short-term storage) or -80°C (for longer-term storage).

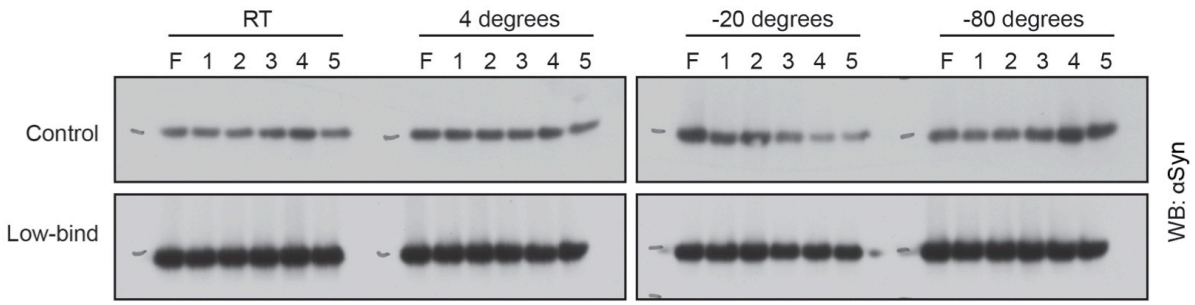

Figure 3.4: Testing of storage conditions for partially purified samples.

SEC fractions were stored either in standard tubes (control) or low-protein-binding tubes at room temperature (RT), 4°C, -20°C, or -80°C and monitored periodically for detectable levels of full-length αSyn. Samples were run fresh (F) or after storing in the indicated conditions. Number 1-5 correspond either to days in storage (for RT and 4°C samples) or number of freeze-thaw cycles (for samples stored at -20°C and -80°C). Storage at -20°C led to a loss of protein upon multiple freeze thaw cycles that was partially prevented with the use of low-binding tubes.

Key contaminants and their removal:

Overall, the procedure described above reproducibly led to pure αSyn; however, four noteworthy proteins occasionally hindered purification due to their abundance and apparently similar biochemical properties. These contaminating proteins were initially revealed by Coomassie stain. Bands at ~50, 45, and 40 kDa were excised and analyzed by in-gel digestion and tandem LC-MS/MS, which revealed their identity to be ATP-synthase beta subunit (ATP5B), gamma-enolase (NSE), creatine kinase B-type (CKB), respectively. These results were later confirmed by Western blotting with specific antibodies (Figure 3.5A). A single incubation with TS6b resin was usually enough to completely purify αSyn (Figure 3.1B); however, in some cases, these contaminating proteins were so abundant that a second incubation with the resin was needed to achieve sufficient purity for further analysis (Figure 3.5B). In later preparations, before pooling αSyn-containing SEC fractions for AEC, we routinely probed a range of SEC fractions with specific antibodies that recognize the principal contaminating proteins in addition to an antibody that detects αSyn (Figure 3.5C). This approach allowed for the strategic reduction in the amount of these contaminants that would reach the thiopropyl Sepharose step.

The other common contaminant that was present through the early stages of the purification was βSyn, which co-purified with αSyn through the SEC step (Figure 3.5C). βSyn was generally separated from αSyn using the AEC step, during which it eluted later (i.e. at a slightly higher salt concentration) than αSyn (Figure 3.5D) - as anticipated due to its lower predicted isoelectric point (pI αSyn = 4.67, pI βSyn = 4.41) (UniProt Consortium, 2014). Only αSyn-containing AEC fractions that lacked βSyn (when AEC sufficiently resolved these two

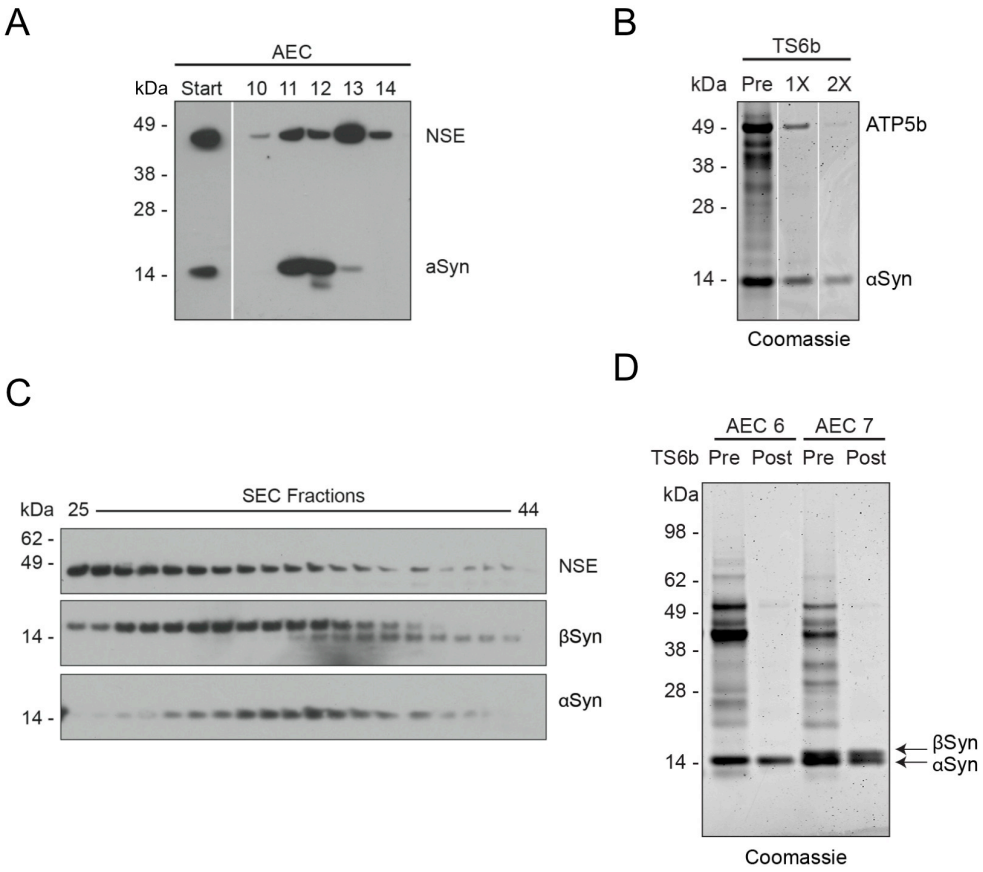

Figure 3.5: Principal contaminating proteins.

A. WB for γ-enolase (NSE) and αSyn in the AEC fractions shows an overlap in the elution profiles of these two proteins. Start refers to pooled SEC fractions that were used for AEC. B. Coomassie staining of an αSyn-rich AEC fraction prior to and after 1x and 2x TS6b incubation steps. In some cases, two incubation steps were necessary to remove contaminants such as ATP5b and produce αSyn of >90% purity. C. WB for NSE, βSyn, and αSyn in the SEC fractions shows considerable overlap in the elution profiles of these three proteins; however the peak of αSyn immunoreactivity is shifted relative to these two contaminants. D. Some αSyn-rich AEC fractions also contained abundant βSyn (as confirmed by mass spectroscopy) that was not separated from αSyn by the TS6b incubation step.

proteins) were incubated with thiopropyl Sepharose since βSyn also lacks cysteines and was not be separated from αSyn by this technique (Figure 3.5D).

Brain-derived αSyn contains variable helical content:

We and others have recently provided evidence that endogenous aSyn in intact cells exists in substantial part as a tetramer and related oligomers (Bartels et al., 2011; Dettmer et al., 2013; Klucken et al., 2006; Newman et al., 2013; Westphal and Chandra, 2013) that, unlike monomeric αSyn, display α-helical structure when purified (Bartels et al., 2011; Trexler and Rhoades, 2012; Wang et al., 2011; Westphal and Chandra, 2013). We therefore performed circular dichroism (CD) spectroscopy to determine the secondary structure of αSyn purified from human brain. In contrast to recombinant αSyn, which consistently showed the expected random coil secondary structure (with a predictable minimum of ellipticity at 196 nm), the CD spectra of human brain αSyn purified using this protocol was more variable. In some cases, the spectra contained significant α-helical content (Figure 3.6A, red trace), while in others, the protein appeared almost completely unfolded (Figure 3.6A, blue trace). We quantified the helical content of brain-derived and recombinantly-expressed αSyn by comparing the ellipticity values at 222 nm to those of completely helical and unfolded peptides (Scholtz et al., 1991). Recombinant αSyn, as expected, displayed little helical content with a mean of 4%. On average, brain-derived αSyn possessed significantly more helical content, ranging from 7-21%, with a mean of ~12% (Fig. 6B). As a point of comparison, vesicle-folded recombinant αSyn, an accepted helical form of αSyn (Davidson et al., 1998), contains ~43% helicity by these calculations. We did, on occasion, observe a spontaneous increase in α-helical content of brain-derived αSyn samples that

Figure 3.6: Purified human brain αSyn is partially helically folded.

Circular dichroism (CD) spectroscopy was used to estimate the secondary structure of purified αSyn samples. A. CD spectra obtained from two samples of αSyn purified from human brain highlighting the variability in helical content. A partially helical sample is shown in red and largely unfolded sample is shown in blue. CD spectroscopy of monomeric recombinant αSyn in the absence (unfolded - solid black trace) and presence of POPC/POPS small unilamellar vesicle (α-helical – solid gray trace) are shown for reference. B. The helicity of αSyn samples purified from human brain are compared to recombinant monomer and are expressed as the percentage of vesicle-folded recombinant αSyn. Relative helicity was determined using the ellipticity value at 222 nm. * = $p < 0.01$ using an unpaired *t*-test. Error bars represent the standard deviation of 6 or 8 independent experiments for recombinant and brain-derived αSyn, respectively. C. CD spectra of human brain αSyn before (blue trace) and after room temperature (RT) incubation (green traces) were compared to unfolded and vesicle-folded recombinant αSyn (black and gray traces, respectively). The raw data obtained after room temperature incubation (light green trace) was scaled to adjust for changes in protein concentration (dark green trace).

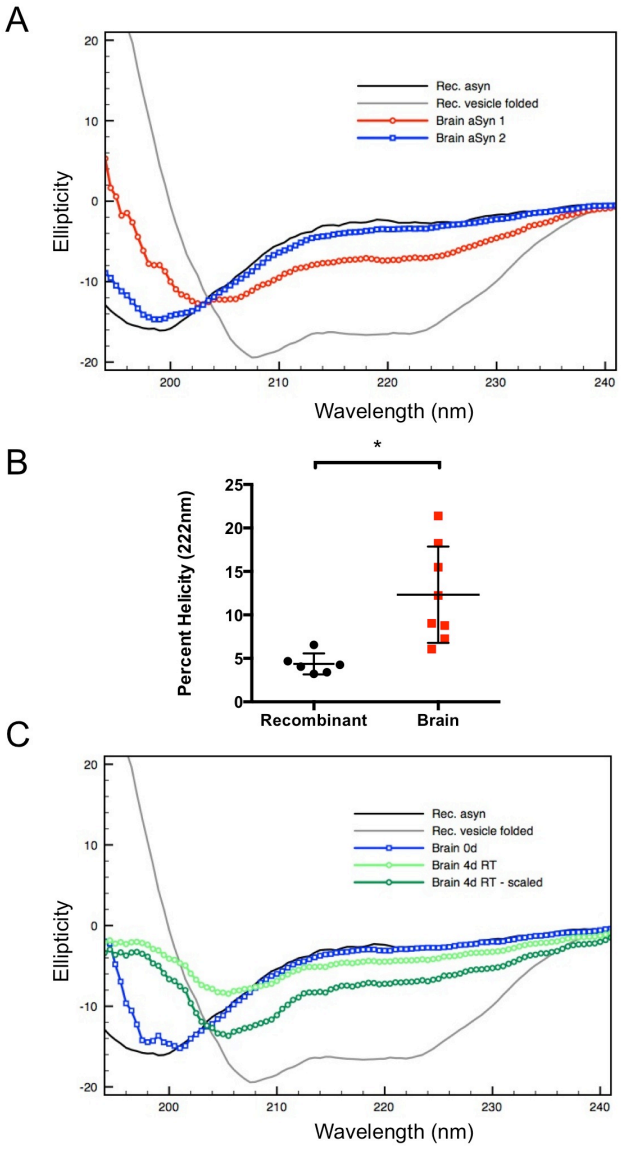

Figure 3.6 (Continued): Purified human brain αSyn is partially helically folded.

initially were determined to be of a random coil conformation (Figure 3.6C). In these cases, reanalysis after 4-5 d at RT showed a relative loss of unfolded character and gain in helicity (Figure 3.6B). When the spectra were scaled so that they passed through the isosbestic point at approximately 204 nm (i.e. adjusted for soluble protein concentration), the spectra appeared quite similar to the samples that were partially folded immediately following purification (compare red trace in Figure 3.6A to dark green trace in Figure 3.6C). Together, these data suggest that the human cortex contains helical αSyn but that there are factors that can influence its stability over the purification procedure.

Abundant αSyn oligomers occur in human brain:

We examined the oligomerization state of the aSyn purified from human brain with the expectation, based on the partially α-helical CD spectra in Figure 3.6A, that these samples would contain both oligomeric and monomeric protein. Crosslinking using the homo-bifunctional, lysine-reactive crosslinker disuccinimidyl glutarate (DSG) revealed a pattern of αSyn-immunoreactive bands that is similar to what was obtained from the diffusion-controlled, stochastic crosslinking of recombinant monomeric αSyn (a ladder of monomers, dimers, trimers, tetramers etc.) (Figure 3.7A). Preliminary quantification indicated that the oligomeric content of partially α-helical cortical αSyn is greater than that of the bacterially expressed protein, but the presence of unfolded, monomeric αSyn in the brain samples precludes a meaningful comparison.

Because our previous work indicated that rat neurons and other cells contain abundant, physiological αSyn oligomers (Bartels et al., 2011; Dettmer et al., 2013; Newman et al., 2013), we crosslinked intact human brain cells (*in vivo* crosslinking) using DSG to determine whether mid-molecular weight oligomers could similarly be trapped in human cortical cells. SDS-PAGE/

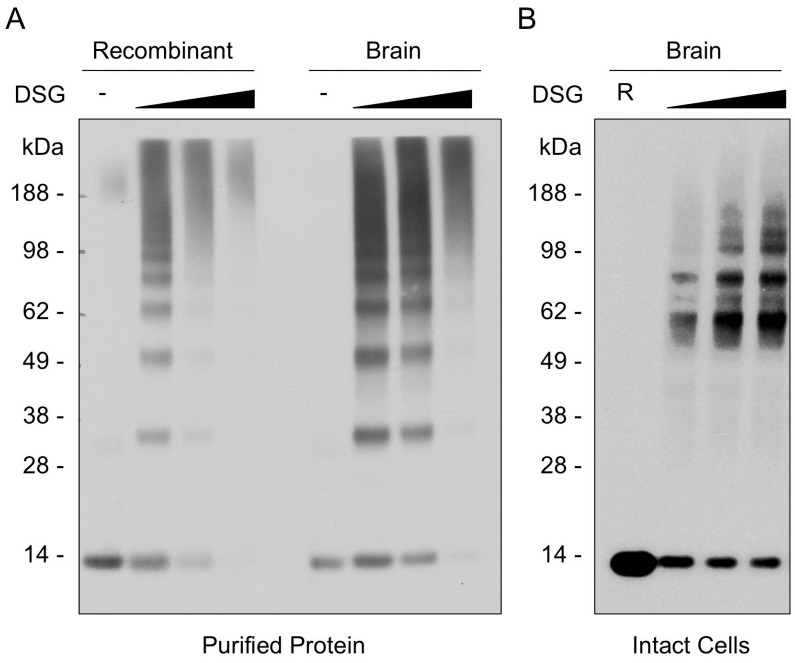

Figure 3.7: Pattern of immunoreactivity for pure crosslinked αSyn differs from αSyn trapped within cells.

A. Recombinant αSyn purified from bacteria and partially helical αSyn purified from human brain were suspended at 10 μg/ml and crosslinked with 0.25, 0.5, or 1 mM DSG. Recombinant αSyn shows a ladder of oligomers whose abundance decreases as their size increases. A similar pattern is seen for brain-derived αSyn. Smearing of the immunoreactivity in the mid-to-high molecular weight region precludes a meaningful quantitative comparison of the oligomer to monomer ratio. B. Crosslinking of intact cells from human cortex using a range of DSG from 0.5 mM to 1.5 mM revealed abundant oligomers of distinct apparent sizes (60 kDa, 80 kDa, and a doublet at 100 kDa). The sample run in the lane marked "R" was crosslinked with 1 mM of the cleavable crosslinker DSP and then reduced (cleaved) by boiling in sample buffer containing βME, and served as a non-crosslinked control.

Western blotting of the 100,000 soluble lysate of cells crosslinked with DSG revealed a major 60 kDa species (as well as 80 and 100 kDa αSyn-immunoreactive bands that may be conformers or oligomers composed of additional αSyn monomers (Dettmer et al., 2013; Gould et al., 2014) in addition to a minor 14 kDa monomer (Figure 3.7B). This suggests that soluble oligomers constitute a major pool of physiological αSyn in non-diseased human neurons. Taken together with the crosslinking of purified, brain-derived αSyn, this suggests that cortical neurons possess abundant αSyn oligomers but either the purification protocol is biased toward monomeric αSyn or the majority of these oligomers are destabilized at some point in the purification.

To further address this issue, we crosslinked αSyn-containing fractions at all intermediate stages of purification. Crosslinking of the total brain homogenate, the 230,000 *g*-soluble homogenate, and the re-solubilized ammonium sulfate precipitated material revealed an abundant ~80 kDa oligomeric band that comigrated with the ~80 kDa oligomer trapped by crosslinking of lysed cells that we reported recently (Dettmer et al., 2013; Newman et al., 2013) (Figure 3.8). Note that the crosslinking efficiency of the DSG in the ammonium sulfate precipitated material is dramatically reduced due to the presence of residual free amines that act to quench this lysine-reactive crosslinker. Crosslinking of this material following SEC (with no ammonium sulfate present) again revealed abundant mid molecular weight oligomers (Figure 3.9). By crosslinking a wide range of SEC fractions and probing with a panel of αSyn antibodies, we were able to observe a consistent elution profile for a variety of αSyn species. Moreover, the species themselves (~14, 60, 80, 100 kDa bands) were in accord with our previous observations of crosslinked αSyn, though the 100 kDa band was often seen as a doublet in these experiments. Oligomers were still readily detectable in the peak αSyn-containing fractions following AEC, but their relative abundance was less than at earlier stages of purification (Figure 3.9A). This

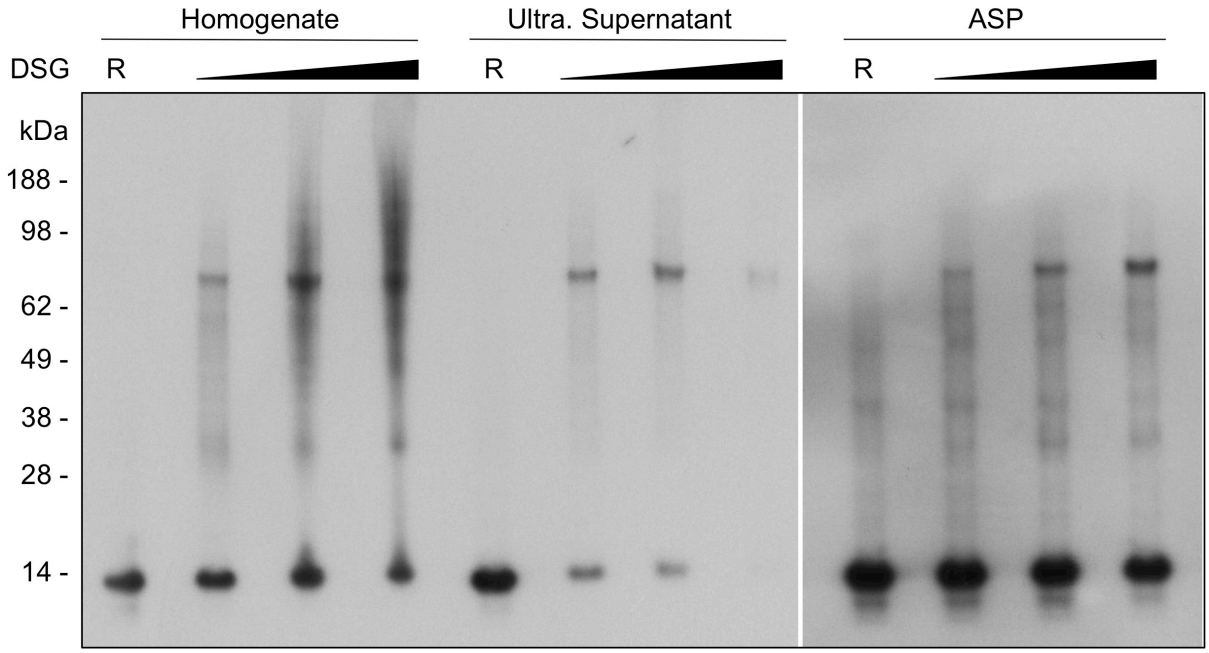

Figure 3.8: Abundant αSyn oligomers are detected after initial chromatography steps. Total brain homogenate, soluble protein (ultra. supernatant), and ammonium sulfate precipitated protein (ASP) samples were protein normalized and crosslinked with a range of DSG concentrations from 0.5-1 mM. A clear 80 kDa band was visible in crosslinked samples from each of these three stages of purification. Residual ammonium sulfate present in the re-solubilized ASP samples led to a reduced DSG crosslinking efficiency in those samples. "R" lanes were crosslinked with 1 mM of the cleavable crosslinker DSP and then reduced (cleaved) by boiling in sample buffer containing βME. They served as non-crosslinked controls.

Figure 3.9: TS6b incubation precludes the detection of oligomeric αSyn.

A. A range of SEC fractions, a sample taken from SEC fractions pooled for AEC (i.e. AEC start (St.), and a range of AEC fractions were crosslinked with either DSG or DSP at 250 μM. DSP-crosslinked samples were cleaved by boiling in βME-containing sample buffer prior to loading and are labeled "R". All samples were probed with an antibody for αSyn. Oligomeric species, especially the 60 kDa and 100 kDa doublet bands, are predominant in SEC fractions. These oligomeric species are also readily detectable following AEC, though the relative abundance of monomer in the main αSyn-containing fractions is higher compared to after SEC. B. An oligomer-rich AEC fraction was crosslinked with a range of DSG from 50-250 μM of before and after TS6b incubation. The 60 kDa band seen before TS6b incubation was only faintly visible afterwards and the strongly immunoreactive 100 kDa band was completely undetectable. Higher crosslinker concentration did not result in the trapping of oligomers, but rather resulted in "over-crosslinking" and a loss of protein able to enter the gel.

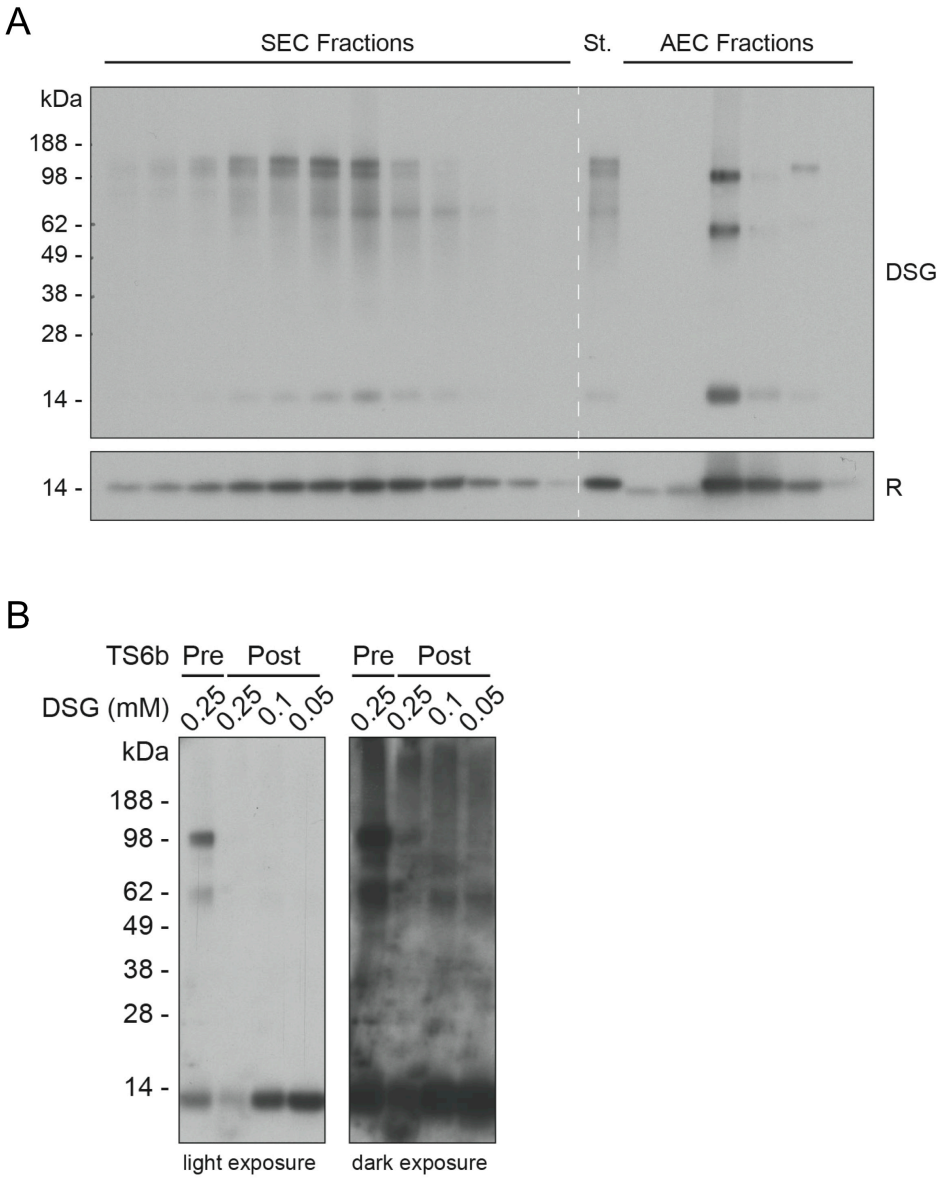

Figure 3.9 (Continued): TS6b incubation precludes the detection of oligomeric αSyn

indicates that the AEC step may contribute to a destabilization of αSyn oligomers during our purification. Interestingly, oligomers were prevailing in later AEC fractions (suggesting that they have a greater negative charge than monomer); however these fractions were not pooled for thiopropyl Sepharose incubation due to the presence of βSyn (see above).

TS6b incubation destabilizes αSyn oligomers:

Crosslinking of oligomer-rich fractions before and after TS6b incubation revealed a striking loss of crosslinker-stabilized oligomers following this chromatography step (Figure 3.9B, compare lanes 1 and 2). Because there is substantial loss of total protein, the DSG concentration used to trap oligomers before the TS6b incubation may result in an "over-crosslinking" of the material and a reduction in the ability of αSyn to enter the gel. To overcome this, we titrated DSG at lower concentrations (Figure 3.9B, lanes 3 and 4); however, we were unable to trap more than relatively small amounts of oligomeric αSyn compared to monomer, and not in the ratios predicted by the crosslinked pre-TS6b sample (Figure 3.9B dark exposure). The difference in crosslinking pattern seen here compared to what was observed in Figure 3.7A is likely the result of the ammonium acetate buffer used for CD spectroscopy; ammonium ions reduce the crosslinking efficiency of DSG and prevent over-crosslinking until higher concentrations are used.

We then asked whether our inability to detect αSyn oligomers was due to their depolymerization or a reduction in crosslinking efficiency. To answer this we took advantage of samples that were contaminated with NSE after TS6b incubation. Western blotting for NSE after DSG crosslinking revealed that residual NSE could still be efficiently crosslinked into its

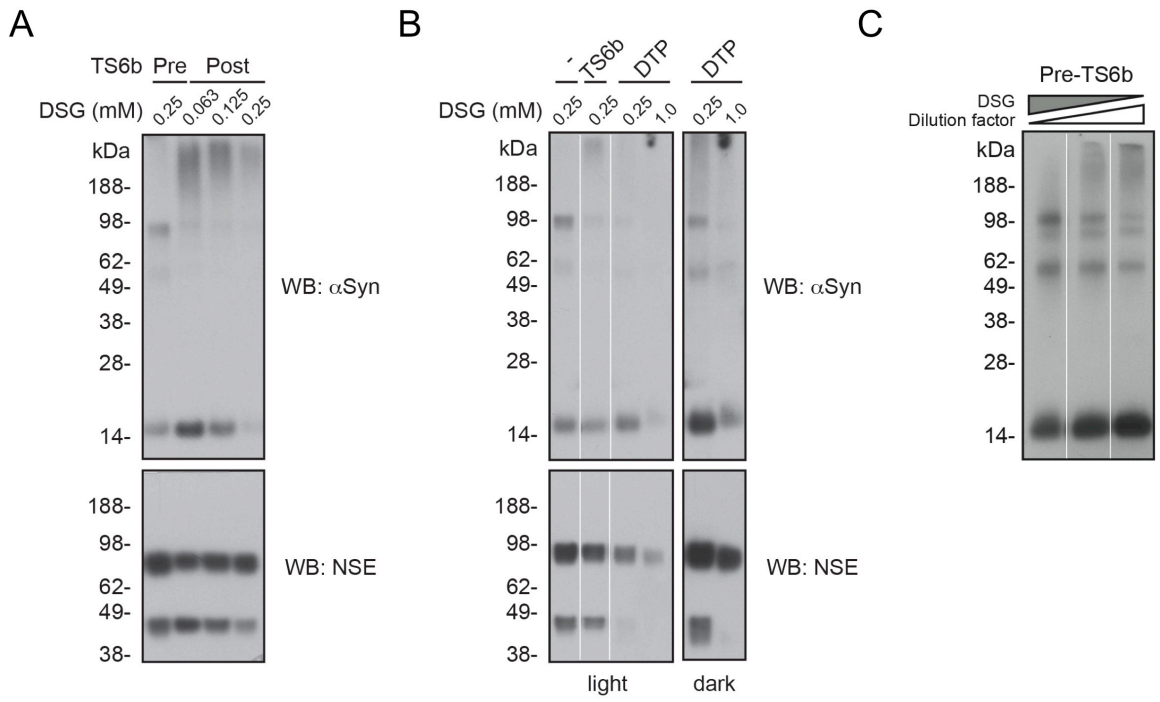

Figure 3.10: αSyn oligomers are destabilized by TS6b resin and a related chemical.

A. AEC fraction containing αSyn and NSE oligomers was incubated with TS6b resin for 1 hour and then crosslinked with a range of DSG concentrations. Samples were blotted for αSyn (top) and NSE (bottom). B. AEC fraction from A was incubated with TS6b resin or dithiopyridine (DTP) for 10 min and then crosslinked with the indicated DSG concentrations. Samples were blotted for αSyn (top) and NSE (bottom). A light and dark exposure are shown for DTP-incubated samples. C. AEC fraction containing αSyn oligomers was left undiluted (lane 1) or diluted 1:2 (lane 2) or 1:3 (lane 3). Samples were then crosslinked with DSG that was diluted to keep the crosslinker : protein ratio the same across samples and then blotted for αSyn.

physiological, dimeric form (Chai et al., 2004) (Figure 3.10A). This suggests that αSyn oligomers are preferentially destabilized by this step. Potential mechanisms of destabilization include reduction of the total protein content and depletion or disruption of a specific stabilizing factor by the resin, To exclude these possibilities, we incubated αSyn oligomer-containing AEC fractions with 2,2'-dithiopyridine (DTP) at a concentration equivalent to that of the active groups on the TS6b resin. DTP is the disulfide of 2-thiopyridine, the compound released from TS6b resin upon protein binding. Its addition creates an environment similar to that resulting from the TS6b resin incubation without removing cysteine-containing proteins from solution, thereby also avoiding a reduction in protein concentration. As we had observed upon TS6b incubation, addition of DTP reduced our ability to trap oligomeric αSyn, but not NSE dimers (Figure 3.10B). Higher DSG concentrations did not lead to the recovery of these oligomers (as would be expected if crosslinking inefficiency were to blame), but instead to a greater amount of gel-excluded material - mostly at the expense of monomer (Figure 3.10B dark exposure). This implies that mid molecular weight αSyn assemblies have been greatly depolymerized but that residual oligomers are somewhat resistant to over-crosslinking. To confirm that dilution specifically did not affect our ability to detect αSyn oligomers, we diluted oligomer-containing AEC fractions 1:2 and 1:3 - in the range of total protein reduction caused by TS6b incubation (as determined by BCA assay). Diluted samples were effectively crosslinked by the DSG when the ratio of DSG : protein was adjusted accordingly to avoid over-crosslinking (Figure 3.10C). As shown earlier, similarly reducing the DSG concentration used in samples incubated with TS6b resin did not lead to the recovery of αSyn oligomers (Figure 3.9B). These data suggest that the depolymerizing effect of TS6b resin is due, at least in part, to a chemical interaction induced by its leaving group**.** Our results demonstrate that physiological αSyn oligomers are carried through

our purification protocol until the final step at which point incubation with TS6b destabilizes oligomers and selectively enriches for monomeric αSyn. Though the specific reasons for this have yet to be elucidated**,** this finding is a potential explanation for our inability to consistently purify helical αSyn.

Purification of β-synuclein:

While optimizing our protocol to purify αSyn, we serendipitously discovered that we could simultaneously purify βsyn. As mentioned above, βSyn co-purified with αSyn until the AEC step, at which point βSyn eluted at a higher concentration of NaCl than aSyn, as predicted by its lower isoelectric point (Figure 3.5D). βsyn-containing AEC fractions occasionally also contained αSyn, but in the event that αSyn was not detectable, we were able to completely purify βSyn using the TS6B resin. Like αSyn, βSyn lacks cysteines, and thus it can also be separated from remaining contaminating proteins using this step (Figure 3.11A). Following TS6b incubation, the identity of βSyn was confirmed by LC-MS/MS (Figure 3.11B). Crosslinking of βSyn-containing fractions following SEC and AEC demonstrated that human neurons contain βSyn oligomers (Figure 3.11C) that migrate and elute in a patter similar to what was observed for αSyn (Figure 3.9A). This finding is in agreement with of crosslinked βSyn oligomers trapped within rat primary neurons (Dettmer et al., 2013).

Discussion

αSyn is an intensely studied protein, and it is extremely abundant in the human nervous system, with estimates that it accounts for up to 1% of total brain protein (Iwai et al., 1995).

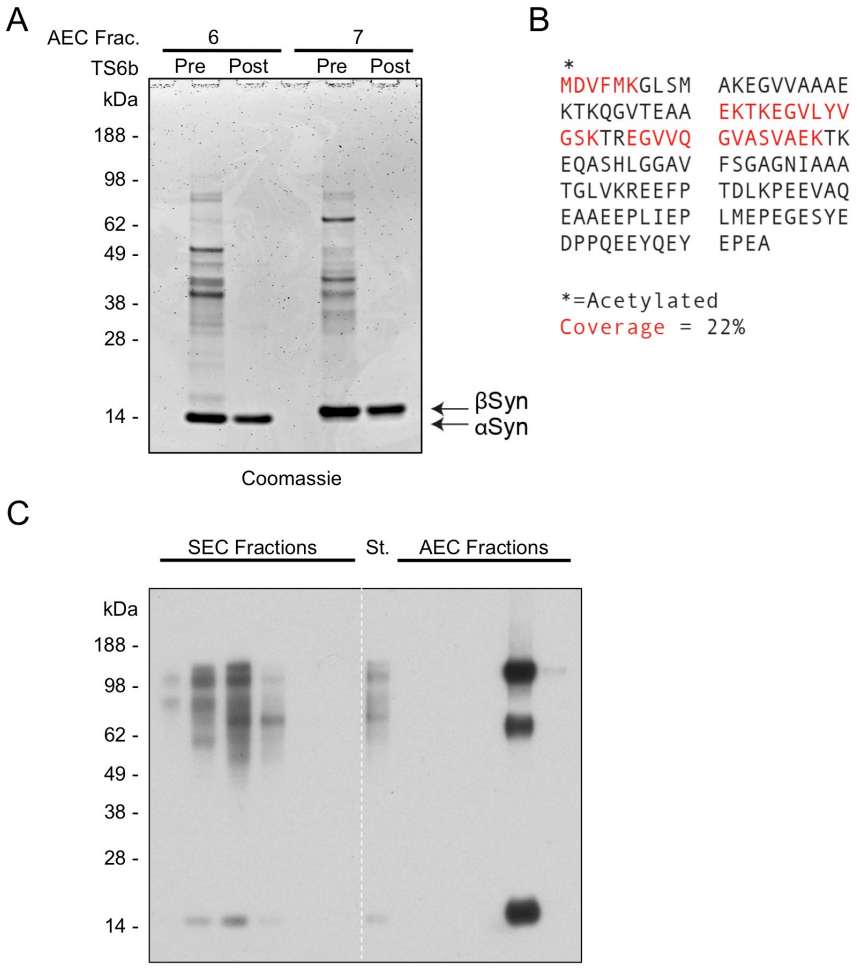

Figure 3.11: Purification of βSyn. A. Coomassie stain of AEC fractions illustrating that βSyn elutes later (at a higher salt concentration) than αSyn and is also able to be purified away from contaminating proteins using TS6b incubation. B. Mass spectroscopy was performed on the final purified sample. The βSyn sequence covered by observed peptide fragments is shown in red. C. DSG crosslinking of SEC and AX fractions, as well as the AEC start (St.), shows that abundant oligomers of βSyn can also be trapped after these intermediate purification steps.

Anderson and colleagues (2006) isolated insoluble αSyn from the brains of synucleinopathy patients, but studies of non-pathologic αSyn isolated from human brain are lacking. This report is the first to describe the purification of soluble human brain αSyn. βSyn was similarly purified from the same starting material with only slight modifications to the penultimate step of the protocol. This set of protocols will be useful in further studies of the physiological function of these two members of the synuclein family.

In recent years, the secondary structure and oligomerization state of native αSyn have been vigorously debated. Our lab and others have provided evidence that the endogenous protein can exist, in large part, as a helical oligomer (Bartels et al., 2011; Dettmer et al., 2013; Westphal and Chandra, 2013) while other groups maintain that it exists exclusively (or almost exclusively) as an unfolded monomer (Burré et al., 2013; Fauvet et al., 2012). We show here that we can purify αSyn with significant helical content from human brain, but that the degree of helicity is variable. We also observed instances in which αSyn that had initially appeared unfolded by CD spectroscopy later showed a partially helical spectrum after room temperature incubation. This phenomenon could be interpreted as an initial induction of helicity in the purified samples, a re-folding of protein that had become unfolded at some point in the purification, or an apparent folding due to an increase in relative abundance of folded protein. Based on other observations in this report and in previously published work (Burré et al., 2013), we favor the third interpretation. We have previously reported that, unlike the unfolded monomer, helical αSyn oligomers are resistant to aggregation (Bartels et al., 2011). Based on this finding, one would predict that in a mixed sample containing both unfolded and helical αSyn and under conditions that favor aggregation, helical αSyn would remain soluble while unfolded αSyn will aggregate and become insoluble. Since insoluble protein does not contribute to the CD spectrum, the

sample will appear to have undergone a random coil-to-α-helical transition when, simply, a larger percentage of the measureable αSyn is helical. In line with this interpretation, we observed a reduction in the amplitude of the CD signal following the apparent increase in helicity suggesting that there is less soluble protein. A similar phenomenon was reported by Burré and colleagues (2013) in their recent characterization of αSyn purified from mouse brain. They detected a degree of helical content in their purified αSyn that is in line with our partially folded samples. Moreover, they also observed an increase in helical content and an accompanying reduction in protein concentration after room temperature incubation, as inferred by a reduction in CD amplitude. Our findings, as well as those of Burré et al., are consistent with the idea that cortical tissue contains a pool of helical αSyn that is aggregation resistant. Furthermore, they reinforce the idea that therapeutics designed to stabilize helical conformations of αSyn may reduce the relative abundance of aggregation prone monomer, thereby interfering with pathological processes in PD and related synucleinopathies.

Our purified brain-derived αSyn did not consistently contain as much helical character as αSyn isolated from RBCs and neuroblastoma cells (Bartels et al., 2011). A simple explanation for this could be related to the tissue from which these samples originate. The source material dictates the nature and array of contaminating proteins, which, in turn, determine what chromatographic techniques are best for isolating αSyn. We optimized the protocol presented here to remove contaminants that are highly expressed in brain but may not be abundant in these other cell types, for example, CKBB and βSyn (Su et al., 2004; Thompson et al., 1980). As discussed further below, overnight TS6b incubation as a polishing step is not favorable for the recovery of helical αSyn. This step will, accordingly, be the subject of further investigation. To

better directly compare brain- and RBC-derived αSyn, we are currently testing the ability of our previously published RBC protocol to yield helical αSyn from brain tissue.

The variation in helical content of our final purified samples can likely be attributed to differences in the retention of oligomeric material during the purification. By its very nature, protein isolation involves sacrificing yield for purity. It is possible that, in the case of our protocol and the one used by Burré et al. (2013) to isolate αSyn from mouse brain, the most straightforward way to achieve pure samples (choosing αSyn-containing fractions that have the least amount of key contaminants) may have resulted in the loss of a pool of αSyn enriched in oligomers. In agreement with our published *in vivo* crosslinking studies (Dettmer et al., 2013), the crosslinking data presented here consistently showed that cortical homogenates contain oligomers of αSyn (and the non-aggregation-prone βSyn) (Hashimoto et al., 2001) at early and intermediate steps of the purification. In fact, until the final chromatography step (the TS6b incubation) we observed abundant oligomeric material that co-migrated with oligomeric αSyn trapped using *in vivo* crosslinking, suggesting that they are representative of species that can be trapped within intact cells. Coomassie blue staining coupled with Western blotting of crosslinked αSyn-containing AEC fractions revealed that oligomer-enriched fractions elute later and are often less pure then monomer-rich fractions. In particular, oligomer-enriched fractions often contained high levels of βSyn, from which αSyn cannot be separated with our current polishing step. Even when AEC resulted in a complete resolution of αSyn and βSyn by Coomassie staining, other contaminants, such as NSE or CKB, were more plentiful in later fractions, making complete purification of αSyn from these oligomer-rich fractions more difficult. Differences in the degree of contamination by these proteins across preparations can influence what fractions are used for successive steps and therefore the amount of purified oligomeric αSyn.

While we cannot presently explain the apparent destabilizing effect of incubation with TS6b resin, the effect of DTP on its own supports the idea that destabilization is not due to the dilution of αSyn nor the pull-down of a stabilizing factor. DTP is an oxidant but its high specificity for thiols makes it unlikely that αSyn itself is a target. Reaction of DTP with a cysteine-containing protein would create 2-thiopyridine, a mild reducing agent. Whatever the biochemical mechanism behind this depolymerization, our data suggest that the stability of physiological oligomers is particularly vulnerable to changes in the chemical environment caused by this leaving group. We therefore suggest that laboratories attempting to purify native αSyn from brain be aware of potential changes in chemical conditions, especially in the later stages of purification when there will be less endogenous redox buffering capacity. We are currently investigating alternative polishing steps for our protocol to better preserve the oligomeric content present after AEC. Though the current protocol will require said optimization before high quantities of oligomeric protein can be isolated, the purification strategy presented here can still be useful in studying the function of brain-derived αSyn (and βSyn) oligomers. We are currently able to obtain ~50% pure samples that contain abundant αSyn oligomers. These samples can be examined in functional studies (for example, assays of vesicle fusion) and compared to samples from which αSyn has been immunodepleted.

Our findings support the existence of helical αSyn oligomers in human cortical neurons. They also highlight the difficulty of purifying such labile species unless great care is taken throughout the purification process to avoid any conditions that destabilize native protein-protein interactions. The apparent ease in which crosslinkable oligomers can be lost during purification provides an explanation for why some groups have difficulty obtaining fully helical material even from established sources of folded protein (Fauvet et al., 2012). Once fully optimized, this

protocol could be used to analyze qualitative and quantitative differences in the pool of soluble αSyn between control and diseased brain tissue. It will also be a key tool in identifying other conditions that destabilize oligomeric αSyn and promote the relative abundance of aggregation prone monomer.

References

Abeliovich, A., Schmitz, Y., Fariñas, I., Choi-Lundberg, D., Ho, W.H., Castillo, P.E., Shinsky, N., Verdugo, J.M., Armanini, M., Ryan, A., Hynes, M., Phillips, H., Sulzer, D., Rosenthal, A., 2000. Mice lacking alpha-synuclein display functional deficits in the nigrostriatal dopamine system. Neuron 25, 239–252.

Anderson, J.P., Walker, D.E., Goldstein, J.M., de Laat, R., Banducci, K., Caccavello, R.J., Barbour, R., Huang, J., Kling, K., Lee, M., Diep, L., Keim, P.S., Shen, X., Chataway, T., Schlossmacher, M.G., Seubert, P., Schenk, D., Sinha, S., Gai, W.P., Chilcote, T.J., 2006. Phosphorylation of Ser-129 is the dominant pathological modification of alpha-synuclein in familial and sporadic Lewy body disease. J. Biol. Chem. 281, 29739–29752.

Bartels, T., Choi, J.G., Selkoe, D.J., 2011. α-Synuclein occurs physiologically as a helically folded tetramer that resists aggregation. Nature 477, 107–110.

Boassa, D., Berlanga, M.L., Yang, M.A., Terada, M., Hu, J., Bushong, E.A., Hwang, M., Masliah, E., George, J.M., Ellisman, M.H., 2013. Mapping the subcellular distribution of α-synuclein in neurons using genetically encoded probes for correlated light and electron microscopy: implications for Parkinson's disease pathogenesis. Journal of Neuroscience 33, 2605–2615.

Breydo, L., Wu, J.W., Uversky, V.N., 2012. A-synuclein misfolding and Parkinson's disease. Biochim. Biophys. Acta 1822, 261–285.

Burré, J., Sharma, M., Tsetsenis, T., Buchman, V., Etherton, M.R., Südhof, T.C., 2010. Alpha-synuclein promotes SNARE-complex assembly in vivo and in vitro. Science 329, 1663–1667.

Burré, J., Vivona, S., Diao, J., Sharma, M., Brunger, A.T., Südhof, T.C., 2013. Properties of native brain α-synuclein. Nature 498, E4–6– discussion E6–7.

Chai, G., Brewer, J.M., Lovelace, L.L., Aoki, T., Minor, W., Lebioda, L., 2004. Expression, purification and the 1.8 angstroms resolution crystal structure of human neuron specific enolase. Journal of Molecular Biology 341, 1015–1021.

Chandra, S., Gallardo, G., Fernández-Chacón, R., Schlüter, O.M., Südhof, T.C., 2005. Alpha-synuclein cooperates with CSPalpha in preventing neurodegeneration. Cell 123, 383–396.

Chartier-Harlin, M.-C., Kachergus, J., Roumier, C., Mouroux, V., Douay, X., Lincoln, S., Levecque, C., Larvor, L., Andrieux, J., Hulihan, M., Waucquier, N., Defebvre, L., Amouyel, P., Farrer, M., Destée, A., 2004. Alpha-synuclein locus duplication as a cause of familial Parkinson's disease. Lancet 364, 1167–1169.

Cookson, M.R., van der Brug, M., 2008. Cell systems and the toxic mechanism(s) of alpha-synuclein. Experimental Neurology 209, 5–11.

Davidson, W.S., Jonas, A., Clayton, D.F., George, J.M., 1998. Stabilization of alpha-synuclein secondary structure upon binding to synthetic membranes. J. Biol. Chem. 273, 9443–9449.

Dettmer, U., Newman, A.J., Luth, E.S., Bartels, T., Selkoe, D., 2013. In vivo cross-linking reveals principally oligomeric forms of α-synuclein and β-synuclein in neurons and non-neural cells. J. Biol. Chem. 288, 6371–6385.

DeWitt, D.C., Rhoades, E., 2013. α-Synuclein Can Inhibit SNARE-Mediated Vesicle Fusion through Direct Interactions with Lipid Bilayers 52, 2385–2387.

Fauvet, B., Mbefo, M.K., Fares, M.-B., Desobry, C., Michael, S., Ardah, M.T., Tsika, E., Coune, P., Prudent, M., Lion, N., Eliezer, D., Moore, D.J., Schneider, B., Aebischer, P., El-Agnaf, O.M., Masliah, E., Lashuel, H.A., 2012. α-Synuclein in central nervous system and from erythrocytes, mammalian cells, and Escherichia coli exists predominantly as disordered monomer. J. Biol. Chem. 287, 15345–15364.

George, J.M., Jin, H., Woods, W.S., Clayton, D.F., 1995. Characterization of a novel protein regulated during the critical period for song learning in the zebra finch. Neuron 15, 361–372.

Gould, N., Mor, D., Lightfoot, R., Malkus, K., Giasson, B., Ischiropoulos, H., 2014. Evidence of Native α-Synuclein Conformers in the Human Brain. J. Biol. Chem.

Hashimoto, M., Rockenstein, E., Mante, M., Mallory, M., Masliah, E., 2001. beta-Synuclein inhibits alpha-synuclein aggregation: a possible role as an anti-parkinsonian factor. Neuron 32, 213–223.

Hsu, L.J., Mallory, M., Xia, Y., Veinbergs, I., Hashimoto, M., Yoshimoto, M., Thal, L.J., Saitoh,

T., Masliah, E., 1998. Expression pattern of synucleins (non-Abeta component of Alzheimer's disease amyloid precursor protein/alpha-synuclein) during murine brain development. Journal of Neurochemistry 71, 338–344.

Iwai, A., Masliah, E., Yoshimoto, M., Ge, N., Flanagan, L., de Silva, H.A., Kittel, A., Saitoh, T., 1995. The precursor protein of non-A beta component of Alzheimer's disease amyloid is a presynaptic protein of the central nervous system. Neuron 14, 467–475.

Kahle, P.J., Neumann, M., Ozmen, L., Muller, V., Jacobsen, H., Schindzielorz, A., Okochi, M., Leimer, U., van Der Putten, H., Probst, A., Kremmer, E., Kretzschmar, H.A., Haass, C., 2000. Subcellular localization of wild-type and Parkinson's disease-associated mutant alpha -synuclein in human and transgenic mouse brain. J. Neurosci. 20, 6365–6373.

Kamp, F., Exner, N., Lutz, A.K., Wender, N., Hegermann, J., Brunner, B., Nuscher, B., Bartels, T., Giese, A., Beyer, K., Eimer, S., Winklhofer, K.F., Haass, C., 2010. Inhibition of mitochondrial fusion by α-synuclein is rescued by PINK1, Parkin and DJ-1. EMBO J 29, 3571–3589.

Kara, E., Lewis, P.A., Ling, H., Proukakis, C., Houlden, H., Hardy, J., 2013. α-Synuclein mutations cluster around a putative protein loop. Neurosci. Lett. 546, 67–70.

Kim, J., 1997. Evidence that the precursor protein of non-A beta component of Alzheimer's disease amyloid (NACP) has an extended structure primarily composed of random-coil. Mol. Cells 7, 78–83.

Klucken, J., Outeiro, T.F., Nguyen, P., McLean, P.J., Hyman, B.T., 2006. Detection of novel intracellular alpha-synuclein oligomeric species by fluorescence lifetime imaging. The FASEB Journal 20, 2050–2057.

Larsen, K.E., Schmitz, Y., Troyer, M.D., Mosharov, E., Dietrich, P., Quazi, A.Z., Savalle, M., Nemani, V., Chaudhry, F.A., Edwards, R.H., Stefanis, L., Sulzer, D., 2006. Alpha-synuclein overexpression in PC12 and chromaffin cells impairs catecholamine release by interfering with a late step in exocytosis. Journal of Neuroscience 26, 11915–11922.

Nemani, V.M., Lu, W., Berge, V., Nakamura, K., Onoa, B., Lee, M.K., Chaudhry, F.A., Nicoll, R.A., Edwards, R.H., 2010. Increased expression of alpha-synuclein reduces neurotransmitter release by inhibiting synaptic vesicle reclustering after endocytosis. Neuron 65, 66–79.

Newman, A.J., Selkoe, D., Dettmer, U., 2013. A new method for quantitative immunoblotting of endogenous α-synuclein. PLoS ONE 8, e81314.

Polymeropoulos, M.H., Lavedan, C., Leroy, E., Ide, S.E., Dehejia, A., Dutra, A., Pike, B., Root, H., Rubenstein, J., Boyer, R., Stenroos, E.S., Chandrasekharappa, S., Athanassiadou, A., Papapetropoulos, T., Johnson, W.G., Lazzarini, A.M., Duvoisin, R.C., Di Iorio, G., Golbe, L.I., Nussbaum, R.L., 1997. Mutation in the alpha-synuclein gene identified in families with Parkinson's disease. Science 276, 2045–2047.

Scholtz, J.M., Qian, H., York, E.J., Stewart, J.M., Baldwin, R.L., 1991. Parameters of helix-coil transition theory for alanine-based peptides of varying chain lengths in water. Biopolymers 31, 1463–1470.

Scott, D.A., Tabarean, I., Tang, Y., Cartier, A., Masliah, E., Roy, S., 2010. A pathologic cascade leading to synaptic dysfunction in alpha-synuclein-induced neurodegeneration. Journal of Neuroscience 30, 8083–8095.

Shevchenko, A., Wilm, M., Vorm, O., Mann, M., 1996. Mass spectrometric sequencing of proteins silver-stained polyacrylamide gels. Anal. Chem. 68, 850–858.

Singleton, A.B., Farrer, M., Johnson, J., Singleton, A., Hague, S., Kachergus, J., Hulihan, M., Peuralinna, T., Dutra, A., Nussbaum, R., Lincoln, S., Crawley, A., Hanson, M., Maraganore, D., Adler, C., Cookson, M.R., Muenter, M., Baptista, M., Miller, D., Blancato, J., Hardy, J., Gwinn-Hardy, K., 2003. alpha-Synuclein locus triplication causes Parkinson's disease. Science 302, 841.

Spillantini, M.G., Schmidt, M.L., Lee, V.M., Trojanowski, J.Q., Jakes, R., Goedert, M., 1997. Alpha-synuclein in Lewy bodies. Nature 388, 839–840.

Su, A.I., Wiltshire, T., Batalov, S., Lapp, H., Ching, K.A., Block, D., Zhang, J., Soden, R., Hayakawa, M., Kreiman, G., Cooke, M.P., Walker, J.R., Hogenesch, J.B., 2004. A gene atlas of the mouse and human protein-encoding transcriptomes. Proc. Natl. Acad. Sci. U.S.A. 101, 6062–6067.

Thompson, R.J., Graham, J.G., McQueen, I.N., Kynoch, P.A., Brown, K.W., 1980. Radioimmunoassay of brain-type creatine kinase-BB isoenzyme in human tissues and in

serum of patients with neurological disorders. J. Neurol. Sci. 47, 241–254.

Trexler, A.J., Rhoades, E., 2012. N-Terminal acetylation is critical for forming α-helical oligomer of α-synuclein. Protein Sci. 21, 601–605.

UniProt Consortium, 2014. Activities at the Universal Protein Resource (UniProt). Nucleic Acids Res. 42, D191–8.

Varkey, J., Isas, J.M., Mizuno, N., Jensen, M.B., Bhatia, V.K., Jao, C.C., Petrlova, J., Voss, J.C., Stamou, D.G., Steven, A.C., Langen, R., 2010. Membrane curvature induction and tubulation are common features of synucleins and apolipoproteins. J. Biol. Chem. 285, 32486–32493.

Volles, M.J., Lansbury, P.T., 2003. Zeroing in on the pathogenic form of alpha-synuclein and its mechanism of neurotoxicity in Parkinson's disease. Biochemistry 42, 7871–7878.

Wang, W., Perovic, I., Chittuluru, J., Kaganovich, A., Nguyen, L.T.T., Liao, J., Auclair, J.R., Johnson, D., Landeru, A., Simorellis, A.K., Ju, S., Cookson, M.R., Asturias, F.J., Agar, J.N., Webb, B.N., Kang, C., Ringe, D., Petsko, G.A., Pochapsky, T.C., Hoang, Q.Q., 2011. A soluble α-synuclein construct forms a dynamic tetramer. Proceedings of the National Academy of Sciences 108, 17797–17802.

Weinreb, P.H., Zhen, W., Poon, A.W., Conway, K.A., Lansbury, P.T., 1996. NACP, a protein implicated in Alzheimer's disease and learning, is natively unfolded. Biochemistry 35, 13709–13715.

Westphal, C.H., Chandra, S.S., 2013. Monomeric synucleins generate membrane curvature. J. Biol. Chem. 288, 1829–1840.

Yavich, L., Jäkälä, P., Tanila, H., 2006. Abnormal compartmentalization of norepinephrine in mouse dentate gyrus in alpha-synuclein knockout and A30P transgenic mice. Journal of Neurochemistry 99, 724–732.

Yavich, L., Tanila, H., Vepsäläinen, S., Jäkälä, P., 2004. Role of alpha-synuclein in presynaptic dopamine recruitment. Journal of Neuroscience 24, 11165–11170.

Chapter 4

Discussion

Altered proteostasis of αSyn is an important factor in the pathogenesis of familial and sporadic PD. In this thesis, I addressed two central questions pertaining to the role of this abundant, soluble protein in health and disease: 1) what is the assembly state of αSyn within and upon purification from non-diseased neurons? and 2) how does the aberrant accumulation of misfolded αSyn contribute to the vulnerability of select neuronal populations? Since the discovery of it association with PD, the field has focused largely on the pathological properties of the protein and on debating the various potentially toxic species. Originally, Lewy bodies and their amyloid fibril components were thought to be toxic (Goedert et al., 2013), but more recently, there has been renewed emphasis on soluble oligomers as the culprit in neurodegeneration (Haass and Selkoe, 2007). On the other hand, initial characterization of recombinant αSyn as an unfolded monomer (Weinreb et al., 1996) was immediately accepted as representative of the physiological state of this protein within mammalian cells. Recent data from our lab, to which I contributed, challenged this assumption and proposed a model in which two fundamentally different types of soluble oligomers exist: misfolded oligomers associated with pathology, and helical oligomers that play a physiological role. Purified helical oligomers are aggregation resistant *in vitro* and may require depolymerization before proceeding down an aggregation pathway *in vivo*. Accumulation of aggregated αSyn is associated with, among other things, mitochondrial dysfunction and eventual cell death. Figure 4.1 illustrates the proposed relationship of αSyn species with each other and with mitochondria, a principal target of their toxic effects. There is much to be learned about the biochemical and cellular mechanisms linking all of these players. This thesis work provides a platform for the discussion of several of these processes.

Figure 4.1: The proposed relationship of αSyn species with each other and of prefibrillar oligomers with mitochondria.

Under physiological conditions, αSyn is localized presynaptically and exists in an equilibrium between helical oligomers and unfolded monomers. Monomeric αSyn adopts a helical conformation when biding highly curved membranes composed of acidic phospholipids, like synaptic vesicles, where it can negatively regulate vesicle fusion with the plasma membrane. Membrane-induced folding may promote the formation of helical oligomers prior to or upon membrane detachment. Helical oligomers may become depolymerized later to yield unfolded monomers under conditions that favor membrane localization. Under pathological conditions, unfolded monomers, but not helical oligomers, aggregate into soluble, prefibrillar oligomers and then insoluble amyloid fibrils. Pathology is also associated with increased αSyn in proximal compartments such as neurites and the soma. Genomic multiplication of *SNCA*, reduced clearance of αSyn due to mutations in glucocerebrosidase (*GBA1* gene), or other conditions that elevate αSyn expression increase the amount of both helical oligomers and unfolded monomers without necessarily altering the ratio. Higher absolute levels of unfolded monomer favor aggregation. PD-linked mutations in αSyn skew this ratio toward the monomer, thereby promoting aggregation, and can also speed up pathological oligomerization. Prefibrillar oligomers serve as a template for additional aggregation of monomer and can interact with mitochondria to inhibit complex I-dependent function, possibly by reducing its enzymatic activity. When complex I dysfunction coincides with mitochondrial Ca^{2+} uptake, complex I may

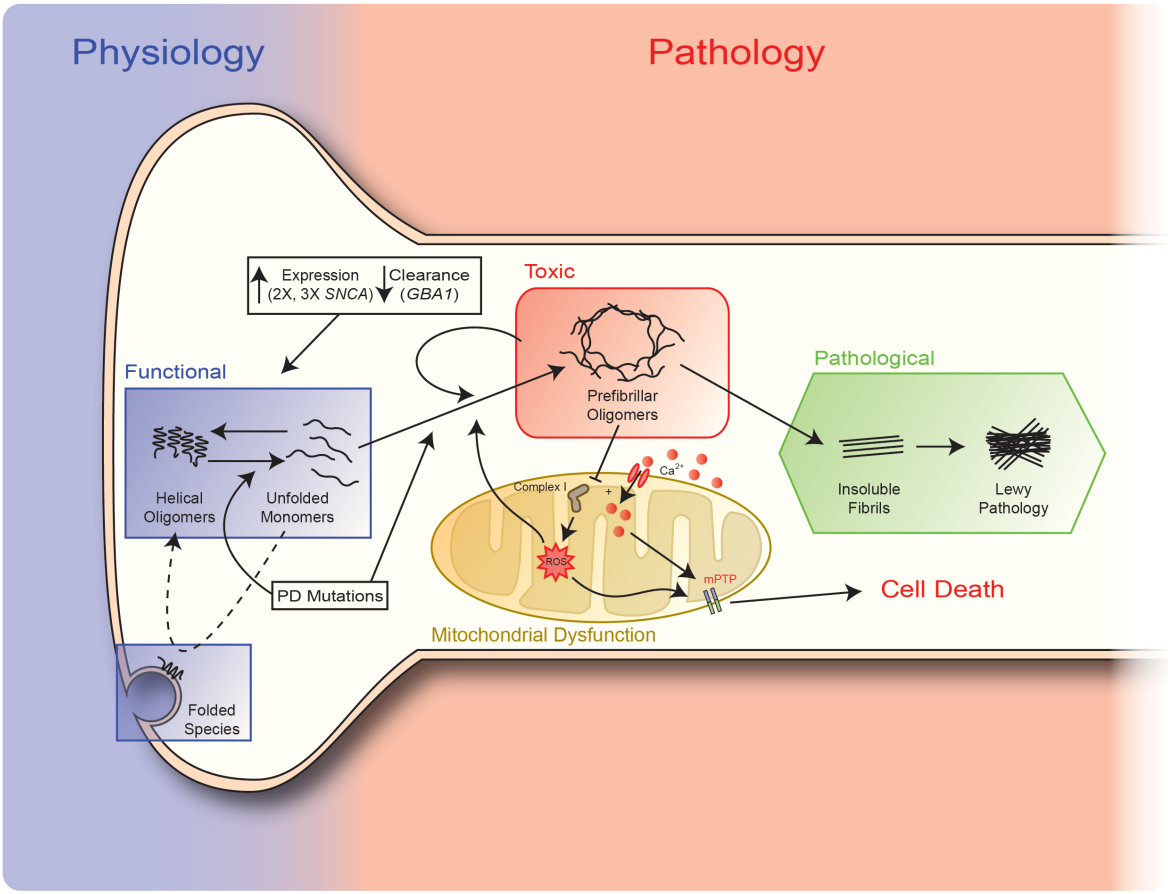

Figure 4.1 (Continued): The proposed relationship of αSyn species with each other and of prefibrillar oligomers with mitochondria.

generate excessive ROS that further promotes aggregation and the opening of the mPTP, leading to cell death. Prefibrillar oligomers further aggregate into insoluble fibrils that coalesce to form Lewy bodies. Formation of these fibrils is a pathological phenomenon, but it may sequester mitotoxic species into a form that does not directly disrupt mitochondrial function.

Destabilization and Formation of Physiological Oligomers

During purification

We have shown that, in addition to an unstructured monomer, αSyn exists physiologically in cells as an oligomer that is helically folded and sizes as a tetramer upon purification (Bartels et al., 2011; Dettmer et al., 2013). Because our data indicate that tetrameric αSyn is aggregation resistant (Bartels et al., 2011), the identification of factors that promote the formation of physiological oligomers (or their depolymerization back into monomers) could have profound functional and pathological consequences. While our previous studies both support the existence of oligomers within cells under normal conditions, we observed in the latter report (and in Appendix 3) that these oligomers are largely lysis sensitive; crosslinking of cells immediately after lysis revealed little oligomeric content (Dettmer et al., 2013). And yet, helical oligomers can be purified (Bartels et al., 2011; Westphal and Chandra, 2013). How does one reconcile these findings?

In this thesis we used crosslinking to probe the array of oligomeric αSyn species present in brain tissue, in crude homogenates, and at various states of purification. DSG crosslinking of intact brain cells trapped species that migrate at approximately 60, 80, and 100 kDa, as we have previously reported with rodent neurons(Dettmer et al., 2013), but we are only able to trap an 80 kDa species immediately following cell lysis. Though we are presently unable to identify the precise relationship of the oligomers represented by these bands, our published data argue against the likelihood of hetero-oligomers with other proteins (Dettmer et al., 2013). It is possible that they represent discrete αSyn oligomers made up of a distinct number of monomeric subunits or that they are conformational variants that are differentially crosslinked by DSG. We are currently distinguishing between these possibilities using intact mass spectrometry of

purified, crosslinked species. Crosslinking of brain homogenates after our first two purification steps (ultracentrifugation and ammonium sulfate precipitation) similarly trapped only the 80 kDa band (in addition to monomer). To further complicate matters, we observed here that 60 and 100 kDa species could be "recovered", apparently at the expense of 80 kDa αSyn, by crosslinking with DSG after size exclusion chromatography, and that they persisted until the final step of purification. The depolymerizing effect of this last step is further discussed below.

Our previous findings suggest that that 80 kDa band may be fundamentally different from the 60 and 100 kDa bands: as mentioned above, the 60 and 100 kDa bands, but not the 80 kDa band, are lysis sensitive, and the addition of recombinant monomer to cell lysate prior to crosslinking led to the enhancement of the 80 kDa, but not 60 or 100 kDa bands (Dettmer et al., 2013). One hypothesis is that the 80 kDa band observed after crosslinking may represent an assembly composed of unfolded αSyn – whether it originates from recombinant protein or endogenous oligomers that have been destabilized – while the 60 and 100 kDa bands (to which recombinant protein does not contribute) consist of helical oligomers. The inability to crosslink 60 and 100 kDa bands after cell lysis could be explained by the presence of a factor (or factors) in the lysate that actively destabilizes helical oligomers. In the context of an intact cell, this destabilization may be regulated by other proteins or by spatial separation of αSyn and this factor. Cell lysis may interfere with this regulation, allowing greater access to oligomers, thereby resulting in their depolymerization. Based on the data presented here, this potential destabilizing agent shares similar solubility properties with αSyn, since the only the 80 kDa band can be trapped by DSG after both the ultracentrifugation and ASP steps. Upon further purification by SEC, after which αSyn exists in solution only with proteins of similar hydrodynamic radii, the 60 and 100 kDa bands are again observed upon crosslinking. Because buffer conditions were

otherwise unchanged, their reappearance after this chromatography step suggests that the removal of a contaminating factor allows for oligomerization. Macromolecular dilution that occurs upon membrane rupture may be partly responsible for the loss of detectable oligomers after cell lysis, but this phenomenon cannot explain the reappearance of these species after SEC – especially because the SEC step further dilutes the sample by over 10 fold. If such an oligomer-destabilizing factor exists, it may be associated with a membranous compartment in intact cells since the Triton X-100-soluble fraction contain exclusively monomeric αSyn (with oligomeric bands detectable only in the PBS-soluble fractions) (Dettmer et al., 2013). Cytosolic αSyn can be efficiently crosslinked as oligomers in intact cells but not in the PBS-soluble phase of lysed cells. This would suggest that cell lysis acts to increase the interaction of this factor with cytosolic αSyn and would imply a weak membrane association. The existence of such a factor would be supported by experiments in which the spiking in of brain homogenate (or the soluble fraction thereof) can prevent the crosslinking of 60 and 100 kDa oligomers in samples that would otherwise show αSyn immunoreactivity at these positions (for example, in SEC or AEC fractions).

Oligomer to monomer ratio in PD and disease models

The data presented here and in our previous publication (Bartels et al., 2011) suggest that helical αSyn oligomers are aggregation resistant and unfolded monomers are aggregation prone. The presence of αSyn-rich Lewy bodies in patient brains (Spillantini et al., 1997) and reports of the pathological effects of prefibrillar αSyn oligomers described here and elsewhere strongly implicate αSyn aggregation in the pathogenesis of PD (Chen et al., 2009; Volles and Lansbury, 2003; Winner et al., 2011). Therefore, if physiological oligomers are indeed non-toxic, one might

predict that manipulations that lead to disease-associated αSyn aggregation may act by altering the ratio of crosslinked oligomer to monomer ratio in favor of the monomer. In support of this hypothesis, recent data from our lab demonstrate that all 5 familial PD-linked mutations in αSyn do indeed lead to an increase in the relative abundance of monomeric αSyn as revealed by crosslinking and fluorescence complementation studies (unpublished data). These data make sense in light of the fact that there is no clear connection between all PD mutant variants and the *in vitro* aggregation propensity of their recombinantly expressed unfolded monomer. *In vivo*, these mutations could indirectly promote aggregation by either preventing the formation or decreasing the stability of aggregation resistant physiological oligomers. It should be noted that we also observe that changes in αSyn expression levels (up to an order of magnitude) do not appear to alter the ratio of 60 to 14 kDa bands trapped by multiple crosslinking reagents. Increasing the absolute abundance of aggregation-prone monomer without necessarily altering this ratio, for example with a genomic multiplication of the αSyn-encoding *SNCA* gene (Chartier-Harlin et al., 2004; Singleton et al., 2003), is also sufficient to cause PD. The same could be true for mutations in glucocerebrosidase (*GBA1*), the most common genetic risk factor for PD, which can elevate αSyn protein levels, perhaps via reduced lysosomal degradation (Cullen et al., 2011).

αSyn-induced toxicity in *in vitro* and *Drosophila* models can be rescued by the expression of human Hsp70 (Auluck et al., 2002; Klucken et al., 2006). Based on the accompanying reduction in αSyn aggregation in these systems, it was suggested that this chaperone prevented the misfolding of αSyn into toxic species; subsequent work by Danzer et al.(2011) supports this interpretation. Complementarily, Hsp70 could also be acting to preserve the folding of helical oligomers, thereby reducing the proportion of unfolded, aggregation prone

monomers. Additional crosslinking studies following the knockdown or overexpression of chaperones in cells with endogenous αSyn expression levels or in those overexpressing low levels of oligomer-destabilizing PD mutants would help address this possibility.

Other models of PD implicate ROS production in the aggregation of αSyn (Betarbet et al., 2000; Sherer et al., 2002). While ROS-induced damage to protein degradation systems will almost certainly lead to an accumulation of αSyn (and other proteins), oxidative stress may also promote αSyn aggregation more specifically. In our purification of αSyn from human brain, we observed an apparent conversion of soluble 60 and 100 kDa αSyn oligomers into monomers by addition of the oxidant DTP. This implies that changes to environmental redox conditions can promote the depolymerization of aggregation-resistant oligomers and suggests an interesting potential feedback mechanism between αSyn-induced mitochondrial dysfunction (Chapter 2) and further aggregation.

The αSyn functional unit

The aforementioned possibility of a membrane-associated factor that promotes the depolymerization of physiological oligomers could be relevant to the function of αSyn. Such regulation could ensure that oligomeric αSyn remains cytosolic while monomers are permitted access to membranes. It is widely believed that the function of αSyn lies at membranes; *in vitro* and *in vivo* studies reviewed by Bendor et al. (2013) suggest that αSyn plays a role in membrane/vesicle dynamics. Though we observed that purified helical tetramers derived from human cells avidly bound artificial membranes, *in vitro* membrane binding assays do not reflect the complexity of the neuronal environment and do not take into consideration possible regulatory mechanisms at play. Using crosslinking agents, we have shown that the majority of

αSyn in normal cells is oligomeric and that these oligomers can be trapped exclusively in the cytosol. Compared to oligomers, the monomeric pool of αSyn is enriched in the membrane fraction (Dettmer et al., 2013). It is possible that the N-terminal conserved repeats in αSyn that are responsible for membrane binding (Bussell and Eliezer, 2003) also participate in physiological self-association (Wang et al., 2011), though not simultaneously. Emerging data from our lab indicate that in-register mutations in these repeat regions completely abolish the ability to crosslink mid-molecular weight oligomers and instead promote the association of αSyn with the Triton-X soluble fraction. This supports the idea that monomeric αSyn associates with membranes where it is in the position to carry out the purported functions for αSyn and suggests that oligomerization may have a greater sensitivity to point mutations in these regions than does membrane binding. Physiological oligomers present in the cytosol may be equally as important in that they may act as a storage form, not only to prevent the aggregation of unfolded monomers as has been proposed (Gurry et al., 2013), but also to modulate the size of the active pool of αSyn.

A recent publication analyzed 26 αSyn variants, including three familial PD mutants (A53T, A30P, E46K) in different model systems and across several assays relevant to proposed physiological and pathological activities (Burré et al., 2012). The authors observed that these mutants (and others) enhanced toxic effects of αSyn, such as neuronal death and impaired motility in mice, without significantly compromising its ability to carry out putative physiological functions, including enhancement of SNARE complex assembly (Burré et al., 2012). Combining this with our crosslinking data, it seems that mutations that lower the tetramer to monomer ratio can increase pathology without losing "functional" effects. This is consistent with the idea that monomeric αSyn is capable of carrying out reported physiological functions.

It would be interesting to examine whether even stronger mutations, for example our engineered mutant that cannot be crosslinked into mid-molecular weight oligomers, can still rescue αSyn-dependent functions in knockout neurons, though low-level expression may be required to avoid aggregation-related phenotypes.

Release from the membrane

In vitro experiments with purified αSyn and artificial membranes demonstrate a high affinity of αSyn for membranes (Beyer, 2007). *In vivo*, however, only a small percentage of αSyn is present at the membrane at any given time (Dettmer et al., 2013; Kahle et al., 2000). It has been proposed that neuronal activity stimulates the release of αSyn from synaptic vesicles (with which is it believed to associate) either by the dilution of specific acidic phospholipids upon vesicle fusion with the presynaptic membrane or by the lessening of membrane curvature that occurs concomitantly (Rhoades et al., 2006; Tao-Cheng, 2006). Based on our unpublished observations, αSyn adheres more tightly to vesicles *in vitro*. Thus, there are also likely to be factors that regulate the release of αSyn from the membrane back into the cytosol where it can assemble into physiological oligomers. Other cytosolic regulators of vesicle trafficking are subject to regulation by soluble factors; for example, rab3 is extracted off of fusing synaptic vesicles by the protein GDP-dissociation inhibitor (Ignatev et al., 2008).

There is evidence that such a factor also exists for αSyn. Using permeabilized synaptosomes, Wislet-Gendebien et al. (2006) demonstrated that addition of brain cytosol promoted the release of αSyn from vesicles. The activity of the added cytosol was sensitive to heat and protease treatment, suggesting the requirement for functional proteins (Wislet-Gendebien et al., 2006). One could investigate the ability of αSyn knockout brain cytosol to

promote αSyn release using *in vitro* assays in which N-acetylated recombinant αSyn (which is more likely to form helical oligomers (Trexler and Rhoades, 2012)) is induced to adopt helical folding in the presence of lipids. After separating the soluble from lipid-bound αSyn via centrifugation, one could examine the oligomerization state soluble αSyn using chemical crosslinking, with cytosol-treated recombinant protein incubated in the absence of lipid as a control. Due to the possibility of a competing factor that may lead to oligomer destabilization (as discussed above) but that would not necessarily be expected to affect release, it would be prudent to test further fractionated cytosol as well.

Mitotoxicity of Prefibrillar αSyn Oligomers

Possible mechanisms of action

We observed that soluble, ThT^{neg}, prefibrillar oligomers, but not monomers or ThT^{pos} fibrils promoted complex I-dependent, Ca^{2+}-induced mitochondrial dysfunction. These results provide a potential subcellular target of prefibrillar αSyn oligomers recently reported to be cytotoxic in cellular and animal models. Karpinar and colleagues (2009) reported greater oligomerization propensity but reduced fibrilization and β-sheet content of recombinant αSyn engineered to contain various proline substitutions. Overexpression of these mutants in rat primary neurons, *C. elegans*, and *Drosophila* was associated with neurotoxicity that was inversely proportional to the β-sheet content of *in vitro* oligomers of the same αSyn proteins (Karpinar et al., 2009), but mitochondrial dysfunction was not specifically addressed. Recent work by Winner et al. (2011) is also in line with our findings: αSyn mutants that preferentially form β-sheet-poor oligomers rather than β-sheet-rich fibrils *in vitro* were associated with more neurotoxicity in lentiviral-infected human mesencephalic cells and rat brain. Moreover,

interaction of these oligomers with cellular membranes was suggested as a potential mediator of toxicity (Winner et al., 2011), but again mitotoxicity was not examined.

It remains unclear whether the prefibrillar αSyn used in our system directly reduces complex I activity, though in light of existing literature, this is a likely explanation for our findings. A specific deficit in complex I activity has been reported in dopaminergic neurons overexpressing mutant αSyn (Chinta et al., 2010), and Devi et al. (2008) observed an inverse correlation between mitochondrial αSyn and complex I activity in the substantia nigra of PD patients**.** Furthermore**,** spectrophotometric analyses of complex I enzymatic activity from αSyn-treated mitochondria and mitoplasts has revealed a dose-dependent inhibition by αSyn (Devi et al., 2008; Liu et al., 2009). We are currently performing these experiments with our bioactive, prefibrillar oligomers.

In our reductionist system, we did not observe αSyn-induced reduction of basal $\Delta\Psi_m$. This would imply a mild reduction in complex I activity that is exacerbated by Ca^{2+} influx. Previous reports suggest that overexpressing αSyn in cells or animals can lead to alterations in mitochondrial function in the absence of overt Ca^{2+} stress (Chinta et al., 2010; Choubey et al., 2011; Devi et al., 2008; Hsu et al., 2000; Lee et al., 2001; Parihar et al., 2008; Shavali et al., 2008). These results could be explained by one or more of the following possibilities. *First,* toxic αSyn species could affect the function of other organelles or cellular pathways leading to intracellular Ca^{2+} dyshomeostasis. *Second,* when overexpressed in cell lines or animals (vs. briefly incubated with mitochondria *in vitro* as here), there may be greater opportunity for αSyn to exert its effects, such that mild alterations of mitochondrial function (which could be exacerbated by our acute Ca^{2+} challenge) can accumulate chronically. In this context, physiological Ca^{2+} transients in neurons could be a sufficient stress in the presence of

prefibrillar, oligomeric αSyn (Loew et al., 1994). Furthermore, endogenous toxins such as the monoamine oxidase product of dopamine, 3,4-dihydroxyphenylacetaldehyde, have also been shown to facilitate mitochondrial permeability transition (Kristal et al., 2001) and may act synergistically with pathological αSyn in dopaminergic neurons. And *third*, the ability of Ca^{2+} to exacerbate the mitochondrial effects of αSyn may not be due to Ca^{2+} uptake *per se* but rather the associated increase in ETC activity. Mitochondrial Ca^{2+} influx comes at the expense of $\Delta\Psi_m$, which must be re-established in order to generate ATP and buffer further Ca^{2+} loads. One possibility is the increased electron transport through a compromised complex I could increase the generation of ROS, thereby accelerating mPTP opening.

Prefibrillar αSyn oligomers could act to inhibit complex I function either by directly associating with protein subunits or indirectly via perturbations of mitochondrial membrane lipids. A recent paper described reduced $\Delta\Psi_m$ and increased ROS in mitochondria of αSyn transgenic mice; however co-immunoprecipitation revealed no specific association of αSyn with complex I protein subunits (Sarafian et al., 2013), although a thorough investigation into the biochemical interaction between αSyn and complex I, an integral membrane protein with its 45 subunits, would require extensive optimization and analysis. αSyn's well-demonstrated tendency to bind negatively charged phospholipids, especially cardiolipin (Nakamura et al., 2008), which is critical for proper electron transfer by complexes I and III (Fry and Green, 1981; Zhang et al., 2002), suggests that membrane association of pathological αSyn oligomers could impair complex I activity. Consistent with this idea and the nature of the toxic αSyn species we identified, Smith and colleagues (Smith et al., 2008) observed that soluble, prefibrillar αSyn oligomers populated during the aggregation lag phase bind to negatively charged membranes with an affinity approximately two orders of magnitude higher than unaged protein and

significantly higher than ThT^{pos} species. Moreover, electron microscopy of these oligomers revealed a striking similarity to our bioactive αSyn.

Mitoxicity in the context of PD

In PD associated with an established alteration of αSyn homeostasis, such as in familial PD caused by mutations in or genomic multiplications of αSyn or in sporadic PD linked to other risk factors known to increase αSyn levels, it is reasonable to assume that aberrant αSyn accumulation is an initial pathogenic stimulus. Furthermore, the presence of Lewy pathology in sporadic PD underscores the relevance of dysfunctional αSyn proteostasis in the vast majority of PD cases. That said, the precise sequence of specific pathological events is not known. Under physiological conditions, αSyn is localized primarily at the presynaptic terminals of mature neurons (Kahle et al., 2000). The insoluble αSyn inclusions characteristic of PD are found in the soma and neurites. Thus, there is an apparent subcellular redistribution of αSyn in the disease state. Does this precede mitochondrial dysfunction or does it occur as a result? Accumulation of αSyn in proximal compartments is likely the result of either impaired axonal transport of αSyn destined for the presynaptic terminal or an inability to clear αSyn that is normally degraded from these areas (Cuervo et al., 2004). Both of these processes are highly dependent on ATP.

Because of their prominent transmembrane Ca^{2+} currents associated with pacemaking activity and their low expression of Ca^{2+} buffering proteins, the neurons vulnerable in PD continuously require ATP to pump large amounts of Ca^{2+} out of the cytosol. This high basal demand for ATP translates to a modest bioenergetic reserve (the difference between the maximum capacity for ATP generation and basal ATP consumption) and puts these neurons at risk of being unable to meet additional bioenergetic demands (Surmeier and Schumacker, 2013). Therefore, they may be less able to energetically handle the proteostatic challenge brought on by

elevated αSyn. This may be particularly true of nigral dopaminergic neurons in which normal aging leads to progressive energy impairment due to accumulated mtDNA mutations (Kraytsberg et al., 2006). A shortage of ATP could compromise transport and degradation machinery, thereby leading to an accumulation and mislocalization of αSyn, which subsequently misfolds and aggregates. Prefibrillar αSyn may then associate with mitochondria, resulting in complex I dysfunction and perhaps increased ROS generation. Elevated ROS levels would further compromise mitochondrial function and promote αSyn aggregation (Hashimoto et al., 1999). Therefore neuronal populations operating near their respiratory capacity may be more likely to accumulate αSyn and more vulnerable to its toxic effects. Our results suggest that excessive Ca^{2+} uptake under these circumstances could more easily lead to the formation of the mPTP. Pore opening could result in apoptosis or necrosis depending on the number of mitochondria having undergone permeability transition and, therefore, the supply of ATP required to form the apoptosome from components released by damaged mitochondria (Rasola and Bernardi, 2011). It is believed that apoptosis is more prevalent in PD (Kostrzewa, 2000), so it is likely that only a subset of mitochondria are terminally affected.

We used a reductionist system in order to directly test the effect of defined αSyn species on Ca^{2+}-induced mitochondrial permeability transition. Though the role of mitochondrial permeability transition in PD-related cell death requires further study, two recent reports support the *in vivo* relevance of our data. Findings from Martin et al. (2013) indicate that the genetic ablation of cyclophilin D, the mPTP modulator and target of CsA, delayed the onset of mitochondrial abnormalities and neuronal apoptosis in Thy1-αSyn A53T transgenic mice. Also, Büttner et al. (2013) showed that overexpression of αSyn in yeast led to cell death and a redistribution of the pro-apoptotic nuclease EndoG from mitochondria to the nucleus. These

effects could both be rescued by genetic modulation of the mPTP components. Moreover, nuclear translocalization of EndoG was preferentially detected in the brain sections of PD patients compared to age-matched controls (Büttner et al., 2013).

Temporal Spreading of PD Pathology

The potential spreading of αSyn pathology to synaptically-connected neurons has emerged as a popular hypothesis and possible alternative to the idea of selective vulnerability. Based on an ever-expanding literature, there can be no doubt that this occurs in cell and animal models with high amounts of αSyn introduced exogenously (Hansen and Li, 2012). In controlled models like this, it is possible to establish a temporal spread of pathology. Defining such a chronological progression from the brains of disparate individuals at different ages is much more challenging. Even if one were to accept the premise of a pathogenic spread model, synaptic connectivity is not enough to explain which neurons display αSyn pathology; areas that exhibit αSyn pathology are invariably connected to others that do not (Surmeier et al., 2010). Ultimately, this reinforces the idea that, at some level, there must be certain populations of neurons that are predisposed to develop αSyn aggregates or are more vulnerable to their effects.

Implications for PD Diagnosis and Treatment

Classical treatment strategies for PD are focused on enhancing dopaminergic transmission in the nigrostriatal pathway, either by augmenting the production of dopamine by presynaptic nigral neurons or stimulating postsynaptic striatal neurons directly (Olanow and Schapira, 2013). These are purely symptomatic treatments that do not address the underlying cause of neurodegeneration and eventually lose their efficacy. This highlights the need for disease modifying, neuroprotective therapeutics that can be effective over the long term.

As discussed earlier, my working hypothesis is that αSyn sensitizes mitochondria to Ca^{2+}-induced permeability transition by increasing ROS generation at complex I. Based on this and other reports of oxidative stress in PD, one would expect that antioxidant therapies, such as Coenzyme Q10 could be effective neuroprotective agents. Data from a number of clinical trials, however, do not provide strong evidence of protection. Studies indicate that some antioxidants, like monoamine oxidase-B inhibitors, do provide some benefit to patients, but it is possible that these are due to symptomatic effects resulting from an increase in synaptic dopamine. Analysis of these clinical trials points to problems of dosing and bioavailability in the brain (Schapira and Olanow, 2004). If these hurdles can be surmounted and appropriate doses can reach at-risk neurons, then I would expect some degree of neuroprotection – especially if these treatments were coupled with drugs like dihydropyridines (DHPs) that may target a source of oxidative stress.

Epidemiological studies have shown that use of DHPs, antagonists of the L-type Ca^{2+} channels that are the source of much of the Ca^{2+} influx in vulnerable pacemaking neurons, to treat hypertension are associated with a reduced risk of PD (Pasternak et al., 2012; Ritz et al., 2010). Though L-type Cav1.3 channels contribute to pacemaking in mature nigral dopaminergic neurons, earlier in development they do not. It was recently shown that, upon blockade of Cav1.3 channels in adult nigral neurons, mitochondrial oxidant stress is reduced and pacemaking persists due to the compensatory activity of Na^{+}-permeable hyperpolarization activated cyclic nucleotide channels that are normally used in immature neurons (Chan et al., 2007; Guzman et al., 2010). This suggests that targeting these channels would not significantly impair dopaminergic transmission. It should be noted that it is unknown whether the physiology of other vulnerable populations that exhibit high transmembrane Ca^{2+} flux can be similarly manipulated without

dramatic functional consequences. Of course by the time symptoms appear, nigral neurons may already be significantly compromised by cycles of energetic stress and mitochondrial dysfunction. This could potentially be overcome by prospective treatment, but predictive biomarkers are lacking.

Biomarkers

The best way to protect neurons from disease related loss is to target the source of the problem, and to do it as early as possible. By the time patients present with PD, most of their SN dopaminergic neurons have been lost forever (Bernheimer et al., 1973; Riederer and Wuketich, 1976), and in order to better treat these individuals, we need a means to detect the disease earlier. One possibility would be to examine the ratio of physiological oligomers to monomers. Based on our unpublished analysis of familial PD variants, pathogenic mutations in αSyn alter the ratio of specific oligomeric bands to the 14 kDa monomer. Based on the presence of Lewy pathology and other factors implicating altered αSyn proteostasis, it is likely that a portion of sporadic PD also arises from a shift toward aggregation prone monomers. Though analysis of brain tissue would not be recommended (especially for such diagnostic purposes), we and others have shown that αSyn is highly expressed in erythrocytes, a renewable and easily accessible source (Barbour et al., 2008; Bartels et al., 2011). Live cell crosslinking of erythrocytes for analysis by Western blotting is unlikely to be suitable for diagnostic purposes for two reasons. The semiquantitative nature of Western blotting may reduce diagnostic accuracy, and the abundance of hemoglobin in erythrocytes can interfere with specific αSyn-αSyn crosslinking, thereby confounding interpretation. Another possibility is an ELISA using conformation-specific antibodies for

monomers and physiological oligomers, and our lab is currently pursuing the development of these potentially useful tools.

Neuroprotective therapeutics

Our observation of mitochondrial dysfunction induced by prefibrillar αSyn oligomers, but not monomeric αSyn, is supportive of efforts to inhibit αSyn aggregation as a neuroprotective strategy, but they call into question a current approach. ThT, which binds strongly to highly aggregated species with a particular amyloid structure (Biancalana and Koide, 2010), is often used to screen the ability of compounds to inhibit αSyn aggregation. Our work and the work of others suggest that the formation of toxic αSyn species occurs earlier in the timeline of aggregation than onset of ThT positivity. Thus, compounds that prevent amyloid aggregation will not necessarily inhibit the formation of toxic αSyn species and may, in fact, stabilize them. The fact that we observed effects of prefibrillar ThT^{neg}, but not ThT^{pos} aggregates on mitochondrial function suggests that our results are in agreement with the concept of Lewy pathology as a protective mechanism, at least temporarily (Reeve et al., 2012; Tompkins and Hill, 1997). Alternatively, one could attempt to accelerate the fibrilization process to decrease levels of potentially toxic oligomers, although it is likely that they are in equilibrium, and fibrils could release smaller oligomers that promote aggregation of monomeric protein via a secondary nucleation mechanism (Cohen et al., 2013; Cremades et al., 2012)**.** Other well-validated dyes or antibodies that detect αSyn at earlier aggregation states would need to be developed so that they can be used as a new benchmark for pathological aggregation.

An alternative therapeutic strategy to developing aggregation inhibitors is to find ways to stabilize native, aggregation-resistant, helical oligomers(Bartels et al., 2011; Dettmer et al., 2013); however, it is still unclear what form of αSyn represents the (or a) functional unit.

Stabilizers would be expected to reduce pathological aggregation of unfolded monomers, but it is also possible that they could compromise the physiological function of the protein. It is therefore crucial to understand specifically how αSyn functions within neurons so that we may undertake an extensive functional characterization of purified helical oligomers. Until that can be achieved, emphasis should be placed on early diagnosis (as discussed above) and on neutralizing the effects of small, soluble, prefibrillar oligomers - either by preventing their formation using aggregation inhibitors, or by promoting the clearance of excess unfolded monomer or toxic oligomers using immunotherapy with specific antibodies.

Future Work

One limitation of my work characterizing the assembly state of αSyn in human brain homogenates and in intermediate purification steps is that I only looked at oligomerization by crosslinking. Unfortunately, there are a limited number of techniques able assess the assembly state of a single, endogenously expressed protein in a complex mixture of other proteins. Aside from the crosslinking approach used in this work, native gels could theoretically be used to size αSyn complexes. Recently, we have been unsuccessful in consistently distinguishing between unfolded, monomeric αSyn (recombinant protein) and helical αSyn oligomers on native gels. A new paper by the Ischiropoulos group (2014), however, has successfully employed the technique to detect multiple conformers of αSyn in human brain extract, and it will be worth examining our homogenates and partially purified samples using their optimized conditions. Another alternative, an ELISA specific for physiological oligomers, is currently under development in our lab. An important short-term goal for this project is to gain a better understanding of the 60, 80, and 100 kDa crosslinked bands. As mentioned above, intact mass spectrometry of these purified,

crosslinked species may distinguish between conformers or oligomers made up of a different number of subunits.

Additional analysis will provide greater insight into the scope and mechanism of αSyn's effects on mitochondria. Our results indicate that mitochondria treated with prefibrillar αSyn exhibit defective complex I-dependent function, and we are now specifically addressing whether the activity of complex I in this system is also reduced. Alternatively, it is possible that αSyn is limiting complex I substrate availability by impeding transport of glutamate or malate into mitochondria. Thus far we have used mitochondria isolated from liver because they provide a high yield of stable mitochondria suitable for testing an array of αSyn species and respiratory conditions in a single experiment. Now that we have identified a consistent source of bioactive αSyn, we are beginning to examine the effects of this material on the activity brain-derived mitochondria. Expanding to this more disease-relevant source of mitochondria will also enable us to measure ROS production that we hypothesize is behind the αSyn-induced sensitivity to mPTP; the amount of catalase present in liver mitochondria preparations precludes accurate quantification.

Ultimately, I think it would be of great interest to further bridge the two parts of my thesis, and there are interesting questions at the interface of my two projects. Does mitochondrial Ca^{2+} stress alter the ratio of native oligomers to monomers *in situ*? From my preliminary results with partially purified αSyn samples, I can speculate that ROS produced by mitochondria may lead to a destabilization of native oligomers, but this would need to be tested directly in a cellular context. Do αSyn mutants that are incapable of forming native oligomers (or are more likely to form prefibrillar oligomers (Winner et al., 2011)) show greater evidence of mPTP activation compared to wild type αSyn when overexpressed within neurons? How does αSyn extracted

from human brain affect the functioning of isolated mitochondria? An initial experiment suggests that helical oligomers have no effect on mitochondrial Ca^{2+} retention, and if confirmed, this would further support the non-pathological nature of this species. As illustrated by the ThT aggregation data presented here, the behavior of recombinant αSyn can be quite variable. Recombinant αSyn can be induced to aggregate in a variety of different ways to produce numerous species with different structural and functional properties. The fact that two independent preparations resulted in bioactive oligomeric αSyn with similar functional effects on mitochondria reduces the likelihood that our observations are due to artifactual effects related to specific aggregation conditions. That being said, the most relevant source of potentially toxic, prefibrillar αSyn is the brain tissue from synucleinopathy patients, and we aim to purify these species for testing on mitochondria. The experiments proposed here would build upon the groundwork laid by my thesis and provide even greater understanding of the role of αSyn in neurodegenerative disease.

References

Auluck, P.K., Chan, H.Y.E., Trojanowski, J.Q., Lee, V.M.-Y., Bonini, N.M., 2002. Chaperone suppression of alpha-synuclein toxicity in a Drosophila model for Parkinson's disease. Science 295, 865–868.

Barbour, R., Kling, K., Anderson, J.P., Banducci, K., Cole, T., Diep, L., Fox, M., Goldstein, J.M., Soriano, F., Seubert, P., Chilcote, T.J., 2008. Red blood cells are the major source of alpha-synuclein in blood. Neurodegener Dis 5, 55–59.

Bartels, T., Choi, J.G., Selkoe, D.J., 2011. α-Synuclein occurs physiologically as a helically folded tetramer that resists aggregation. Nature 477, 107–110.

Bendor, J.T., Logan, T.P., Edwards, R.H., 2013. The function of α-synuclein. Neuron 79, 1044–1066.

Bernheimer, H., Birkmayer, W., Hornykiewicz, O., Jellinger, K., Seitelberger, F., 1973. Brain dopamine and the syndromes of Parkinson and Huntington. Clinical, morphological and neurochemical correlations. J. Neurol. Sci. 20, 415–455.

Betarbet, R., Sherer, T.B., MacKenzie, G., Garcia-Osuna, M., Panov, A.V., Greenamyre, J.T., 2000. Chronic systemic pesticide exposure reproduces features of Parkinson's disease. Nat. Neurosci. 3, 1301–1306.

Beyer, K., 2007. Mechanistic aspects of Parkinson's disease: alpha-synuclein and the biomembrane. Cell Biochem. Biophys. 47, 285–299.

Biancalana, M., Koide, S., 2010. Molecular mechanism of Thioflavin-T binding to amyloid fibrils. Biochim. Biophys. Acta 1804, 1405–1412.

Burré, J., Sharma, M., Südhof, T.C., 2012. Systematic mutagenesis of α-synuclein reveals distinct sequence requirements for physiological and pathological activities. Journal of Neuroscience 32, 15227–15242.

Bussell, R., Eliezer, D., 2003. A structural and functional role for 11-mer repeats in alpha-synuclein and other exchangeable lipid binding proteins. Journal of Molecular Biology 329, 763–778.

Büttner, S., Habernig, L., Broeskamp, F., Ruli, D., Vögtle, F.N., Vlachos, M., Macchi, F., Küttner, V., Carmona-Gutierrez, D., Eisenberg, T., Ring, J., Markaki, M., Taskin, A.A., Benke, S., Ruckenstuhl, C., Braun, R., Van den Haute, C., Bammens, T., van der Perren, A., Fröhlich, K.-U., Winderickx, J., Kroemer, G., Baekelandt, V., Tavernarakis, N., Kovacs, G.G., Dengjel, J., Meisinger, C., Sigrist, S.J., Madeo, F., 2013. Endonuclease G mediates α-synuclein cytotoxicity during Parkinson's disease. EMBO J 32, 3041–3054.

Chan, C.S., Guzman, J.N., Ilijic, E., Mercer, J.N., Rick, C., Tkatch, T., Meredith, G.E., Surmeier, D.J., 2007. 'Rejuvenation' protects neurons in mouse models of Parkinson's disease. Nature 447, 1081–1086.

Chartier-Harlin, M.-C., Kachergus, J., Roumier, C., Mouroux, V., Douay, X., Lincoln, S., Levecque, C., Larvor, L., Andrieux, J., Hulihan, M., Waucquier, N., Defebvre, L., Amouyel, P., Farrer, M., Destée, A., 2004. Alpha-synuclein locus duplication as a cause of familial Parkinson's disease. Lancet 364, 1167–1169.

Chen, L., Periquet, M., Wang, X., Negro, A., McLean, P.J., Hyman, B.T., Feany, M.B., 2009. Tyrosine and serine phosphorylation of alpha-synuclein have opposing effects on neurotoxicity and soluble oligomer formation. J. Clin. Invest. 119, 3257–3265.

Chinta, S.J., Mallajosyula, J.K., Rane, A., Andersen, J.K., 2010. Mitochondrial α-synuclein accumulation impairs complex I function in dopaminergic neurons and results in increased mitophagy in vivo. Neurosci. Lett. 486, 235–239.

Choubey, V., Safiulina, D., Vaarmann, A., Cagalinec, M., Wareski, P., Kuum, M., Zharkovsky, A., Kaasik, A., 2011. Mutant A53T alpha-synuclein induces neuronal death by increasing mitochondrial autophagy. J. Biol. Chem. 286, 10814–10824.

Cohen, S.I.A., Linse, S., Luheshi, L.M., Hellstrand, E., White, D.A., Rajah, L., Otzen, D.E., Vendruscolo, M., Dobson, C.M., Knowles, T.P.J., 2013. Proliferation of amyloid-β42 aggregates occurs through a secondary nucleation mechanism. Proceedings of the National Academy of Sciences 110, 9758–9763.

Cremades, N., Cohen, S.I.A., Deas, E., Abramov, A.Y., Chen, A.Y., Orte, A., Sandal, M., Clarke, R.W., Dunne, P., Aprile, F.A., Bertoncini, C.W., Wood, N.W., Knowles, T.P.J., Dobson, C.M., Klenerman, D., 2012. Direct observation of the interconversion of normal and toxic forms of α-synuclein. Cell 149, 1048–1059.

Cuervo, A.M., Stefanis, L., Fredenburg, R., Lansbury, P.T., Sulzer, D., 2004. Impaired degradation of mutant alpha-synuclein by chaperone-mediated autophagy. Science 305, 1292–1295.

Cullen, V., Sardi, S.P., Ng, J., Xu, Y.-H., Sun, Y., Tomlinson, J.J., Kolodziej, P., Kahn, I., Saftig, P., Woulfe, J., Rochet, J.-C., Glicksman, M.A., Cheng, S.H., Grabowski, G.A., Shihabuddin, L.S., Schlossmacher, M.G., 2011. Acid β-glucosidase mutants linked to Gaucher disease, Parkinson disease, and Lewy body dementia alter α-synuclein processing. Ann. Neurol. 69, 940–953.

Danzer, K.M., Ruf, W.P., Putcha, P., Joyner, D., Hashimoto, T., Glabe, C., Hyman, B.T., McLean, P.J., 2011. Heat-shock protein 70 modulates toxic extracellular α-synuclein oligomers and rescues trans-synaptic toxicity. The FASEB Journal 25, 326–336.

Dettmer, U., Newman, A.J., Luth, E.S., Bartels, T., Selkoe, D., 2013. In vivo cross-linking reveals principally oligomeric forms of α-synuclein and β-synuclein in neurons and non-neural cells. J. Biol. Chem. 288, 6371–6385.

Devi, L., Raghavendran, V., Prabhu, B.M., Avadhani, N.G., Anandatheerthavarada, H.K., 2008. Mitochondrial import and accumulation of alpha-synuclein impair complex I in human dopaminergic neuronal cultures and Parkinson disease brain. Journal of Biological Chemistry 283, 9089–9100.

Fry, M., Green, D.E., 1981. Cardiolipin requirement for electron transfer in complex I and III of the mitochondrial respiratory chain. J. Biol. Chem. 256, 1874–1880.

Goedert, M., Spillantini, M.G., Del Tredici, K., Braak, H., 2013. 100 years of Lewy pathology. Nat Rev Neurol 9, 13–24.

Gould, N., Mor, D., Lightfoot, R., Malkus, K., Giasson, B., Ischiropoulos, H., 2014. Evidence of Native α-Synuclein Conformers in the Human Brain. J. Biol. Chem.

Gurry, T., Ullman, O., Fisher, C.K., Perovic, I., Pochapsky, T., Stultz, C.M., 2013. The dynamic structure of α-synuclein multimers. J. Am. Chem. Soc. 135, 3865–3872.

Guzman, J.N., Sanchez-Padilla, J., Wokosin, D., Kondapalli, J., Ilijic, E., Schumacker, P.T., Surmeier, D.J., 2010. Oxidant stress evoked by pacemaking in dopaminergic neurons is attenuated by DJ-1. Nature 468, 696–700.

Haass, C., Selkoe, D.J., 2007. Soluble protein oligomers in neurodegeneration: lessons from the Alzheimer's amyloid beta-peptide. Nat. Rev. Mol. Cell Biol. 8, 101–112.

Hansen, C., Li, J.-Y., 2012. Beyond α-synuclein transfer: pathology propagation in Parkinson's disease. Trends Mol Med 18, 248–255.

Hashimoto, M., Takeda, A., Hsu, L.J., Takenouchi, T., Masliah, E., 1999. Role of cytochrome c as a stimulator of alpha-synuclein aggregation in Lewy body disease. J. Biol. Chem. 274, 28849–28852.

Hsu, L.J., Sagara, Y., Arroyo, A., Rockenstein, E., Sisk, A., Mallory, M., Wong, J., Takenouchi, T., Hashimoto, M., Masliah, E., 2000. alpha-synuclein promotes mitochondrial deficit and oxidative stress. Am. J. Pathol. 157, 401–410.

Ignatev, A., Kravchenko, S., Rak, A., Goody, R.S., Pylypenko, O., 2008. A structural model of the GDP dissociation inhibitor rab membrane extraction mechanism. J. Biol. Chem. 283, 18377–18384.

Kahle, P.J., Neumann, M., Ozmen, L., Muller, V., Jacobsen, H., Schindzielorz, A., Okochi, M., Leimer, U., van Der Putten, H., Probst, A., Kremmer, E., Kretzschmar, H.A., Haass, C., 2000. Subcellular localization of wild-type and Parkinson's disease-associated mutant alpha - synuclein in human and transgenic mouse brain. J. Neurosci. 20, 6365–6373.

Karpinar, D.P., Balija, M.B.G., Kügler, S., Opazo, F., Rezaei-Ghaleh, N., Wender, N., Kim, H.-Y., Taschenberger, G., Falkenburger, B.H., Heise, H., Kumar, A., Riedel, D., Fichtner, L., Voigt, A., Braus, G.H., Giller, K., Becker, S., Herzig, A., Baldus, M., Jäckle, H., Eimer, S., Schulz, J.B., Griesinger, C., Zweckstetter, M., 2009. Pre-fibrillar alpha-synuclein variants with impaired beta-structure increase neurotoxicity in Parkinson's disease models. EMBO J 28, 3256–3268.

Klucken, J., Outeiro, T.F., Nguyen, P., McLean, P.J., Hyman, B.T., 2006. Detection of novel intracellular alpha-synuclein oligomeric species by fluorescence lifetime imaging. The FASEB Journal 20, 2050–2057.

Kostrzewa, R.M., 2000. Review of apoptosis vs. necrosis of substantia nigra pars compacta in Parkinson's disease. Neurotox Res 2, 239–250.

Kraytsberg, Y., Kudryavtseva, E., McKee, A.C., Geula, C., Kowall, N.W., Khrapko, K., 2006. Mitochondrial DNA deletions are abundant and cause functional impairment in aged human substantia nigra neurons. Nat Genet 38, 518–520.

Kristal, B.S., Conway, A.D., Brown, A.M., Jain, J.C., Ulluci, P.A., Li, S.W., Burke, W.J., 2001. Selective dopaminergic vulnerability: 3,4-dihydroxyphenylacetaldehyde targets mitochondria. Free Radical Biology and Medicine 30, 924–931.

Lee, M., Hyun, D., Halliwell, B., Jenner, P., 2001. Effect of the overexpression of wild-type or mutant alpha-synuclein on cell susceptibility to insult. Journal of Neurochemistry 76, 998–1009.

Liu, G., Zhang, C., Yin, J., Li, X., Cheng, F., Li, Y., Yang, H., Uéda, K., Chan, P., Yu, S., 2009. α-Synuclein is differentially expressed in mitochondria from different rat brain regions and dose-dependently down-regulates complex I activity. Neurosci. Lett. 454, 187–192.

Loew, L.M., Carrington, W., Tuft, R.A., Fay, F.S., 1994. Physiological cytosolic Ca2+ transients evoke concurrent mitochondrial depolarizations. Proc. Natl. Acad. Sci. U.S.A. 91, 12579–12583.

Martin, L.J., Semenkow, S., Hanaford, A., Wong, M., 2013. The mitochondrial permeability transition pore regulates Parkinson's disease development in mutant α-synuclein transgenic mice. Neurobiol. Aging 10.1016–j.neurobiolaging.2013.11.008.

Nakamura, K., Nemani, V.M., Wallender, E.K., Kaehlcke, K., Ott, M., Edwards, R.H., 2008. Optical reporters for the conformation of alpha-synuclein reveal a specific interaction with mitochondria. Journal of Neuroscience 28, 12305–12317.

Olanow, C.W., Schapira, A.H.V., 2013. Therapeutic prospects for Parkinson disease. Ann. Neurol. 74, 337–347.

Parihar, M.S., Parihar, A., Fujita, M., Hashimoto, M., Ghafourifar, P., 2008. Mitochondrial association of alpha-synuclein causes oxidative stress. Cell. Mol. Life Sci. 65, 1272–1284.

Pasternak, B., Svanström, H., Nielsen, N.M., Fugger, L., Melbye, M., Hviid, A., 2012. Use of calcium channel blockers and Parkinson's disease. Am. J. Epidemiol. 175, 627–635.

Rasola, A., Bernardi, P., 2011. Mitochondrial permeability transition in Ca(2+)-dependent apoptosis and necrosis. Cell Calcium 50, 222–233.

Reeve, A.K., Park, T.-K., Jaros, E., Campbell, G.R., Lax, N.Z., Hepplewhite, P.D., Krishnan, K.J., Elson, J.L., Morris, C.M., McKeith, I.G., Turnbull, D.M., 2012. Relationship between mitochondria and α-synuclein: a study of single substantia nigra neurons. Arch. Neurol. 69, 385–393.

Rhoades, E., Ramlall, T.F., Webb, W.W., Eliezer, D., 2006. Quantification of alpha-synuclein binding to lipid vesicles using fluorescence correlation spectroscopy. Biophysj 90, 4692–4700.

Riederer, P., Wuketich, S., 1976. Time course of nigrostriatal degeneration in parkinson's disease. A detailed study of influential factors in human brain amine analysis. J. Neural Transm. 38, 277–301.

Ritz, B., Rhodes, S.L., Qian, L., Schernhammer, E., Olsen, J.H., Friis, S., 2010. L-type calcium channel blockers and Parkinson disease in Denmark. Ann. Neurol. 67, 600–606.

Sarafian, T.A., Ryan, C.M., Souda, P., Masliah, E., Kar, U.K., Vinters, H.V., Mathern, G.W., Faull, K.F., Whitelegge, J.P., Watson, J.B., 2013. Impairment of mitochondria in adult mouse brain overexpressing predominantly full-length, N-terminally acetylated human α-synuclein. PLoS ONE 8, e63557.

Schapira, A.H.V., Olanow, C.W., 2004. Neuroprotection in Parkinson disease: mysteries, myths, and misconceptions. JAMA 291, 358–364.

Shavali, S., Brown-Borg, H.M., Ebadi, M., Porter, J., 2008. Mitochondrial localization of alpha-synuclein protein in alpha-synuclein overexpressing cells. Neuroscience Letters 439, 125–128.

Sherer, T.B., Betarbet, R., Stout, A.K., Lund, S., Baptista, M., Panov, A.V., Cookson, M.R.,

Greenamyre, J.T., 2002. An in vitro model of Parkinson's disease: linking mitochondrial impairment to altered alpha-synuclein metabolism and oxidative damage. Journal of Neuroscience 22, 7006–7015.

Singleton, A.B., Farrer, M., Johnson, J., Singleton, A., Hague, S., Kachergus, J., Hulihan, M., Peuralinna, T., Dutra, A., Nussbaum, R., Lincoln, S., Crawley, A., Hanson, M., Maraganore, D., Adler, C., Cookson, M.R., Muenter, M., Baptista, M., Miller, D., Blancato, J., Hardy, J., Gwinn-Hardy, K., 2003. alpha-Synuclein locus triplication causes Parkinson's disease. Science 302, 841.

Smith, D.P., Tew, D.J., Hill, A.F., Bottomley, S.P., Masters, C.L., Barnham, K.J., Cappai, R., 2008. Formation of a high affinity lipid-binding intermediate during the early aggregation phase of alpha-synuclein. Biochemistry 47, 1425–1434.

Spillantini, M.G., Schmidt, M.L., Lee, V.M., Trojanowski, J.Q., Jakes, R., Goedert, M., 1997. Alpha-synuclein in Lewy bodies. Nature 388, 839–840.

Surmeier, D.J., Guzman, J.N., Sanchez-Padilla, J., Goldberg, J.A., 2010. What causes the death of dopaminergic neurons in Parkinson's disease? Prog. Brain Res. 183, 59–77.

Surmeier, D.J., Schumacker, P.T., 2013. Calcium, bioenergetics, and neuronal vulnerability in Parkinson's disease. J. Biol. Chem. 288, 10736–10741.

Tao-Cheng, J.-H., 2006. Activity-related redistribution of presynaptic proteins at the active zone. Neuroscience 141, 1217–1224.

Tompkins, M.M., Hill, W.D., 1997. Contribution of somal Lewy bodies to neuronal death. Brain Research 775, 24–29.

Trexler, A.J., Rhoades, E., 2012. N-Terminal acetylation is critical for forming α-helical oligomer of α-synuclein. Protein Sci. 21, 601–605.

Volles, M.J., Lansbury, P.T., 2003. Zeroing in on the pathogenic form of alpha-synuclein and its mechanism of neurotoxicity in Parkinson's disease. Biochemistry 42, 7871–7878.

Wang, W., Perovic, I., Chittuluru, J., Kaganovich, A., Nguyen, L.T.T., Liao, J., Auclair, J.R.,

Johnson, D., Landeru, A., Simorellis, A.K., Ju, S., Cookson, M.R., Asturias, F.J., Agar, J.N., Webb, B.N., Kang, C., Ringe, D., Petsko, G.A., Pochapsky, T.C., Hoang, Q.Q., 2011. A soluble α-synuclein construct forms a dynamic tetramer. Proceedings of the National Academy of Sciences 108, 17797–17802.

Weinreb, P.H., Zhen, W., Poon, A.W., Conway, K.A., Lansbury, P.T., 1996. NACP, a protein implicated in Alzheimer's disease and learning, is natively unfolded. Biochemistry 35, 13709–13715.

Westphal, C.H., Chandra, S.S., 2013. Monomeric synucleins generate membrane curvature. J. Biol. Chem. 288, 1829–1840.

Winner, B., Jappelli, R., Maji, S.K., Desplats, P.A., Boyer, L., Aigner, S., Hetzer, C., Loher, T., Vilar, M., Campioni, S., Tzitzilonis, C., Soragni, A., Jessberger, S., Mira, H., Consiglio, A., Pham, E., Masliah, E., Gage, F.H., Riek, R., 2011. In vivo demonstration that alpha-synuclein oligomers are toxic. Proceedings of the National Academy of Sciences 108, 4194–4199.

Wislet-Gendebien, S., D'Souza, C., Kawarai, T., St George-Hyslop, P., Westaway, D., Fraser, P., Tandon, A., 2006. Cytosolic proteins regulate alpha-synuclein dissociation from presynaptic membranes. J. Biol. Chem. 281, 32148–32155.

Zhang, M., Mileykovskaya, E., Dowhan, W., 2002. Gluing the respiratory chain together. Cardiolipin is required for supercomplex formation in the inner mitochondrial membrane. J. Biol. Chem. 277, 43553–43556.

Appendix 1

Investigating the Ability of α-Synuclein to Sensitize Cells to Ca^{2+}-Induced Toxicity

Contributions:

Experiments were designed by Eric Luth and Dennis Selkoe.

All experiments were performed by Eric Luth.

Introduction

In addition to its role in familial forms of PD, αSyn contributes to the pathogenesis of the more common sporadic forms of the disease. Intracellular aggregates of αSyn are the main component of Lewy bodies and Lewy neurites, the pathological hallmarks of PD (Spillantini et al., 1997). It is becoming increasingly clear that soluble αSyn oligomers, rather than insoluble fibrils, are the main neurotoxic species in PD and other such synucleinopathies (Volles and Lansbury, 2003). PD selectively targets neurons of the SNc, DMV, LC, and other brain regions that are characterized by intracellular Ca^{2+} oscillations and low expression of cytosolic Ca^{2+} buffering proteins (Surmeier and Schumacker, 2013). Proper regulation of cytosolic Ca^{2+} levels by ATP-dependent plasma membrane pumps and uptake by Ca^{2+}-buffering organelles is necessary to prevent Ca^{2+}-associated apoptotic or necrotic cell death. Elevated cytosolic Ca^{2+} can therefore burden mitochondria in two ways: mitochondrial generation of ATP is required to actively pump Ca^{2+} into the extracellular space or internal stores such as the endoplasmic reticulum, and mitochondria themselves act as Ca^{2+} buffering organelles. Mitochondrial Ca^{2+} uptake also presents a potential risk to the cell. Physiological Ca^{2+} uptake is favorable for ATP production because Ca^{2+} stimulates the activity of the tricarboxylic acid cycle; however, excessive Ca^{2+} uptake can compromise ATP production by reducing the mitochondrial membrane potential that is used to drive oxidative phosphorylation or by leading to the formation of the mPTP (Brookes et al., 2004). Despite the physiological phenotype of cells at risk in PD and the important role of αSyn accumulation in most forms of the disease, there has been little investigation into the ability of αSyn to sensitize cells to Ca^{2+}-induced toxicity.

To investigate αSyn-induced changes to Ca^{2+} homeostasis, we used a neuroblastoma cell line that can be induced to overexpress αSyn. Our results suggest that regulated overexpression

of αSyn results in higher levels of mitochondrial matrix Ca^{2+} ($[Ca^{2+}]_m$) as measured by Rhod2 fluorescence, and sensitizes neuroblastoma cells to toxicity resulting from exposure to the Ca^{2+} ionophore A23187. Preliminary experiments indicate that αSyn overexpression also renders cells more susceptible to toxicity caused by a more targeted elevation of $[Ca^{2+}]_m$ induced by exposing cells to NMDA.

Results and Discussion

Inducible overexpression of αSyn:

We used 3D5 cells, a human dopaminergic neuroblastoma cell line that can be induced to overexpress α-synuclein in a tetracycline-off system (Ko et al., 2008). *3*D5 cells were cultured in the presence of tetracycline, which acts to repress αSyn overexpression. We induced αSyn overexpression by culturing the cells in tetracycline-free conditions and harvested them after different durations of induction. A protein normalized (see actin loading control) Western blot for αSyn confirms this overexpression beginning at, in this case, 4 d of induction (Figure A1.1A). In this example, the minimal increase in αSyn overexpression earlier could result from residual tetracycline in the media that acts to keep the cells in a relatively repressed state. Inducing αSyn overexpression for longer in this system leads to the presence of a small amount SDS-resistant αSyn oligomers (Ko et al., 2008). At 7 d of induction, but not before, a mid-to-high molecular weight smear of αSyn immunoreactivity is observed in this cell line (Figure A1.1B). Though we believe this 14 kDa band represents both monomeric and helical tetrameric αSyn that is not stable in the presence of SDS (see Chapter 3 and Appendix 3), to distinguish these species from SDS-resistant, perhaps pathological oligomers, we refer collectively to the species that run at 14 kDa under denaturing conditions as “monomers”. In subsequent

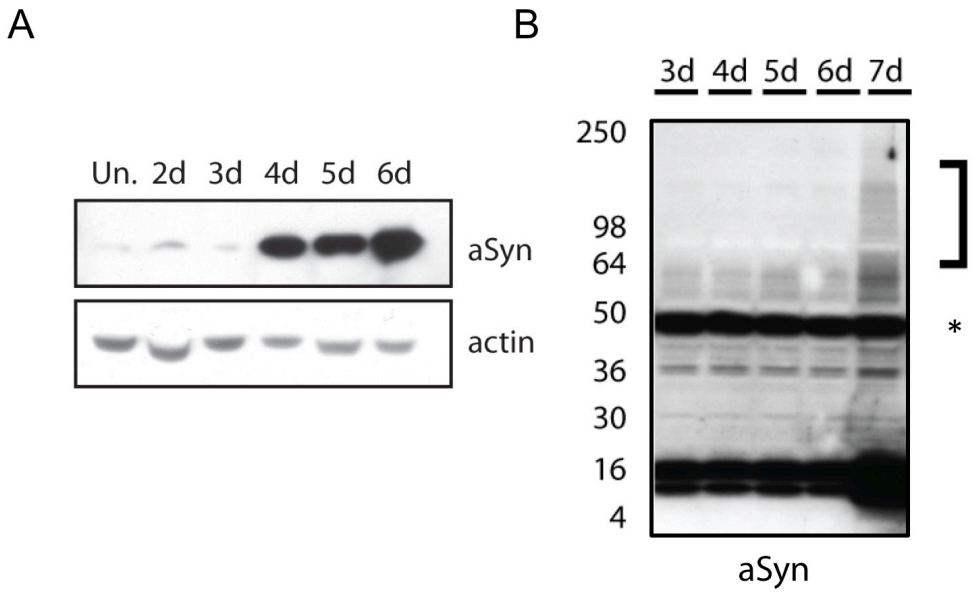

Figure A1.1: Time-dependent induction of Monomeric and Oligomeric αSyn in 3D5 Neuroblastoma cells.

A. 3D5 human neuroblastoma cells express αSyn in a tetracycline-off manner. Uninduced cells (Un.) cultured in the presence of tetracycline express minimal endogenous αSyn, possibly resulting from promoter leak. After, at most, 4 days of culturing in the absence of tetracycline (induction), cells massively overexpress αSyn. B. SDS-resistant αSyn oligomers(noted by bracket) can be detected after 7 days of induction, but not before. * indicates a non-specific band detected by the Syn1 αSyn antibody.

experiments, uninduced (repressed) cells were compared to cells expressing monomers or monomers plus SDS-resistant oligomers.

Examination of Resting $[Ca^{2+}]_m$:

We first used 3D5 cells to examine whether αSyn overexpression, specifically the induction of oligomers, alters the basal $[Ca^{2+}]_m$. To address this, we compared the $[Ca^{2+}]_m$ of cells overexpressing monomeric or monomeric plus oligomeric αSyn to uninduced cells using the $[Ca^{2+}]_m$ indicator Rhod-2AM, which is trapped within cells after cleavage to Rhod-2. In contrast to the cytosolic Ca^{2+} indicator Fluo-3 that exhibits a diffuse fluorescence when loaded into cells, Rhod-2 shows a punctate fluorescence corresponding to mitochondrial localization (Figure A1.2A). We used flow cytometry to quantify the fluorescence of cells loaded with Rhod-2 and the dye MitoTracker green that was used a control for mitochondrial mass. To ensure that only live cells were analyzed, we first excluded debris and dead cells by gating based on forward and side scatter parameters in the Flow Jo software (Figure A1.2B). A histogram of the Rhod-2 fluorescence of live cells is displayed in Figure A1.2C. Cells induced for 4 d (blue) show a slightly shifted histogram compared to uninduced cells (green), and the histogram for cells induced for 7 d is shifted toward an even greater fluorescence. When normalizing for mitochondrial mass, we observed that the level of mitochondrial Ca^{2+} (Rhod-2/MitoTracker fluorescence) was elevated in cells overexpressing αSyn for 7-10. Though the data did not reach significance ($p = 0.06$ with paired comparisons to uninduced and 3-4 d induced cells from the same parental stock), they suggest that in 3D5 cells that overexpress αSyn to the point where oligomers can be detected, the mitochondria contain higher levels of Ca^{2+} under basal conditions than uninduced cells or those in which only monomer can be detected.

Figure A1.2: Extended induction of αSyn expression correlates with higher levels of mitochondrial Ca^{2+}.

A. 3D5 cells loaded with the cytosolic Ca^{2+} indicator Fluo-3 (at 2 uM) and mitochondrial Ca^{2+} indicator Rhod-2AM at 500 nM and analyzed by fluorescence microscopy. Note the cytosolic diffuse fluorescence for fluo-3 and the punctate fluorescence for Rhod 2 corresponding to mitochondrial localization. B. Individual cells analyzed by flow cytometry and plotted according their forward and side scattering (their size and complexity/granularity, respectively). Live cells were gated based on these parameters and this population was subsequently analyzed for fluorescence. C. A histogram showing the relative distribution of live cells according to their fluorescence in the DsRed fluorescence channel, corresponding to Rhod-2 fluorescence intensity. Uninduced (0d) cells and cells induced to overexpress αSyn for 4 and 7 days are compared. D. The ratio of median fluorescence intensity of Rhod-2 to mitotracker (control for mitochondrial mass) is plotted for uninduced, 3-4d induced, and 7d induced cells. Each color/symbol represents data collected using the same stock of cells that were either induced or uninduced. The level of mitochondrial Ca^{2+} (Rhod-2/mitotracker fluorescence) was elevated in cells overexpressing αSyn for 7-10 d.

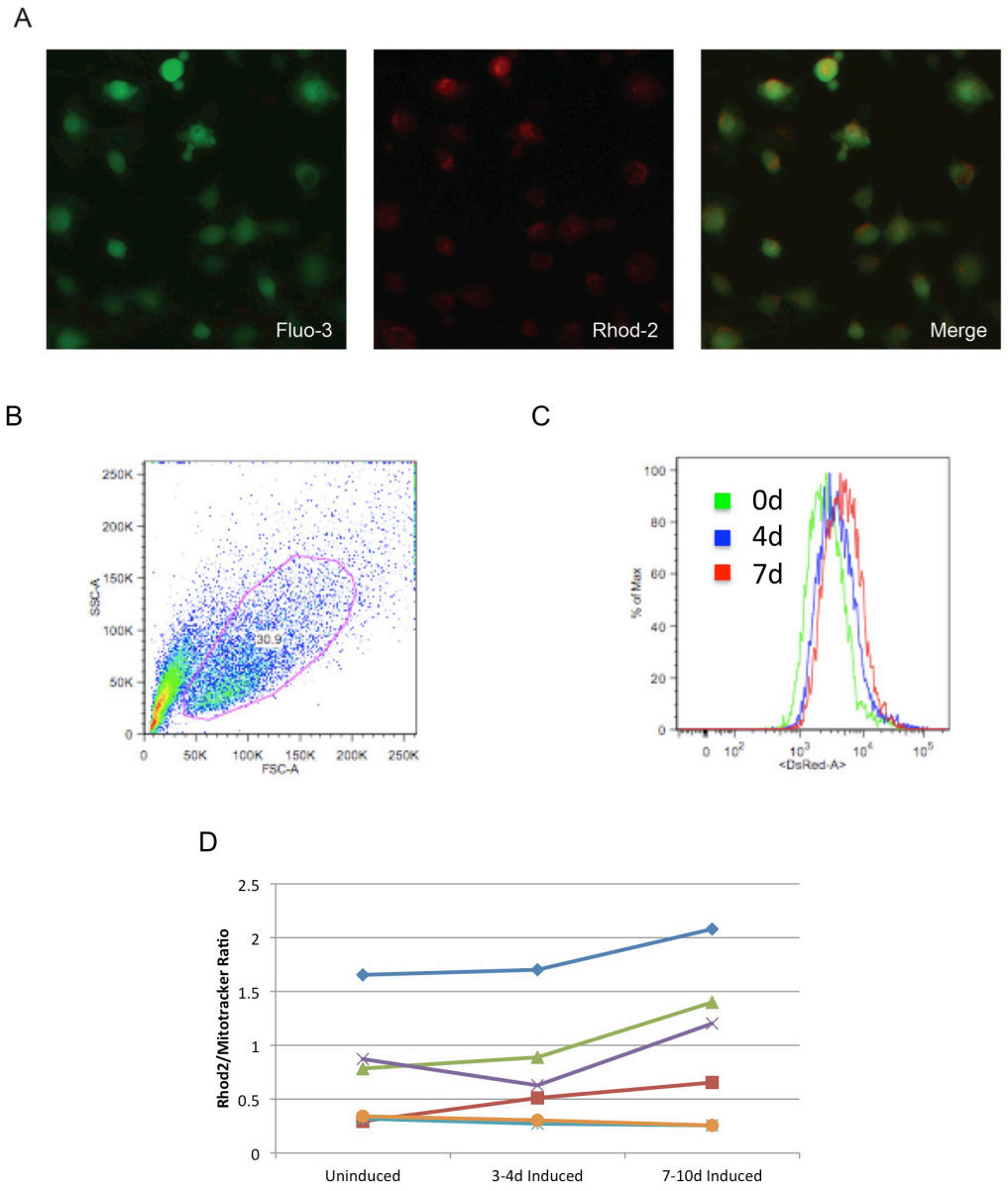

Figure A1.2 (Continued): Extended induction of αSyn expression correlates with higher levels of mitochondrial Ca^{2+}.

Ca^{2+} ionophore-induced toxicity:

We then asked whether overexpression of αSyn sensitizes cells to Ca^{2+}-induced toxicity. For these experiments, we compared uninduced 3D5 cells to those that had been induced to overexpress αSyn for 8 d. Cells were cultured in the presence of the Ca^{2+} ionophore A23187 for 24 h and then analyzed for the degree of toxicity using flow cytometry. After ionophore treatment, cells were incubated with fluorescent "live cell" indicator calcein-AM and the "dead cell" dye ethidium homodimer-1 that binds to the DNA of cells with permeable membranes. As seen in Figure A1.3A, a percentage of uninduced cells were killed by exposure to A23187. Cells were considered "live" when they displayed calcein, but not ethidium homodimer-1 fluorescence (lower right quadrant). "Dead" cells were those that exhibited ethidium homodimer-1, but not calcein fluorescence (upper left quadrant). Examination of 8 d-induced 3D5 cells showed that A23187 treatment led to a reduction in the number of live cells and a corresponding increase in the number of dead cells compared to uninduced cells. Using a range of A23187 concentrations, we observed a dose-dependent increase in the percentage of dead cells for both uninduced and induced cells, and at each concentration we observed more cell death when αSyn was overexpressed (Figure A1.3B). When sets of induced and uninduced cells from the same experiment were analyzed pairwise, there were significantly more dead cells upon αSyn overexpression at concentrations ranging from 0.5–2 uM as exemplified by the data shown in Figure A1.3C.

To rule out the possibility that the observed effects of induction were due to the removal of tetracycline rather than the overexpression of αSyn, we utilized the parental cell line to the 3D5 cells (BE(2)M17D) that does not overexpress αSyn in response to tetracycline removal. We compared the percentages of dead cells in response to A23187 treatment in the presence or

Figure A1.3: Induced αSyn overexpression sensitizes cells to Ca^{2+}-induced toxicity.

A. Flow cytometry of uninduced and 8 d induced 3D5 cells treated with 1 uM A23187 Ca^{2+} ionophore for 24 hours and then loaded with calcein and ethidium homodimer 1. Each dot represents an individual cell. Quadrants were defined using samples containing unstained cells, cells stained with only calcein, and cells stained only ethidium homodimer 1. Induced samples contain more cells in the calcein-negative, ethidium homodimer 1-positive quadrant and less in the calcein-positive, ethidium homodimer-1-negative quadrant. B. Induced and uninduced cells were treated with vehicle or 0.5-4 uM A23187 and the percent dead cells (calcein-negative, ethidium homodimer 1-positive) was analyzed as in A. Error bars represent the standard deviation of 4 independent experiments. C. Statistical significance ($p < 0.05$) was reached when pairwise analysis was used for uninduced and induced sample pairs. Examples with 1 and 2 uM A23187 are shown.

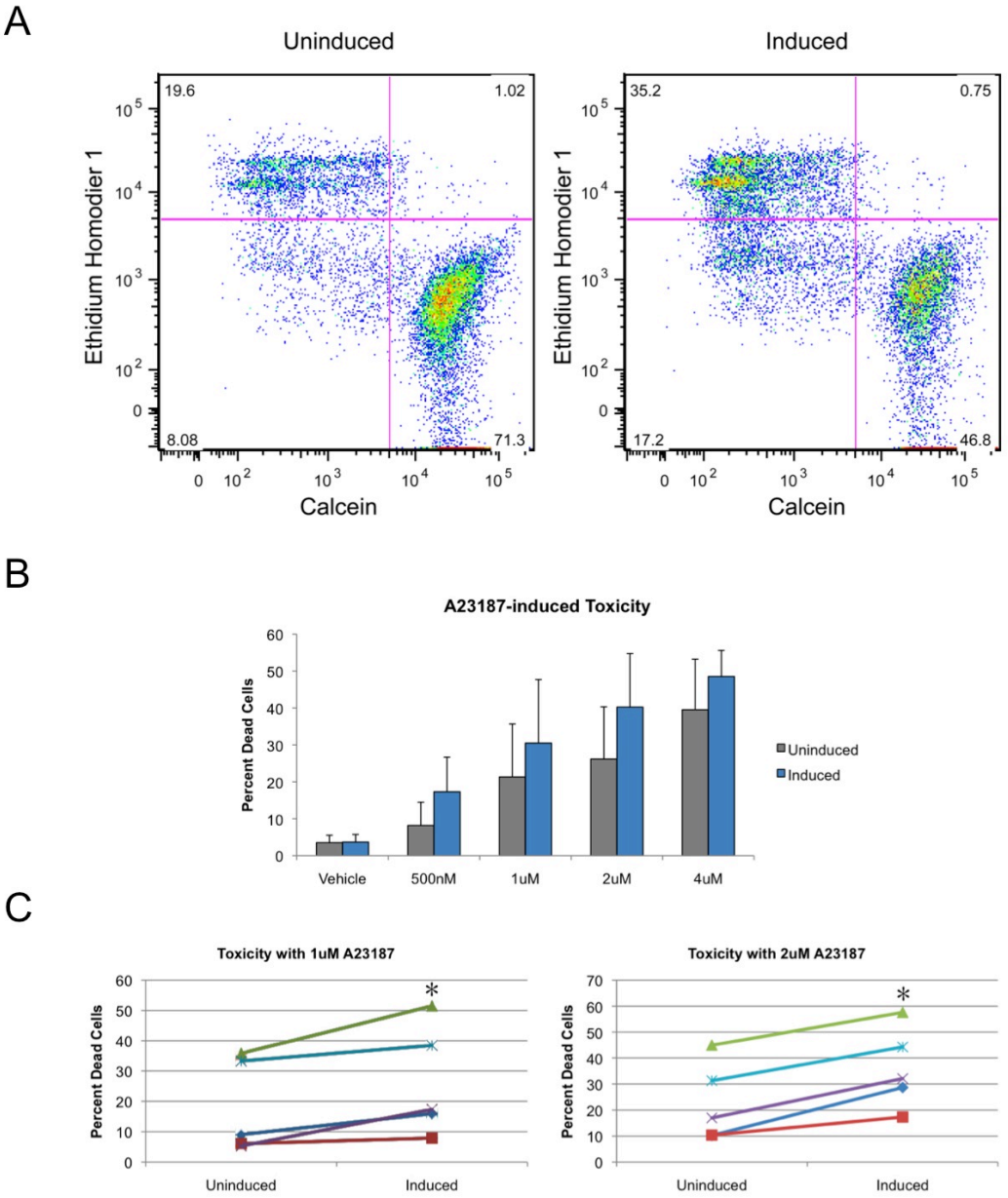

Figure A1.3 (Continued): Induced αSyn overexpression sensitizes cells to Ca^{2+}-induced toxicity.

absence (after 8 d) of tetracycline. We did observe a roughly-dose-dependent effect of A23187 on cell survival, but we did not see any effect of tetracycline removal on the percent of dead cells (Figure A1.4). This suggests that αSyn overexpression and not tetracycline removal is responsible for the sensitization effects of induction.

NMDA-induced changes in mitochondrial metabolism

To test whether αSyn overexpression is associated with impaired mitochondrial function in response to Ca^{2+} uptake, we exposed uninduced and 8 d-induced cells to NMDA and assessed the metabolism of 3-(4,5-dimethylthiazol-2-yl)-2,5-diphenyl tetrazolium bromide (MTT) by mitochondrial dehydrogenases. NMDA stimulation is known to increase $[Ca^{2+}]_m$ in neurons (Peng and Greenamyre, 1998; Peng et al., 1998). Preliminary results indicated that 25 and 50 uM NMDA application had no effect on MTT metabolism in uninduced cells, but it dose-dependently reduced MTT metabolism in cells overexpressing αSyn (Figure A1.5). Treatment of cells with 0.1% Triton X-100 was used as a positive control to kill cells, thereby eliminating mitochondrial metabolism and MTT conversion.

We observed that αSyn overexpression, in particular to the degree that SDS-resistant oligomers can be detected, is associated with elevated resting $[Ca^{2+}]_m$, increased sensitivity to Ca^{2+} ionophore-induced toxicity, and reduced mitochondrial function in response to NMDA treatment. While these results are potentially interesting, there are many control experiments that need to be conducted. To gain more insight into the role of oligomeric αSyn, all experiments, including toxicity and mitochondrial function assays, need to be conducted with both 3-6 d-induced as well as ≥ 7 d induced cells. Before claiming that treatments associated with toxicity

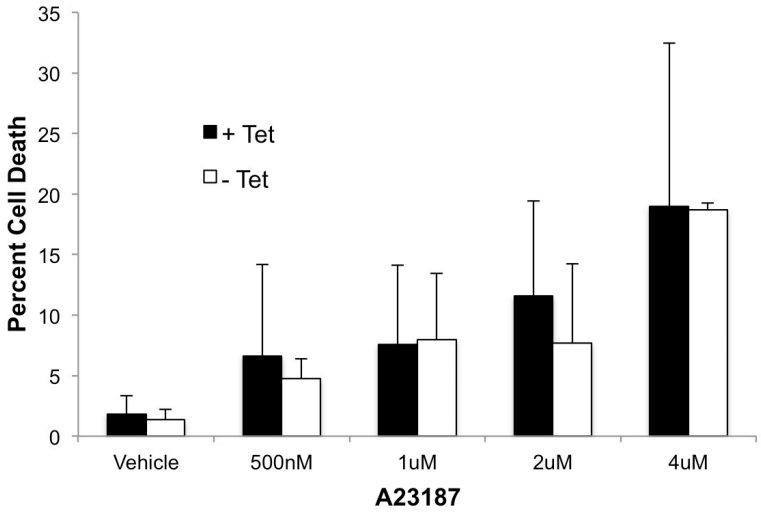

Figure A1.4: Sensitization of induced cells to Ca^{2+}-induced toxicity is not due to the removal of tetracycline.

The parental cell line of 3D5, called BE(2)M17D cells, dot no overexpress αSyn in response to tetracycline removal. BE(2)M17D cells were treated and analyzed as in Figure 3. Error bars represent the standard deviation of 3 independent experiments.

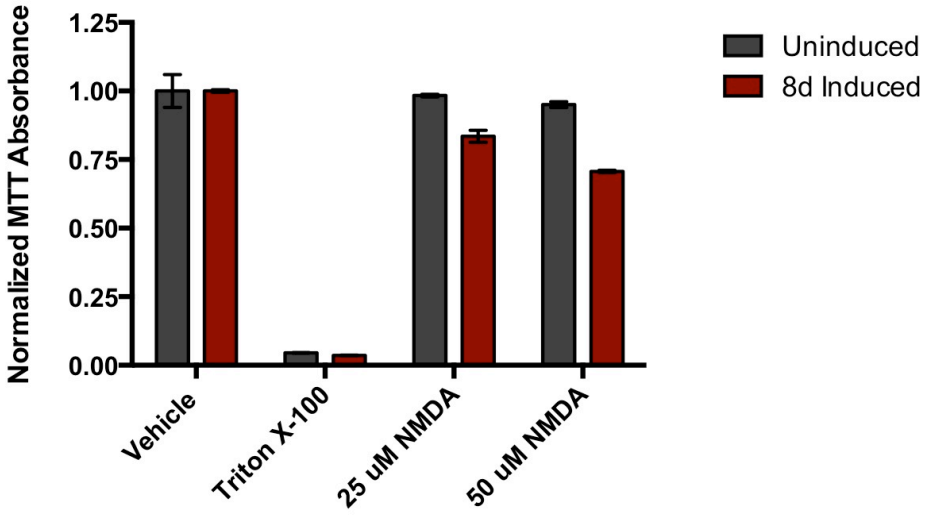

Figure A1.5: Induction of αSyn oligomer expression is correlated with increased sensitivity to NMDA.

Uninduced and 8d induced cells were cultured in 1.8mM Ca^{2+} and treated for 1 hour with 25-50 uM NMDA. Cells were then assessed for their ability to metabolize MTT reagent. The results for uninduced and induced cells are normalized to the NMDA vehicle for each group. Error bars represent the standard deviation of 3 biological replicates analyzed on the same day.

(A23187) and reduced mitochondrial function (NMDA) are related to mitochondrial Ca^{2+}, it will be necessary to determine whether these stimuli do indeed raise $[Ca^{2+}]_m$. This can be accomplished by treating the cells with these chemicals, incubating them with Rhod-2AM (and also Fluo-3AM to measure cytosolic Ca^{2+}), and then analyzing them via flow cytometry. The literature suggests that Ca^{2+} influx through NMDA receptors targets mitochondria (Peng et al., 1998; Peng and Greenamyre, 1998); however, we would need additional controls to show that mitochondrial Ca^{2+} uptake is required for the reduction in MTT absorbance after NMDA treatment that we see in induced cells. This experiment should be repeated in the presence of an extracellular Ca^{2+} chelator (such as EGTA) or Ru360, an inhibitor of mitochondrial Ca^{2+} uptake. It would also be important to examine the sensitivity to Ca^{2+}-induced toxicity using a technique that targets mitochondria more specifically. A23187 is an ionophore that will ultimately lead to the equilibration of Ca^{2+} across all cell membranes. Application of thapsigargin, the ER Ca^{2+} pump inhibitor, acts to deplete ER Ca^{2+} stores and trigger Ca^{2+} uptake into mitochondria (Hom et al., 2007) and would provide a more elegant means to examine the role of mitochondria in Ca^{2+}-mediated toxicity and possible sensitizing effects of αSyn.

These preliminary results are in agreement with those of Parihar and colleagues (2008) who also observed elevated Rhod-2 fluorescence in αSyn overexpressing neuroblastoma cells. Elevated $[Ca^{2+}]_m$ would be expected to result in reduced resting $\Delta\Psi_{m,}$, a phenomenon observed by other labs (Li et al., 2013; Marongiu et al., 2009; Parihar et al., 2009) and one that can be rescued by inhibiting mitochondrial Ca^{2+} uptake (Marongiu et al., 2009). It is possible that cells in which mitochondria exhibit higher $[Ca^{2+}]_m$ at rest would be more vulnerable to the type of intracellular Ca^{2+} stress that is characteristic of neurons vulnerable in PD (Surmeier and Schumacker, 2013). Mitochondrial Ca^{2+} overload triggers the formation of the mPTP. In αSyn

overexpressing cells, this critical threshold of $[Ca^{2+}]_m$ could potentially be reached with a more mild intracellular Ca^{2+} elevation that would not cause toxicity (or would cause less toxicity) in cells without overexpressed αSyn simply because overexpressing cells are effectively starting from a position of higher $[Ca^{2+}]_m$. It will therefore be interesting to determine whether mPTP inhibitors like CsA can rescue Ca^{2+}-induced toxicity in αSyn overexpressing cells. Our isolated mitochondria data (Chapter 2) suggest that oligomeric αSyn can act directly on mitochondria to increase their susceptibility to Ca^{2+}; however, in the context of a cell there are many potential sites of action for pathological αSyn species that could affect cellular and mitochondrial Ca^{2+} homeostasis. There is evidence that αSyn can affect Ca^{2+} flux at the endoplasmic reticulum and plasma membranes as well (Hettiarachchi et al., 2009; Marongiu et al., 2009), and it is possible that all of these pathways contribute to cell death in PD.

Experimental Techniques

SDS-PAGE / Western blotting (WB):

Tet-off 3D5 human neuroblastoma cells (Ko et al., 2008) were induced to overexpress αSyn for the indicated number of days. Supernatant from 3,000 x g spins were used for Western blotting. Samples were prepared using MilliQ water and 4x sample buffer containing LDS plus 20% β-mercaptoethanol (βME) Samples were electrophoresed on Nu-PAGE 4-12% Bis-Tris gels with MES-SDS running buffer. Gels were then transferred onto 0.45 μm Immobilon-P PVDF membranes for 60 min at 400 mA constant current at 4°C in transfer buffer consisting of 25 mM Tris, 192 mM glycine, and 20% methanol. After transfer, membranes were blocked in 5% non-fat milk in PBS with 0.1% v/v Tween-20 (PBS-T) for 30 min at room temperature and then incubated in primary antibody either overnight at 4 °C or for 60 min at room temperature.

Membranes were then washed 3 times for 5 min in PBS-T, incubated with secondary antibody, washed 3 more times for 5 min in PBS-T, and then developed with ECL Plus or ECL Prime according to the manufacturer's directions.

Rhod2 Fluorescence Assay: Induced and uninduced 3D5 cells were gently scraped into microcentrifuge tubes in 1 ml of culture medium. Cells were incubated with 200nM Rhod2-AM and 100nM MitoTracker Green for 15min in the dark. Cells were then spun down, resuspended with ice cold PBS, and analyzed using an LSRII flow cytometer at using PE settings for Rhod-2 and FITC settings for MitoTracker. Flow cytometry data were analyzed using Flow Jo software.

Cell Viability Assay:

3D5 cells were treated for 24hr with A23187 to induce Ca^{2+} influx and downstream effects. 1 ml of cells was transferred to microcentrifuge tubes at a concentration of 0.1-5x10^6 cells/ml in warm culture medium. Calcein and ethidium homodimer 1 were added to cell suspensions to a final concentration of 100 nM and 8 uM, respectively, and the cells were incubated at room temperature in the dark for 15 min. Cells were pelleted and resuspended in 300-500 μl ice cold PBS. Analysis was performed by flow cytometry using an LSRII flow cytometer and a 488 nm excitation laser, measuring emission at 530 nm (calcein) and 610 nm (ethidium homodimer 1). Data were analyzed using Flow Jo software.

MTT Toxicity Assay:

M17D neuroblastoma cells were seeded at a density of 1.5x10^5 cells/ml and treated at 37˚ for 24hr with PBS or 25-50 uM NMDA after which media was replaced with 50 μL of 0.5

mg/mL MTT in DMEM and incubated for 2hrs at 37°C. 200 μL of MTT lysis buffer (50% dimethyl formamide, 20% SDS, pH 7.4, 0.025N HCl, 2% acetic acid) was added to each well to solubilize the cells, and the plates were incubated at 37°C overnight and absorbance was determined using a luminometer. Plates were read at 570 nm for the reduction of MTT, subtracting baseline readings at 650 nm from each well.

References

Brookes, P.S., Yoon, Y., Robotham, J.L., Anders, M.W., Sheu, S.-S., 2004. Calcium, ATP, and ROS: a mitochondrial love-hate triangle. Am. J. Physiol., Cell Physiol. 287, C817–33.

Hettiarachchi, N.T., Parker, A., Dallas, M.L., Pennington, K., Hung, C.-C., Pearson, H.A., Boyle, J.P., Robinson, P., Peers, C., 2009. α-Synuclein modulation of Ca 2+signaling in human neuroblastoma (SH-SY5Y) cells. Journal of Neurochemistry 111, 1192–1201.

Hom, J.R., Gewandter, J.S., Michael, L., Sheu, S.-S., Yoon, Y., 2007. Thapsigargin induces biphasic fragmentation of mitochondria through calcium-mediated mitochondrial fission and apoptosis. J. Cell. Physiol. 212, 498–508.

Ko, L.-W., Ko, H.-H.C., Lin, W.-L., Kulathingal, J.G., Yen, S.-H.C., 2008. Aggregates assembled from overexpression of wild-type alpha-synuclein are not toxic to human neuronal cells. J. Neuropathol. Exp. Neurol. 67, 1084–1096.

Li, L., Nadanaciva, S., Berger, Z., Shen, W., Paumier, K., Schwartz, J., Mou, K., Loos, P., Milici, A.J., Dunlop, J., Hirst, W.D., 2013. Human A53T α-synuclein causes reversible deficits in mitochondrial function and dynamics in primary mouse cortical neurons. PLoS ONE 8, e85815.

Marongiu, R., Spencer, B., Crews, L., Adame, A., Patrick, C., Trejo, M., Dallapiccola, B., Valente, E.M., Masliah, E., 2009. Mutant Pink1 induces mitochondrial dysfunction in a neuronal cell model of Parkinson's disease by disturbing calcium flux. Journal of Neurochemistry. 108, 1561–1574.

Parihar, M.S., Parihar, A., Fujita, M., Hashimoto, M., Ghafourifar, P., 2008. Mitochondrial association of alpha-synuclein causes oxidative stress. Cell. Mol. Life Sci. 65, 1272–1284.

Parihar, M.S., Parihar, A., Fujita, M., Hashimoto, M., Ghafourifar, P., 2009. Alpha-synuclein overexpression and aggregation exacerbates impairment of mitochondrial functions by augmenting oxidative stress in human neuroblastoma cells. International Journal of Biochemistry. 41, 2015–2024.

Peng, T.I., Greenamyre, J.T., 1998. Privileged access to mitochondria of calcium influx through N-methyl-D-aspartate receptors. Molecular Pharmacology 53, 974–980.

Peng, T.I., Jou, M.J., Sheu, S.S., Greenamyre, J.T., 1998. Visualization of NMDA receptor-induced mitochondrial calcium accumulation in striatal neurons. Experimental Neurology 149, 1–12.

Spillantini, M.G., Schmidt, M.L., Lee, V.M., Trojanowski, J.Q., Jakes, R., Goedert, M., 1997. Alpha-synuclein in Lewy bodies. Nature 388, 839–840.

Surmeier, D.J., Schumacker, P.T., 2013. Calcium, bioenergetics, and neuronal vulnerability in Parkinson's disease. J. Biol. Chem. 288, 10736–10741.

Volles, M.J., Lansbury, P.T., 2003. Zeroing in on the pathogenic form of alpha-synuclein and its mechanism of neurotoxicity in Parkinson's disease. Biochemistry 42, 7871–7878.

Appendix 2

Differential Effects of Recombinant and Erythrocyte-Derived α-Synuclein on the Fusion of Small Unilamellar Vesicles

Contributions:

Experiments were designed by Eric Luth, Tim Bartels, and Dennis Selkoe.

Spectrophotometric assays of vesicle fusion were performed by Eric Luth and Vidiya Sathananthan. Electron microscopy was performed by Eric Luth with the help of Maria Ericsson.

Purified αSyn from human erythrocytes was provided by Tim Bartels and Nora Kim.

Introduction

For over two decades, αSyn has been thought to exist solely as an unstructured monomer under physiological conditions. Our lab recently described the purification and biophysical characterization of helical, oligomeric αSyn from human neuroblastoma cells and erythrocytes (Bartels et al., 2011). Because the purified helical αSyn is resistant to aggregation (unlike the unfolded monomer) and the pathological activity of αSyn is related to its aggregation (Volles and Lansbury, 2003), we hypothesized that helical oligomers represent a physiological form of the protein. This hypothesis would be supported by data showing that helical αSyn oligomers can carry out the physiological function of the protein; however, because the precise function of αSyn is has not been determined, there is no established functional assay for αSyn. *In vitro* experiments with recombinant protein (DeWitt and Rhoades, 2013; Varkey et al., 2010) and *in vivo* studies of knockout mice (Abeliovich et al., 2000; Anwar et al., 2011) support a physiological role for αSyn in the modulation of membrane dynamics – specifically related to synaptic vesicle release, though there is debate as to whether this occurs directly or via interactions with membrane proteins (Burré et al., 2010; DeWitt and Rhoades, 2013). In one recent study, Kamp and colleagues (Kamp et al., 2010) showed that recombinant αSyn dose-dependently inhibits the fusion of small unilamellar vesicles (SUVs), a finding is consistent with one purported *in vivo* function. We therefore adopted this facile assay to begin to functionally characterize αSyn oligomers isolated from erythrocytes (RBC αSyn) and to gain insight into whether this form of αSyn behaved in a manner that could be considered "physiological".

Recombinant and RBC αSyn were compared in their ability to inhibit the fusion of SUVs as determined by light scattering, fluorescence and electron microscopy. Based on our previous observations that purified RBC αSyn can more avidly bind to a membrane surface, we

hypothesized that RBC αSyn would have a similar but stronger effect in inhibiting vesicle fusion. We observed that recombinant αSyn acted as expected based on the literature (Kamp et al., 2010), but RBC αSyn behaved qualitatively different from recombinant protein in that it promoted vesicle fusion, but only to a certain extent. Our data suggest that RBC αSyn acts to stabilize a particular size of vesicle, but further studies are needed to confirm the specificity of this effect.

Results and Discussion

Static light scattering:

We examined the effects of recombinant and RBC-derived αSyn on the fusion of SUVs composed of 1,2-dipalmitoyl-*sn*-glycero-3-phosphocholine (DPPC). We first used a static light scattering assay in which we added a non-ionic detergent, octaethylene glycol monododecyl ether ($C_{12}E_8$), to stimulate vesicle fusion after a stable baseline absorbance was achieved in the presence of vehicle, recombinant αSyn, or RBC αSyn (Figure A2.1A). The fusion of vesicle increases the average particle size, which corresponds to an increase in the absorbance of light at 500 nm. In vehicle-treated samples (red trace), $C_{12}E_8$ steadily induced vesicle fusion until a stable plateau in scattering was reached after approximately 12 min. In agreement with published data, submicromolar concentrations of recombinant αSyn (blue and light blue traces) dose-dependently reduced the rate of vesicle fusion (Kamp et al., 2010). In contrast, RBC-derived αSyn (orange) accelerated $C_{12}E_8$-induced fusion of DPPC vesicles. Interestingly, the increase in particle size stopped abruptly at a lower absorbance value than was achieved with vehicle addition. Quantification of the initial rate of fusion over the first 30 s showed that this acceleration was significant when compared to both vehicle and recombinant αSyn-treated

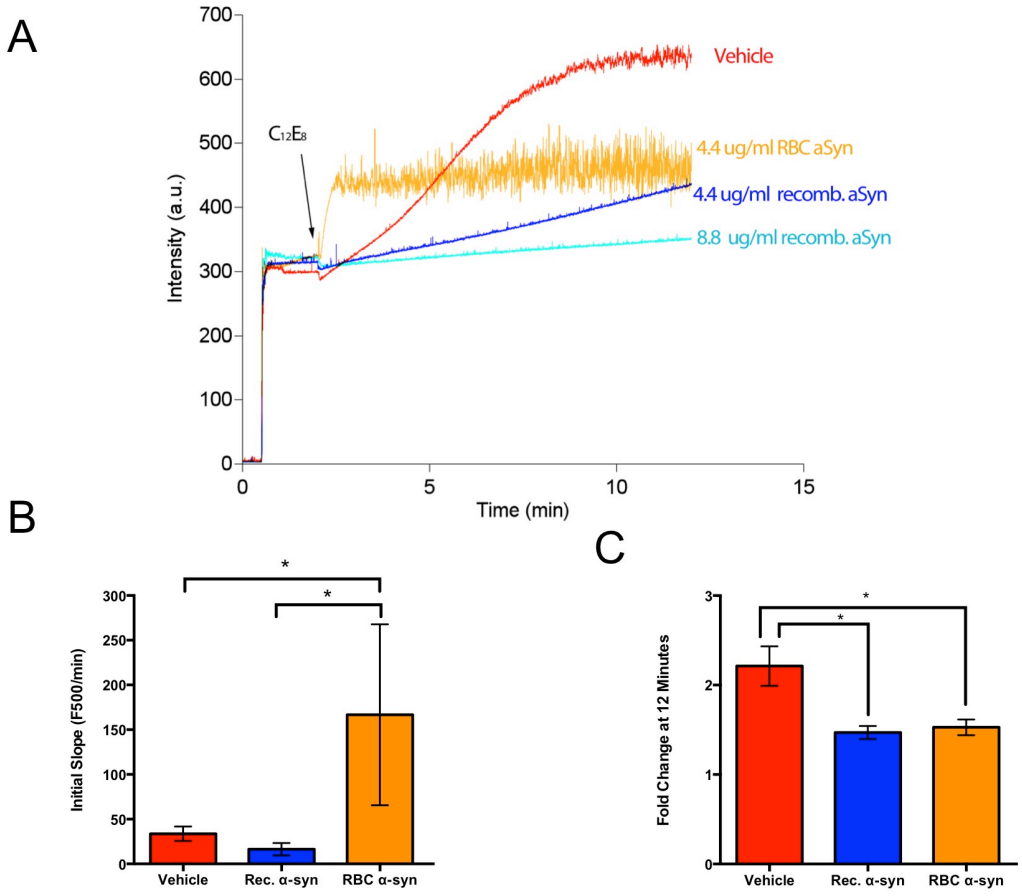

Figure A2.1: DPPC SUV fusion as measured by static light scattering.

A. Representative traces of vehicle-, recombinant αSyn-, and RBC αSyn-treated vesicles. The time of C12E8 addition and initiation of vesicle fusion is noted. B. Quantification of the initial increase in light scattering in the 30 sec after C12E8 addition. C. the fold change in scattering from before C12E8 addition to 12 min after. Error bars represent the standard deviation of 3 independent experiments. * = $P < 0.05$

vesicles (Figure A2.1B). To illustrate that this did not ultimately equate to an overall increase in scattering compared to vehicle-treated vesicles, we also quantified the fold increase in absorbance at 12 min, the time at which vehicle-treated vesicles reached a plateau (Figure A2.1C). At this time point, both recombinant αSyn- and RBC αSyn-treated vesicles were significantly smaller than vehicle-treated vesicles, but were roughly the same size as each other.

Measurement of lipid mixing:

An increase in static light scattering intensity can correspond either to the fusion of vesicles or their clustering without fusion. To exclude the second possibility, we used a lipid mixing assay of vesicle fusion. This assay is conducted similarly to the static light scattering assay except that 10% of the lipids are labeled with both donor and acceptor fluorescent lipid probes such that the donor fluorescence emission is quenched by the acceptor fluorophore under conditions of limited lipid mixing. Initiation of fusion leads to mixing of the fluorescently labeled lipids with the unlabeled lipids and therefore a spatial separation of the donor and acceptor fluorophore. Fluorescence emission of the donor fluorophore is quantified over the course of the assay (Figure A2.2). We have carried out fewer experiments with this system, but initial studies confirm published data in that recombinant αSyn dose-dependently reduced the rate of lipid mixing compared to vehicle-treated vesicles (Kamp et al., 2010). As we had seen with static light scattering, RBC αSyn-treated vesicles fused and then reached a plateau faster than vehicle-treated vesicles. Together with the static light scattering results, this data suggest that recombinant acts to simply slow the fusion of SUVs, but RBC αSyn seems to rapidly promote the formation of and stabilize vesicles of a particular size and, presumably, curvature.

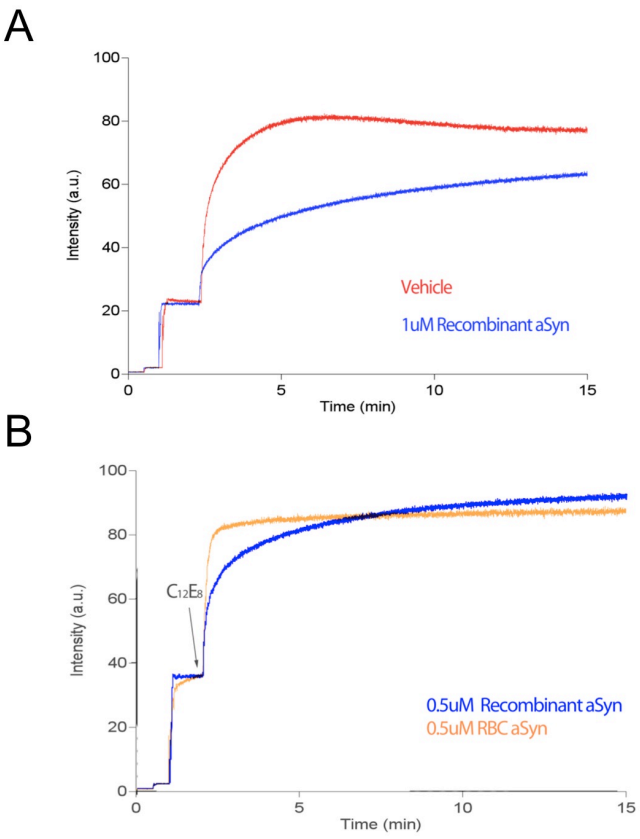

Figure A2.2: Lipid mixing of DPPC vesicles.

A. Preliminary data showing lipid mixing in the presence of vehicle or recombinant αSyn. B. Preliminary qualitative comparison of the effects of recombinant and RBC αSyn on DPPC SUV fusion.

Additional controls:

To show that the observed effects were specific, we incubated vesicles with cytochrome c, another small protein that associates with lipids. Addition of cytochrome c at concentrations up to 10 times what was used for αSyn had no effect on the rate or plateau in either static light scattering or lipid mixing assays (Figure A2.3A). Since some of the RBC αSyn samples contained glycerol, we also tested the effects of vehicle with 15% glycerol. As with cytochrome c, there was no effect of 15% glycerol in either assay of vesicle fusion.

Electron microscopy of fused vesicles:

We next attempted to confirm the effect of the different αSyn species on vesicle fusion using an independent technique. To do this, we prepared samples as in the static light scattering assay but removed aliquots of the vesicle suspension for electron microscopy ~5 min after addition of $C_{12}E_8$, at a time when we could expect to see the greatest difference between all three samples (Figure A2.1A). Representative electron micrographs for these samples are shown in Figure A2.4A. Vehicle-, recombinant αSyn-, and RBC αSyn-treated samples are highlighted in red, blue, and orange, respectively. We measured the diameter of the vesicles and plotted their distributions (Figure A2.4B). As expected based on the light scattering data, recombinant αSyn-treated vesicles showed a shift to the left indicating a smaller average vesicle diameter and confirming reduced fusion. Interestingly, the mean diameter of RBC αSyn-treated vesicles was similar to that of vehicle-treated vesicles (though slightly smaller), but there was a much narrower distribution of the vesicle sizes. This again suggests that RBC αSyn promotes the formation and/or stabilization of DPPC vesicles of a particular size (~60-65 nm in diameter).

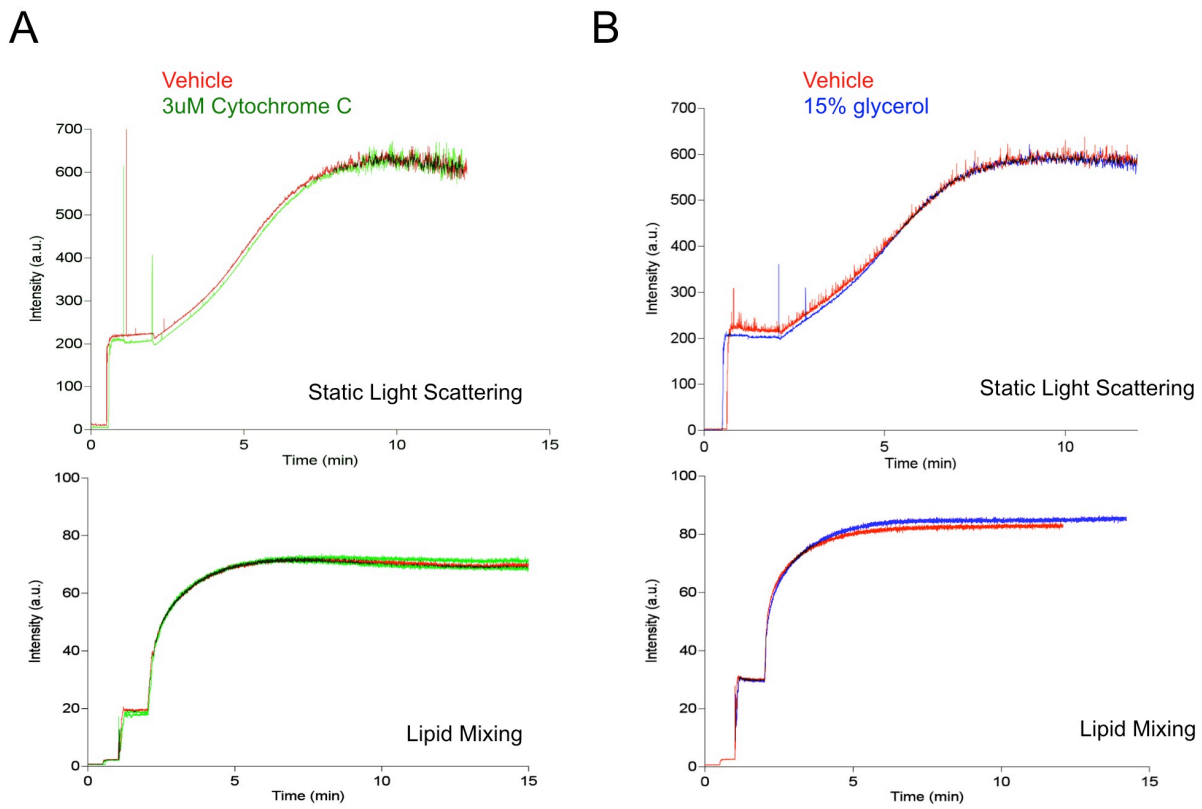

Figure A2.3: Cytochrome C and 15% glycerol do not affect DPPC fusion.

A. DPPC SUVs were mixed with cytochrome at a greater than 10 fold higher concentration compared to what was used or αSyn in the previous figures. B. We occasionally stored RBC αSyn samples in glycerol, but observed no alteration of vesicle fusion by this concentration of glycerol by itself.

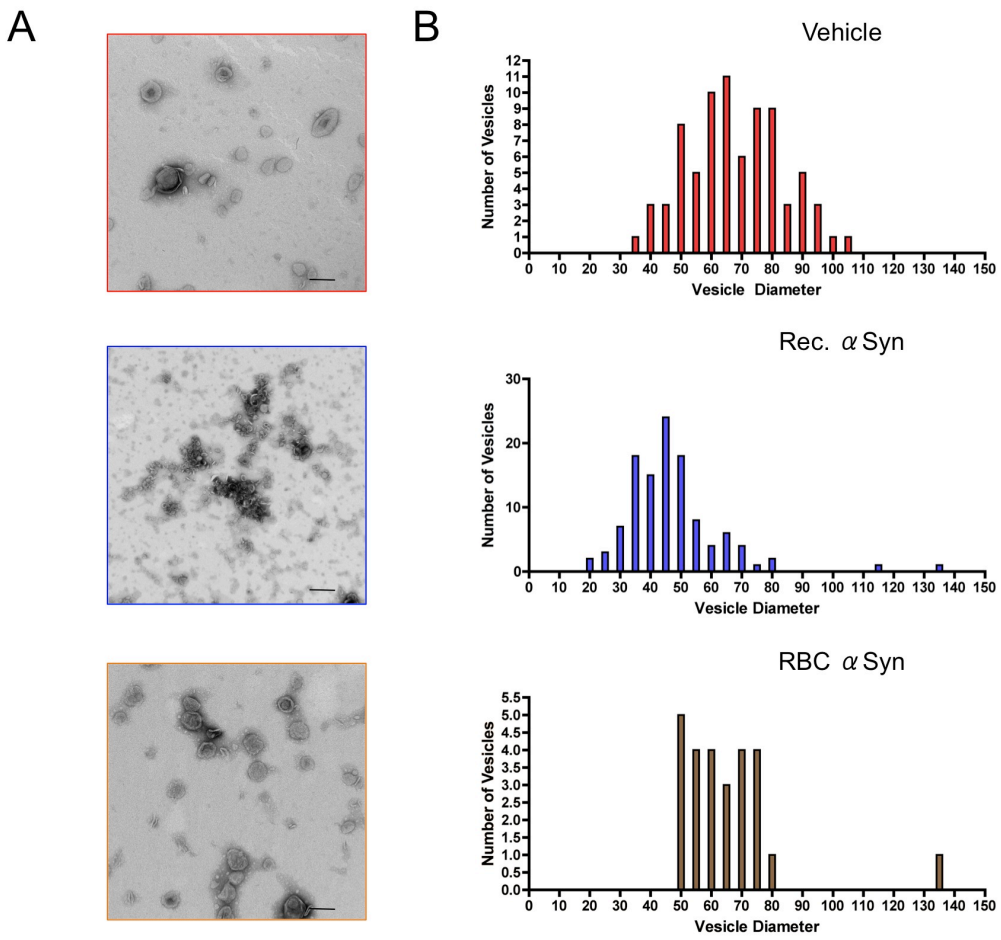

Figure A2.4: Electron microscopy of fused vesicles supports spectrophotometric data.

A. Representative electron micrographs of DPPC vesicles 5 min after initiation of fusion in the presence of vehicle (top panel, red outline), recombinant αSyn (middle panel, blue outline), and RBC αSyn (bottom panel, orange outline). Scale bar = 100nm B. The average diameter of vehicle-, recombinant αSyn-, and RBC αSyn-treated vesicles was measured from electron micrographs as in A and presented as histograms.

Hemoglobin behaves similarly to RBC αSyn:

In addition to αSyn, erythrocytes also abundantly express another helical tetramer: hemoglobin. We decided to test whether this potential contaminant also affected vesicle fusion. Hemoglobin-treated DPPC vesicles behaved similarly to RBC αSyn-treated vesicles in both static light scattering and fluorescent lipid mixing fusion assays (Figure A2.5A). We then asked whether our RBC αSyn samples were contaminated with hemoglobin. Western blot of 200 ng recombinant and RBC αSyn (Figure A2.5B, top panel, lanes 1 and 4, respectively) showed immunoreactivity for αSyn (though RBC αSyn was more difficult to detect), but not for hemoglobin (Figure A2.5B, bottom panel). A separate WB (Figure A2.5C) showed that we were able to detect as little as 100 ng of hemoglobin suggesting that at least 50% of the sample was not hemoglobin. That being said, considering the similarity in behavior of hemoglobin and RBC αSyn samples, the possibility of hemoglobin contamination must be carefully ruled out for each RBC αSyn samples tested in these functional assays.

Our results suggest that recombinant αSyn and RBC αSyn have qualitatively and quantitatively different effects on the fusion of SUVs composed of DPPC. In agreement with published data, recombinant αSyn inhibits SUV fusion and lipid mixing. Based on the increased fusion rate and rapid plateau of light scattering and fluorescence changes, helical αSyn may act to stabilize a preferred size/curvature of vesicles. Electron micrographs of vesicles supported this interpretation. One important caveat is the effect of potential hemoglobin contamination in our RBC samples, though we were unable to detect hemoglobin. It is conceivable that similar secondary and quaternary structures of helical αSyn and hemoglobin (small, helical tetramers) may be responsible for their comparable effects on vesicle fusion. That being said, subsequent

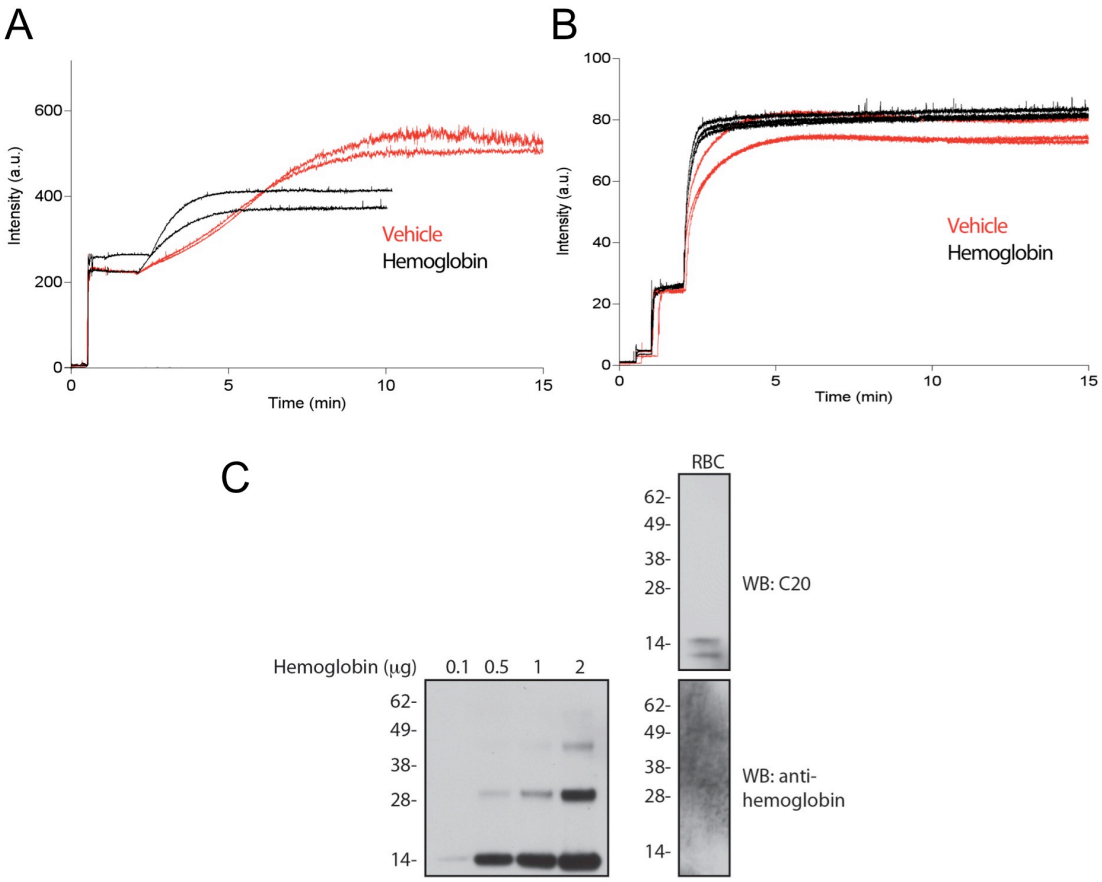

Figure A2.5: Hemoglobin behaves similarly to RBC αSyn in assays of vesicle fusion.

A. Static light scattering analysis of DPPC SUVs treated with vehicle or hemoglobin at the same concentration as used for RBC αSyn in other figures. B. Fusion of DPPC SUVs incubated with vehicle or hemoglobin measured by the increase in increase in donor fluorophore fluorescence due to lipid mixing. C. The left panel shows a Western blot of a range of hemoglobin samples. Hemoglobin exists as a tetramer and loading high quantities of sample results in the detection of low amounts of species incompletely broken down by SDS. The right panels show 200 ng RBC αSyn probed for αSyn (C20) and hemoglobin.

studies of helical αSyn should be performed using a source that does not contain significant amounts of hemoglobin, such as human brain. We could find no publications describing the observed effects for hemoglobin, and it may be interesting to further examine this activity in future studies.

These preliminary results should be followed up in several ways. A dose-response titration of RBC αSyn would allow us to determine at what protein:lipid molar ratio the effects of αSyn are saturated for comparison to published data for recombinant αSyn. Though Kamp et al. (2010) showed that recombinant protein inhibits the fusion of a variety of SUVs, it is possible that there may be preferential effects of RBC αSyn on different lipid types. Importantly, RBC αSyn is acetylated at its N terminus, a post-translational modification absent in recombinantly expressed protein. Unpublished observations from our lab indicate that N-acetylated αSyn binds with greater affinity to monosialoganglioside GM1, a lipid enriched in presynaptic membranes, than does non-acetylated protein. In the future it will also be interesting to compare the ability of helical and unfolded αSyn to inhibit the fusion of purified synaptic vesicles.

Mitochondria provide another potential subcellular target for the activity of αSyn (Kamp et al., 2010; Nakamura et al., 2011; 2008). We could apply RBC and recombinant αSyn to suspensions of isolated mitochondria and monitor changes in size by light scattering and electron microscopy, though higher a protein:lipid ratio may be needed. High concentrations of recombinant αSyn have been shown to fragment large and giant unilamellar vesicles (Varkey et al., 2010). Findings from a recent paper from Westphal and Chandra (2013) suggest that RBC αSyn may have less of an effect on larger membrane structures. They show that monomeric but not RBC-derived tetrameric αSyn caused membrane tabulation of large vesicles. It has been suggested that fragmentation of mitochondria by αSyn is a potential neurotoxic mechanisms for

αSyn oligomers (Nakamura et al., 2011), and the reported curvature-sensing of αSyn (Jensen et al., 2011) may manifest as curvature-generation when the concentration of αSyn is sufficiently high – perhaps due to the formation of misfolded oligomers. A negative result with RBC αSyn in such an assay would further support that idea the abundant oligomers our lab detects under physiological conditions (Bartels et al., 2011; Dettmer et al., 2013) represent a physiological form of the protein and not one that is associated with disease.

Experimental Techniques

Purification of αSyn:

Purification of recombinant αSyn was performed as described by Weinreb et al. (1996), and RBC αSyn was purified as described by Bartels et al. (2011).

Preparation of vesicles:

DPPC (at a final concentration of 4 mM) was suspended in 20 mM Tris pH 7.4 and incubated for 30 min at 65°C. This suspension was then sonicated for 5 min to produce ~30 nm vesicles and spun for 5 min at maximum speed on a benchtop centrifuge. The supernatant (unlabeled vesicles) was stored at 65°C until use. For fluorescently labeled vesicles to be used in lipid mixing assays, 13 mM DPPC in chloroform was also prepared in glass vials. *N*-(7-Nitrobenz-2-Oxa-1,3-Diazol-4-yl)-1,2-Dihexadecanoyl-*sn*-Glycero-3-Phosphoethanolamine (NBD-PE) fluorescence donor and rhodamine B 1,2-Dihexadecanoyl-*sn*-Glycero-3-Phosphoethanolamine **(***N*-Rh-PE) acceptor probe were added at 1 and 2 mol%, respectively, to 13 mM DPPC. Labeled lipid solutions were dried using an air hose, lyophilized, and then

brought up in 20 mM Tris pH 7.4 to a concentration of 13 mM DPPC. Labeled lipids were then sonicated as described above for unlabeled vesicles.

Assays of vesicle fusion:

For static light scattering, 2100 μl of 20 mM Tris pH 7.4 were added to a quartz cuvette and 400 ul of 4 mM unlabeled vesicles were added after 30 sec of recording. At 60 s either vehicle, αSyn, or other controls were added, and at 120 s 15 μl of the non-ionic detergent $C_{12}E_8$ was added to initiate vesicle fusion. Fusion was monitored continuously for 12-15 min by the increase in light scattering at 500 nm. For fluorescent lipid mixing assays, 2100 μl of 20 mM Tris pH 7.4 were added to a quartz cuvette along with αSyn or control samples. At 30 s into recording, 364 μl of unlabeled vesicles were added. At 60 s 36 u μl l of labeled vesicles were mixed in, and at 120 sec 15 μl of $C_{12}E_8$ was added to initiate vesicle fusion. The reduction in donor fluorescence quenching (an indicator of lipid mixing) was monitored at excitation/emission of 450/530 nm for 15 min. All experiments were performed in a Cary Eclipse fluorescence spectrophotometer at 40°C with stirring.

Electron microscopy:

10 ul Aliquots from vesicle suspensions were adsorbed for 1 minute to a carbon coated grid that had been made hydrophilic by a 30 s exposure to a glow discharge. Excess liquid was removed with filter paper and the samples were stained with 0.75% uranyl formate for 30 s. After removing the excess uranyl formate with filter paper, the grids were examined using a TecnaiG² Spirit BioTWIN transmission electron microscope. Images were acquired with an AMT 2k CCD camera. Vesicles diameters were measured using ImageJ.

References

Abeliovich, A., Schmitz, Y., Fariñas, I., Choi-Lundberg, D., Ho, W.H., Castillo, P.E., Shinsky, N., Verdugo, J.M., Armanini, M., Ryan, A., Hynes, M., Phillips, H., Sulzer, D., Rosenthal, A., 2000. Mice lacking alpha-synuclein display functional deficits in the nigrostriatal dopamine system. Neuron 25, 239–252.

Anwar, S., Peters, O., Millership, S., Ninkina, N., Doig, N., Connor-Robson, N., Threlfell, S., Kooner, G., Deacon, R.M., Bannerman, D.M., Bolam, J.P., Chandra, S.S., Cragg, S.J., Wade-Martins, R., Buchman, V.L., 2011. Functional alterations to the nigrostriatal system in mice lacking all three members of the synuclein family. Journal of Neuroscience 31, 7264–7274.

Bartels, T., Choi, J.G., Selkoe, D.J., 2011. α-Synuclein occurs physiologically as a helically folded tetramer that resists aggregation. Nature 477, 107–110.

Burré, J., Sharma, M., Tsetsenis, T., Buchman, V., Etherton, M.R., Südhof, T.C., 2010. Alpha-synuclein promotes SNARE-complex assembly in vivo and in vitro. Science 329, 1663–1667.

Dettmer, U., Newman, A.J., Luth, E.S., Bartels, T., Selkoe, D., 2013. In vivo cross-linking reveals principally oligomeric forms of α-synuclein and β-synuclein in neurons and non-neural cells. J. Biol. Chem. 288, 6371–6385.

DeWitt, D.C., Rhoades, E., 2013. α-Synuclein Can Inhibit SNARE-Mediated Vesicle Fusion through Direct Interactions with Lipid Bilayers. Biochemistry. 52, 2385–2387.

Jensen, M.B., Bhatia, V.K., Jao, C.C., Rasmussen, J.E., Pedersen, S.L., Jensen, K.J., Langen, R., Stamou, D., 2011. Membrane curvature sensing by amphipathic helices: a single liposome study using α-synuclein and annexin B12. J. Biol. Chem. 286, 42603–42614.

Kamp, F., Exner, N., Lutz, A.K., Wender, N., Hegermann, J., Brunner, B., Nuscher, B., Bartels, T., Giese, A., Beyer, K., Eimer, S., Winklhofer, K.F., Haass, C., 2010. Inhibition of mitochondrial fusion by α-synuclein is rescued by PINK1, Parkin and DJ-1. EMBO J 29, 3571–3589.

Nakamura, K., Nemani, V.M., Azarbal, F., Skibinski, G., Levy, J.M., Egami, K., Munishkina, L.,

Zhang, J., Gardner, B., Wakabayashi, J., Sesaki, H., Cheng, Y., Finkbeiner, S., Nussbaum, R.L., Masliah, E., Edwards, R.H., 2011. Direct membrane association drives mitochondrial fission by the Parkinson disease-associated protein alpha-synuclein. J. Biol. Chem. 286, 20710–20726.

Nakamura, K., Nemani, V.M., Wallender, E.K., Kaehlcke, K., Ott, M., Edwards, R.H., 2008. Optical reporters for the conformation of alpha-synuclein reveal a specific interaction with mitochondria. Journal of Neuroscience 28, 12305–12317.

Varkey, J., Isas, J.M., Mizuno, N., Jensen, M.B., Bhatia, V.K., Jao, C.C., Petrlova, J., Voss, J.C., Stamou, D.G., Steven, A.C., Langen, R., 2010. Membrane curvature induction and tubulation are common features of synucleins and apolipoproteins. J. Biol. Chem. 285, 32486–32493.

Volles, M.J., Lansbury, P.T., 2003. Zeroing in on the pathogenic form of alpha-synuclein and its mechanism of neurotoxicity in Parkinson's disease. Biochemistry 42, 7871–7878.

Weinreb, P.H., Zhen, W., Poon, A.W., Conway, K.A., Lansbury, P.T., 1996. NACP, a protein implicated in Alzheimer's disease and learning, is natively unfolded. Biochemistry 35, 13709–13715.

Westphal, C.H., Chandra, S.S., 2013. Monomeric synucleins generate membrane curvature. J. Biol. Chem. 288, 1829–1840.

Appendix 3

Visualization of Cellular α-Synuclein Oligomers Using Intact Cell Crosslinking

Contributions:

Experiments were designed by Eric Luth and Dennis Selkoe.

All experiments were performed by Eric Luth and Vidiya Sathananthan.

Introduction

The secondary structure and oligomerization state of αSyn under physiological conditions is a matter of great interest and debate. We recently challenged the longstanding view that αSyn normally exists exclusively as an unstructured monomer by demonstrating that αSyn purified from human erythrocytes and neuroblastoma cells exists as a helically-folded oligomer that sizes as a tetramer and resists aggregation (Bartels et al., 2011). Independent laboratories have since confirmed the existence of helical oligomers of αSyn purified from erythrocytes (Westphal and Chandra, 2013) or, under favorable conditions, from bacteria (Trexler and Rhoades, 2012; Wang et al., 2011). Another group was unable to detect such species (Fauvet et al., 2012). Our goal was to further probe the assembly state of αSyn as it exists within cells by developing a facile and reproducible method for detecting oligomers. Evidence of abundant cellular oligomers under non-pathological conditions would support the idea that our previous findings are not an artifact of purification but rather represent an endogenous state of the protein.

To this end, we applied cell permeable crosslinking reagents to live cells in order to stabilize intermolecular αSyn-αSyn interactions. We elected to use a crosslinker-based strategy since an alternative FRET/FLIM approach would require the use of fluorescent tags, which could affect these interactions. We restricted our efforts to amine-reactive crosslinking agents because sulfhydryl crosslinkers would be ineffective, due to the absence of cysteine residues in the αSyn protein sequence. We first worked out favorable crosslinking and detection conditions in cells overexpressing the protein and then applied our protocol to the detection of αSyn oligomers under endogenous expression conditions. Application of the 7.7 Å crosslinker disuccinimidyl glutarate (DSG) at a concentration of 0.5-1 mM at room temperature was most effective in trapping midrange oligomeric species for detection on SDS-PAGE. αSyn oligomers could be

detected by multiple αSyn antibodies and also immunoprecipitated. We also show that certain oligomeric assemblies are apparently destabilized by cells lysis. These preliminary results provide a basis for future investigations into factors that affect the stability of αSyn oligomers in intact cells.

Results and Discussion

The 7.7 Å crosslinker DSG effectively traps αSyn oligomers within cells:

We applied a variety of crosslinking agents to intact 3D5 human neuroblastoma cells overexpressing αSyn with the goal of covalently stabilizing αSyn-αSyn interactions that exist within intact cells. We exclusively tested homobifunctional, amine reactive crosslinkers. αSyn lacks cysteines, and therefore thiol reactive agents would not be effective at crosslinking the protein. The 3 Å crosslinker 1,5-difluoro-2,4-dinitrobenzene (DFDNB) did not trap any αSyn oligomers as seen by SDS-PAGE of the lysed cells (Figure A3.1). Additional monomeric protein was detected after crosslinking, but this is due to the fact that crosslinker-induced modification of αSyn monomer allows for improved immunodetection upon Western blotting (Newman et al., 2013). We were able to trap abundant oligomeric species with the 12 Å crosslinker dithiobis(succinimidylpropionate) (DSP). After running lysed cells on SDS-PAGE, the dominant band ran at the position of an αSyn dimer (αSyn-35) with weaker bands migrating around 60 and 80 kDa as well as some high molecular weight smearing (Figure A3.1). Based on the 14.5 kDa molecular weight of the αSyn monomer, we interpreted the αSyn-60 band as a tetramer (4 x 14.5 kDa = 58 kDa). Application of the 7.7 Å crosslinker DSG consistently led to a reduction in the amount of detectable αSyn monomer (an expected consequence of trapping oligomeric protein) and a prominent stabilization of the putative tetramer, with a less immunoreactive dimer band

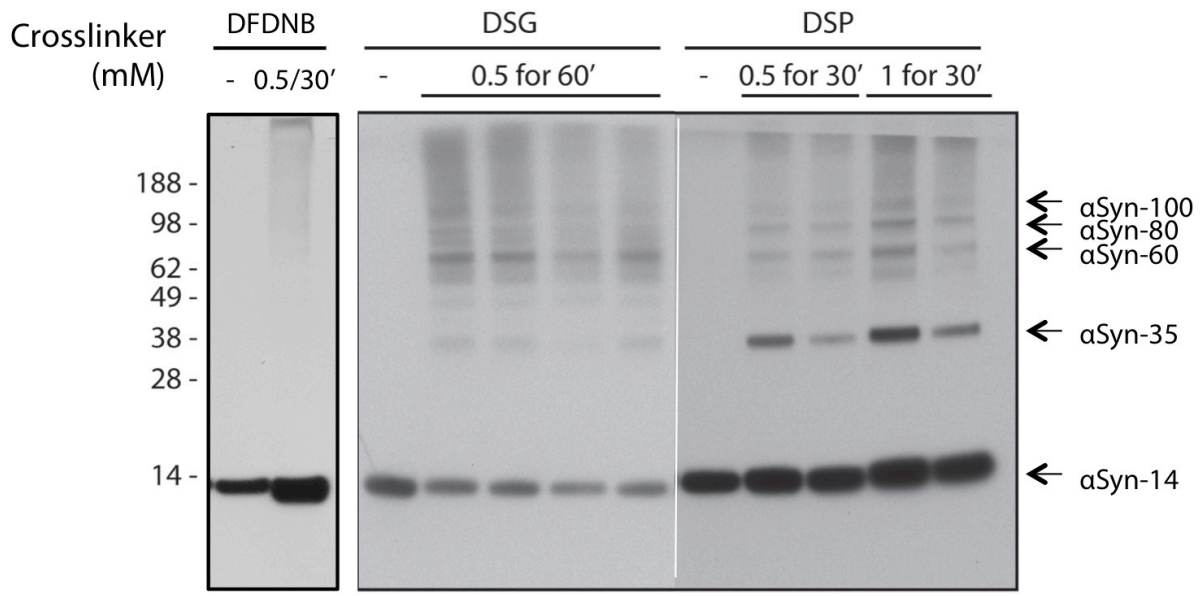

Figure A3.1: The 7.7 Å crosslinker effectively traps a 60 kDa αSyn species.

Intact neuroblastoma cells overexpressing αSyn were crosslinked with either the 3 Å crosslinker DFDNB, the 7.7 Å crosslinker DSG, or the 12 Å crosslinker DSP at the concentrations and times (in minutes) as indicated. The lystates were run on denaturing gels and blotted for αSyn. The positions of specific αSyn immunoreactive bands are noted. Monomeric αSyn runs at 14.5 kDa and a crosslinked tetramer would be expected to run at 58 kDa. DFDNB fails to trap oligomeric αSyn. DSP traps mostly dimeric αSyn. The predominant oligomeric band trapped by DSG is at 60 kDa.

(Figure A3.1). Under these conditions, we also observed some smearing with DSG. Because of our recent publication that characterized αSyn purified from both human erythrocytes and this neuroblastoma cell line as a tetramer, we chose to pursue crosslinking conditions that favored the stabilization of the αSyn-60 tetrameric band – in this case the crosslinker DSG.

Optimization of crosslinking conditions:

We tested a multiple DSG concentrations within the range recommended by the manufacturer and saw the best results with 0.5-1 mM (shown in Figure A3.2A). With 0.5 mM DSG, we observed a time-dependence of both monomer reduction and tetramer stabilization. At 1 mM DSG, the intensity of oligomeric bands was less time dependent, but there was a greater presence of smearing in the mid-to-high molecular weight region that is indicative of non-specific crosslinking to a variety of other molecules. We then compared DSG crosslinking at room temperature and 4°C in their ability trap putative tetramers. We consistently observed that crosslinking at 4°C, even for twice as long, was less efficient that crosslinking at ambient temperature. At room temperature, we saw strong stabilization of the αSyn-60, -80, and -100 kDa bands (Figure A3.2B). The precise relationship between these bands is currently under investigation. On the other hand, αSyn-35 (dimer) was readily detected after crosslinking at 4°C, and we interpreted this as a partial crosslinking of tetramers (Figure A3.2B). This was true when samples were probed with two different αSyn antibodies, C20 and Syn1. While a variety of αSyn antibodies can detect the trapped oligomeric species, they occasionally exhibit preferences for different species. For example, C20 more readily detects monomer compared to Syn1 (Figure A3.2B).

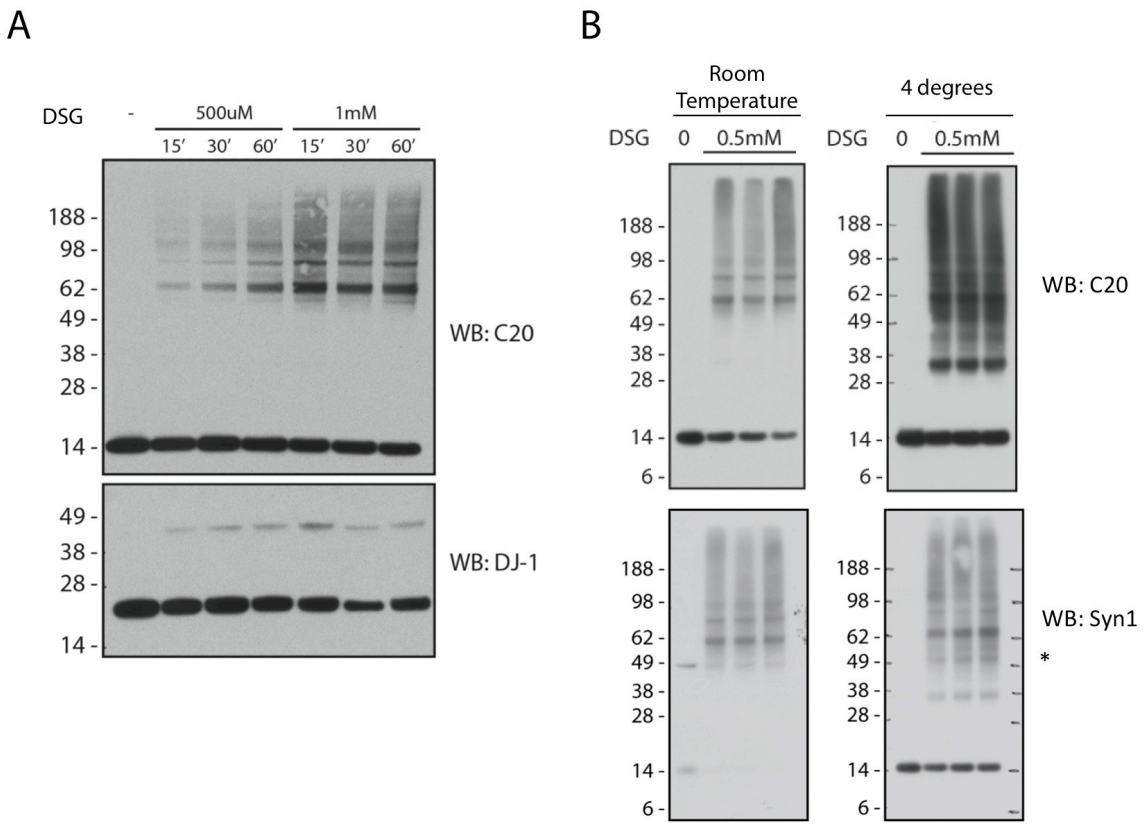

Figure A3.2: Optimization of DSG crosslinking conditions.

A. The ability of 0.5 and 1 mM DSG for various durations to crosslink αSyn (top) and DJ1 (bottom) at room temperature were compared. B. Two different αSyn antibodies (C20 and Syn1) were used to compare the ability of 0.5 mM DSG to trap mid-molecular weight αSyn oligomers after 60 min incubations at either room temperature or 4°C. Note the presence of dimers (i.e. less efficient crosslinking) associated with crosslinking performed at 4°C. *= non-specific Syn1 immunoreactive band.

Crosslinked oligomers can be immunoprecipitated:

As a means of laying the groundwork for future pulse-chase studies to look at the stability of oligomeric αSyn, we asked whether any of our αSyn antibodies could immunoprecipitate (IP) crosslinked species. As shown with non-crosslinked samples, Syn1 could efficiently IP αSyn from cell lysate. When we used Syn 1 to IP from lysate that was prepared after crosslinking intact cells with DSG, it was able to pull down both monomeric and oligomeric αSyn (Figure A3.3A) Based on the presence of monomer in the post-IP supernatant, it is possible that Syn1 IPs relatively more oligomeric αSyn than monomeric αSyn, but this will need to be examined further. Two other αSyn antibodies, LB509 and 5C2 failed to IP any αSyn species (Figure A3.3B), suggesting that their epitopes may be inaccessible under native conditions regardless of whether the protein is in a monomeric or oligomeric assembly state.

Crosslinking of endogenous αSyn oligomers in intact cells:

Thus far, we have demonstrated an ability to trap oligomeric αSyn in overexpressing cells. It is possible that the formation of these assemblies of αSyn is a result of overexpression and/or pathological accumulation of the protein. We therefore sought to similarly trap oligomeric species in cell expressing endogenous or near endogenous levels of αSyn. The overexpression of αSyn in 3D5 cells is induced when the cells are cultured in the absence of tetracycline. In the presence of tetracycline, there is minimal αSyn overexpression. Though higher concentrations of crosslinker were required when compared to overexpressing 3D5 cells, we were able to detect oligomeric αSyn-immunoreactive bands (αSyn-35, -60, -80, -100) in uninduced cells (Figure A3.4A). We then tested a completely endogenous neuroblastoma system, SKNMC cells. Intact cell crosslinking in SKNMC cells revealed the same pattern of oligomeric bands that we

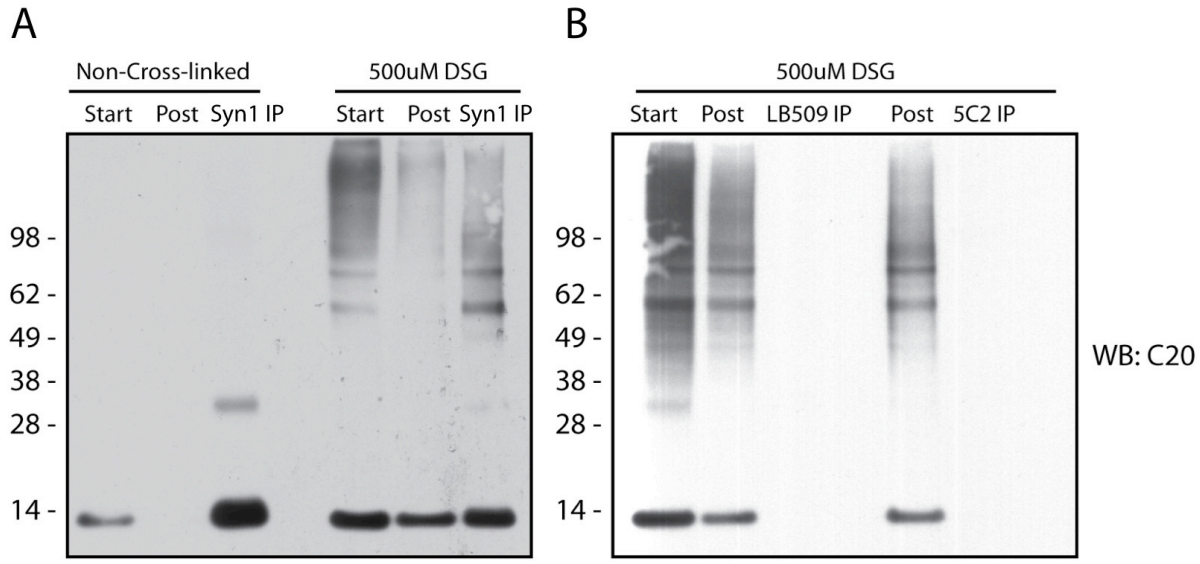

Figure A3.3: Immunoprecipitation of crosslinked αSyn oligomers.

A. αSyn was immunoprecipitated from the lysates of non-crosslinked and crosslinked neuroblastoma cells by the Syn1 antibody. Post = the supernatant following immunoprecipitation of αSyn. IP lanes = precipitated samples boiled in sample buffer containing βME to elute precipitated protein from agarose beads. B. Immunoprecipitations from crosslinked cells were carried out using the αSyn antibodies LB509 and 5C2. Note the strong signal in the Post but not IP lanes.

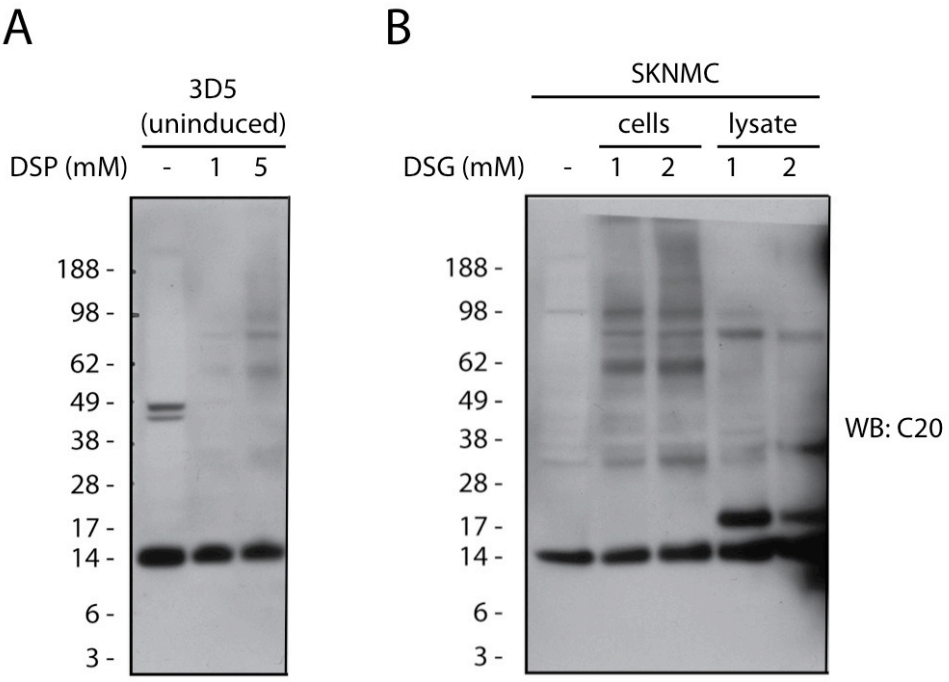

Figure A3.4: Crosslinking of endogenous αSyn oligomers within cells.

A. DSP crosslinking of human neuroblastoma cells under conditions that repress αSyn overexpression. Note the presence of 35, 60, 80, and 100 kDa bands in lanes with 1 and 5 mM DSP. B. DSG crosslinking of SKNMC human neuroblastoma cells expressing only endogenous αSyn. Crosslinking of intact cells (lanes 2 and 3) was compared to crosslinking of cell lysate (lanes 4 and 5). The standard pattern of oligomers is observed upon intact cell crosslinking, but much of the mid-molecular weight oligomers were not observed after crosslinking of cell lysates. Only the 80 kDa band appeared resistant to lysis.

observed in induced and uninduced 3D5 cells (Figure A3.4B). When SKNMC cells were lysed prior to crosslinking, DSG trapped a different pattern of oligomers; we saw a profound destabilization of the 60 and 100 kDa bands in favor of a strong 17 kDa band and enhanced immunoreactivity for the 80 kDa band. This suggests some of the oligomeric assemblies trapped within live cells by DSG are lysis sensitive.

An attempt to alter the oligomer to monomer ratio:

It has previously been reported that HSP-70 expression can affect the intermolecular interactions of lysis-sensitive αSyn oligomers within cells (Klucken et al., 2006). To learn more about the potential role of HSP-70 in the formation of oligomers in our system, we transfected induced 3D5 cells with an siRNA for HSC-70 (a constitutively active isoform) and examined the pattern of crosslinker-trapped oligomers. Untransfected cells showed the familiar strong 60, 80, and 100 kDa band with a faint dimer band (Figure A3.5). Cells transfected with HSC-70 siRNA showed a somewhat reduced staining for oligomeric bands, but a similar effect was seen with mock-transfected cells. Moreover, probing for HSC-70 showed no evidence of lower protein expression levels. Though this experiment failed to alter the oligomer to monomer ratio (perhaps due to technical issues with the siRNA transfection), live cell crosslinking promises to be an effective tool for analyzing conditions that modulate the native cellular state of αSyn.

The crosslinking technique that I developed for the detection of αSyn oligomers has been further optimized by my colleagues and recently published (Dettmer et al., 2013). In that paper, we show that removing membranous components using an ultracentrifugation step after cell lysis dramatically reduced smearing in the mid-to-high molecular weight region. The use of cells with

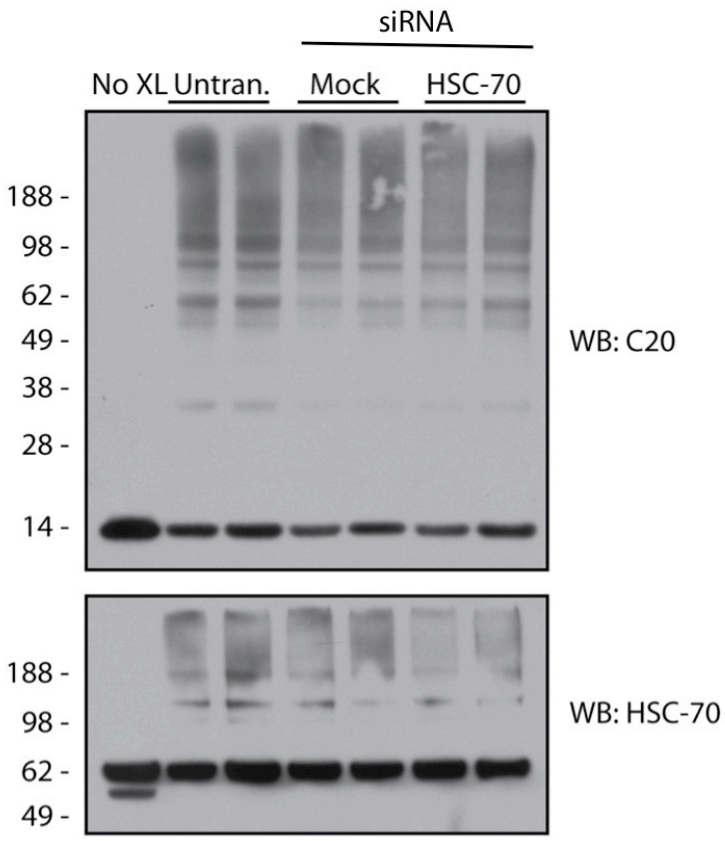

Figure A3.5: An attempt to alter the oligomer to monomer ratio.

Intact 3D5 cells were crosslinked after transfection with siRNA to the chaperone HSC-70 and the pattern of αSyn immunoreactivity was compared to untransfected and mock transfected cells (top). Western blot for HSC-70 (bottom) shows no reduction of protein levels with siRNA transfection.

higher endogenous αSyn expression, such as human erythroleukemia cells and primary rat neurons, coupled with more sensitive αSyn antibodies have improved the detection of endogenously expressed oligomeric species trapped within cells. The diffusion controlled crosslinking of recombinant protein produced a pattern of oligomeric bands whose intensity decreased as their size increased. This is distinct from the strong 60 kDa band that we observe after crosslinking live cells, arguing against the likelihood that the pattern of immunoreactivity we observe with intact cell crosslinking is due to a stochastic process. We expanded upon my initial observation that certain immunoreactive oligomeric bands are lysis sensitive by showing that they can be recovered when cells are lysed at high protein concentrations (above 15 mg/ml). This suggests that macromolecular crowding is favorable for stability of oligomeric species, specifically the 60 and 100 kDa bands. We are currently trying to identify the relationship between these oligomeric bands to determine whether they are distinct oligomeric species or conformers that are differentially modified by DSG. To this end, we are purifying crosslinked species for intact mass determination by mass spectroscopy.

We used multiple approaches, including the co-immunoprecipitation of differentially tagged αSyn species and the exclusion of putative interactors by Western blot or other means to show that these mid-molecular weight oligomers are homo-oligomers rather than monomer crosslinked to a distinct protein. Furthermore, we showed that non-aggregation prone βSyn and αSyn lacking an intact NAC domain can be similarly crosslinked in a pattern that mirrors that for αSyn (Dettmer et al., 2013). These observations further support the idea that the oligomers we trap by live-cell crosslinking are physiological and not pathological species.

This now-optimized technique will be useful in identifying intracellular factors that influence the formation or stability of physiological αSyn oligomers. Such factors can be

intrinsic to αSyn, such as mutations or extrinsic, such as the activation of other cellular pathways. We have preliminary data suggesting that PD-linked αSyn missense mutations reduce the ratio of αSyn-60 : αSyn-14. These data further highlight the physiological nature of these αSyn oligomers and support the hypothesis that toxic αSyn species arise from the aggregation of unfolded monomers but not helical oligomers. It will also be important to investigate whether other conditions, such as chronic rotenone treatment (Sherer et al., 2002) that promote αSyn aggregation are also associated with a reduction in endogenous mid-molecular weight oligomers in favor of monomers.

Experimental Techniques

Crosslinking:

For intact cell crosslinking, cells were crosslinked in 10 cm culture dishes. Culture media was aspirated and cells were gently washed with Dulbecco's phosphate buffered saline (DPBS) after which 4 ml of DPBS plus a crosslinking agent (dissolved in DMSO) or DSMO vehicle was carefully added so as not to disturb the monolayer of cells. Dishes were rocked at room temperature or 4°C for the indicated time. To quench the crosslinking reaction Tris pH 7.6 was added to a final concentration of 50 mM and dishes were rocked at room temperature for an additional 15 min. The liquid was then aspirated from the dishes and cells were scraped in 1 ml PBS into microcentrifuge tubes. Cells were pelleted by spinning at 1,000 *g* for 5 min at 4°C, resuspended in 150 μl PBS and sonicated 3 times for 15 s each. Lysates were spun at 20,000 *g* for 30 min and the supernatant was collected. For crosslinking of lysed cells, cells were scraped in 1 ml DPBS into microcentrifuge tubes and spun at 1,000 *g* for 5 min at 4°C. The intact cell pellets were resuspended in 200 ul DPBS and homogenized by sonication for 3 times for 15 s.

Lysates were spun at 20,000 *g* for 30 min and the supernatant was collected. DSG was added to a final concentration of 1 or 2 mM in DMSO and the samples were incubated for 30 min at room temperature under nutation. To quench the crosslinking reaction Tris pH 7.6 was added to a final concentration of 50 mM and samples were incubated for an additional 15 min at room temperature.

Immunoprecipitation:

Protein A or G agarose beads stored in ethanol were washed in PBS. For pre-clearing, 500 μg of crosslinked or non-crosslinked samples were incubated with 10 ul protein A or G agarose beads and PBS for a total of 300 ul. In parallel, agarose beads were conjugated to antibodies directed against αSyn. 1 μg of antibody was incubated with 20 ul of agarose beads and PBS for a total of 300 μl. Samples were nutated at 4°C for 90 min after which the supernatant from the pre-clear step was added to the pelleted antibody-bead conjugates and then incubated overnight at 4°C. The following day, beads were pelleted by spinning at 5,000 *g* for 5 min at 4°C. The post-IP supernatant was collected. The pellet was washed with PBS and spun again and the protein in the resultant pellet was eluted by boiling the beads in 2x LDS sample buffer without βME for 5 min at 85°C.

SDS-PAGE / Western blotting (WB):

Samples were prepared using MilliQ water and 4x sample buffer containing LDS plus 20% βME Samples were electrophoresed on Nu-PAGE 4-12% Bis-Tris gels with MES-SDS running buffer. Gels were then transferred onto 0.45 μm Immobilon-P PVDF membranes for 60 min at 400 mA constant current at 4°C in transfer buffer consisting of 25 mM Tris, 192 mM

glycine, and 20% methanol. After transfer, membranes were blocked in 5% non-fat milk in PBS with 0.1% v/v Tween-20 (PBS-T) for 30 min at room temperature and then incubated in primary antibody either overnight at 4 °C or for 60 min at room temperature. Membranes were then washed 3 times for 5 min in PBS-T, incubated with secondary antibody, washed 3 more times for 5 min in PBS-T, and then developed with ECL Plus or ECL Prime according to the manufacturer's directions.

References

Bartels, T., Choi, J.G., Selkoe, D.J., 2011. α-Synuclein occurs physiologically as a helically folded tetramer that resists aggregation. Nature 477, 107–110.

Dettmer, U., Newman, A.J., Luth, E.S., Bartels, T., Selkoe, D., 2013. In vivo cross-linking reveals principally oligomeric forms of α-synuclein and β-synuclein in neurons and non-neural cells. J. Biol. Chem. 288, 6371–6385.

Fauvet, B., Mbefo, M.K., Fares, M.-B., Desobry, C., Michael, S., Ardah, M.T., Tsika, E., Coune, P., Prudent, M., Lion, N., Eliezer, D., Moore, D.J., Schneider, B., Aebischer, P., El-Agnaf, O.M., Masliah, E., Lashuel, H.A., 2012. α-Synuclein in central nervous system and from erythrocytes, mammalian cells, and Escherichia coli exists predominantly as disordered monomer. J. Biol. Chem. 287, 15345–15364.

Klucken, J., Outeiro, T.F., Nguyen, P., McLean, P.J., Hyman, B.T., 2006. Detection of novel intracellular alpha-synuclein oligomeric species by fluorescence lifetime imaging. The FASEB Journal 20, 2050–2057.

Newman, A.J., Selkoe, D., Dettmer, U., 2013. A new method for quantitative immunoblotting of endogenous α-synuclein. PLoS ONE 8, e81314.

Sherer, T.B., Betarbet, R., Stout, A.K., Lund, S., Baptista, M., Panov, A.V., Cookson, M.R., Greenamyre, J.T., 2002. An in vitro model of Parkinson's disease: linking mitochondrial impairment to altered alpha-synuclein metabolism and oxidative damage. Journal of Neuroscience 22, 7006–7015.

Trexler, A.J., Rhoades, E., 2012. N-Terminal acetylation is critical for forming α-helical oligomer of α-synuclein. Protein Sci. 21, 601–605.

Wang, W., Perovic, I., Chittuluru, J., Kaganovich, A., Nguyen, L.T.T., Liao, J., Auclair, J.R., Johnson, D., Landeru, A., Simorellis, A.K., Ju, S., Cookson, M.R., Asturias, F.J., Agar, J.N., Webb, B.N., Kang, C., Ringe, D., Petsko, G.A., Pochapsky, T.C., Hoang, Q.Q., 2011. A soluble α-synuclein construct forms a dynamic tetramer. Proceedings of the National Academy of Sciences 108, 17797–17802.

Westphal, C.H., Chandra, S.S., 2013. Monomeric synucleins generate membrane curvature. J. Biol. Chem. 288, 1829–1840.